Phase 2.1 Report

DOE Award: DE-EE0002777

AltaRock Energy, Inc.

March 10, 2014

Contributing Authors

AltaRock Energy

Trenton T. Cladouhos, Susan Petty, Yini Nordin, Geoff Garrison,

Matt Uddenberg, Michael Swyer, Kyla Grasso

Consultants and Sub-recipients

Paul Stern (PLS Environmental)

Eric Sonnenthal (LBNL)

Dennise Templeton (LLNL)

Pete Rose (EGI)

Gillian Foulger and Bruce Julian (Foulger Consulting)

Acknowledgment: This material is based upon work supported by the Department of Energy under Award Number DE-EE0002777.

Table of Contents

TABLE OF FIGURES

TABLE OF TABLES

APPENDICES

1 INTRODUCTION

1.1 PROJECT DESCRIPTION

The Newberry EGS Demonstration will develop an Enhanced Geothermal System (EGS) reservoir in the high-temperature, low-permeability resource present in volcanic formations on the northwest flank of the Newberry Volcano. The EGS Demonstration Project is being executed in multiple stage-gated phases, and this report summarizes the activities of Phase 2.1.

During the field portion of Phase 2.1, AltaRock Energy, Inc. (AltaRock) successfully deployed, monitored, tracked, and recorded seismic activity using a specialized seismic array. Stimulation equipment was installed, tested, and operated, including water piping, high pressure pumps and electrical control equipment, diverter and tracer injection equipment. High level systems controls and data acquisition systems were operated that enabled high accuracy data collection. As a result, the project team definitively demonstrated quantitative stimulation techniques that successfully induced and sustained fluid flow into an EGS injection well. However, a failure in the surface casing of the stimulation well allowed the majority of the injected water to leave the casing and enter the subsurface at a depth shallower than was intended in the project plan. The casing will need to be repaired before additional work can be done.

Figure 1-1. Location map for the EGS Demonstration at Newberry Volcano, showing Newberry National Volcanic Monument, geothermal leases, and the communities of Bend, Sunriver, Three Rivers and La Pine.

The project is located about 37 km (23 miles) south of Bend, Oregon, with the nearest small community about 11 km (7 miles) away at Newberry Estates, and the nearest town of La Pine about 16 km (10 miles) away (Figure 1-1). The project site was developed on land leased from the Bureau of Land Management

(BLM) with the surface controlled by both the BLM and the US Forest Service (USFS). The geothermal leases lie adjacent to the Newberry National Volcano Monument (NNVM), which was created in 1990 to preserve the scenic beauty and the volcanic features inside the Newberry Volcano caldera while also providing for geothermal resource development and other uses on adjacent lands.

With the completion of Phase 2.1, the Newberry site has proven to be a favorable area to demonstrate EGS technologies. The well utilized in this project provided access to a large, high-temperature, very low permeability geothermal resource at a depth of 10,000 feet below ground surface (bgs), with multiple zones where potential flow pathways are suitable for stimulation.

1.2 SUMMARY OF PHASE 1 ACCOMPLISHMENTS

Phase 1 was successfully completed when the BLM approved the Environmental Assessment (EA) in April, 2012 (BLM, 2011). Both the EA and the Phase 1 Progress Report (AltaRock, 2011a) served as a basis for the Stage Gate Review conducted by the Department of Energy (DOE), after which the DOE then granted approval to proceed with Phase 2.1 on February 15, 2012. Phase 1 accomplishments included:

- Obtaining necessary permits to compliance with all applicable regulations (including NEPA); permits required are listed in Table 1-1;
- Communicating with the public, regulators and other stakeholders;
- Evaluating existing geoscience data and collecting additional field data, including a static pressure-temperature (PT) survey, an injectivity test and a borehole televiewer survey (Osborn et al., 2011);
- Develop a Thermal-Hydrological-Chemical (THC) conceptual resource model (Figure 1-2), including simulation of the reservoir under supercritical steam conditions using the TOUGH2 modeling code developed and maintained at Lawrence Berkeley National Lab (LBNL);
- Evaluate the two candidate injection wells and select the best well for stimulation;
- Formulate a detailed Stimulation Plan for Phase 2.1;
- Initial microseismic array (MSA) deployment and calibration, followed by final MSA design;
- Calibration shot and background seismic monitoring;
- A study of the potential for induced seismicity and seismic hazards by independent consultants using a temporary seismic array (URS, 2010);
- Develop an Induced Seismicity Mitigation Plan (ISMP) with procedures to evaluate, monitor, and mitigate the risk of felt or potentially damaging induced seismicity (AltaRock, 2011b);
- Develop a Water Usage Plan for all Phase II activities (part of the permitting process; AltaRock, 2011c); and
- Develop a Groundwater Monitoring Plan to characterize local water resources before, during, and after the stimulation.

Table 1-1. Permits required for Phase 2.1.

Permit and Agency	Permit Trigger
1. ODEQ Simple Air Contaminant Discharge Permit	Diesel generator air emissions
2. ODEQ Letter Permit of Authorization	Sump design for Pads S-16 and S-29
3. USFS Temporary Special Use Permit	Surface microseismic stations
4. USFS Road Use Permit	Use of Forest Service roads
5. BLM Geothermal Drilling Permit	Geothermal use of well NWG 55-29
6. DOGAMI Geothermal Well Permit	Geothermal use of well NWG 55-29
7. ODEQ Underground Injection Control (UIC) Permit	Injection of groundwater into well NWG 55-29
8. OWRD Limited Use License	Groundwater use from water supply wells
9. BLM Authorization of Notice of Intent	Geothermal Resource Exploration Operations
10. Deschutes County Building Permit	Use of modular office units
11. BLM Geothermal Sundry Notice	Stimulation of well NWG 55-29
12. DEQ UIC Permit	Injection of diverter products into well NWG 55-29

DOGAMI - Oregon Department of Geology and Mineral Industries
ODEQ - Oregon Department of Environmental Quality ORWD - Oregon Water Resources Department

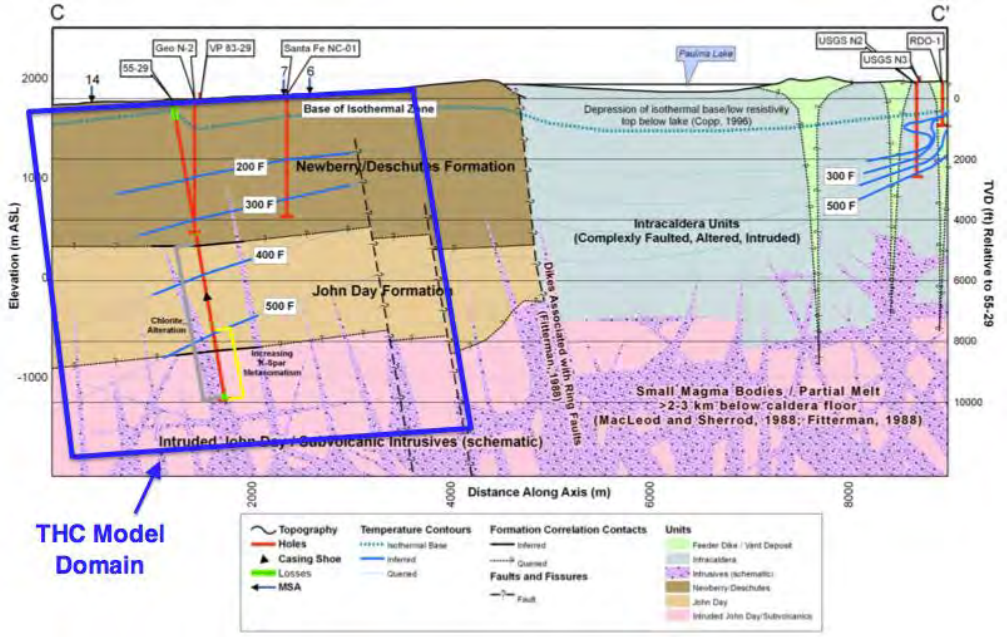

Figure 1-2. THC model of initial thermal and hydrologic conditions at Newberry Volcano. Section runs ENE-WNW from caldera through NWG 55-29 (after AltaRock, 2011a); the upper surface of the model follows the surface contour, and gravity is vertical in the model.

1.3 PHASE 2.1 GOALS AND PURPOSE

The primary objective of Phase 2.1 was to stimulate the existing fracture network around one of the two existing geothermal wells completed by Davenport Newberry in 2008. The stimulation was designed to allow significant movement of geofluids through the reservoir.

The work conducted under Phase 2.1 was guided by the permit requirements, the geologic conceptual resource model, the Stimulation Plan, the ISMP, Water Usage Plan, and the Groundwater Monitoring Plan, all of which were included in the Phase 1 Progress Report (AltaRock, 2011a).

The stimulation well was originally completed as one of two exploratory wells prospecting for a traditional hydrothermal resource. Both wells were completed to more than 10,000 feet bgs, and water could only be injected at a rate of 0.02 gallons per minute per pound per square inch (gpm/psi) (Osborn et al., 2011).

The Phase 2.1 plan called for stimulation of three zones using thermally degrading zonal isolation materials (TZIM) to block permeable areas and create multiple stimulated fracture systems. These stimulations targeted deep, high-temperature areas of the reservoir while isolating and preventing stimulation of shallow, low-temperature rock. The objective was to increase injectivity by one to two orders of magnitude.

1.4 NEXT STEPS

The next phase of development, Phase 2.2, is planned to start spring of 2014. Section 6 of this report details the scope and objectives of Phase 2.2, including:

- onsite maintenance;
- well casing repair of NWG 55-29;
- restimulation of NWG 55-29;
- borehole televiewer run;
- planning production well trajectory; and
- production well construction.

Phase 2.2 will allow for further development of the Newberry site, including improved characterization of the stimulated reservoir. Repairing the casing will allow the reservoir around well NWG 55-29 to be more completely stimulated. The borehole televiewer will provide high resolution data on the effect of stimulation on fractures intersecting the wellbore. Such data is important in characterizing the effects of stimulation and will provide researchers invaluable data regarding the use of EGS in locations similar to Newberry.

2 PHASE 2.1 INSTALLATION AND OPERATIONS

The Phase 2.1 build-out of the project site consisted of the following critical tasks:

- **Permitting**

The permitting process included an Environmental Assessment (EA) on which the BLM issued a Finding of No Significant Impact (FONSI), Forest Service Special Use and Road Permits, a Forest Service Industrial Fire Precaution Level Waiver, a State Special Letter Permit for injection, and a State Geothermal Well Modification Permit.

- **Public Outreach**

Public outreach and education was an integral part of Phase 2.1 activities, including public meetings, reports and publications, and outreach through online social media. Monthly public outreach meetings were held during stimulation and were conducted in Bend, La Pine and Sunriver.

- **Road and Pad Preparation for Seismometer Installation and Development of Pad S-29**

Roads required repair and grading from over-use, and watering for dust mitigation was needed during times of extreme dust and heat. Certain roads accessing borehole sites needed widening and grading to make the road serviceable during drilling and seismometer installation.

- **Drilling Boreholes for Seismometers**

Between May and August of 2012, four new boreholes were drilled and one existing borehole was deepened to depths ranging between 213 m to 248 m bgs (700 ft to 815 ft) using a combination of air hammer and tricone drill bits. The boreholes were completed with steel casing and cement along the full length for seismometer installation.

- **Installation of Borehole and Surface Seismometers**

A seismic monitoring array of 15 seismometers was installed in August 2012 with the assistance of GeoTech Instruments, Inc., out of Dallas, Texas, and Hasting Microseismic Consulting out of Ridgecrest, California. Eight seismometers were installed in boreholes, and 7 were installed at surface stations. Each station was equipped with surface equipment for digitizing, recording, and transmitting seismic data.

- **Installation of Distributed Temperature Sensing (DTS) Cable**

A high-temperature VHM 3000 Distributed Temperature Sensing (DTS) cable approximately 3,000 m (9,843 ft) in length, with three optical fibers was obtained and then deployed into NWG 55-29 on October 17. This cable lost signal during stimulation and was replaced by a second 3-fiber DTS on November 25. Further information on DTS performance and results is provided in Section 3.4.

- **Rehabilitation of the 46-16 Sump and Installation of Temporary Water Pipeline**

The two principal well pads used in the stimulation work were Pad S-29, where the stimulation was to be performed, and Pad S-16, which was made available for backup injection water and additional flowback capacity. Drilling mud remaining from 2009 had to be removed from the 46-16 pad sump, and the sump had to be relined to receive potential flowback water from Pad S-29. A 25.4 cm (10 in) diameter 4.3 km (2.7 mi) long temporary aluminum pipeline was then laid between the two pads to facilitate water transfer as needed.

- **Modification of the NWG 55-29 Wellhead**

Early in Phase 2.1 it was determined that the existing American National Standards Institute (ANSI) 900 Series wellhead should be replaced to meet safety standards for the fluid temperatures and pressures that were expected to be produced. An ANSI 1500 Series wellhead, a new wellhead cross, and new inlet and outlet control valves were procured. TNG Energy Services Inc., out of Bakersfield, California, installed the new wellhead in August.

- **Commissioning Pad S-29 and the Water Transfer System**

Infrastructure used at Pad S-29 to facilitate water transfer between sumps, the water supply well, and the injection well included: water storage tanks, booster pumps, specialized stimulation pumps and associated drives and electrical control equipment, and inlet and outlet piping manifolds. Three 980 kW and two smaller diesel generators were mobilized to the pad to provide power capacity for all the pumps and a mobile office. Infrastructure was installed downstream of the injection wellhead to manage geofluid flowback, including: flow line piping, a control valve, a liquid phase/steam phase separator, and a flow metering weir box. Flow back infrastructure is designed to separate steam and water phases to enable both measurement and sampling of water and steam flows. A site office, sanitary facilities, and storage for fuel, tools and other items were installed in addition to well infrastructure.

Detailed descriptions of the most significant tasks are below.

2.1 PERMITTING

2.1.1 PHASE 2.1 PERMITS

The following permits were obtained during the 2012 field season to allow the stimulation to proceed.

Environmental Assessment (EA)

The Bureau of Land Management (BLM) completed an environmental analysis (EA) entitled Newberry Volcano Enhanced Geothermal System (EGS) Demonstration Project Environmental Assessment No. DOI-BLM-OR-P000-2011-003-EA (DOE/EA-1897). Because the project is located on National Forest system lands administered by the U.S. Forest Service (USFS), and because the Department of Energy (DOE) was providing partial financing through a grant utilizing American Reinvestment and Recovery Act funds, the Deschutes National Forest, Bend-Fort Rock District and the DOE were cooperating agencies on the EA.

The EA was completed and published for public comment on December 21, 2011. The EA was completed in response to a Notice of Intent to Conduct Geothermal Resource Exploration Operations along with a Plan of Exploration, Operations Plan and Drilling Program application submitted to the BLM by Davenport Newberry Holdings, LLC, and AltaRock Energy, Inc., in May, 2010.

Based upon a review of the EA and its supporting documents, BLM determined that the project was not a major federal action that would significantly affect the quality of the human environment nor would any of the environmental effects be significant. As a result, BLM determined an environmental impact statement was not required and issued a Finding of No Significant Impact (FONSI) on April 5, 2012.

The BLM received 11 comment letters following publication of the environmental assessment. After a review of the comments received (BLM prepared a summary of substantive comments and BLM responses to those comments) and based on the EA and the FONSI, BLM approved the application to proceed with the project on April 5, 2012. DOE provided a link on the DOE Golden Field Office Public Reading Room website to the EA located on BLM's website. Based on the information presented in the EA, DOE

determined an environmental impact statement (EIS) was not required and issued their FONSI concurrently on April 5, 2012.

As part of the Decision Record, BLM stated they would monitor the drilling and stimulation procedures via adherence to the Conditions of Approval in Geothermal Sundry Notices (GSN) and Geothermal Drilling Permits (GDP) (for the production wells in Phase 2.2). The GSNs were issued in phases. The first GSN was for the construction of the downhole MSA stations under the jurisdiction of the BLM (NN-17, NN-18, NN-19, NN-21 and NN-24). This was issued on May 9, 2012. The second GSN was issued for the stimulation, after BLM had received written approval from the DOE that a functioning MSA had been installed that met all requirements of the ISMP. This GSN was issued on September 6, 2012.

Forest Service Special Use Permit

Seven of the surface MSA stations and the Strong Motion Sensor (SMS) were located on National Forest system lands that were not on BLM geothermal leases. As a result, the Forest Service has jurisdiction and issued a special use permit (BEN841) permitting these stations. The Special Use Permit was issued on June 18, 2012.

Forest Service Road Use Permit

In order to access the MSA drill sites and stations, USFS roads were used. As a result, Forest Service issued a Road Use Permit on July 3, 2012.

Forest Service Industrial Fire Precaution Level (IFPL) Waivers

Due to forest fires during the dry summer field season, we applied for and the Forest Service issued two waivers to allow conditional field operations. These IFPL waivers were issued on July 27, 2012 (IFPL level II waiver) and August 14, 2012 (IFPL level III waiver). All fire restrictions were lifted on October 16, 2012.

Oregon Department of Environmental Quality (DEQ) Water Quality Permit

The Oregon DEQ issued a Special Letter Permit allowing stimulation and injection of diverters and tracers into well NWG 55-29. This permit was effective October 1, 2012 and later modified to be effective November 25, 2012 to take into account operational delays.

Oregon Department of Geology and Mineral Industries (DOGAMI) Geothermal Well Modification Permit

DOGAMI reviewed the application to conduct EGS activities within geothermal well NWG 55-29 and issued a Permit to Drill Geothermal Well—Modification on October 1, 2012.

2.1.2 PHASE 2.2 PERMITS

The following permits will be needed for the planned 2015 field season (Phase 2.2). The current water use license LL-1441 (and associated mitigation permit) is good until December 2017 for additional stimulations. The Deschutes River Conservancy has been notified for to purchase the necessary groundwater mitigation credits.

BLM Geothermal Drilling Permit (GDP)

As stated in the Decision Record, BLM will require a GDP for the drilling of each of the new production wells to be drilled off of NGW 55-29 well pad.

DOGAMI Geothermal Well Permit

DOGAMI will also require a Geothermal Well Permit for each of the new production wells to be drilled off of the 55-29 well pad.

Oregon Department of Environmental Quality (DEQ) Water Quality Permit

The Oregon DEQ issued a General Geothermal Exploration Permit on April 24, 2013. This permit will cover the planned field activities for 2014 allowing for any injection of water and geothermal fluids. Another Special Letter Permit would be required to allow for stimulation and injection of diverters and tracers.

Oregon Water Resources Department (OWRD)

On January 9th, 2013, the OWRD issued a limited water use license to allow the withdrawal of groundwater for use in the project. As a condition of the license, a 22 million gallon temporary groundwater mitigation credit was purchased to offset the water used for stimulation, which ended up being only 11 million gallons. This credit was purchased by Davenport Newberry Holdings with funds outside the DOE grant.

2.2 PUBLIC OUTREACH

Public outreach and education during Phase 2.1 was accomplished through three primary mechanisms: public outreach meetings, reports and publications, and outreach through online social media. Reporting and publications completed in Phase 2.1 include quarterly and annual project updates to the DOE, publication and presentation of peer-reviewed reports to the geothermal industry, and this Phase 2.1 report.

Data collected and analyzed during Phase 2.1, as well as the overall project technical plan, will be published in various geothermal industry and scientific forums, as appropriate. Papers and presentations have already been made at the annual meetings of the American Geophysical Union, Geothermal Resources Council, and Stanford Geothermal Workshop, and SMU Geothermal Energy Utilization Conference.

Monthly public outreach meetings were held during stimulation and were conducted in Bend, La Pine and Sunriver. Attendance at these meetings was between 20 and 100 people. Booths at the weekend-long Bend Spring and Fall festivals were also staffed to provide public outreach about the Newberry project. The La Pine Chamber of Commerce and local politicians toured the field site at Newberry in mid-August.

Outreach via social media during Phase 2.1 included regular updates to the Newberry EGS blog, Facebook™ and Twitter™ webpages, as well as the AltaRock Energy website. An informational hotline number was also established for public comments and questions and published on all of the webpages. The Newberry EGS blog, Facebook and Twitter pages were updated on a regular basis with updates from the field. Articles published to these web pages during Phase 2.1 include updates on the stimulation, seismicity, environmental monitoring and photos from the field.

2.3 BOREHOLE COMPLETION AND MICROSEISMIC ARRAY INSTALLATION

To complete the planned network of monitoring boreholes around well NWG 55-29, four new wells were completed and one pre-existing well was deepened to accommodate installation of borehole seismometers (Figure 2-1). Drilling was completed by Tacoma Pump & Drilling, based in Graham, Washington. Borehole drilling began in late May, 2012 at site NN-21 and concluded three months later with the completion of borehole NN-24.

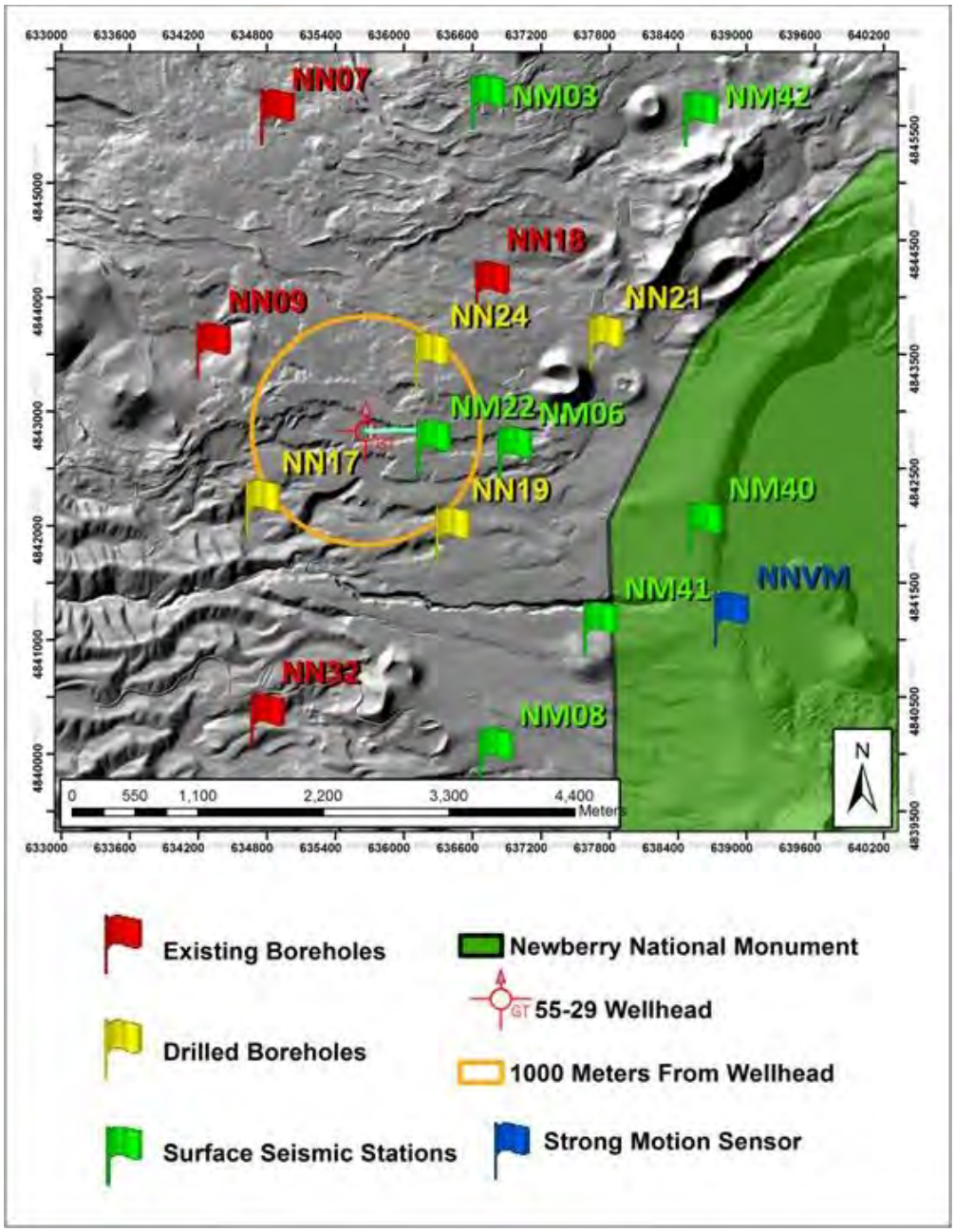

Figure 2-1. Location of existing boreholes, new boreholes, and surface stations.

2.3.1 SCOPE AND OBJECTIVES

The microseismic array (MSA) was designed to monitor and provide accurate location of seismic events occurring 1 to 3 km away from NWG 55-29 (BLM, 2011; Foulger Consulting, 2010). Sites were chosen based on proximity to the injection well and use of three pre-existing boreholes (NN-07, NN-09, and NN-32) drilled by Davenport Newberry Holdings as part of an exploration project (Figure 2-1). Environmental impact from drilling was reduced by ensuring prospective locations were accessible via existing roads. Pre-existing road pull-outs were used at all sites except for NN-17 where small trees had to be cleared and a gravel pad constructed to provide a level area for the drill rig.

To maximize coupling of the geophones to the earth and minimize attenuation, the depth of MSA boreholes were required to be below the water table, in sections of competent rock at least 30 m long and below the highly attenuating cinders and debris flows on the flanks of the Newberry Volcano. Geologic and hydrologic data from previously drilled wells in the area indicated the top of the local aquifer began at +/-200 m below ground surface (650 ft bgs), and competent rock was noted below the water table. Target depths for each borehole were based on local geologic, hydrologic and drilling conditions in the field, and the initial target depth of 213-307 m (700-1,000 ft).

All five MSA boreholes were designed to accommodate 12.7 cm (5 in) borehole seismometers. In addition, wells NN-17 and NN-18 were completed with perforated sections to allow groundwater to fill the wellbore so that a pressure transducer could monitor water level, and a bladder pump could sample groundwater.

2.3.2 DRILLING METHODS

Tacoma Pump & Drilling completed all five MSA boreholes using a Foremost DR-24 air hammer drill rig. AltaRock technical staff (Drill Site Geologist and/or Project Manager) was on-site during all drilling days to monitor progress and ensure compliance with permitting conditions. All drilling-related equipment was pressure washed prior to mobilization to mitigate introducing noxious weeds to the project site. The requirements of the BLM Sundry Notice were reviewed with Tacoma Pump and Drilling personnel prior to activities on site.

With the exception of site NN-18, drill cuttings were collected in a trailer and hauled off site for disposal after drilling. NN-18 was deepened 12.8 m (42 ft) to accommodate seismometer installation in competent rock; cuttings and fluid (water) were dispersed on the drill pad after USFS verbal approval. Excess water from the other borehole sites was either hauled to La Pine Redi Mix for disposal (NN-21, NN-19), spread on roads for dust abatement (NN-19, NN-17, NN-24) or passed through a sprinkler system and spread over the forest floor surrounding the drill pad (NN-17; NN-24).

2.3.2.1 DRILLING AND CASING

The initial 6 m (20 ft) of each borehole was drilled with a 30 cm (12 in) air hammer bit and casing (Figure 2-2). After surface casing was installed, the bit was changed to a 20 cm (8 in) under reaming hammer bit with wings that extended to drill a 21 cm (8.25 in) hole and allowed 20 cm (8 in) diameter casing to be advanced behind the bit using the rig's bottom drive. The casing while drilling program was adopted to counter hole collapse problems experienced by Davenport Newberry's project while drilling similar holes (NN-09, NN-07, NN-32, and 4 others). Upon reaching the water table and stable bottom hole formations the open-hole drilling began. Once final depth was reached, 12.7 cm (5 in) casing was installed to total depth in the hole. Cementing was carried out by pumping cement through the 12.7 cm (5 in) casing to fill the annulus between the 20 cm (8 in) and 12.7 cm (5 in) casings from below. Because the cement did not reach the surface, the cement job was completed by pumping down the annulus from above (top job) (Figure 2-3). After curing, cement remaining in the 12.7 cm (5 in) casing was drilled out, completing the well to final depth. Inclination and standing water level were monitored at each borehole as drilling progressed. A dummy seismometer, an 11.5 cm x 92.7 cm (4.5 in x 36.5 in) steel pipe filled with cement, was run to total depth in each borehole after completion to ensure clearance for seismometer installation.

Figure 2-2. Left: advancement of casing while drilling; Center: under reaming air hammer bit with wings extended; Right: tricone drill bit used for wet borehole intervals.

Figure 2-3. Setup for pumping cement at NN-19.

Wells NN-17 and NN-18 were perforated upon completion and installed with water sampling equipment (Table 2-1). Well NN-18 was previously drilled by California Energy, Inc., with a screened interval between 211.2-235.6 m (693-773 ft bgs) which was preserved during drilling activities. Water was air-lifted to test production both before and after drilling activities at NN-18, and no significant impact on water production was detected.

Table 2-1. Summary of MSA borehole drilling and completion details.

Well ID	Completion date	Days (on hole/working)	Final depth (ft bgs)	Competent rock (ft from bottom of hole)	Inclination (° from horizontal)	8 in casing (ft bgs)	5 in casing (ft bgs)	Perforation interval (ft bgs)	Initial depth to water (ft bgs)	Static water level (ft bgs)	Water production minimum/maximum (gpm)
NN-17	4-Aug	19/10	715	43	89.5	680	723	480-580	420	350	20/500+
NN-18	16-Jul	6/2	815	20	89	793*		693-773		556.1	40/60
NN-19	10-Jul	32/18	792	93	89.5	707	800	n/a	484	373	30/500
NN-21	7-Jun	20/10	693	95	89.6	603	698	n/a	603	495	15/30
NN-24	22-Aug	17/8	694	34	89	660	694	n/a	630		50

* NN-18 (*aka* CE Water Well #2) was completed with 7 in casing in 1995

2.3.2.2 SAMPLE COLLECTION AND LOGGING

Rock samples were collected at 3 m (10 ft) intervals for all boreholes except NN-18, which was sampled at 1.5 m (5 ft) intervals. Samples were dried, described in the field, and bagged for archiving. Field interpretations were used in compiling the lithologic columns shown in below in Figure 2-6 to Figure 2-10 and the well descriptions below. Zones of cinder and scoria encountered during drilling caused occasional partial or complete loss of drilling fluid circulation at four of the five borehole sites (Figure 2-4). Field notes reflect where loss of circulation occurred and sample collection was not possible due to lack of returns.

Figure 2-4. Example of the heterogeneity of volcanic rock types encountered while drilling.

2.3.3 DRILLING RESULTS

MSA drilling began on May 23, 2012 with borehole NN-21 and was finished on August 22, 2012 with the completion of well NN-24 (Table 2-1). After completion of drilling, Tacoma Pump and Drilling was released from the project site on August 23. Newly drilled boreholes took an average of 11.5 days to complete. Final depths for all five sites ranged between 211 and 248 m bgs (693 – 815 ft). Where water was produced

during drilling, production varied from 1.8 - 31.5 L/s (30 - 500 gpm) (Table 2-1). Borehole NN-17 was so productive that drilling was impeded and the borehole was completed 15 m (50 ft) above the target depth. Figure 2-5 summarizes the drilling rates to complete the initial hole, not including cementing and re-drilling to final depth. The sections below summarize the geology encountered at each borehole and details well completion specifics at each location.

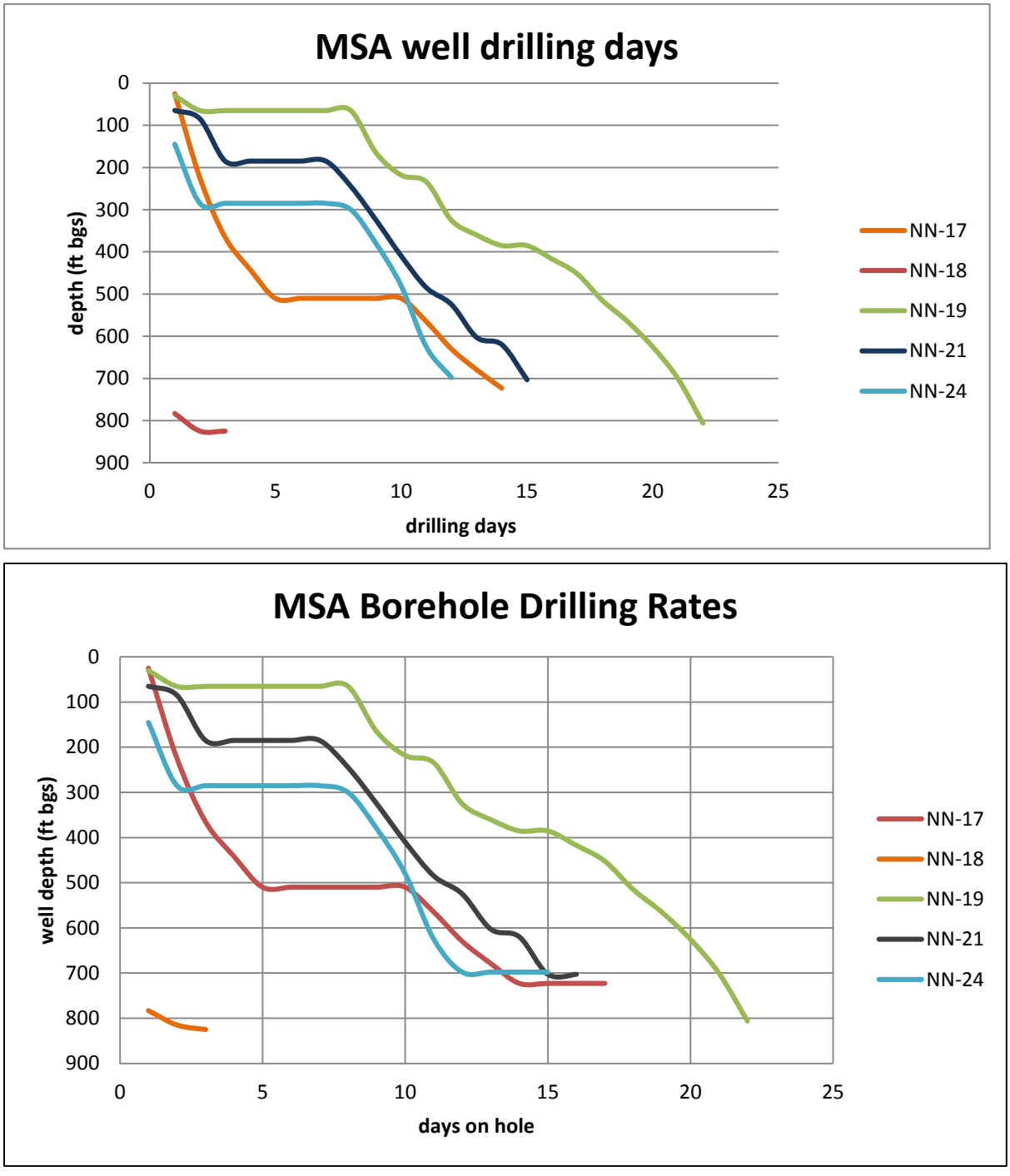

Figure 2-5. Comparison of MSA borehole drilling rates.

2.3.3.1 WELL NN-21

This borehole was located on the reclaimed CalEnergy 88-21 pad which had been constructed in 1995, and been the site of a 1,486.2 m (4,876 ft) deep temperature core hole (TCH 88-21) and a planned deep exploration hole (88-21). A 33.5 m (110 ft) deep, 76 cm (30 in) diameter conductor pipe had been installed but 88-21 was not drilled, when CalEnergy abandoned Newberry exploration in 1996. To ease permitting and the first 33.5 m (110 ft) of drilling, NN-21 was drilled through the 88-21 conductor.

Lithology at this site is characterized by interbedded scoria and cinder zones with basaltic to andesitic flows and occasional lithified ash layers (Figure 2-6). Possible rhyodacite flows were encountered at depths greater than 183 m (600 ft); interpretations of the lithology for these flows are confirmed by the mud logs from well TCH 88-21 made available to AltaRock. Flow units range in thickness from less than 3 m (10 ft) to 40 m (130 ft), while interbedded scoria and cinder zones were typically 1.5 - 15 m (5 - 50 ft) thick. Water production of 0.94 - 1.89 L/s (15 - 30 gpm) began at 184 m (603 ft), and the standing water level was measured at 151 m (495 ft) after well completion.

Wellbore NN-21 is cased with 33.5 m (110 ft) of 76 cm (30 in) steel conductor pipe with 184 m (603 ft) of 20.3 cm (8 in) steel well casing inside and below it. The annular space between the 76 cm (30 in) conductor pipe and 20.3 cm (8 in) casing is filled with pea gravel and a 2 m (6.5 ft) thick cement cap. Internal to the 8 inch casing 213 m (698 ft) of 132.7 cm (5 in) steel well casing was installed and cemented in place. Two cement jobs were required to complete the well; 3 m^3 (4 yds^3) were pumped through the 13 cm (5 in) casing to the bottom of the well, and 5.4m^3 (7 yds^3) were pumped into the annulus between the 12.7 cm (5 in) and 20.3 cm (8 in) casing from the top. Cement reached 2.4 m (8 ft) bgs and was drilled out from the 12.7 cm (5 in) casing to a final depth of 211 m (693 ft), completing the well. A 3 m (10 ft) cement plug was left below the 12.7 cm (5 in) casing. Drilling reached a total depth of 214 m (703 ft) bgs at NN-21; final well depth was adjusted based on casing advancement and cement drilling. Inclination was measured at 89.6° after well completion, and the dummy seismometer cleared to total depth with no concerns. Completion of borehole NN-21 required 20 days on-site, including four days of delay due to snow accumulation greater than 30 cm (1 ft).

2.3.3.2 WELL NN-19

Challenges specific to this borehole included accumulation of snow, two broken drill bits, and a broken air hose on the drill rig. Drill bit maintenance was performed more frequently after completion of this hole to prevent further delays due to breakdown. Dense basalt layers made drilling difficult at this site, as did backpressure from high water production which slowed the drilling rate significantly at depths over 152.4 m (500 ft) bgs. Tacoma Pump and Drill staff delivered a stronger drill hammer to the site after several days of slow drilling which increased drilling speed slightly.

Wellbore NN-19 is characterized by dense basalt and basaltic andesite flows and rubble with interbedded cinders, scoria and pumice in some sections (Figure 2-7). Basalt and basaltic andesite flow layers typically ranged from 3.6-18.3 m (12-60 ft) thick. Cinder and scoria layers typically ranged from 3 to 4 m (10 to 20 ft) thick. Water production began with 1.9-2.5 L/s (30-40 gpm) at 147 m (484 ft). This depth marks the beginning of a deposit of well-rounded, mixed composition material ranging from mafic to silicic volcanics leading to general loss of circulation in the well. Water production increased dramatically at 152.4 m (500 ft) to approximately 9.5 L/s (150 gpm) in mixed basalt and cinders, and continued to increase to a maximum of 31.5 L/s (500 gpm) encountered at 190 m (625 ft) in a unit of mixed cinders and pumice overlying basalt. Basaltic flow units were re-encountered at 201 and 207 m (660 and 680 ft); only a few thinly interbedded cinder and lithified ash layers persisted within these flows to total depth at 245.6 m (806 ft).

The well was completed with 20.3 cm (8 in) steel casing installed to 215 m (707 ft) and 12.7 cm (5 in) casing to 243.8 m (800 ft). Seven yards of cement were pumped down-hole through the 12.7 cm (5 in) casing, reaching to 109 m (360 ft) bgs in the annulus. Two more cubic yards of cement were pumped down the annulus from above after drilling cement out of the 12.7 cm (5 in) casing to the well completion depth of 241.4 m (792 ft). Inclination was measured at 89.5°, and the dummy seismometer cleared to total depth with no concerns. Completion of NN-19 required 32 days on-site, including 18 drilling days and 12 days off.

2.3.3.3 WELL NN-18

Site NN-18 required minor brush removal and surface improvements before drilling activities began. Borehole NN-18 was previously drilled to a depth of 245 m (805 ft) by California Energy, Inc., in 1995; Figure 2-8 includes the findings of the original drilling report. Originally completed at 245 m (805 ft), formation collapse had filled the well to 238m (783 ft). New drilling with a 7 inch bit at this site deepened the well 12.8 m (42 ft) to a new total depth of 251 m (825 ft) to accommodate a borehole seismometer. Completion of NN-18 required 6 days on site including two drilling days and 1 day off. Use of a dump bailer was originally planned for cementing, but the bailer caught in the well during a trial run. Once the bailer was removed a tremmie pipe was run down hole and 63 gallons of cement were pumped down the pipe to create a 7 in diameter cement plug at the well bottom. The plug was then drilled out using a 5 inch bit to a completion depth of 248 m (815 ft), leaving a 3 m (10 ft) cement plug at the bottom of the well for the 5 in hole lock and geophone to fit into. Cement drilling returned approximately 10 % rock cuttings to the surface. Water was air-lifted from the well to test production before and after drilling. Production measured 3.2-3.8 L/s (50-60 gpm) both before and after drilling. Production at this well was higher at the time of initial construction in 1995, and the screened interval from 211 to 235 m (693 to 773 ft) may be clogged with cinders and/or scoria. Inclination was measured at 89.0° after well completion, and the dummy seismometer cleared to 248 m (815 ft) with no concerns. The 12.8 m (42 ft) of length drilled at this well are characterized by an upper cinder zone and a lower basalt flow zone. Cinders were encountered from 238 - 245m (783 - 805 ft), and overlie a fine-grained non-vesicular basalt flow that extends from 245 m (805 ft) to total depth at 251 m (825 ft).

2.3.3.4 WELL NN-17

Forest Service road FS-500 was improved to provide drill rig access to site NN-17, where a 100 x 50 ft pad was cleared and leveled for drilling equipment. Basin and Range Heritage Consultants completed an archaeological survey (See Appendix A) prior to surface disturbing activities at site NN-17. The survey included visual inspection, sieving of surface material, trenching and trench wall inspection for evidence of site use by Native Americans. No evidence of past human use at was found at the site. Borehole NN-17 accommodates a borehole seismometer, a pressure transducer for continuous depth monitoring and a bladder pump system for water sampling. Drilling began on July 17, 2012, and completion required 19 days on site including 10 drilling days and 5 days off. Highly productive fractured basalt posed a significant challenge to drilling at this site; backpressure from water production greater than 31.5 L/s (500 gpm) significantly reduced drilling speed past 195 m (640 ft) bgs.

This well is characterized by a thick cinder deposits and high volume water production (>31. 5 L/s or 500 gpm) in fractured basalt layers (Figure 2-9). The initial 40 ft of borehole penetrated dense basalt overlying cinders to a depth of 100 m (330 ft). Weathered basalt deposits overlie cinders to 134.7 m (442 ft) bgs. Mixed basalt and cinders, grading toward basalt with depth, overlie a basalt flow unit extending 168-177 m (550-580 ft). A thick deposit of mixed basalt, cinders and pumice extends from 177-207 m (580-680 ft) and overlies the final unit in the well, a dense, fractured basalt flow from 207 m to 220 m (680 ft to 723 ft).

Drilling was halted at 220 m (723 ft) bgs as water production began increasing, fracture frequency within the basalt unit increased and backpressure forced the drill bit off the bottom of the well.

Well NN-17 was completed with 207 m (680 ft) of 20 cm (8 in) steel casing and 220 m (723 ft) of 12.7 cm (5 in) casing, each slotted to accommodate water flow for sampling along the interval from 146-176.8 m (480-580 ft). Slots were made using an air-driven tool in both the 20 cm (8 in) and 12.7 cm (5 in) well casing. Slots in the 20 cm (8 in) casing measure approximately 3.8 cm x 1.27 cm (1.5 in x 0.5 in); 12.7 cm (5 in) casing was slotted with 2.5 cm x 1 cm (1 in x ⅜ in) slots rotated 90° after each 6 m (20 ft) progression. A gravel pack was installed between the 12.7 cm (5 in) and 20 cm (8 in) casing from 106-202 m (350 - 633 ft), with a bentonite seal above it from 103 - 106 m (340 - 350 ft).

Cement reached only 27.4 m (90 ft) from the bottom of the hole after pumping through the 12.7 cm (5 in) casing into the annulus. Cement in the 12.7 cm (5 in) casing was drilled out to a final well depth of 218 m (715 ft). Inclination was measured at 89.5° after completion, and the dummy seismometer cleared to total depth with no concerns. Standing water was at 106 m (350 ft) at the time of completion.

2.3.3.5 WELL NN-24

The final MSA borehole, site NN-24 was completed on August 22 after 17 days on site including 8 drilling days and 5 days off (Figure 2-5). A thick (>30 m, >100 ft) dense layer of basalt lead to excessive wear on the drill bit in this borehole, causing the bit to break and detach from the drill string on the second drilling day at a depth of 86.8 m (285 ft). Tacoma Pump and Drill assembled a fishing tool in their shop during several days off-site. The broken bit was successfully removed upon their return.

The lithology at this site is characterized by several debris flows composed of mixed volcanics including basalt, cinders, pumice and obsidian (Figure 2-10). Debris flows range from 3 - 15 m (10 - 50 ft) thick and are typically basalt-dominated, although pumice-dominated layers are also present. Most debris flow deposits are composed of angular to sub-angular basalt (25 - 75%), cinders (15 - 45%), and pumice (10 - 20%). One exception was a pumice-dominated debris flow composed of subrounded pumice (60 - 70%), basalt (15 - 35%) and cinders (5 - 10%) comprises the stratigraphic section of this well from approximately 164 - 177 m (540 - 580 ft) bgs. Interbedded basalt and cinder layers range in thickness from 9 - 30 m (30 - 100 ft) thick and separate debris flow deposits in the wellbore. Layered flows of basalt to basaltic andesite complete the bottom segment of the well from 192 m (630 ft) to the final depth of 212.75 m (698 ft) bgs. Water production at NN-24 began at 188 m (620 ft), but was much lower than previously drilled holes, never reaching over 3.2 L/s (50 gpm).

The total depth drilled at this site was 212.7 m (698 ft) bgs, and the well was completed with 201 m (660 ft) of 20 cm (8 in) casing; 12.7 cm (5 in) casing was subsequently installed to the bottom of the well. Six cubic yards of cement were pumped down the 5 in casing and up into the annulus, reaching 19.8 m (65 ft) bgs in the annulus and 91.4 m (300 ft) from the bottom inside the casing. Excess cement was drilled out of the 12.7 cm (5 in) casing to the well completion depth of 211.5 m (694 ft) bgs, leaving a 2.4 m (8 ft) cement plug at the bottom of the wellbore. Inclination of the wellbore after completion was 89.0°, and the dummy seismometer cleared the total bore borehole length.

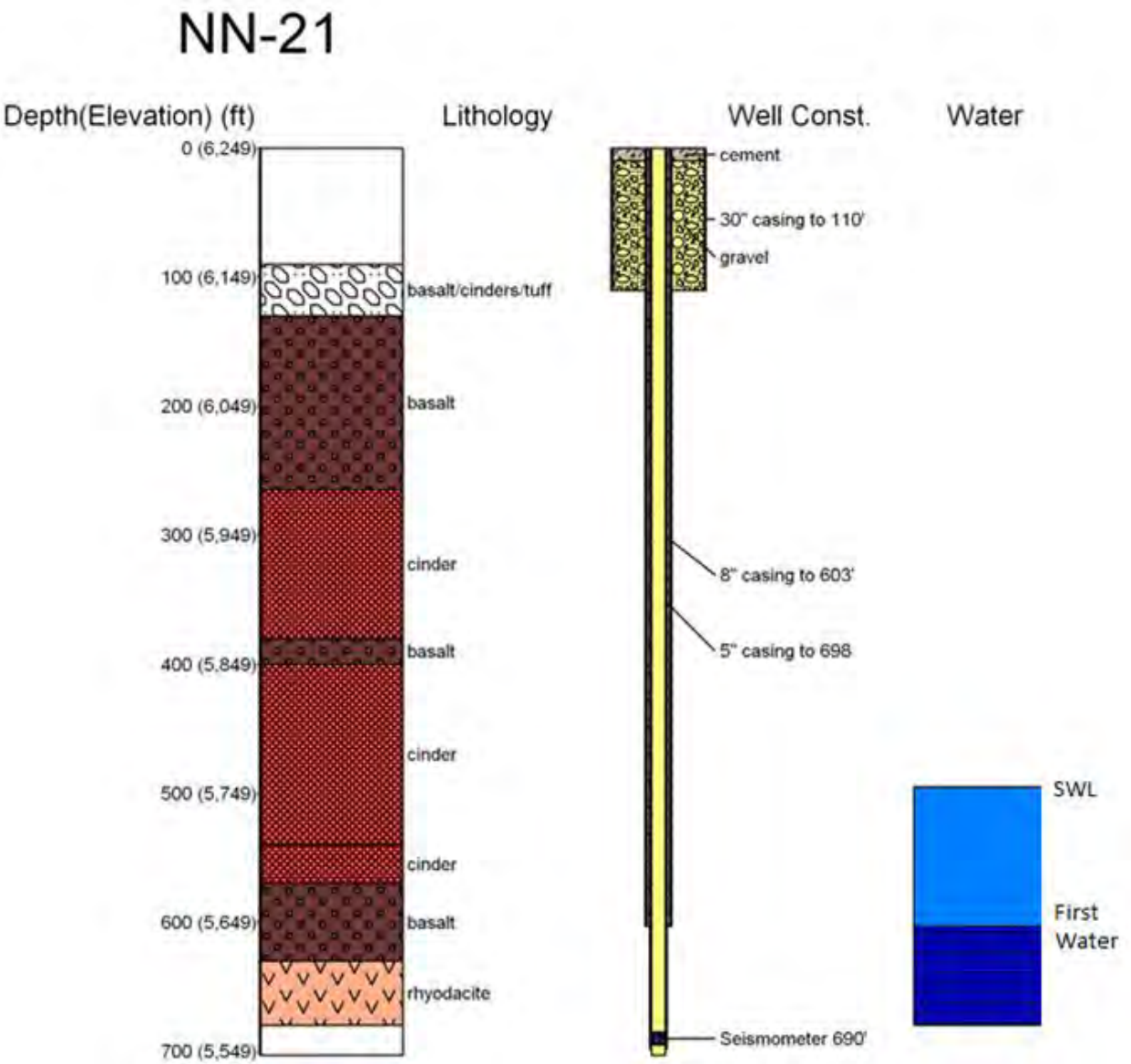

Figure 2-6. Lithology and borehole schematic for borehole NN-21.

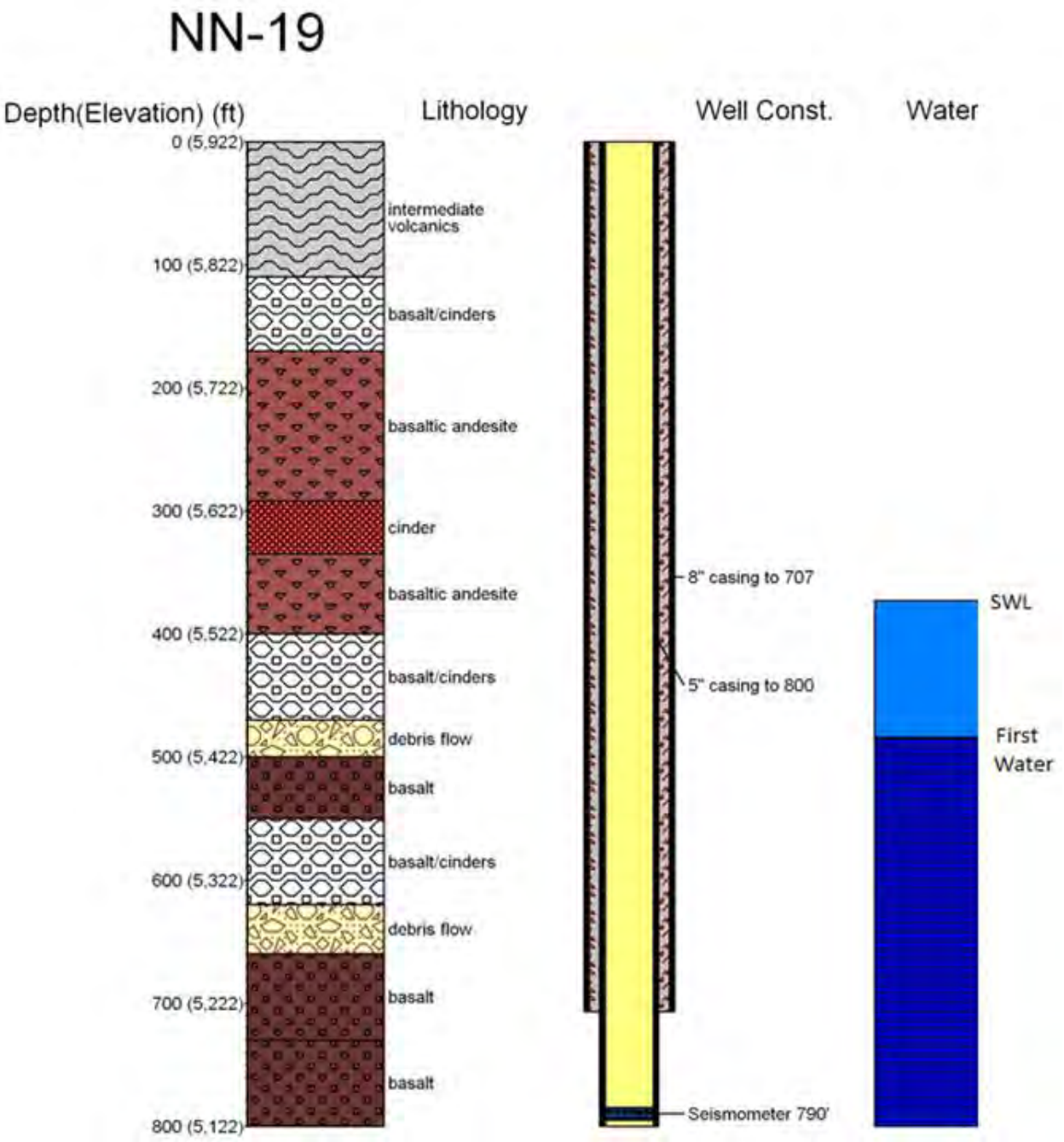

Figure 2-7. Lithology and borehole schematic for borehole NN-19.

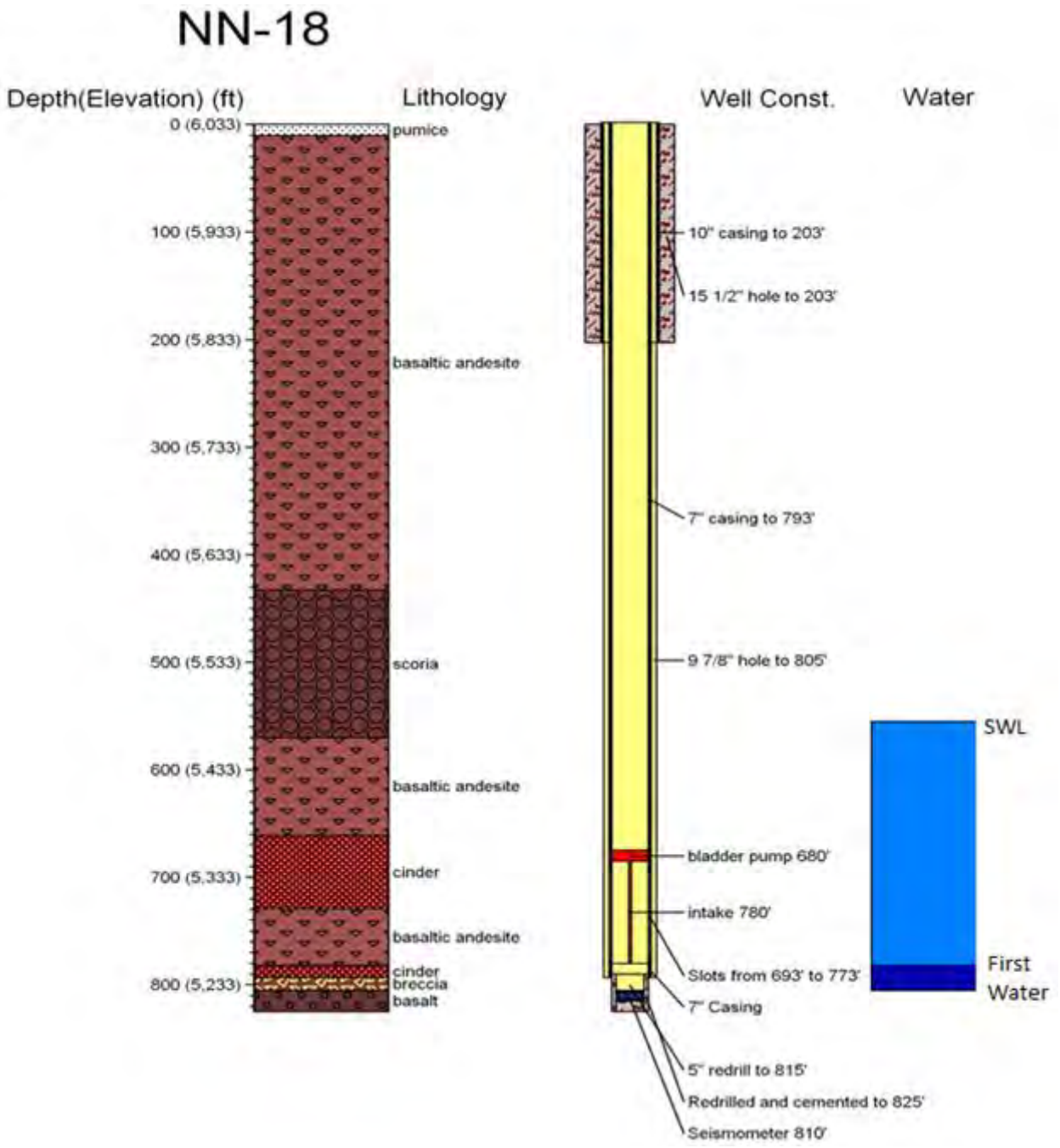

Figure 2-8. Lithology and borehole schematic for borehole NN-18.

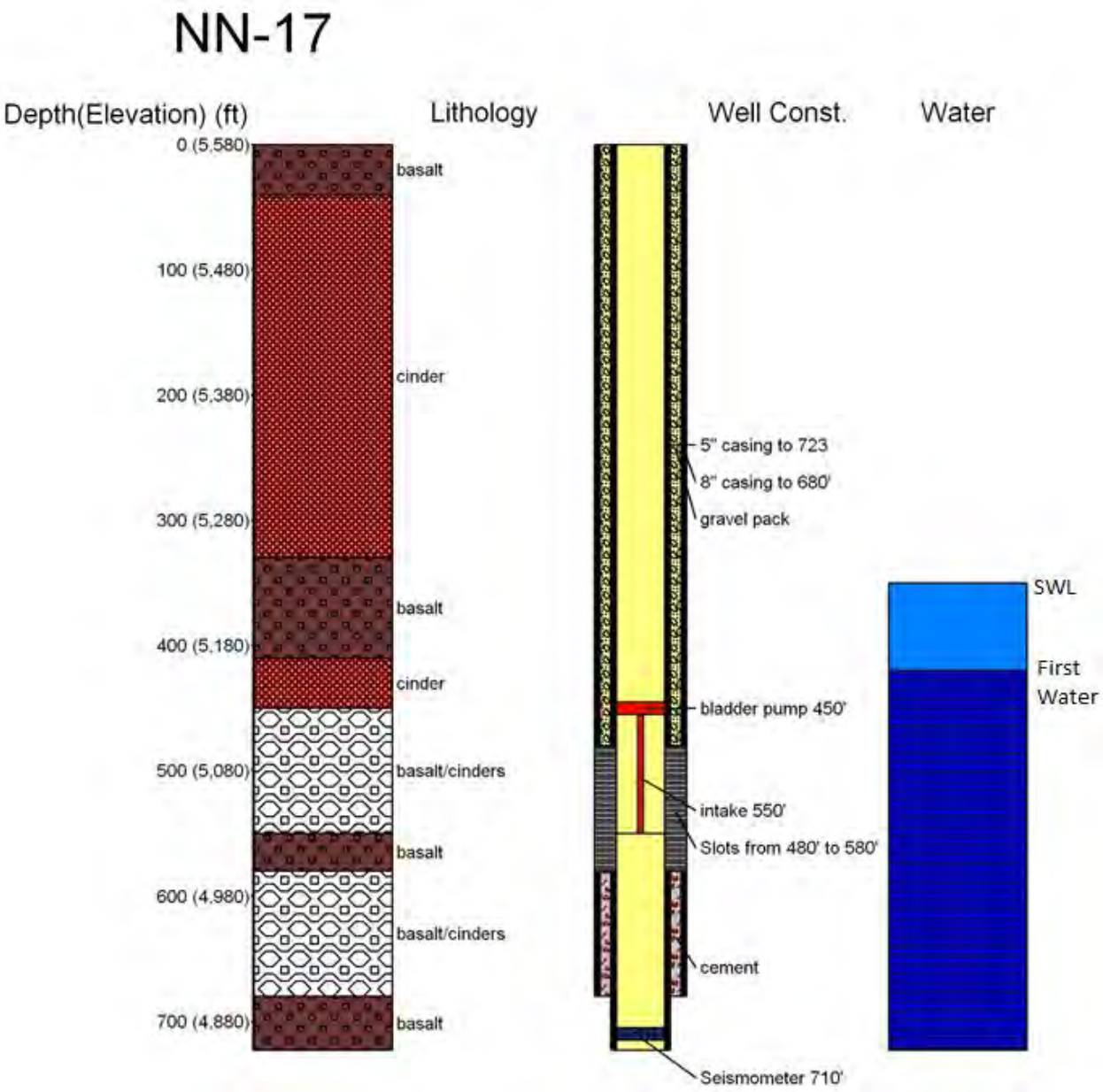

Figure 2-9. Lithology and borehole schematic for borehole NN-17.

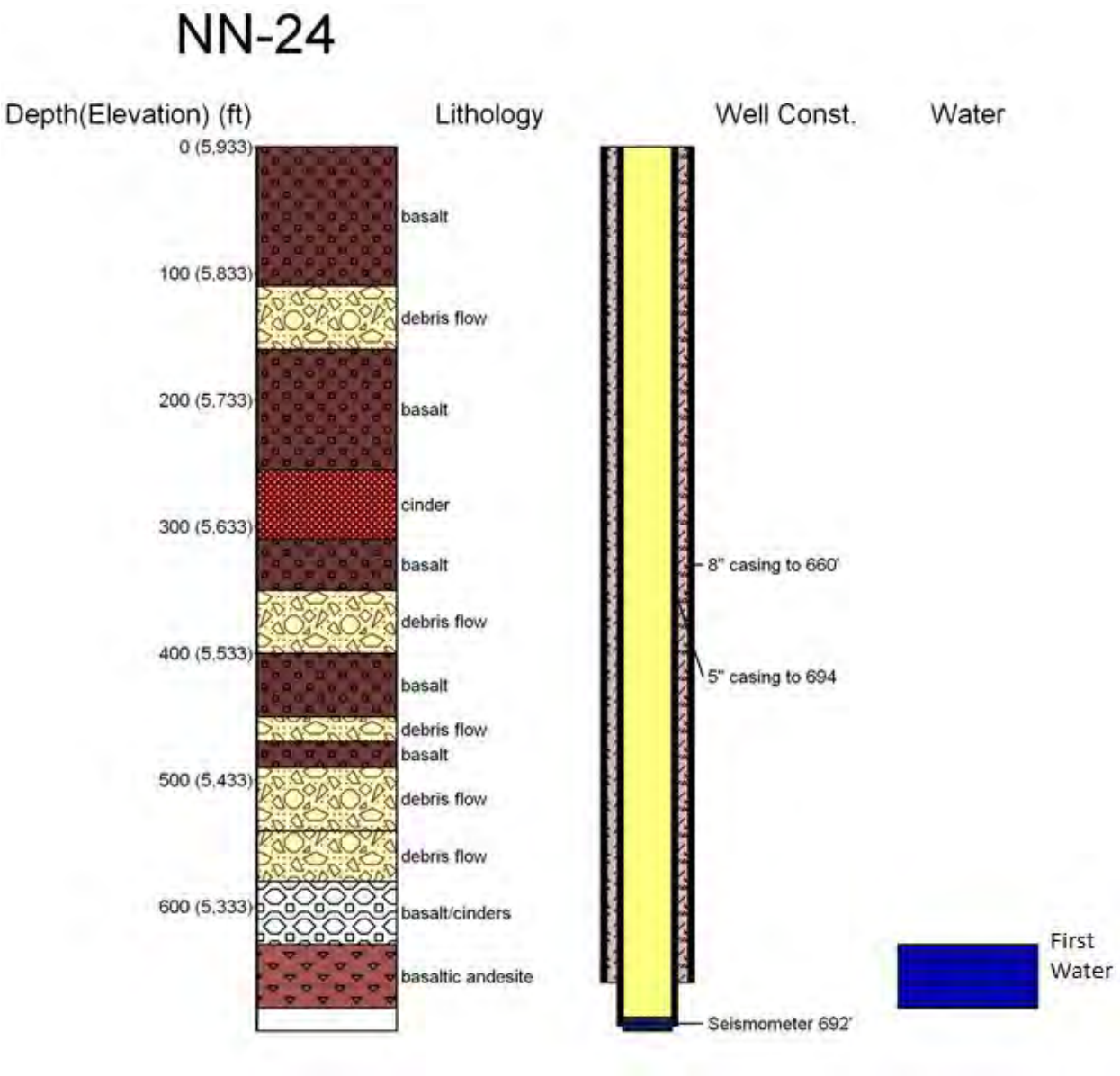

Figure 2-10. Lithology and borehole schematic for borehole NN-24.

2.4 SEISMOMETER NETWORK INSTALLATION

After the FONSI was issued in early April 2012, seismic equipment was ordered. Geotech Instruments had been selected to provide and install oriented hole-locks for the boreholes geophones. AltaRock had procured Geotech Instruments digitizers, DR-24s, for another DOE-supported project, so Geotech was also selected to reconfigure and install the surface equipment at Newberry. The Institute of Earth Science and Engineering (IESE) had been selected to provide the 3-component geophones, both for surface and borehole stations. For the S21g-2.0 Sonde, IESE installed three Oyo-Geospace HS-1 two-hertz geophones into stainless steel cylinders. The borehole geophones are gimbaled, so that they can be installed in a borehole with a deviation from vertical of up to 10 degrees. The sondes and hole-locks had 8 - 12 week lead times, so their manufacture was a critical path item.

Installation of the microseismic array began August 6 after the Geotech Instruments hole locks and IESE geophones had been fabricated and shipped to La Pine. Geophones were installed at the seven surface sites and eight borehole sites shown in Figure 2-1 and listed in Table 2-1. The easier-to-install surface stations were installed first. An auger was used to create a 60-90 cm (2-3 ft) deep 15.2 cm (6 in) hole. At all locations, this was the thickness of the Mazama Ash, which was underlain by basaltic bombs, making it impossible to auger any deeper. A 12.7 cm (5 in) PVC pipe was then placed in each hole and the surface (posthole) sonde with its data cable placed inside the pipe and oriented using a compass. The sand removed from the hole was packed back into hole, on the outside and inside of the PVC pipe, to couple the instrument to the earth.

Borehole geophone installation proceeded in three steps (Figure 2-11). First, the hole-lock was lowered down the hole on a wireline while mounted to a 24 V down-hole impact wrench powered from the surface by an electrical cable. Once lowered to the installation depth, the wrench was activated, which rotated the threaded bottom of the lock relative to the top and pushed out carbide steel teeth that latched the hole-lock to the steel casing. The installation tool was removed, leaving the hole-lock in place. Next, a gyroscope connected to a laptop computer was first oriented (to North) at the surface and then lowered to the installed holelock where it was oriented by a bishop's hat and groove on the hole-lock. The gyroscope's downhole orientation was determined at least twice and then pulled back to the surface, where its orientation was re-checked. Geotech Instrument's hole-lock orientation software, allowed the hole-lock's orientation to be determined. The down-hole lock orientation (in degrees clockwise from north) was then used to orient the key on the geophone's hole-lock adapter. Finally, the geophone was lowered down hole on a Kevlar-reinforced, six conductor data cable.

Figure 2-11. Geophone hole-lock installation equipment. Top left: installation tool (a down-hole impact wrench) with hole-lock mounted. Top right: Hole-lock, stabilizer and geophone adapter. Bottom left: Gyroscope for orienting hole-lock. Bottom right: Geophone on data cable (green) ready to install.

The surface recording and telemetry equipment was installed inside a 91 x 91 x 46 cm (36 x 36 x 18 in) Hoffman instrument box situated within approximately 5 m (16 ft) of the installed sonde. Each box contained two 100 Amp-hour deep cycle gel batteries, a Geotech Instruments DR-24 digitizer, solar panel charge controllers, and a cell phone modem. In a tree adjacent to each box, two 90 W solar panels, a GPS antenna for precision time, and a cell phone antennae were installed. Each cell phone modem was given a static IP address which allowed remote communications to any digitizer.

The 15 MSA stations continuously stream data to be saved and archived on a server running acquisition software at the office of AltaRock Energy in Seattle, Washington. Triggered waveforms are sent to Lawrence Berkeley National Lab (LBNL) to locate the seismic events which were published on their public website (LBNL, 2013). Microseismic events were also analyzed by Foulger Consulting (Foulger and Julian, 2013a), and the Pacific Northwest Seismic Network (PNSN, 2013). Three of the borehole sites (NN-21, NN-17, and NN-19) also stream continuous data directly to the PNSN. This provides partial backup acquisition and a real-time, public website for those seismograms (e.g. http://www.pnsn.org/seismograms/NN17).

Table 2-2. MSA station locations and elevations.

Station Name	Station Type	Longitude (WGS84)	Latitude (WGS84)	Surface Elevation (ft bgs)	Hole Lock Depth (ft bgs)	Seismometer Elevation (ft ASL)	Seismometer Elevation (m ASL)
NM-22	S	-121.308	43.725	5918	4	5911	1.802
NM-06	S	-121.300	43.724	5971	4	5979	1.823
NM-42	S	-121.279	43.750	6616	4	6611	2.016
NM-41	S	-121.291	43.710	6144	4	6158	1.877
NM-08	S	-121.302	43.700	6030	4	6031	1.839
NM-40	S	-121.279	43.718	6461	4	6457	1.969
NM-03	S	-121.302	43.752	6123	4	6119	1.866
NN-07	B	-121.325	43.751	5543	830	4703	1.434
NN-19	B	-121.306	43.718	5914	790	5102	1.555
NN-18	B	-121.302	43.737	6032	810	5223	1.592
NN-21	B	-121.289	43.733	6262	690	5559	1.695
NN-17	B	-121.327	43.720	5576	710	4870	1.485
NN-09	B	-121.332	43.733	5492	859	4625	1.410
NN-32	B	-121.327	43.703	5545	948	4597	1.401
NN-24	B	-121.308	43.732	5946	692	5241	1.598

B – borehole seismometer station
S – surface seismometer station

2.5 WELLHEAD INSTALLATION

Well NWG 55-29 was drilled by Davenport Geothermal in 2008. At the time, the Newberry geothermal development work focused on accessing a potential hydrothermal resource that would have wellhead and wellbore pressure not exceeding 10.3 MPa (1,500 psi). The drilling of this exploratory production well confirmed the presence of heat at depth but found little permeability and no hydrothermal circulation. The Newberry EGS Project and wellbore stimulation activities required significantly higher working pressures than the existing wellhead valve was rated for requiring a new wellhead.

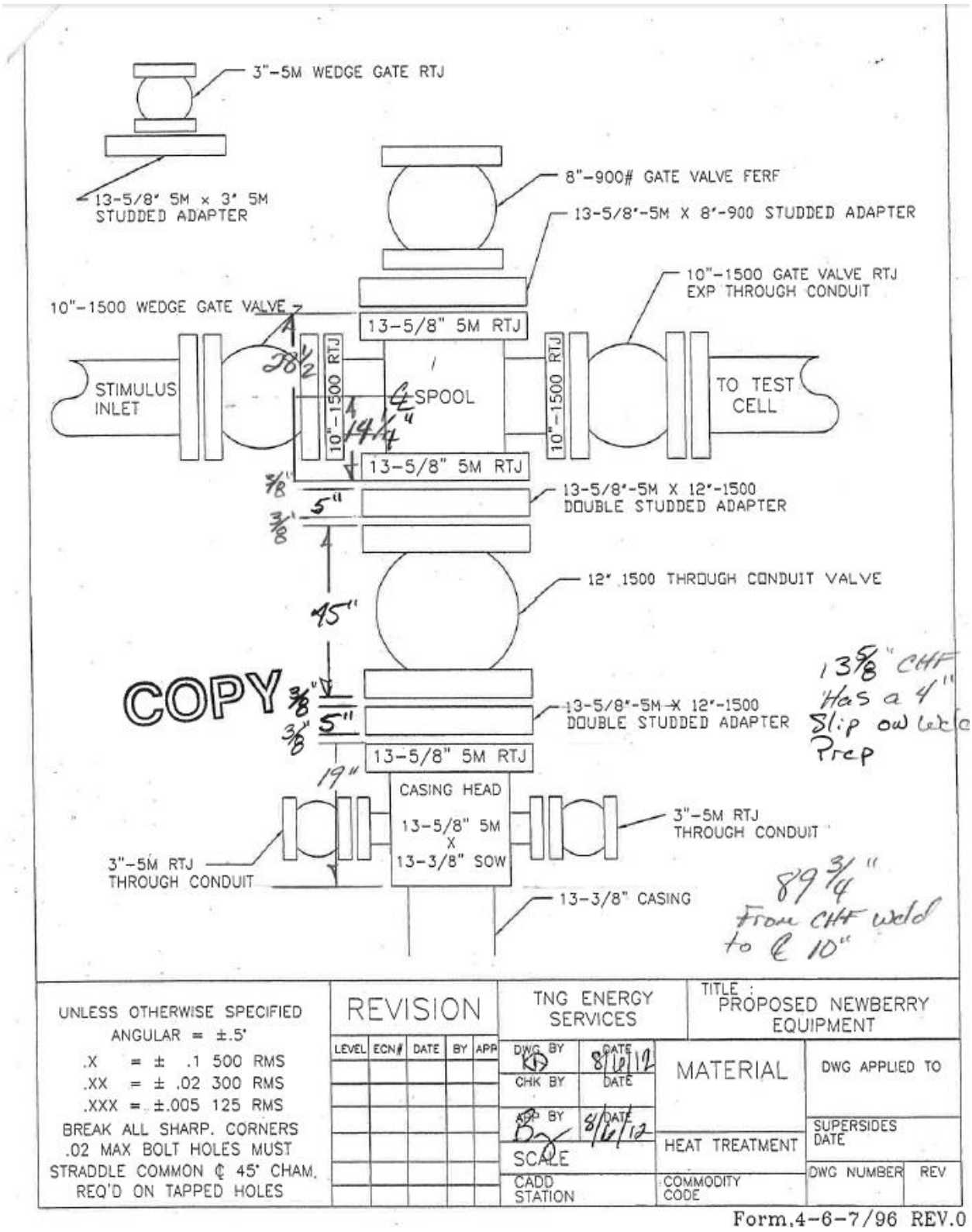

Figure 2-12. Wellhead valve assembly for 55-29 stimulation.

Figure 2-12 is a schematic of the modified wellhead that was installed. The existing wellhead cellar was first demolished and removed (Figure 2-13). The modification required the cutting and removal of the

existing wellhead-to-valve casing flange. Once the new wellhead adapter was installed, welded up and heat treated, the new well valve was installed (Figure 2-14). The well was capable of generating non-condensable gases (NCGs) which pressurized the wellbore to 4.1 MPa (600 psi). As such, it was necessary to use a mechanical packer/isolation device to isolate the gas producing section of the well bore from the surface casing and valve adapter work. It was also necessary to make accommodation for fugitive gas emissions by excavating around the well to prevent a confined space situation while work on the wellhead was taking place. Upon completion of the wellhead work by TNG, the wellhead cellar was rebuilt by AltaRock personnel. This work included form fitting and placing a new 3 m (10 ft) diameter culvert to act as the new cellar and then backfilling and compacting fill material grade. This effort was required to support the installation and operation of the new wellhead connected piping and valve support equipment.

Figure 2-13. Excavation of NWG 55-29 cellar in preparation for the modification of the wellhead for new 30.48 cm (12 in) Series 1500 valve. The valve pictured is the original Series 900 valve installed by Davenport Newberry after well drilling.

Figure 2-14. The new wellhead adapter being installed on existing 34 cm (13 ⅜ in) casing; the mottled surface of the adapter was due to in-place weld heat-treatment. TNG personnel are installing the 30.5 cm (12 in) double studded adapter prior to the installation of the new 30.5 cm (12 in) Series 1500 Wellhead valve.

2.6 HIGH PRESSURE STIMULATION PUMPS AND FLOW-LINES

From analysis of the September and October 2010 injection tests and stimulation modeling (Cladouhos et al., 2011b) it was estimated that stimulation pumps capable of injecting 0.63-50 L/s (10-800 gpm) at pressures ranging from 5.2-20.7 MPa (750-3000 psi) would be required to initiate hydroshearing in NWG 55-29 (Phase I report, Section 7; AltaRock, 2011a). During the bidding process, pump rental and service companies were both considered. Because of the wide injection rate and pressure range anticipated at Newberry, most service company/rental bids included two types of pumping systems: high pressure/low volume and high pressure/high volume. After reviewing options on renting third party pumps to perform the stimulation treatment (Table 2-3), a decision was made to lease centrifugal horizontal pumps from Centrilift Water Systems a division of Baker Hughes, Inc. (BHI).

Table 2-3. A projected cost comparison of pump rental vs. service company hydraulic fracturing truck options based on a 21 day stimulation schedule.

Column1	Baker Hughes	Halliburton	Power Zone Option 1	Power Zone Option 2	Schlumberger	Purchasing Baker Hughs Hpump
Matrix pump unit mob/demob	$ 27,530.00	$ 20,625.50	$ 21,000.00	$ 27,000.00	$ 4,374.00	$ 19,300.00
Matrix pump cost	$ 342,696.00	$ 15,432.50	$ 420,000.00	$ 590,000.00	$ 165,726.00	$ 598,362.97
Frac truck mob/debmob	-	$ 83,230.00	-	-	$ 109,944.00	
Frac truck/Fuel pumping cost	-	$ 945,479.64	$ 52,920.00	$ 52,920.00	$ 3,662,640.00	$ 420,000.00
Batch Mixer cost	$ 67,585.50	$ 111,148.00	$ 67,585.50	$ 67,585.50	-	67585.5
Manifolding	$ 78.20	-	$ 288,000.00	$ 53,000.00	$ 34,560.00	
Crew	$ 214,940.25	-	$ 168,000.00	$ 168,000.00	$ 124,830.00	
Misc.	$ 315,964.80	$ 11,889.00				$ 92,000.00
Total	**$ 968,794.75**	**$ 1,187,804.64**	**$ 1,017,505.50**	**$ 958,505.50**	**$ 4,102,074.00**	**$ 1,197,248.47**

The HPump™ horizontal surface pumping system from BHI is a multistage centrifugal pump with 14 stationary diffusers and rotating impellers. These pumps were custom built by BHI in their Claremore, Oklahoma facility. The pump is mounted on a skid and includes an 800 HP, 60 Hz, 460 V motor. Motor coupling and pump column thrust counter-plate is also included. The skid mounted pump-motor assembly included a separate skid mounted Electrospeed 3© Variable Speed Drive (VSD). The VSD is classified as a variable voltage inverter that uses six or twelve pulse width silicon controlled rectifiers to convert AC power into variable voltage DC Power. Each pump motor was powered by dedicated 1 MW truck mounted diesel driven synchronous generators. The BHI pumps were designed to pump optimally 63 L/s (1,000 gpm) at 6.9 MPa (1,000 psi) each with capability to reach nearly 1350 psi. The pumps were installed with a high-pressure piping and valve configuration which allowed them to operate in series or parallel. The maximum injection pressure that could be achieved by the equipment is approximately 19 MPa (2,700 psi), with an associated flow rate up to 63 L/s (750 gpm), as illustrated in the pump performance curves shown in Figure 2-15.

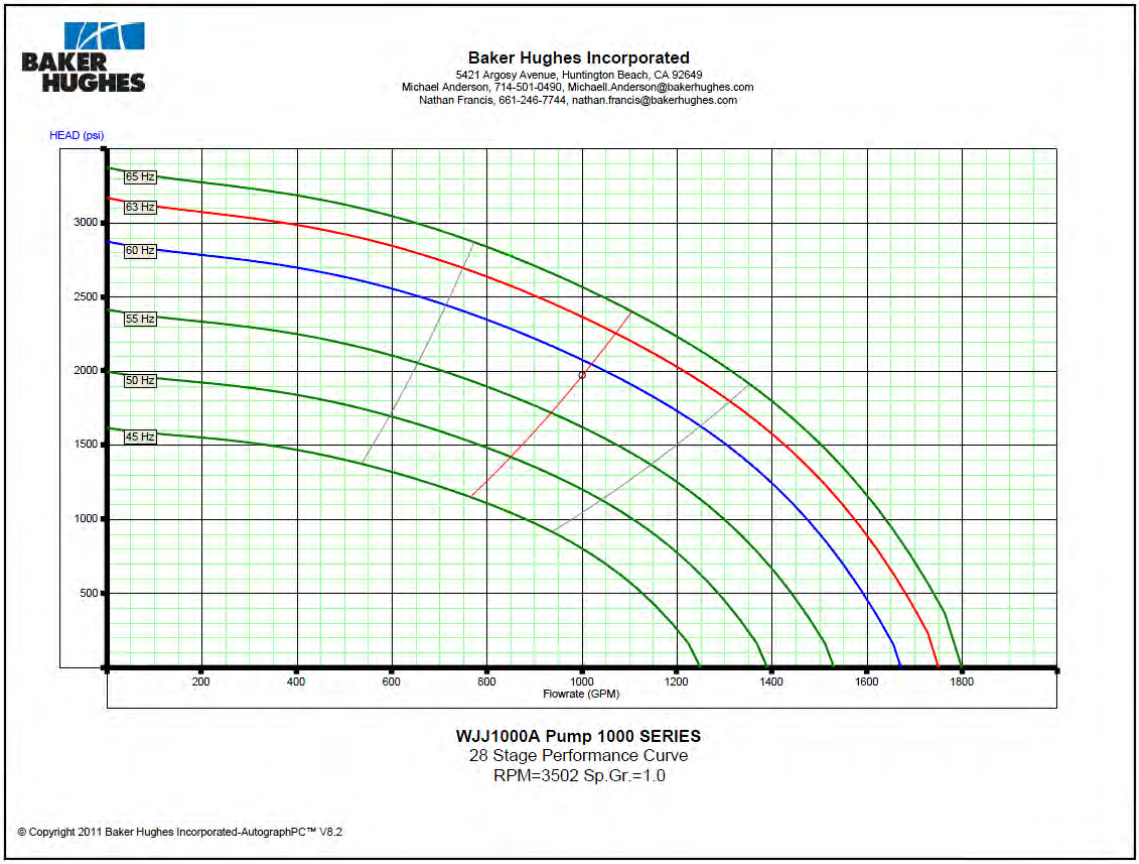

Figure 2-15. Stimulation pump performance operation curves provided by BHI for pumps configured in series

Prior to pump delivery, a concrete pad was poured based on design by Veizades & Associates Inc., to provide a level, anchored installation and provide stability during high pressure operations. Photos of pad installation and pour are shown below in Figure 2-16. Pad installation was in accordance with the design provided by BHI shown in Figure 2-17.

Figure 2-16. Concrete pad for stimulation pump anchor construction.

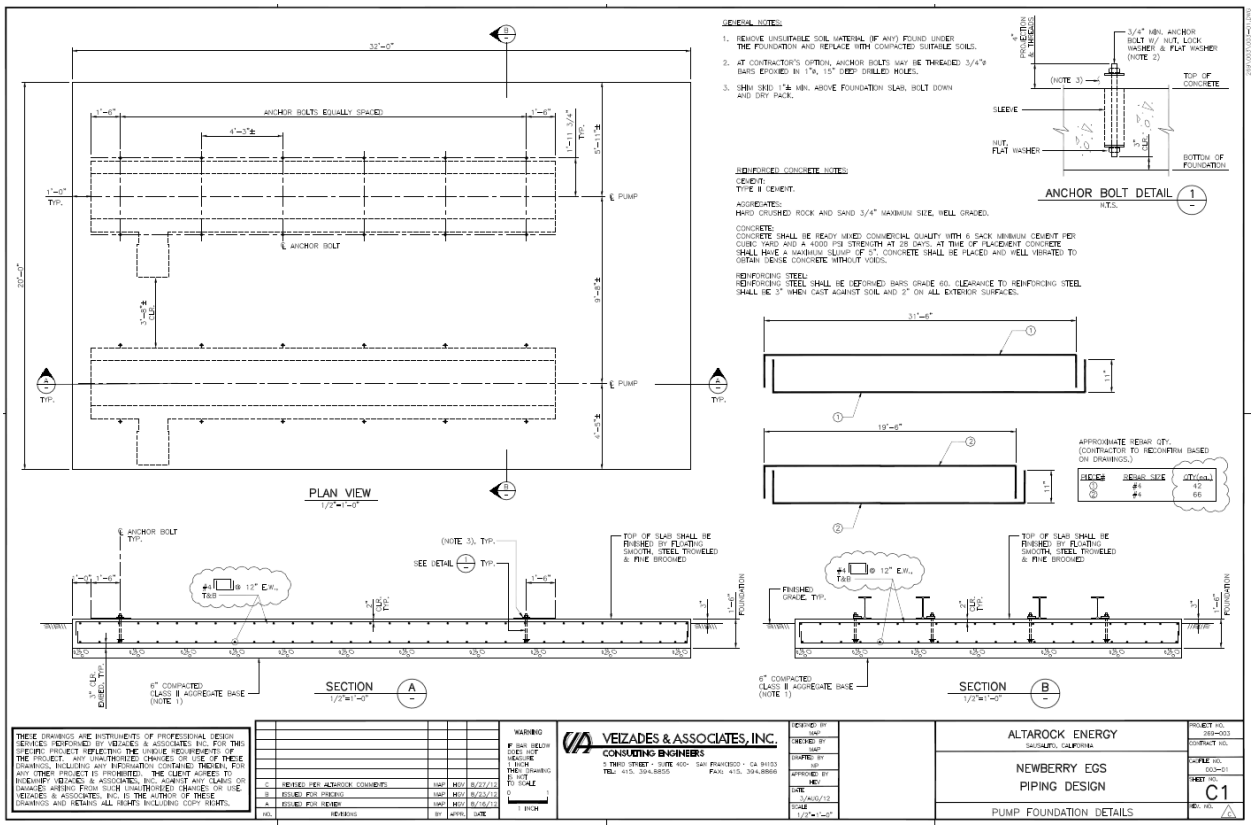

Figure 2-17. Pad S-29 stimulation pump concrete pad design.

The high pressure piping system was also designed by Veizades and Associates, Inc. Due to the low initial pre-stimulation injectivity of NWG 55-29, 50 mm (2.0 in) diameter bypass lines were installed on the discharge side of each pump to extend the pumping range and prevent damaging, low-flow conditions. Since the stimulation pumps require a minimum flow rate at each motor speed and wellhead pressure (WHP) to function under normal operating conditions, bypassed fluid was piped to the atmospheric separator installed for flow back testing.

Hudson Mechanical Inc. constructed the piping from October 2 to 12, 2012. The high pressure piping connecting both stimulation pumps to the wellhead tee consisted of Schedule 160, XXS, XS and Standard grade materials. Many runs of piping were fabricated in the shop and transported to the site to minimize field welding. The final field outfit differed from the Veizades original design as the bypass lines were drained into the atmospheric separator, rather than recirculating into the stimulation pumps, to prevent recirculating fluid from heating up the system.

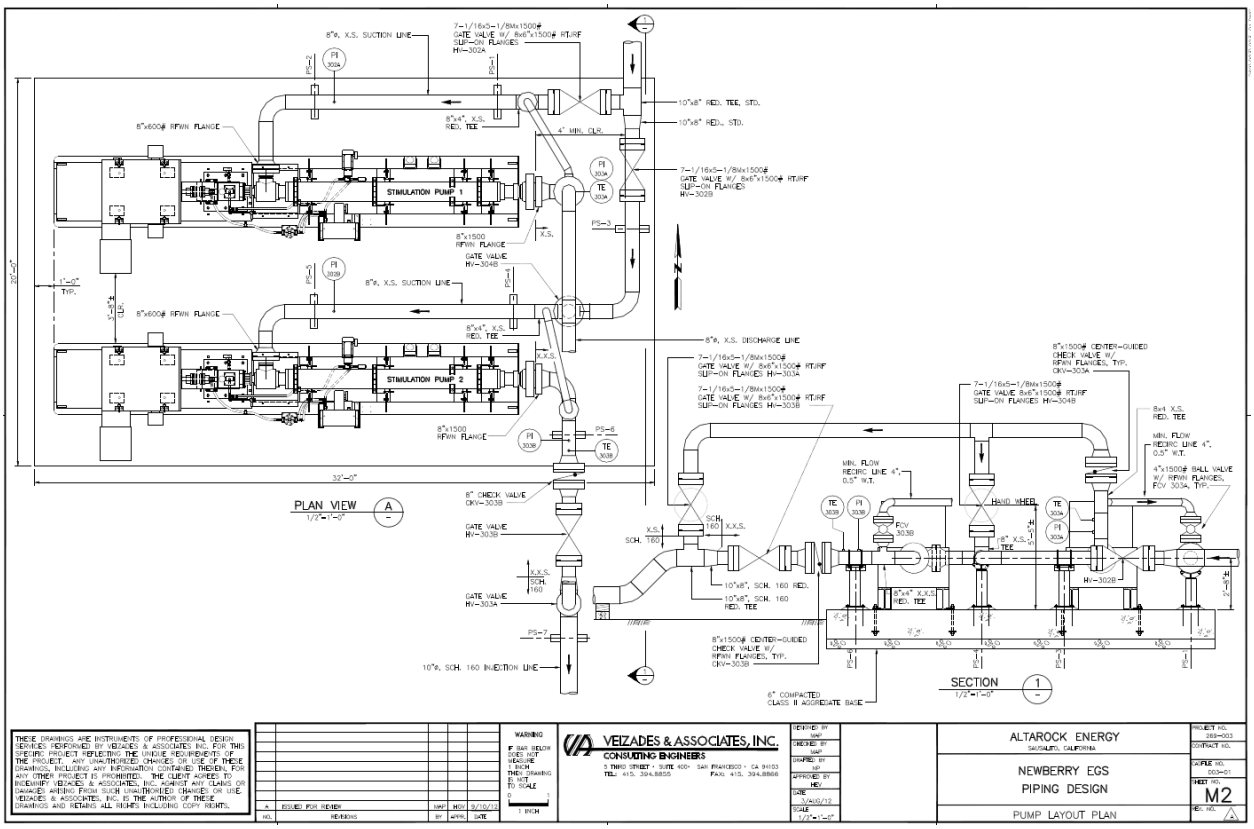

Figure 2-18. High pressure piping system designed by Veizades & Associates, Inc.

Figure 2-19. Newberry stimulation site showing stimulation pump setup, Variable Speed Drive cabinets (white), switchgear, and auto-transfer switches. The high pressure piping manifold is in the foreground. Caterpillar© 1 MW diesel generators that power the stimulation pumps are seen in the background.

2.7 PAD 29 WATER STORAGE

The high pressure stimulation pumps were supplied with water by water tanks, low pressure booster pumps, water transfer lines, and the water well on Pad S-29; plans for the original design are shown in Figure 2-20. The water well on Pad S-29 supplied stimulation water and was originally connected to

eighteen 76 m^3 (20,000 gal) capacity storage tanks using one common 25 cm (10 in) header line (Figure 2-21). 10 cm (4 in) flexible hoses connected a 10 in pipeline to each of the 18 water tanks on site for stimulation. Water flowed from the tanks into the two booster pumps that fed the stimulation pumps. These tanks were meant to provide a surge capacity of 1,400 m^3 (380,000 gal). Water well flow rates and cumulative volumes were continuously recorded by an in-line differential pressure flow meter and a magnetic flow meter downstream of the water well pump. Water level in the tank system was recorded by an in situ digital pressure transducer in the first tank which triggered the water well pump when levels dropped below 1.5 m (5 ft) above the bottom of the tanks. The injection line was tied to a booster pump system that fed the suction side of the stimulation pumps to ensure positive suction pressure. A flow tee also incorporated a batch mixer system between the booster pump and stimulation pumps for TZIM injection.

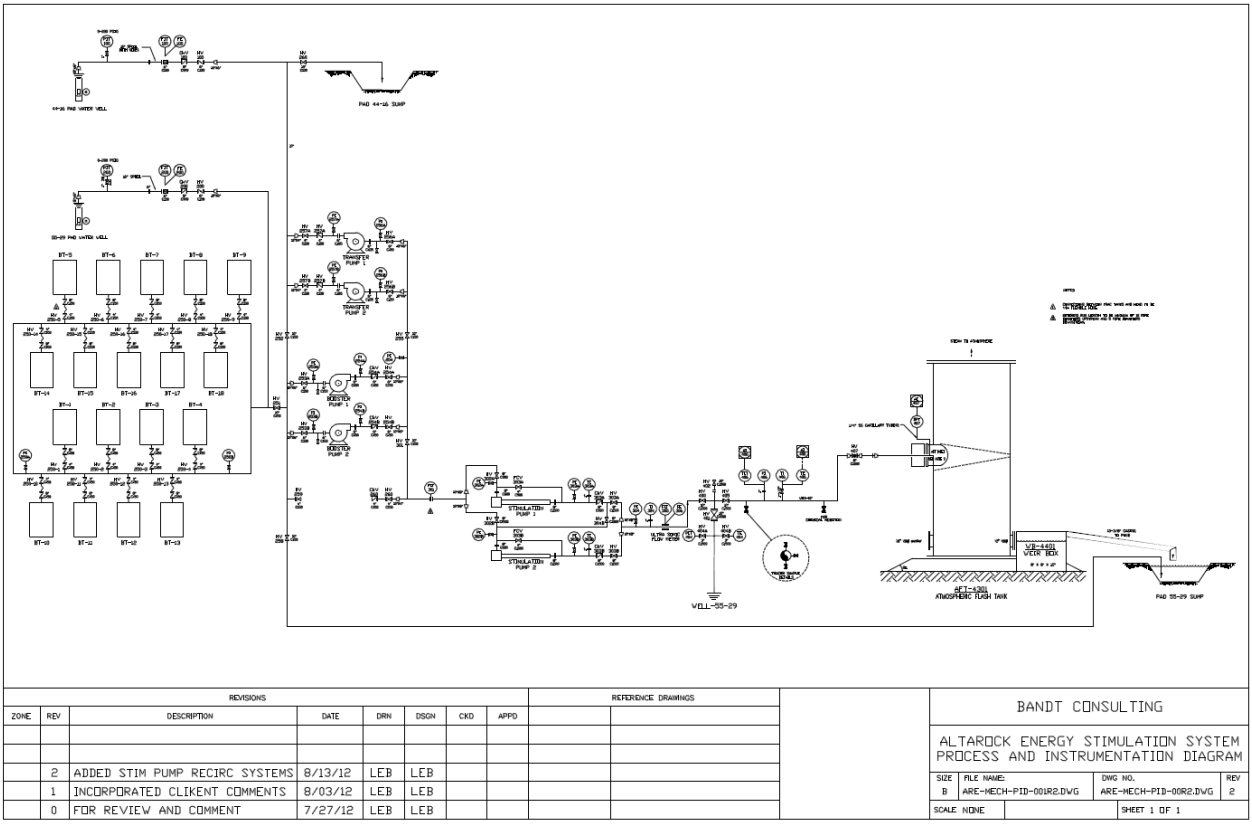

Figure 2-20. Well site schematic. Boxes on the left represent the location of water tanks in the overall system.

Figure 2-21. Water storage tanks connected to 25 cm (10 in) header line.

During start up the dual booster pump system, aligned in parallel, proved to be unstable due to the difference in the pump model specifications. The two electric booster pumps, model DV-150e and DV-150ie, did not perform at the same level. The newer model, DV150 iE overpowered the older DV-150e pump, causing the system to deadhead and cavitate.

Both the difference in pump power and the pressure drop from the tanks to the booster pump inlets created non-optimal conditions for stimulation pump operation. These conditions triggered the Programmable Logic Control (PLC) to trip system shutdown multiple times (Appendix B). After evaluating the performance, a new system (Figure 2-22) was designed using the water well to fill the smaller (north) side of the Pad S-29 sump as a buffer pond and feeding the booster pump system using a submersible pump installed in the sump. This revised system proved to be efficient during the stimulation. Minor setbacks included a broken vacuum chamber on October 26 due to pump construction that was quickly fixed, and partial plugging of stimulation pumps due to suction of debris from the sump.

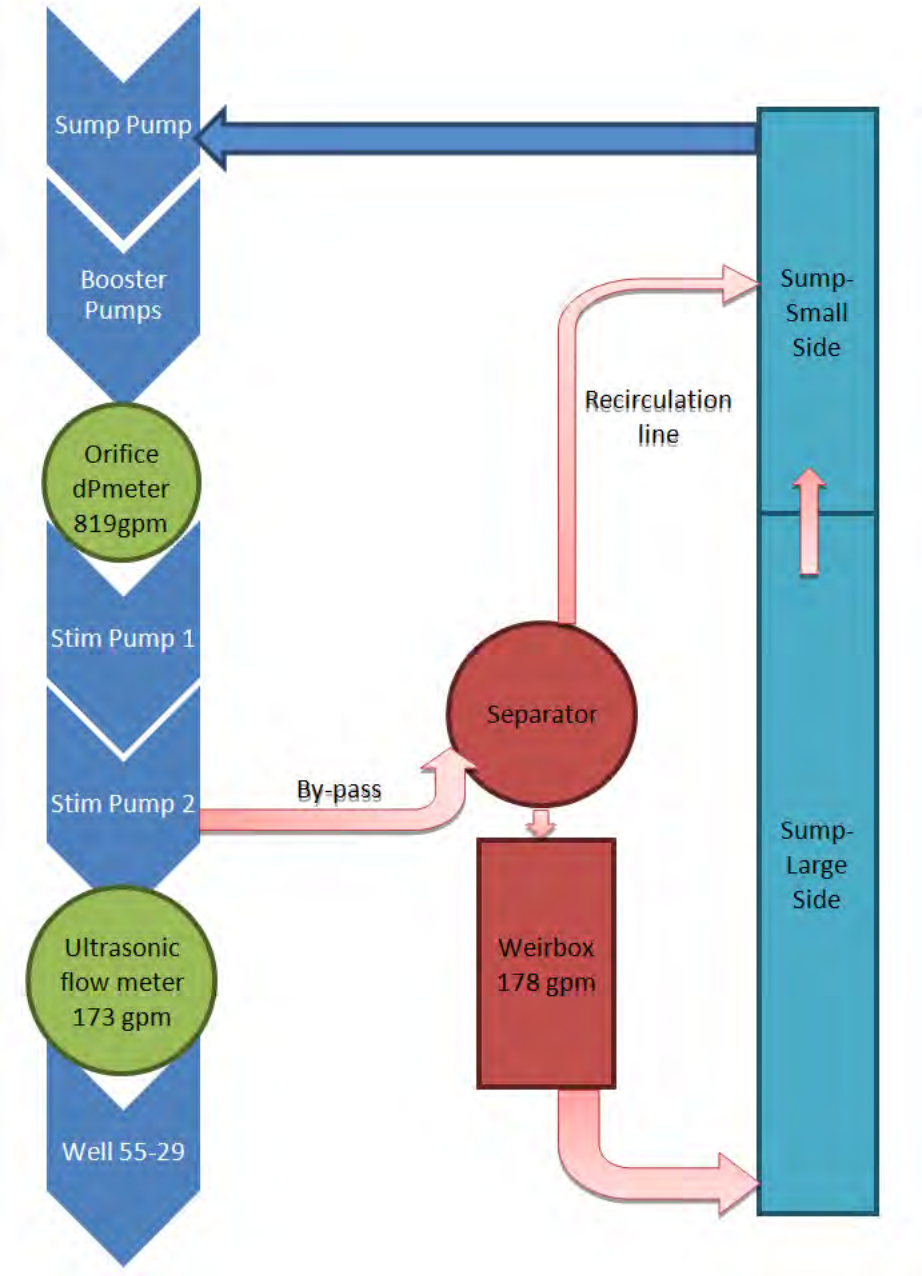

Figure 2-22. Revised NWG 55-29 stimulation pumping system set-up.

2.8 BACKUP WATER SUPPLY PIPELINE

A 25 cm (10 in) diameter Rain for Rent aluminum pipeline was constructed from Pad S-16 to Pad S-29, connecting the water well at Pad S-16 to water supply lines on Pad S-29. The pipeline was intended to provide a backup water supply to the stimulation site and to allow uphill pumping to the sump on Pad S-16 during flowback, in the event the sump holding capacity at Pad S-29 was inadequate. The tanks were connected to two DV150 booster pumps that discharged to the intake line to the stimulation pumps. Two additional diesel powered high pressure pumps (Model 3HA) were tied into the line to move water uphill from the sump on Pad S-29 to the sump on Pad S-16 if needed during flowback (Figure 2-24). The pipeline

was never used for uphill flow during stimulation and was disassembled after stimulation conditions indicated it would be unnecessary for flowback testing.

Figure 2-23. Roadside construction of the backup water supply pipeline from Pad S-16 to Pad S-29.

The total length of the pipeline was approximately 4.3 km (2.7 mi) (Figure 2-23). The pipeline was assembled over a two week period along the side of FS roads 600A and 600B. Pipeline culverts were constructed across FS roads 600A, 600B and 300, to maintain road usability. A third culvert was constructed where the pipeline crossed into the forest from FS road 600A, 1 mile south of the FS 600A-600B split. Chevron signs and delineators were posted on either side of the culverts in accordance with USFS permit requirements.

The pipeline was coupled together in 0.3, 1.5, 3, 6, and 12 m (1, 5, 10, 20 and 40 ft) sections with rubber gaskets and bolted Victaulic couplings. The pipeline was leak-checked after completion, and a partial up-gradient pump test was performed.

Figure 2-24. Model 3HA high pressure pumps used to pump water uphill to Pad S-16.

2.9 ELECTRICAL AND CONTROLS

2.9.1 MEDIUM AND LOW VOLTAGE ELECTRICAL

The Newberry EGS project site on Pad S-29 is approximately 12 km (7.5 mi) from highway US-97 and an equal distance from the nearest electrical transmission or distribution line. As such, Pad S-29 does not have utility electrical services or connectivity to the local grid; all electrical power requirements must be provided by portable diesel generator sets. The full operational load of the test facility was approximately 1,300 kW. This did not include the smaller auxiliary loads that required power, including submersible well pumps and site office facilities. Given the diversity of electrical generator used at the site, it was determined that single-source power supply was not optimal and that separate dedicated power supplies must be provided to various site users. Electrical generation equipment used during the stimulation project is shown in Table 2-4.

Table 2-4. Electrical generator parameters

Requirement	Qty	Output (kW)	Voltage	Phase
Stimulation Pump Generator(s)	3	980	480	3
NWG 55-29 Well Pump	1	175	480/230	3
Site Office/Control Room	1	60	480/230	3
Pad S-16 Well Pump	1	400	480/230	3

For 24/7 operations for the duration of the project, AltaRock required that each stimulation pump have a dedicated 980 kW diesel generator. In addition, should one of the dedicated pump generators fail or require service, a third standby generator of equal size was available for operations. This third generator

also served as a reduced load generator used to conserve fuel during times when dual-pump operations were not possible or maintenance was being performed.

The three 980 kW generators were connected to two Automatic Transfer Switches (ATS). The generator in the center-top of the diagram was designated as the standby generator (Figure 2-25); if one or the other primary generators is disconnected, the standby would engage and start. The purpose for this was to secure dependable operations during the stimulation even in the event of a single-mode generator failure. The two operating generators and their ATS units were connected to a dedicated distribution cubicle (Lineup #1 and #2) which provided electrical breaker control and transformer step-down voltages to associated systems. Each cubicle provided electrical service to the dedicated stimulation pump and booster pump, at 480 V. Finally, a step-down transformer and distribution panel provided power to the remaining 208/120 V loads including the control PLC, the ultrasonic flow meter and electrical bypass control valves.

Figure 2-25 is a schematic electrical single line diagram of the Stimulation Pump electrical system. This 1-line diagram details not only the lineup of the three generators but the required electrical services to ancillary equipment serving the primary pumping systems used in the stimulation work. In Figure 2-26 the generator on the left, generator 1, is dedicated to ATS box 1 and the generator on the far right, generator 3, is dedicated to ATS box 2. The generator in the middle, Generator 2, can switch between both boxes. Setting up the system in this way allows for the aforementioned flexibility when considering maintenance and potential failures. Further downstream are the specific components of the stimulation system. Connected to ATS box 1 are a VSD, components of the Programmable Logic Controller (PLC) and a Rain for Rent booster pump. Connected to ATS box 2 are: another VSD, more components of the PLC , the second rain for rent booster pump and the sump pump, used to supply water to the booster pumps.

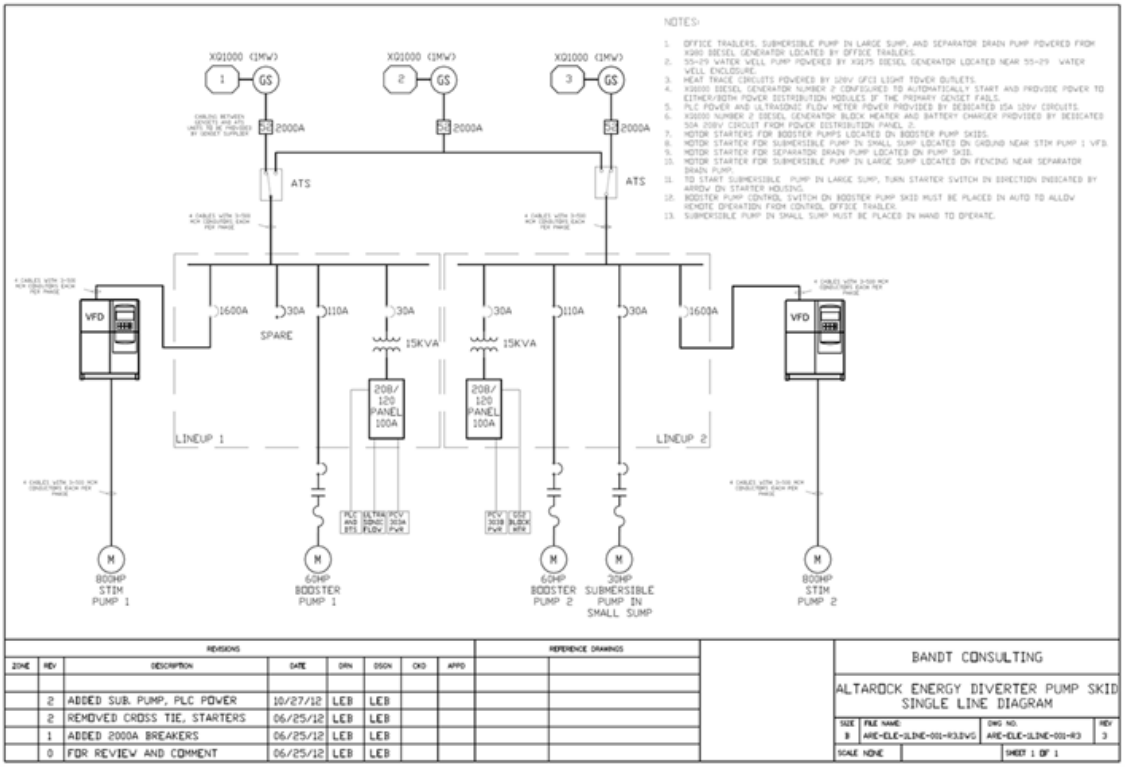

Figure 2-25. Schematic of stimulation pump electrical system.

All equipment and power cabling was installed on grade. The equipment was rated for outdoor use and therefore sealed from weather and elements. The power cabling was designated as special outdoor, armored and surface-installed cable and was selected to mitigate the need for construction of buried or conduit-encased wiring runs.

Figure 2-26. Initial set up of XQ1000 generators (large white containers). From left to right they are labeled Generators 1, 2 and 3.

Grounding of the entire electrical system was required. Initially, installation of independent grounds for generators and equipment were attempted. Due to the sub-grade rock structure of the S-29 pad, ground rods were not successfully installed to the required depth. A single ground point for the entire system was created utilizing the NWG 55-29 wellbore and its 1,981 m (6,500 ft) steel casing as a ground rod. The electrical system design, specification, and configuration were provided by Larry Bandt of Bandt Consulting, from Reno, Nevada.

2.9.2 INSTRUMENTATION AND CONTROLS

The control system for the stimulation project was a combination of instrumentation, for automatic monitoring, and limited automatic control of devices. Active field monitoring and manual adjustment of control valves was also required to change operating settings.

Included in this control scheme are stimulation pump Variable Frequency (or Speed) Drives (VFD) (Figure 2-27). The VFD used in this system is an Electrospeed™ GCS and is classified as a variable voltage inverter (VVI). This particular VFD uses a six-pulse silicon controlled rectifier to convert AC power into variable voltage DC power. It is through the VFD that the speeds of the stimulation pumps are controlled. Initially, there were problems with the VFD connected to ATS box 1. When the stimulation pump connected to this VFD reached speeds greater than 50 Hz the pump began to behave erratically. Typically, these pumps are configured to an Electrical Submersible Pump (ESP) mode which transforms the AC power into a six step

voltage output, which approximates a sinusoidal waveform. When using these pumps at the surface a Full Pulse Width Modulation (FPWM) mode is needed, which is a twelve step voltage output providing a smoother sinusoidal wave. This mode requires added engineered complexity. The reason for the erratic behavior of stimulation Pump 2 was a default in one of the components of this complex drive system. BHI came to the site on October 6, 2012 to fix the drive and could not locate the specific problem. After switching out the old components of the drive with new ones the pump behaved as expected at speeds greater than 50 Hz.

Figure 2-27. Installation of VSD 1 (white box in foreground). The gray box behind VSD 1 is a dedicated breaker cubicle for the VSD. The armored cabling that connected 460V phases between the cubicles and then the 800HP pump drive is placed on the ground prior to termination.

The Programmable Logic Controller is the principal device which allowed for the automation and control of the stimulation system. All sensors, as well as control panels for different equipment, were connected to the PLC. Signal inputs into the PLC came from the sensors located on or within pieces of equipment; outputs went to the different equipment control panels. The PLC uses programmed imbedded logic to take incoming information from the sensors on site and make decisions about trips and alarms for the different pieces of equipment under its control. Choices have to be made about what should be automated and what should be controlled by the operator. Typically, automated decisions consist of sending trip commands to different pieces of equipment when a known operational threshold is crossed. When there is not a clear need to turn off a piece of equipment, but there may be operational concerns about running a certain piece of equipment at a specific state for too long, then an alarm is sent to the operator. This alarm is sent to a Human Machine Interface (HMI) unit located in the control trailers where an operator can see different streams of information in real time and make changes to equipment settings when needed. An inventory of the trips and alarms that occurred during the field work is presented in Appendix B.

At Newberry the HMI used during operations was an Allen-Bradley PanelView Plus 1000. The PanelView is a programmable touch screen which allows an operator to set up controls and access live streaming data in a way that is in accordance with the method of operations. For this first phase at Newberry there were six control and data screens programmed for the HMI. These screens included: pump diagnostics, live data from various sensors, a pump control panel and a stimulation control panel (Figure 2-28).

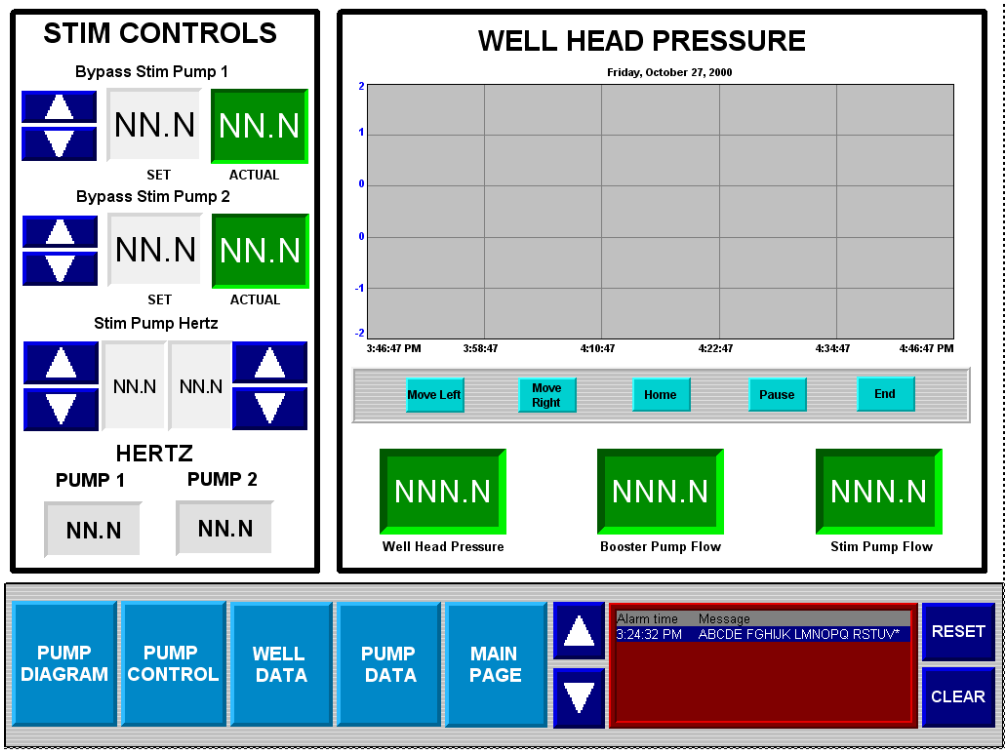

Figure 2-28. Picture of the stimulation control panel.

From the panel shown in Figure 2-28 staff could control the speed of each stimulation pump and the amount each bypass valve was open. The gray square, upper right, displays the current WHP over an hour long increment. The green squares underneath numerically display the current WHP, flow into the stimulation pumps and flow into the well. The blue squares on the bottom of the image are links to the other panels programmed into the touch screen. The red box to the right of these is the alarm display panel, where active alarms and trips are displayed.

This stimulation system provided a means to reasonably influence induced seismicity. Pressure and injection rates during stimulation could flexibly be controlled by changing pump speed or throttling the bypass valve. These control parameters, combined with incoming data from the Micro-Seismic Array, allowed the testing staff to respond to changes in micro-seismic activity with changes in pump operations. Stimulation could therefore be quickly influenced without compromising the integrity of the stimulation pumps.

2.9.3 ACCOMODATING WEATHER

During the course of operations, as weather conditions changed, it became necessary to provide heat tracing (no-freeze) protection to the instruments. Earlier in the project, failure to install no-freeze protection resulted in stimulation pump failure when sensors responsible for monitoring the operational threshold of the pumps became frozen and inoperable (see Section 3.2.3, below). Later in the stimulation it became necessary to enclose the pump drives in a temporary structure in order to protect them from

snow accumulation. Though the cubicles were weather proof, the units contained external cooling coils that became impacted with snow. The structure built to mitigate this problem provided simple cover for the drives and overall protection for the operational end of the drive-pump combination. Furthermore, it provided a dry place for personnel to monitor critical pump operations in the field during both start-up and injection of TZIM.

2.10 FLOWBACK EQUIPMENT

The flow test equipment (Figure 2-29) was connected to the wellhead on NWG 55-29 prior to and during stimulation. One 25.4 cm (10 in) 1500 series wing valve isolated the flow test equipment from high stimulation pressures. After shut-in and thermal recovery, the flow line valves can be opened and the well would be allowed to flow through the separator and weir box into the empty sump on Pad S-29. The water would travel from the wellhead through the flow line and control valve into the James tube assembly. Along the flow line (Figure 2-30), ports were installed for tracer flowback sampling, geochemistry sampling and chemical abatement system injection as needed.

Steam flow would be calculated utilizing the lip pressure method and the James tube assembly. Three different sizes of assembly, 15, 20 and 25 cm (6, 8 and 10 in) were staged on-site to ensure that the steam flow could be calculated accurately at different fluid flow rates. The separator for Newberry is 3.7 m (12 ft) in diameter. The separator allows steam discharge vertically and funnels water into an outlet at the bottom. From that point, the liquid flows through a V-notch weir box (Figure 2-31). Using this configuration liquid and steam flow rates can be measured and calculated separately so that total fluid flow and two-phase enthalpy can be calculated. For this flow back design the weir box discharges into the sump on Pad S-29. Water in the sump is then used to supply the stimulation pumps.

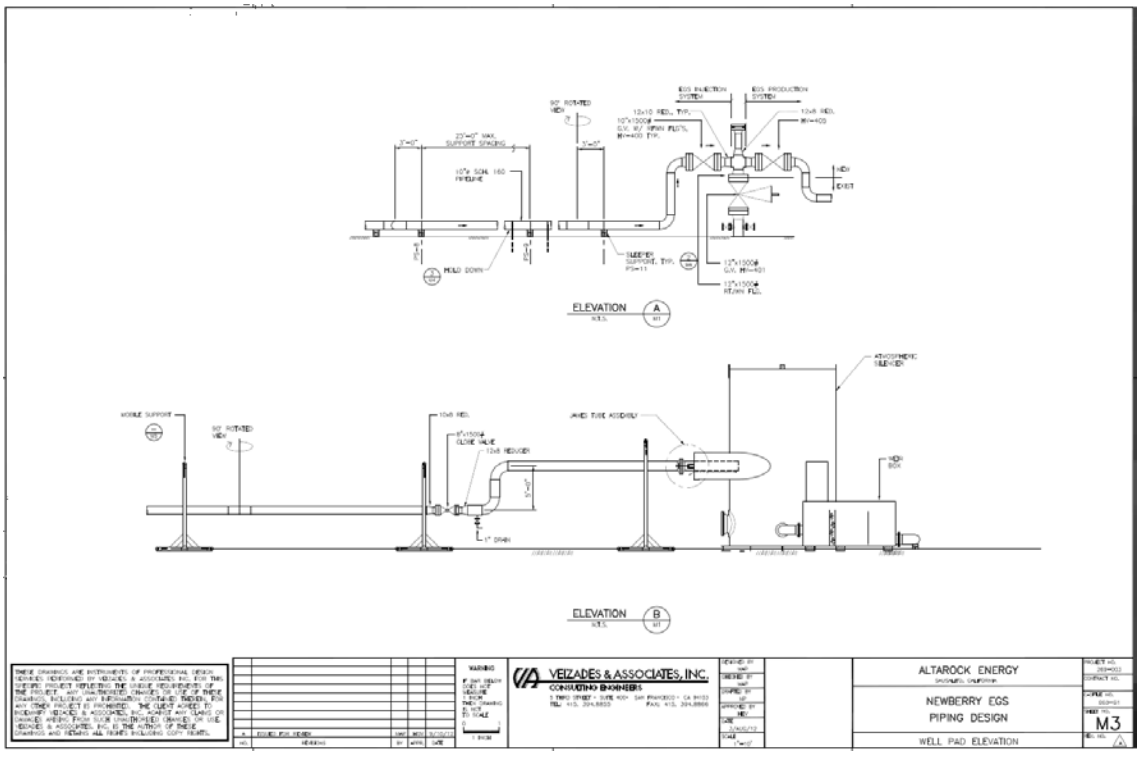

Figure 2-29. Flowback equipment design. Including piping, separator, and weir box.

Figure 2-30. Flow back piping, phase separator (large white cylinder) and wellhead.

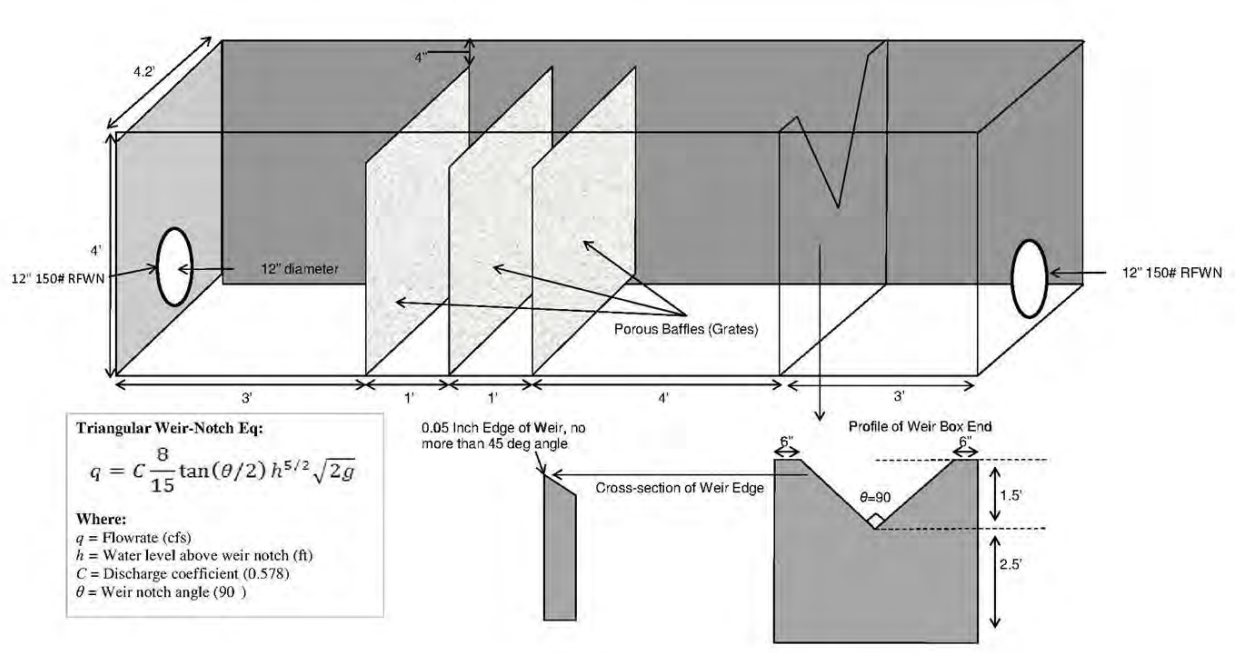

Figure 2-31. Detail of weir box and flow rate measurement formula.

2.11 DIVERTER STAGING

Proprietary thermally degradable zonal isolation material (TZIM) developed by AltaRock (product name AltaVert™) was used in this project to stimulate multiple zones in the subsurface. TZIM material injected between stimulation stages to temporarily reduce permeability of stimulated fractures near the wellbore.

Blocking flow allows for increased WHP and subsequent stimulation of new fractures elsewhere along the wellbore. This method allows for the stimulation of multiple stages in a single well without the use of mechanical isolation. The TZIM applied during each stage contains a distribution of various particle sizes in order to optimize their sealing capability (Figure 2-32).

A total of 1,043 kg (2,300 lbs) of AltaVert 251™ and 12,864 kg (28,360 lbs) of AltaVert 154™ were staged on Pad S-29 in pallets containing 23 kg (50 lb) sacks. These two TZIMs were chosen based on their degradation characteristics. Breakdown characteristics of AltaVert 154™ are shown in Figure 2-33; this material is stable at temperatures lower than 200°C (392° F), but it will degrade completely within four weeks at temperature above 250°C (482° F). Breakdown characteristics of AltaVert 251™ are shown in Figure 2-34; this material is more stable at temperatures above 315°C (599° F). It lasts longer than AltaVert 154™ (though it does break down eventually), and it was staged as a back-up TZIM in case AltaVert 154™ degraded too quickly during stimulation. Coarse AltaVert 154™ was also staged to be used as backup material in the case that fractures below 2,900 m (9,514 ft) could not be plugged for the entire stimulation duration due to lack of cooling.

TZIM injection is described in Section 3.6. Prior to TZIM injection, the AltaVert™ TZIM material was first blended into a slurry using a batch mixer unit supplied by ThermaSource, Inc. out of Santa Rosa, California. Ultimately, only AltaVert 154™ was used. At high temperatures, AltaVert 154™ decomposes to its building blocks, - ethylene glycol ($C_2H_6O_2$) and terephthalic acid ($C_8H_6O_4$). Ethylene glycol decomposes to carbon dioxide in a matter of weeks. Terephthalic acid lasts longer (weeks to months), is insoluble in water, and eventually degrades to CO_2 and H_2O. Thus, nothing of the diverter material is expected to remain by the time the well is eventually flowed.

Figure 2-32. TZIM of varying particle size distribution used during Newberry stimulation.

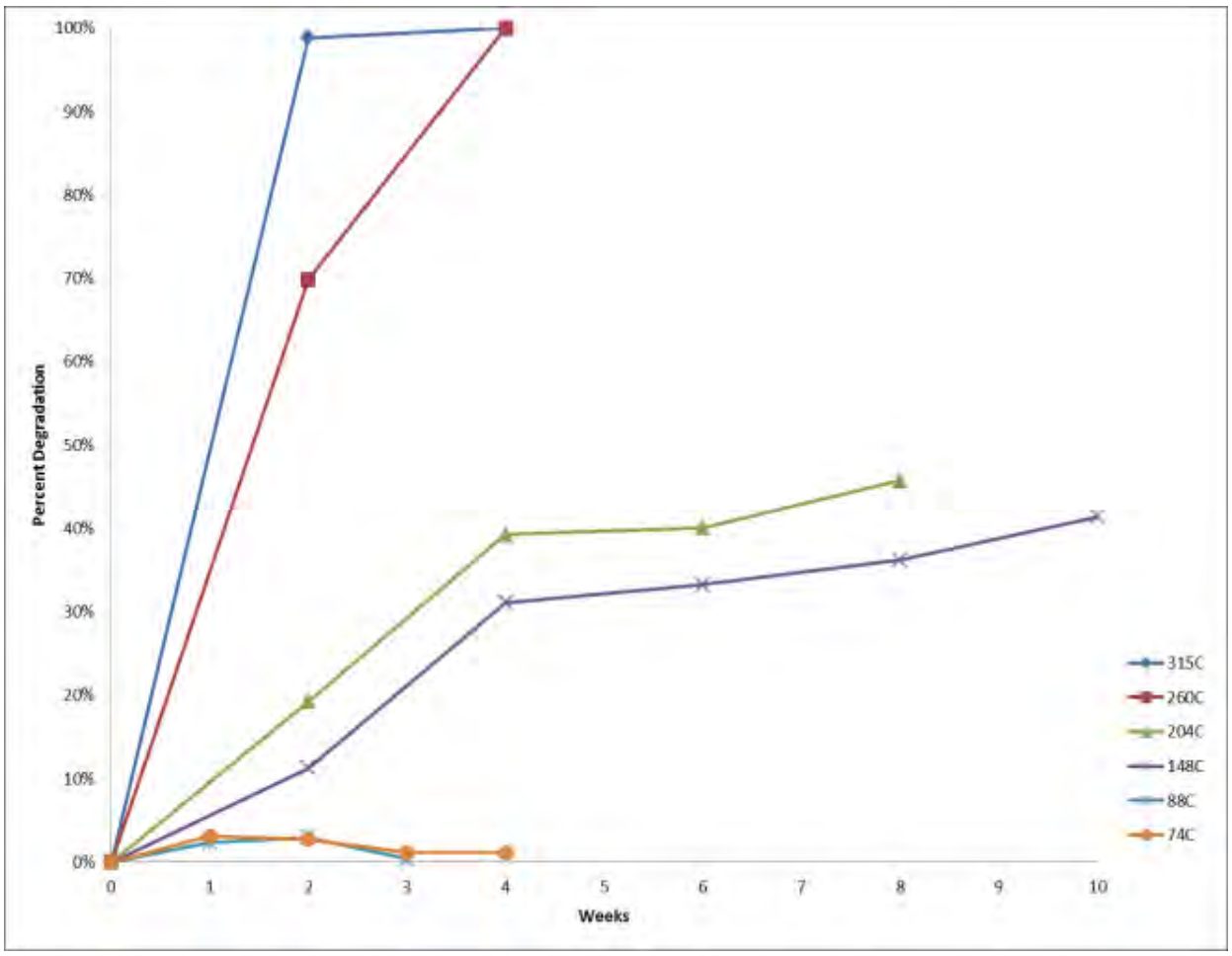

Figure 2-33. AltaVert 154™ thermal degradation curves.

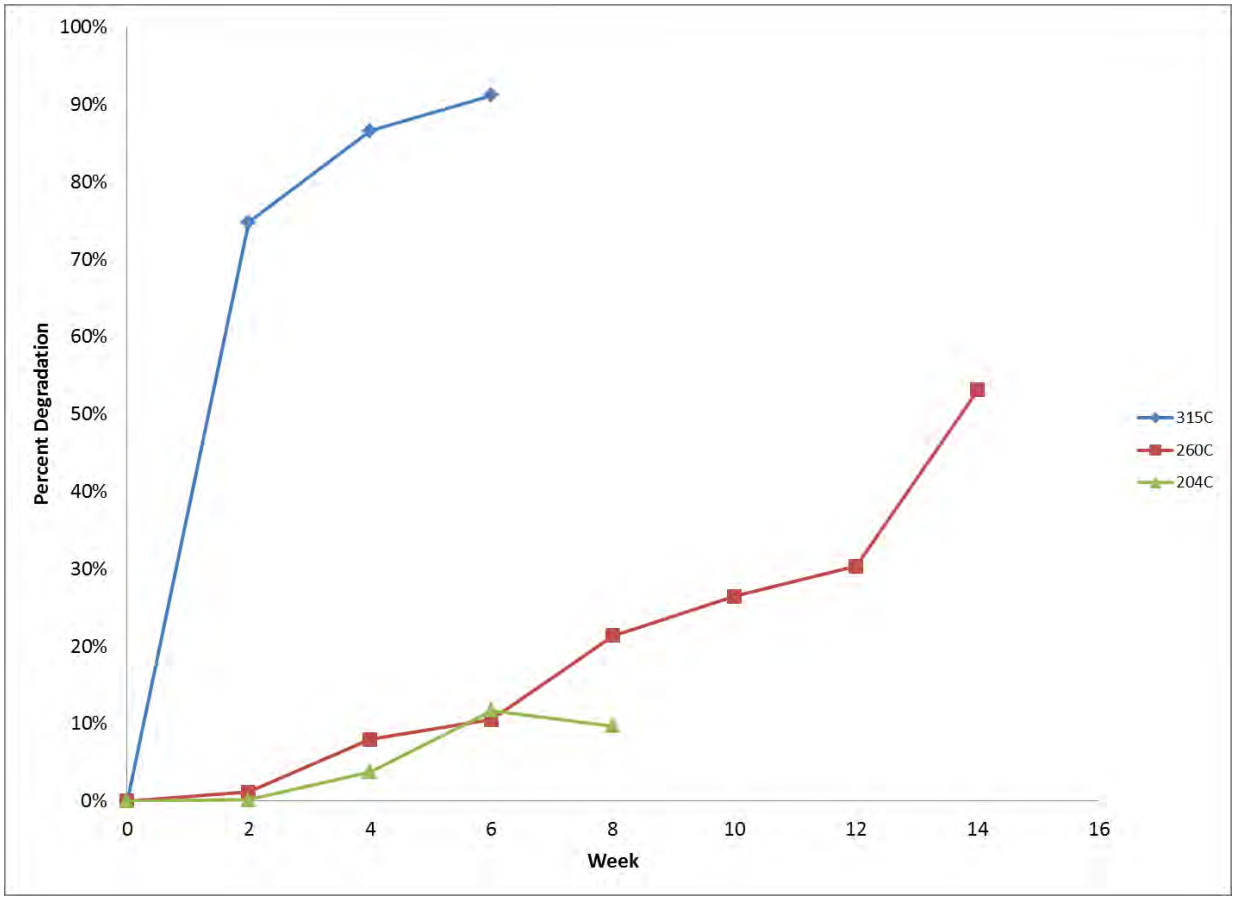

Figure 2-34. AltaVert 251™ thermal degradation curve.

Figure 2-35. ThermaSource batch mixing unit tied into TZIM booster pump. Tracer injection set-up shown to the left of TZIM booster pump.

3 STIMULATION

3.1 STIMULATION TIMELINE

Stimulation at the Newberry EGS Demonstration site began on October 15. Daily summary reports were prepared at the close of each day of stimulation activities and are included as Appendix C. Preceding the commencement of stimulation, two important milestones were passed. Approval for the installed micro-seismic array was received from the DOE on August 30, at which time AltaRock Energy was approved to file a sundry notice for stimulation of well NWG 55-29. Approval of the MSA was a requirement agreed upon in the ISMP and acted as a stage-gate for subsequent development of the stimulation infrastructure. Between August 30 and October 15 the sundry notice for stimulation of NWG 55-29 was approved and the development of the stimulation infrastructure was completed.

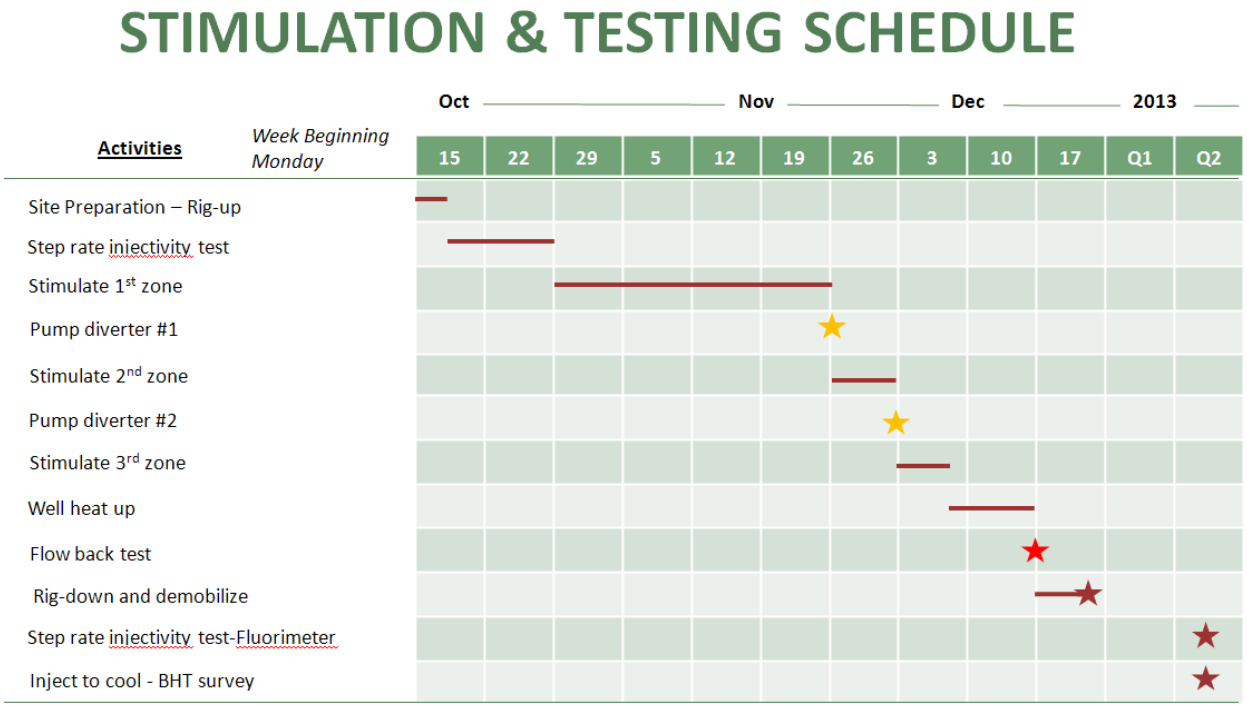

Figure 3-1. Stimulation procedure timeline at the Newberry EGS Demonstration site.

On October 15, rig up and testing of the stimulation system were completed. An initial step rate test began on October 16 (Figure 3-1). Conducting a step rate test allowed initial injectivity to be ascertained and identified critical pressures for different stimulation zones within the well. Once the step rate test was completed, stimulation of the first zone began. The stimulation of this zone took place over a three week period which was lengthened by equipment failure. After the first stimulation, diverter was pumped down the hole, closing off the first stimulation zone. This was followed by the second stimulation, which proceeded much more quickly due to system optimization and significantly fewer equipment failures. The diverter injection process was repeated to block the second zone and allow stimulation to open a third and final zone. Stimulation ended on December 7. Upon conclusion of the stimulation the pad was cleared of essential equipment and the well was shut-in and allowed to thermally equilibrate with the formation. When the well had equilibrated sufficiently, a flow test was initiated to determine different characteristics of the reservoir. Sufficient flow back from the well did not occur, despite an attempt to air lift the well. A flow test will need to be conducted in the next phase of the project.

3.2 HIGH PRESSURE PUMP PERFORMANCE

3.2.1 INITIAL PUMPING PROBLEMS

Initial pump wiring began on October 3. Both pump motors were tested without load and ran smoothly. Pump start-up testing began on October 14. Vibration and system checks cleared the pumps for high pressure operations, but several pump tripping issues persisted including: under voltage, PLC shut down due to low suction pressures, low speed trip shutdown, ride through low speed and phase over current. Both pumps could start up successfully in series or parallel, but increasing the pump speed would often trigger an error message which eventually caused one or both pumps to shut down (Figure 3-2). The 18 water storage tanks were interconnected with a common header to one pipeline with Victaulic couplings. The line appeared to have leaked air into the pumping system which triggered the system to shut down. Initial pump trips occurred when ramping up pump frequency. Inlet leaks are believed to have caused cavitation as indicated by irregular suction pressures (Figure 3-2, bottom). Multiple startup attempts showed early signs of low voltage issues that became increasingly problematic during stimulation. Startup problems were resolved by throttling the bypass line.

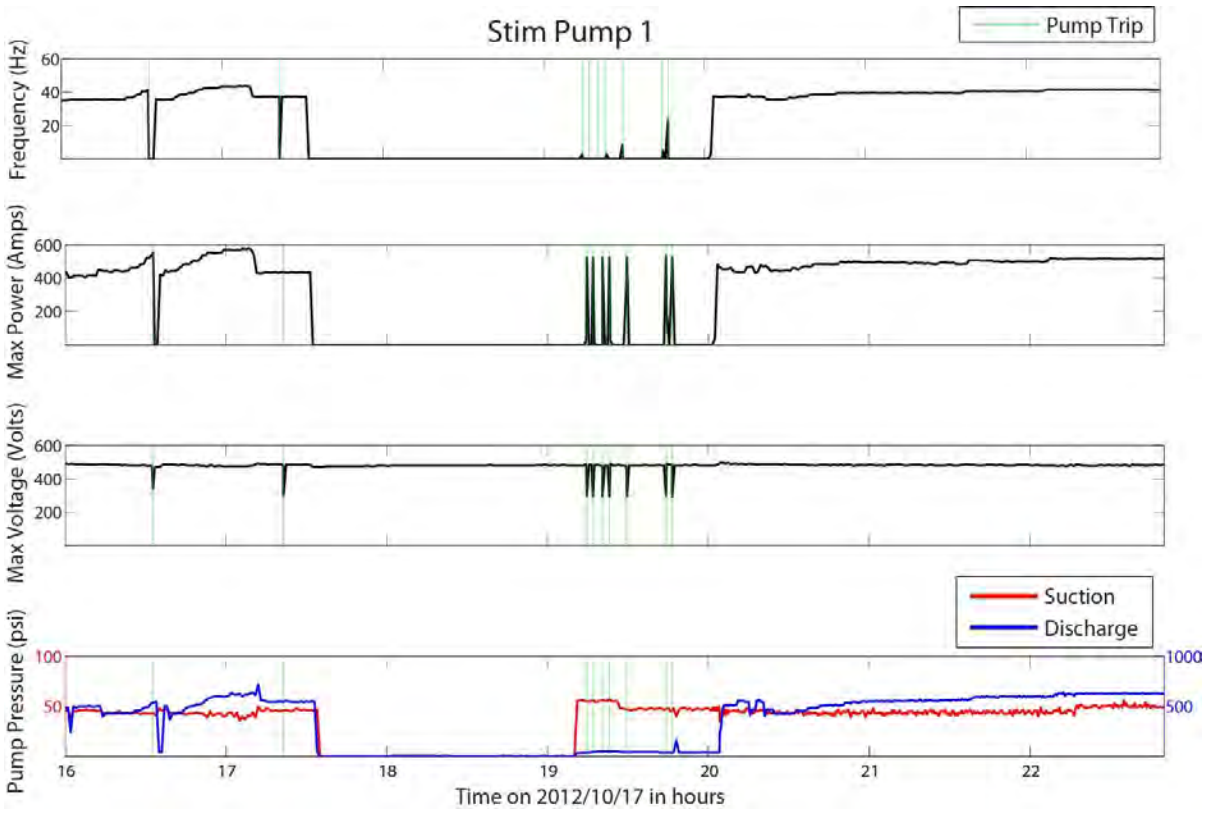

Figure 3-2. Data for Stimulation Pump 1 on the first day of stimulation.

3.2.2 CHANGE OF PUMPING CONFIGURATION

Decisions were made on October 19 to pull out the 18 tank buffer systems and draw water directly from the smaller (north) portion of the sump with the help of a submersible pump. Water pumped from the water well on Pad S-29, along with the recirculating water from the stimulation pumps maintained a constant level in the sump. The submersible pump fed water directly to two booster pumps lined up in parallel. The discharge pressure from the booster pump system was approximately 0.5 MPA (80 psi). The submersible pump approach proved to be more stable than the tank buffer system previously used. WHP

reached 11.3 MPa (1640 psi) on October 19, although suction pressure at the stimulation pumps continued to surge when pumps operated at higher than 35 Hz.

3.2.3 PUMP 1 FAILURE AND DRIVE PROBLEMS WITH PUMP 2

After reaching 12 MPa (1,736 psi) on October 20, Stimulation Pump 2 began to experience low voltage issues and was unable to re-start. In conjunction, sudden cold weather caused multiple sensors to malfunction and accurate flow was not detected. During the restart process, the back-up generator failed to provide power to the submersible pump and caused the stimulation pumps to run dry and overheat. Then a sudden surge of cold water was reintroduced to the stimulation pumps, shattering the tungsten carbide bearings in Stimulation Pump 1.

From October 21 to 24, booster pump injection continued in order to prevent surface piping from freezing. Stimulation Pump 2 was restarted on October 24 while waiting on the back-up replacement pump body for Stimulation Pump 1. The replacement pump barrel from BHI had not been delivered at the start of operations as planned due to manufacturing delays. Figure 3-3 displays data for Stimulation Pump 1 on October 21, 2013. The pump experienced two low voltage trips, followed by two more trips, possibly due to suction pressure. Low speed trips are accompanied by severe drops in voltage and intense spikes in current above 1000 amps. Wellhead pressure is shown in lieu of no suction/discharge data available due to freezing pressure gauges on pumps. When operating solely on Stimulation Pump 2, it became apparent that drive issues prevented Stimulation Pump 2 from operating above 40 Hz. Baker Hughes representatives delivered the new body for Stimulation Pump 1 on October 28. Shortly after installing Stimulation Pump 1, it was determined that the voltage clamp needed to be lowered from 450 V to 440 V; allowing Stimulation Pump 2 to reach higher speeds. The fix allowed both stimulation pumps to operate at high injection pressure from October 28 to November 2 and complete Stage 1 stimulation.

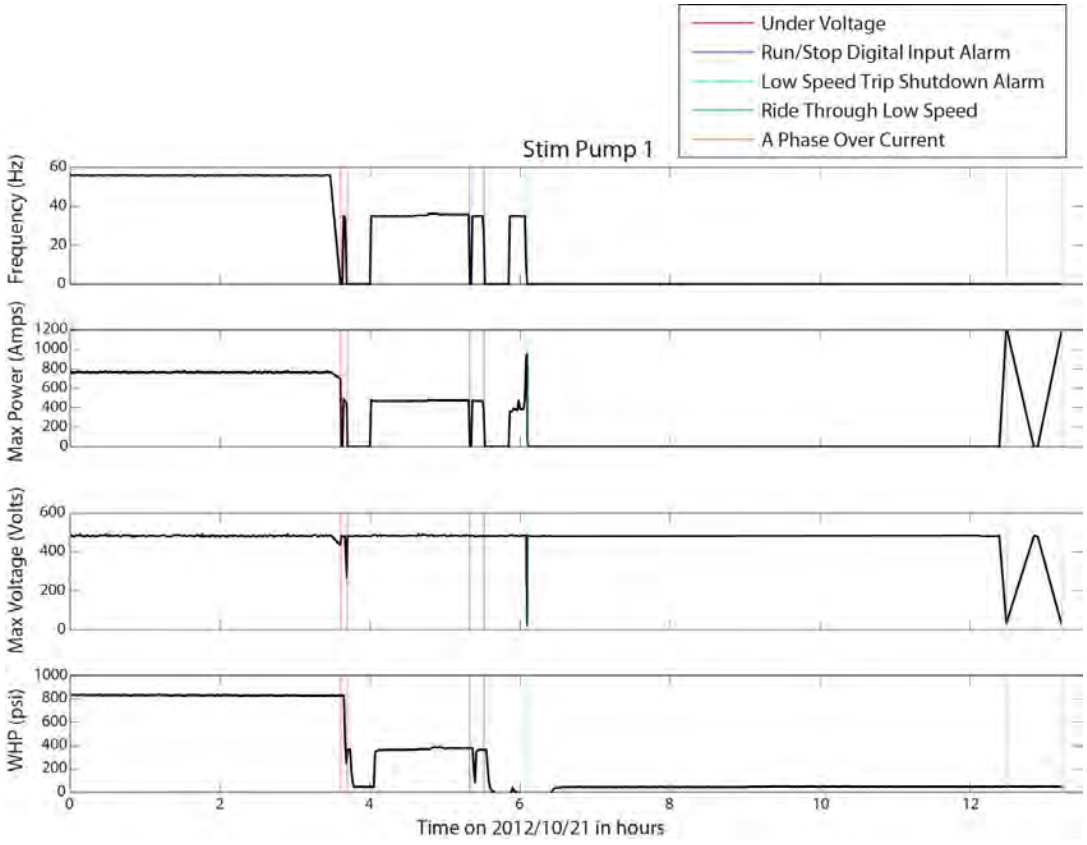

Figure 3-3. Pump data for Stimulation Pump 1 on October 21st.

On November 1, Generator 3 shut down due to overheating and tripped Stimulation Pump 2. After the standby generator was brought online, Stimulation Pump 2 was unable to restart. Start-up issues were caused by high current on one of the legs, and the pulse width modulation (PWM) module in Drive 2 was suspected to be at fault. After checking circuitry and replacing cards, it was found that the front-panel reset switch was not functioning as designed. The reset mode was made temporarily operational by jumping to reset to the PWM operating mode. During the two weeks spent trouble shooting Drive 2, Stimulation Pump 1 operations were mostly maintained; however, a gradual pressure decline was noted. After decoupling the pump, inspection revealed that the shaft no longer turned certain impellers because fibrous material, originally a nylon line and lift strap that has fallen into the sump and been sucked into the submersible pump. This material was pumped into the Stimulation Pump, and had wrapped around the pump shaft.

From November 11 to 25, both pumps were sent to Baker Hughes in Oklahoma for repairs. A new central shaft was machined for Stimulation Pump 1 and straightened to specs. The pump bowls, diffusers, collars, etc. were keyed and taper-fit onto the shaft. Operational testing produced above specification performance with near zero vibration (at the reduced load testing available at the facility). Stimulation Pump 2 was disassembled and it was found that the inlet at stage 1 of the pump was completely blocked with debris (duct tape, pieces of white plastic, shreds of strapping and some shards of poly rope, plus a few pieces of marble-sized pumice). Reduced pump performance was concluded to be the result of this blockage; no significant damage was observed during disassembly of the pump. The disassembled parts were cleaned and reassembled by November 21. An in-line filter system, with purge capability, was also installed between the booster pumps and the intake of the stimulation pumps to prevent additional debris from clogging the pump system from that point forward.

From November 25 to December 7, the re-installed pump-VFD drive system performed smoothly. Dual pump operations allowed injection of TZIM while maintaining moderate WHPs. The highest WHP achieved with series operation was approximately 16.7 MPa (2,422 psi).

3.2.4 PUMP CURVES / OPERATIONS

The stimulation pumps were operated in such a way that flow rates and WHPs were maintained within the pumps' optimum performance parameters (i.e., the pump performance curve). Pump operations were guided by the pump curves provided by Baker Hughes (Figure 3-4). To safely reach the pressures needed to stimulate the well, the outlet flow from the pumps had to be higher than could be injected into the well. This design challenge was overcome by installing a flow bypass manifold which allowed the extra flow needed to run the pumps within the optimal conditions. When flow down the well was not high enough, water was discharged through the bypass line to the northern (smaller) end of the sump for recycle. When the pumps were not behaving erratically because of variable frequency drive failure, they generally operated within the optimal zone defined by the pump curves. Figure 3-4 illustrates smoothly operating pump conditions over a 30-hour period when both stimulation pumps were run in series. Points on the graphs refer to samples taken from time of operations. The bottom graph in the figure shows both pressure and flow rate as a function of time. The upper graph shows the relation of WHP to flow rate. An optimized pumping zone is bounded by two black lines. The red line shows the ideal operations curve for running these pumps in series.

3.2.5 LESSONS LEARNED

Freezing conditions could come at unexpected times and cause significant operational down time. A cold weather mitigation plan should be in place and installed well in advance of when cold weather is projected. Furthermore, procedures should be in place to ensure that foreign material is not allowed to enter pump intakes, particularly when withdrawing water from exposed sources, such as a sump. During

initial pump operations it may be pertinent to maintain a pump subcontractor on-site to diagnose initial pump issues until operations proceed smoothly.

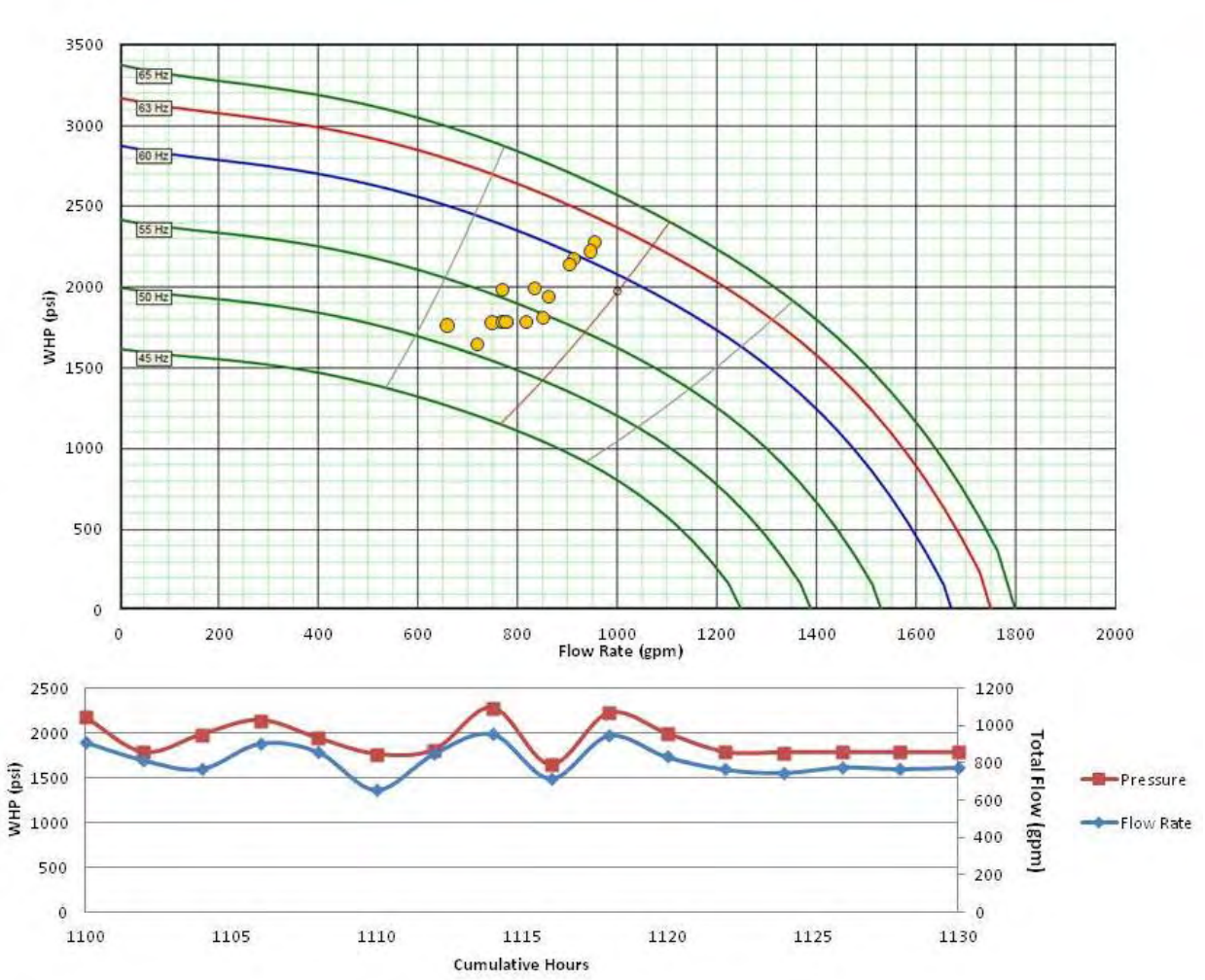

Figure 3-4. Stimulation pump performance curves and operating conditions.

3.3 WATER SUPPLY PERFORMANCE

3.3.1 WATER WELL PERFORMANCE

The primary water source for the Newberry EGS Demonstration Project came from the water well located on Pad S-29. This well was drilled by Abbas Well Drilling in March, 2008, and reached a total depth of 177.6 m (583 ft). The depth to ground water in water well 29 is approximately 98.8 m (324 ft) below ground surface. The well has approximately 61 m (200 ft) of available drawdown before the dynamic water level will reach the minimum required for proper pump operation. A three day drawdown test conducted on water well 29 in 2011 extrapolated a drawdown of only 7.6 m (25 ft) with sustained 21 day pumping. Previous drawdown testing also showed quick aquifer recovery post pump shut-in, indicating adequate reservoir conductivity to sustain Pad S-29 water usage during stimulation. Despite the water well being a fairly reliable source of water, a pipeline connecting Pad S-29 to the water well on Pad S-16 was built as a contingency (see Section 2.8). The potential problems with relying on one well were both well pump failure and a need for a water supply rate of more than 41 L/s (650 gal/min), the maximum output for the water well on Pad S-29. If more than 41 L/s (650 gal/min) were flowing into well NWG 55-29, the pipeline

would provide the extra water necessary to keep operations running. During the course of operations flow into the well never reached greater than 25 L/s (400 gal/min) and the water well had no significant problems; therefore the backup pipeline was never used.

3.3.2 PERFORMANCE OF INITIAL CONFIGURATION

Initially, Pad S-29 was setup with 1,875,710 L (20,000 gal) bi-level water storage tanks to serve as a supply reservoir for the booster pumps. This buffer was designed both to minimize any water well supply problems and also prevent the need to continuously adjust the well pump to meet the stimulation pump intake needs. However, holding tank buffer system performance was poor. The pressure loss due to friction created low intake pressure to the booster pumps during the early stages of stimulation. Evidence suggested air was leaking into the water supply pipeline, and on some occasions when the booster pumps were purged, air would rush out over the course of a few seconds. The flexible supply lines visibly collapsed at times, indicating vacuum conditions inside the line. Much effort was made during operational downtime to fix couplings, replace sections of lines and fix valves, but the problem persisted and an alternate water supply buffer system was needed. It was determined that the 4-inch supply hoses leading from the storage tanks were too small and that pressure loss to friction were too great.

3.3.3 PERFORMANCE OF SECOND CONFIGURATION

It was decided on October 18 to disconnect the storage tanks and use the north end of the Pad S-29 sump as a buffer. On October 20, a submersible pump was installed in the northern end of the sump and connected to the booster pumps, which resolved the air leak problem. Figure 3-5 illustrates the configuration; the pump was connected to the booster pumps via the green hose, and the water level in the sump was maintained by input from the Pad S-29 water well through the blue hose.

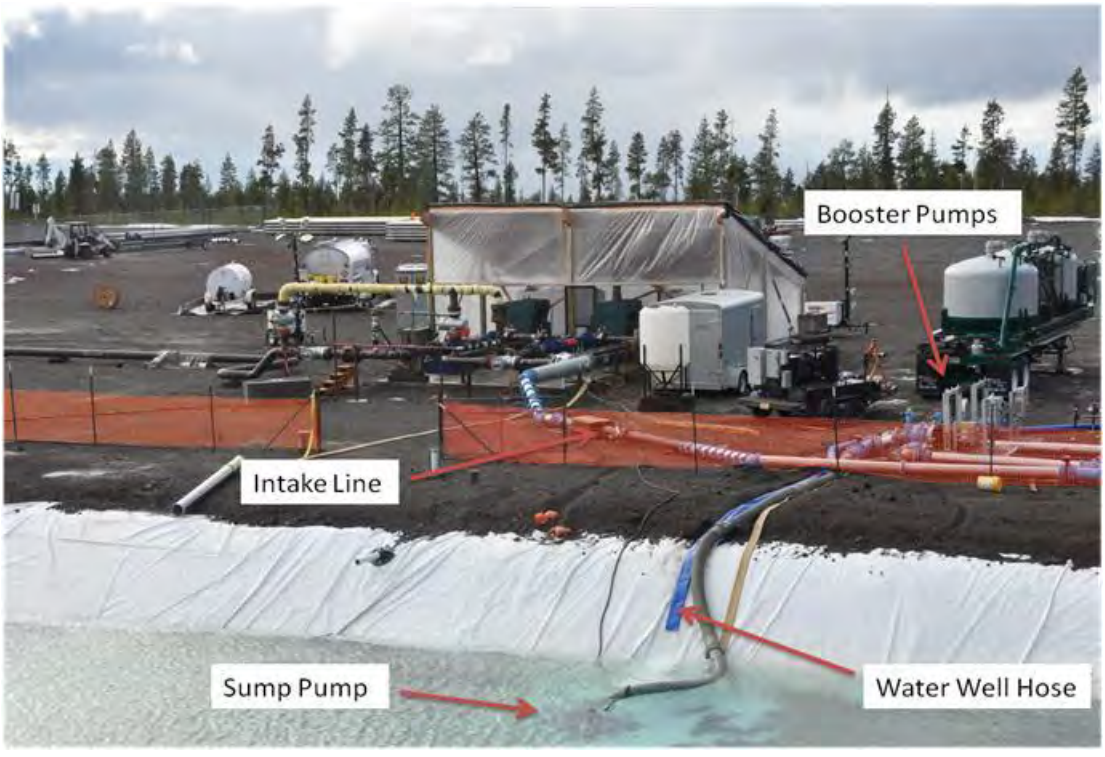

Figure 3-5. Picture of the second water supply configuration.

On October 21, Booster Pump 2 tripped and failed to restart. After installation of the sump pump, the intake pressure to the booster pumps was considerably higher than it had been before. Before tripping,

Booster Pump 2 had been running at a high temperature, with steam visibly escaping from the purge valve. The inevitable failure of this pump led to the discovery that although the two booster pumps were the same model, they were made in different years and were rated to operate at different pressures. The pumps were run in parallel, causing Booster Pump 2, with the lower pressure rating, to unknowingly operate outside the manufacturer's operational threshold for pressure.

A new booster pump was installed on October 24. The pump worked reasonably well at first but began leaking the following day. A hose was installed to collect the leaking water and drain it into the sump. Minor repairs were carried out, but the leak was never fully abated.

3.3.4 LESSONS LEARNED

Performing a three day drawdown test prior to using the water well on Pad S-29 for stimulation was an effective means of assessing well performance and water supply potential over the extended time period anticipated for stimulation. The water supply to stimulation pumps should be protected from particulates; installation of protective screens can prevent particulate matter and large objects from entering the pump systems and causing damage. Water storage tanks may provide an effective buffer to regulate pump intake pressures. However, the potential pressure loss due to friction and air leaks must be taken into account when designing a buffer tank system. Furthermore, the low-pressure booster system must be closely inspected while the subcontractor is on site to ensure it has been installed correctly and with the right equipment.

3.4 DISTRIBUTED TEMPERATURE SENSING

3.4.1 BACKGROUND ON DTS ACQUISITION

Distributed Temperature Sensing (DTS) provides essential information about the depth of fracture initiation and the success or failure of the TZIM in sealing fractures. AltaRock obtained a high-temperature Schlumberger DTS system in 2010. This DTS contains one multi-mode, high-temperature 50/125 fiber with carbon polyimide coating (Table 3-1). The 3,810 m (12,500 ft) DTS fiber is enclosed in 316 L stainless steel capillary tubing that has been temperature hardened. In 2012, this DTS unit was deployed in a low-temperature well and signal loss was noted towards the end of the operation. Plans were then made to purchase a back-up DTS for the Newberry stimulation in case the existing cable failed. Various vendors including Halliburton, Schlumberger, Silixa, and Core Lab were invited to provide support on the project, but all these vendors failed to bid. BMP Enterprises, a company in Houston referred by Core Lab was the only company to submit a bid that included supplying a back-up high-temperature cable, DTS signal capture box with software, and DTS field deployment.

The Schlumberger DTS was then shipped to BMP in September for calibration and testing. During the optical Time Domain Reflectometry (OTDR) shots, the DTS only displayed 2,552 m (8,372.7 ft) signal and the fiber was difficult to splice due to its brittleness. Damage was likely caused during storage and transportation. The original back-up cable was still being manufactured, as new cable with length greater than 3,500 m (11,483 ft) usually requires 10-12 weeks to complete. In the meantime, efforts were made to find another back-up high-temperature DTS tool.

Table 3-1. Description of DTS cables owned or obtained by AltaRock Energy.

Cable Type	Fiber Type	Annulus Fill	Tube Type
Schlumberger DTS	1 single mode fiber	No gel	316L cap tube enclosure
AFL DTS VHM3000	3 fiber (1 single mode, 2 multi-mode)	No gel	316L outer tube with aluminum inner tube
BMP Enterprise DTS VHM5000	3 fiber (1 single mode, 2 multi-mode)	Gel filled	Incoloy 825 outer tube with 304SS inner tube

3.4.2 DEPLOYMENT AND RESULTS OF FIRST DTS

A high-temperature VHM 3000 DTS cable approximately 3,000 m (9,843 ft) in length, with three optical fibers, was available through AFL before the planned start date. This cable was obtained and then deployed on October 17; it lasted until November 24, when signal loss was significant enough that it needed to be pulled from the well. DTS contour visualizations of Stage 1 stimulation show that one main interval, between 2,880 m (9,448.8 ft) and 2,950 m (9,678.4 ft), took the majority of the injected water (Figure 3-6).

Maximum cooling was achieved between hours 300 and 350, when injection pressure was approximately 14 MPa (2,030.5 psi). The gradient below 2,890 m (9,481.6 ft) during high pressure pumping increased, indicating an increasing amount of fluid exiting below 2,890 m (9,481.6). Separations seen within the 2,880-2,950 m (9,481.6-9,678.4 ft) interval of the gradient plot suggest that multiple permeable fractures are taking fluid. Several other zones such as 2,550 m (8,366 ft) 2,670 m (8,760 ft) and 2,850 m (9,350 ft) also showed periodic changes in temperature gradient, suggesting minor fluid loss during stimulation. Signal loss was noted starting on November 8, suggesting higher temperatures were deteriorating the fiber optic cable at depth.

3.4.3 DEPLOYMENT AND RESULTS OF SECOND DTS

In order to complete stimulation Stages 2 and 3 with a functional DTS, the decision was made to deploy the newly available high-temperature DTS purchased from BMP. This cable consists of 3 fibers, and has a nested tube design with gel-filled interstices. The previous cable was pulled on November 24 and the new cable was installed on November 25. The main fluid exit intervals were not monitored during stages II and III of stimulation because of the inability to lower the new DTS below 2,090 m (6,857 ft), (refer to Section 3.4.3). Contour plots of Stage 2 (Figure 3-7) indicate that during stimulation a permeable interval beginning at approximately 2,080 m (6,824 ft) was taking fluid. This zone is marked by strong changes in temperature gradient and located more than 100 m (328 ft) below the casing shoe. Other zones at 2,040 m (6,693 ft) and 2,060 m (6,759 ft) also showed small changes in temperature gradient. These were not stimulated fractures, but were most likely minor permeable zones that reached temperature equilibrium as high pressure injection continued.

One goal of the second TZIM treatment on December 3 was to seal the permeable zone at 2,080 m (6,824 ft). The decrease in the temperature gradient between 2,080-2,090 m (6,824-6,857 ft) following TZIM injection indicated successful occlusion of the reservoir fractures. The constant gradient sustained through the duration of Stage 3 stimulation and heat-up further validated the effectiveness of TZIM.

3.4.4 LESSONS LEARNED

Have a plan in place to cool off the DTS during times when the stimulation pumps are turned off. Overheating of the DTS will quickly cause signal distortion and tool failure.

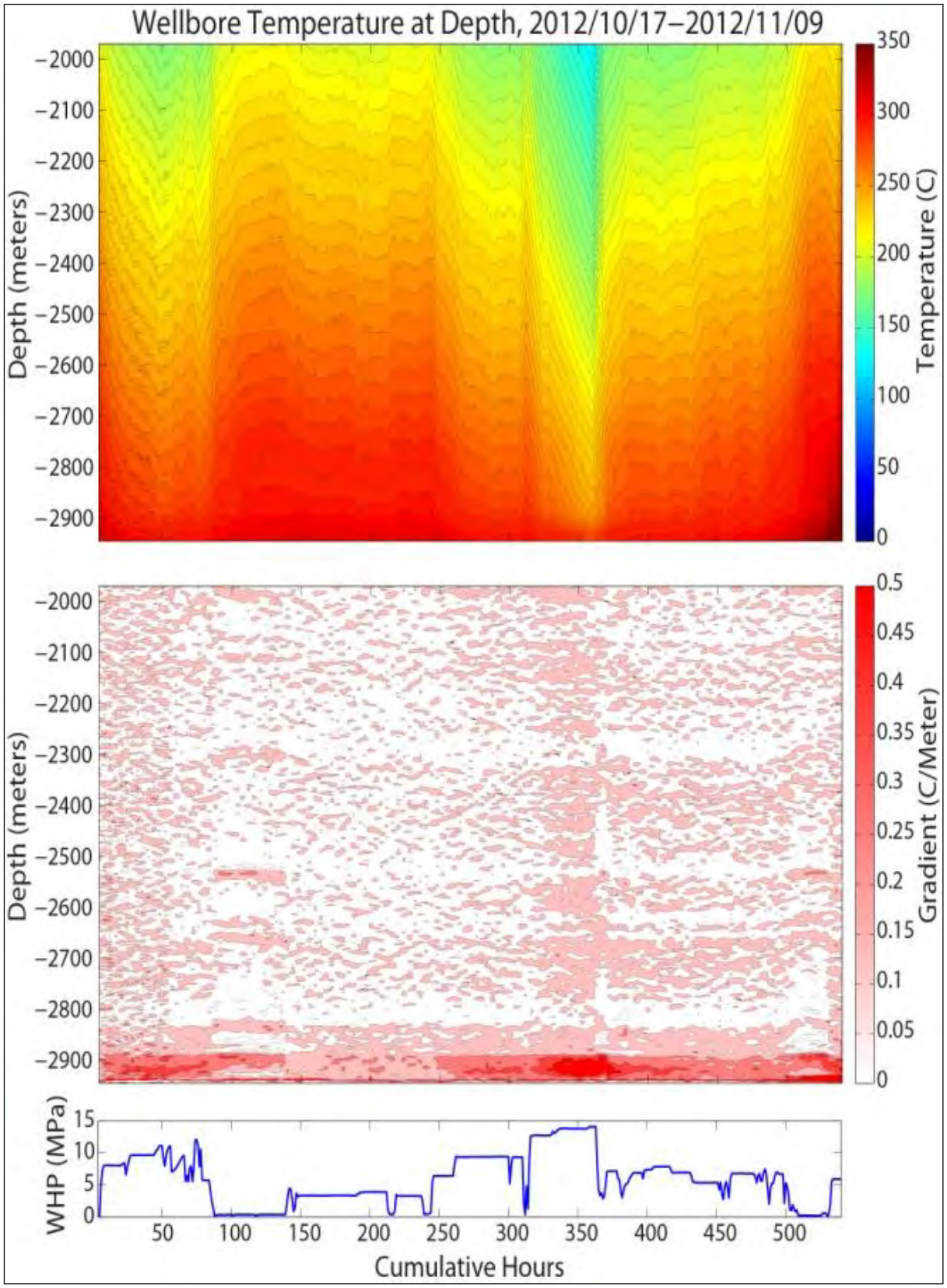

Figure 3-6. DTS visualization showing the temperature contour (upper graph) and gradient (lower graph) with depth and time. The bottom graph shows WHP as a function of time.

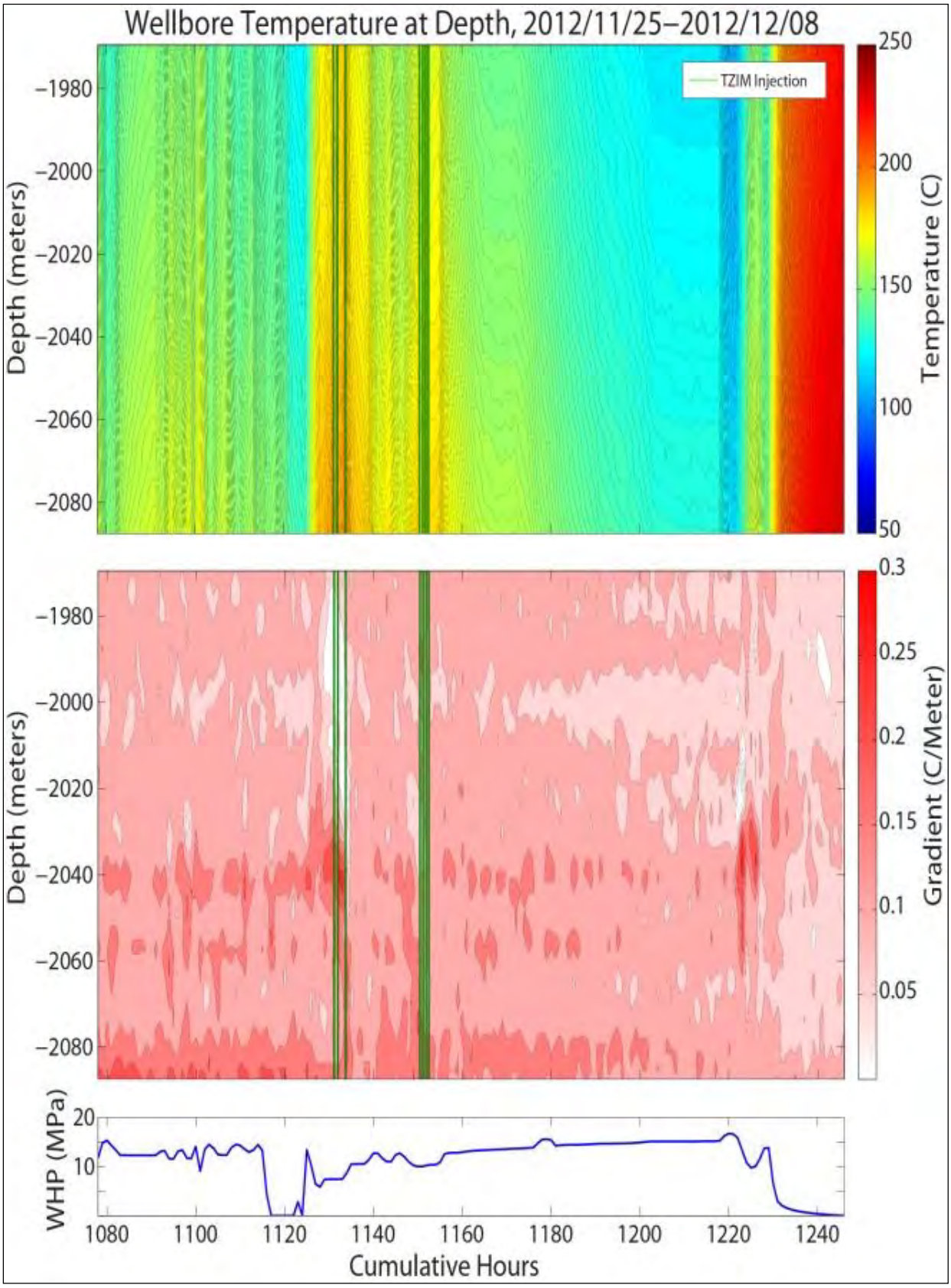

Figure 3-7. DTS visualization showing temperature contour and gradient and WHP for stimulation Stages 2 and 3 and; graphs included TZIM injection (vertical green lines).

3.5 WELLBORE CONDITION AT APPROXIMATELY 6850 FEET BGS

3.5.1 INTIAL ENCOUNTER WITH POTENITAL WASHOUT DOWN HOLE

On November 23, the first DTS used during stimulation was pulled out of the hole due to significant signal loss near the bottom of the well. During this time stimulation was temporarily stalled due to stimulation pump failure. Another DTS was installed on November 25, preceding the recommencement of stimulation. Two sinker bars were installed on to the end of the DTS prior to the first down-hole run. This was done because of a potential ledge which was encountered during the installation of the first DTS. After having trouble getting past a zone at approximately 2,088 m (6,850 ft) the first DTS was pulled out of the hole and three sinker bars were installed. With the sinker bars installed, the first DTS was able to make it past this zone. However, even with three sinker bars installed the second DTS cable was not able pass the zone at 2,088 m (6,850 ft). The cable was pulled out of the hole and a centralizer was installed at the end of the sinker bars. With the centralizer installed the DTS cable was still unable to make it past the same interval. After attempting to get past this potential ledge several times, the decision was made to begin stimulation with the DTS installed to a depth of 2,091 m (6,860 ft).

3.5.2 LOST SINKER BARS AND CENTRALIZER DOWN HOLE

After completing stimulation, the second DTS cable was pulled out of NWG 55-29 on the night of December 8. Initial removal of the DTS went well. However, during the removal of the lubricator the three sinker bars and centralizer were dropped down the hole. The lubricator allows a DTS cable to be connected to instrumentation on the surface while maintaining WHP. This lubricator was roughly 4.6 m (15 ft) tall and connected to the top of the wellhead. Three sinker bars and a centralizer should have been able to fit within the lubricator. The plan was to pull the sinker bars and centralizer into the lubricator and then remove the lubricator using a boom crane. Temperatures on the night of the lubricator's removal were below freezing, and as a consequence the lubricator was filled with ice with only enough room for the DTS cable to pass through (Figure 3-8). The lubricator, therefore, had to be removed with 4.6 m (15 ft) of sinker bar and centralizer hanging from its base. This meant that roughly thirty feet of material had to be removed from a wellhead standing 3 m (10 ft) tall. In order to accomplish this, the boom crane was strapped to just above the middle of the lubricator. The boom crane was roughly 12 m (40 ft) tall, making this operation complex. Using this configuration the lubricator and most of the sinker bars were removed from the wellhead. However, as the last sinker bar came out of the well the DTS cable snapped at the base of the lubricator, sending all three sinker bars and centralizer down the well. It appeared that there was too much torque impingent on the cable and that this eventually led to its failure.

Figure 3-8. Left: ice in the lubricator after removal. Right: the lubricator on top of the wellhead (thin green object) and boom crane with basket.

3.5.3 CHARACTERIZING THE WASHOUT

In the next phase of the Demonstration, a borehole televiewer will be run down NWG 55-29 to look for signs of improved fracture aperture. For the borehole televiewer to be run, the location of the fish (the sinker bar and centralizer) down hole needs to be known. The borehole televiewer operator will not run the instrument down hole if the location of the fish is unknown. The tool may get lost down hole if it gets entangled with the centralizer. Two locations for the fish have been proposed; one at the bottom of the hole and the other at the zone where consistent problems were encountered at 2,088 m (6,850 ft). Characterization of the 2,088 m (6,850 ft) zone began with a review of the bore hole drilling mud log and the original borehole televiewer data.

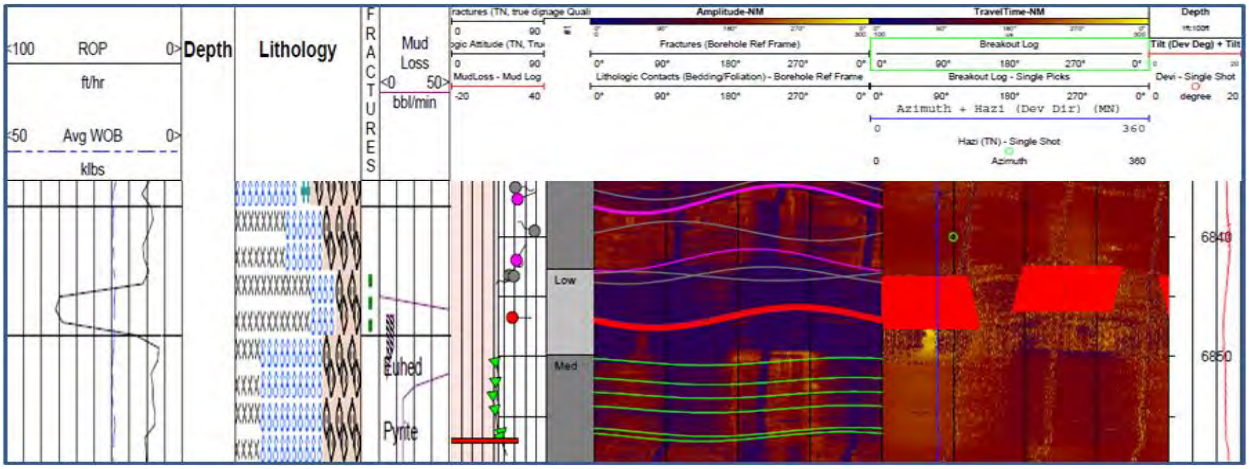

Figure 3-9. Comparison of borehole televiewer and mud log data over the problematic interval. Interval located in region with basalt, black crosses, dacite, blue, and crystalline tuff, pink.

Data show a major fracture located in the zone where DTS deployment had consistent problems. Figure 3-9 shows a side comparison of borehole televiewer data with mud log data over the depth interval where problems were encountered with the DTS. Areas of significant mud loss, rate of penetration, and a significant fracture on the borehole televiewer are all aligned. This fracture is located at 2,088 m (6,850 ft) depth and appears to be open as evident from the significant mud losses associated with the zone (Figure 3-9). The fracture is located along the boundary of what appears to be a dike. As described in the NWG 55-29 mud log the dike was 'Dark gray, very hard and brittle, very little alteration; cross-cuts Tuff with small cryptocrystalline chill margin; contains disseminated pyrite.' Surrounding this dyke was an altered tuff which was 'grayish-green; moderately hard with crunchy to tough tenacity; matrix strongly overprinted with alteration; alteration includes chlorite, epidote, calcite and pyrite.' From this data it is clear that the dyke material was much harder than the surrounding altered tuff. Mud log data appear to indicate that the most probable cause for the ledge at 2,088 m (6,850 ft) is washout occurring during stimulation. A model of the probable downhole conditions was created to get a better idea of how to retrieve the fish potentially stuck in this zone (Figure 3-10).

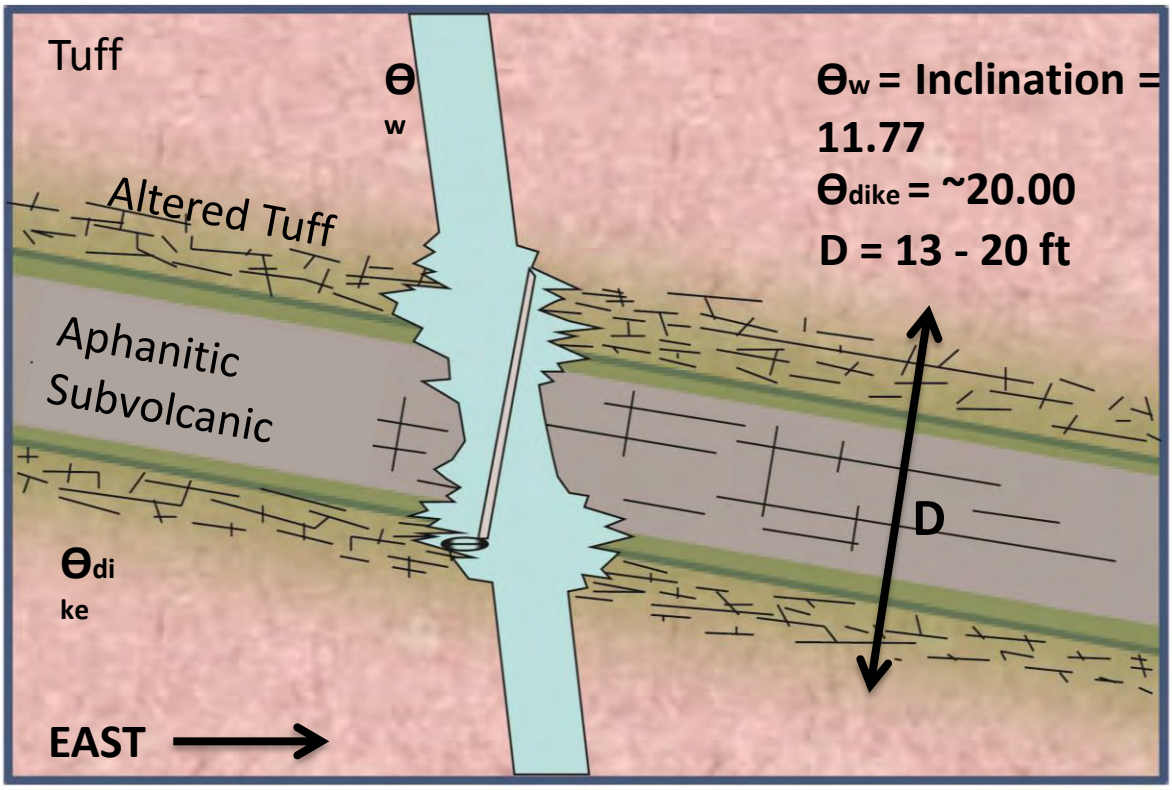

Figure 3-10. Model of the ledge at 2,088 m (6,850 ft). Well inclination was taken from survey data. Strike and dip of aphanitic subvolcanic material was taken from borehole televiewer interpretation. Formation thickness derived from mud log and borehole televiewer data.

3.5.4 LESSONS LEARNED

Again, late season cold weather was problematic. In the course of water injection through the wellhead apparatus and into the wellbore, water and water vapor circulated to all regions of the wellhead apparatus, including the DTS lubricator assembly. In low flow regions of the wellhead, water froze when ambient temperature was below freezing for extended periods. This was the precursor to the DTS cable failure during removal. The lubricator mast was found to be packed with ice to the extent that the sinker bars could not be further extracted from the wellbore. A plan to maintain above-freezing conditions in the wellhead assembly and lubricator tower (with insulation and heat tracing) needs to be in place. Alternatively, if weather is freezing, plan on removing the DTS as soon as stimulation ends. Freezing of the lubricator caused significant trouble and was ultimately responsible for the fish falling down the hole.

3.6 WELL HEAD PRESSURE, FLOW, DIVERTER INJECTION, AND MULTISTAGE STIMULATION

3.6.1 STEP RATE TEST

The stimulation started with a step-rate injection test in order to assess the pre-stimulation parameters and determine hydroshearing initiation pressure (Figure 3-11). Injectivity calculated during the step-rate test averaged 0.37 L/s/MPa (0.04 gpm/psi), which was equivalent to the injectivity and flow testing values measured after drilling in 2008. The highest WHP obtained during the injectivity test was 12.2 MPa (1,770 psi) with 5.5 L/s (87 gpm) injected down hole. Shortly after this critical WHP was reached during the step rate test, the stimulation pumps experienced a series of start-up issues due to malfunctions with the electrical drive.

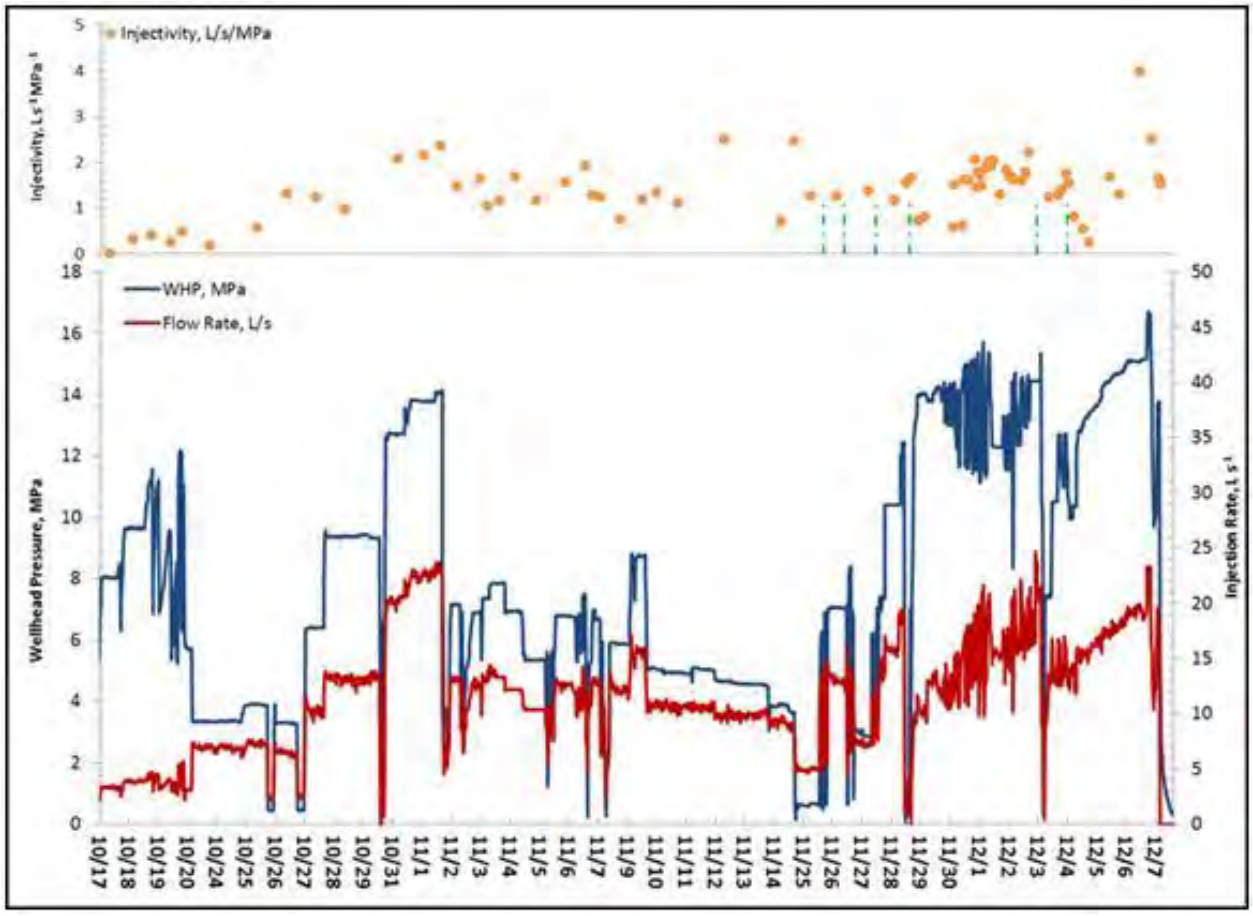

Figure 3-11. Injection well NWG 55-29 stimulation parameters. Pressure (blue) and injection rate (red). Calculated injectivity (orange) and TZIM injection (green). Gap in timeline is when stimulation pumps were offline.

3.6.2 STIMULATION STAGE 1

Stage 1 stimulation began after the step rate test and calibration of the stimulation pumping system on October 27. Injectivity improved when injection pressure exceeded 12.4 MPa (1,798 psi) and the corresponding flow rate reached 20.6 L/s (326 gpm). The improved injectivity rate remained stable with moderate pressure injection until November 14. By November 14, continuing drive, pump and DTS issues needed to be addressed and a two week break was taken during which only booster pumps moved water down hole. On November 25, both stimulation pumps were reinstalled and returned to normal operating conditions. When installing the DTS, however, an obstruction at approximately 2,090 m (6,857 ft) down hole was encountered and prevented the DTS from being lowered deeper. The improvement in injectivity during stimulation Stage 1 was approximately 2 L/s/MPa (0.21 gpm/psi).

3.6.3 STIMULATION STAGE 2

Stage 2 of the stimulation started with injection of lithium chloride (LiCl) salt as a tracer on November 24 (Section 3.7.1), followed by 6 pills of TZIM from November 25 to 28. Approximately 1,340 kg (2,954 lbs) of TZIM were injected over the period of 4 days (Figure 3-12; Table 3-2). After the first pill was injected, the rate of water injection decreased slightly while WHP remained relatively constant. The second, third, fourth and fifth pills were injected over the next two days, while varying the concentration and particle size distribution. Pills one through five consisted mostly of fine grained TZIM, a result of having to get through the injection filter mesh, which was used to protect the stimulation pumps. To test the

effectiveness of the coarse TZIM, the blending unit was disconnected from the Stimulation Pump inlet and connected directly to the wellhead on November 28. After 206 kg (454 lbs) of coarse blend TZIM was injected, the WHP increased beyond the pressure rating of the batch mixer blending unit 1.38 MPa (200 psi). When the stimulation pumps were restarted the injection rate decreased to approximately 9.5 L/s (150 gpm) at 13.8 MPa (2,002 psi). The decrease in injectivity as a result of TZIM injection indicated that the fracture zones enhanced in Stage 1 had been at least 50% blocked and marked the beginning of stimulation of new zones in the wellbore. WHP was maintained at 14 MPa (2,031 psi) with approximately 9 L/s (144 gpm) injection rate overnight. Onset of hydroshearing was noted on November 29, when slight decrease in WHP occurred in conjunction with 4 L/s (60 gpm) increase in injection rate.

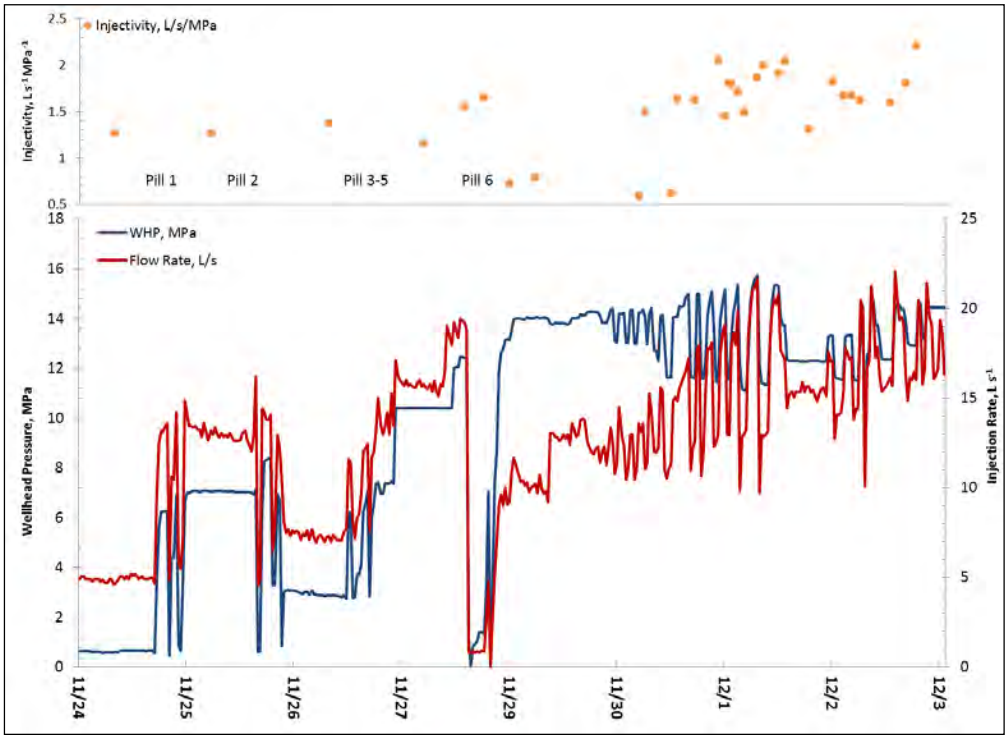

Figure 3-12. TZIM injection and Stage 2 stimulation. Showing pressure (blue), injection rate (red) and calculated injectivity (orange).

In this second stage of stimulation, WHP cycled between 12.4 and 15.2 MPa (1,798-2,205 psi). The pressure cycling method seemed to improve injectivity over time; over the course of the next five days the injectivity of Stage 2 improved from 0.7 L/s/MPa (0.08 gpm/psi) to 2.2 L/s/MPa (0.24 gpm/psi). On December 3, the flow rate reached 19.4 L/s (307 gpm) with a 14.3 MPa (2,049 psi) corresponding WHP.

3.6.4 STIMULATION STAGE 3

Stage 3 of the stimulation began after the second phase of TZIM treatment, pumping 8 pills over two days starting on December 3 (Figure 3-13; Table 3-2). Total TZIM injected in this phase was 1,451.5 kg (3,200 lbs). Four consecutive pills were pumped each day. The flow rate decreased and WHP increased overnight after both TZIM injection efforts. After TZIM application the injectivity decreased to 0.26 L/s/MPa (0.03 gpm/psi). The well responses for the second diversion are shown in Figure 3-13. The WHP for Stage 3 was slowly ramped up over time from 13.3 to 16.7 MPa (1,929 to 2,422 psi). This operation strategy increased injectivity to 2.5 L/s/MPa (0.27 gpm/psi). Stimulation pumping in Stage 3 continued until December 7. That night, cesium bromide (CsBr) salt tracer was injected (Section 3.7.2), and the well was shut-in and allowed to heat-up post-stimulation. The WHP fall-off data was recorded and analyzed. The improvement

in injectivity was found to be approximately 1.3 L/s/MPa (0.14 gpm/psi) during Stage 3 stimulation. The transmissivity was calculated to be 6.46E-13 m^3 (2,147 mD-ft). Assuming a reservoir height of 200 m per stage as presented in Cladouhos et al. (2011), the equivalent permeability is 3.23E-15 m^2 (3.27 mD). Post shut-in, the well did not build static WHP. Attempts were made to lift the well and initiate flow, but winter weather (significant snow accumulation; freezing temperatures) and well conditions (suspected break in the PAS line) made it impossible to successfully flow test the well.

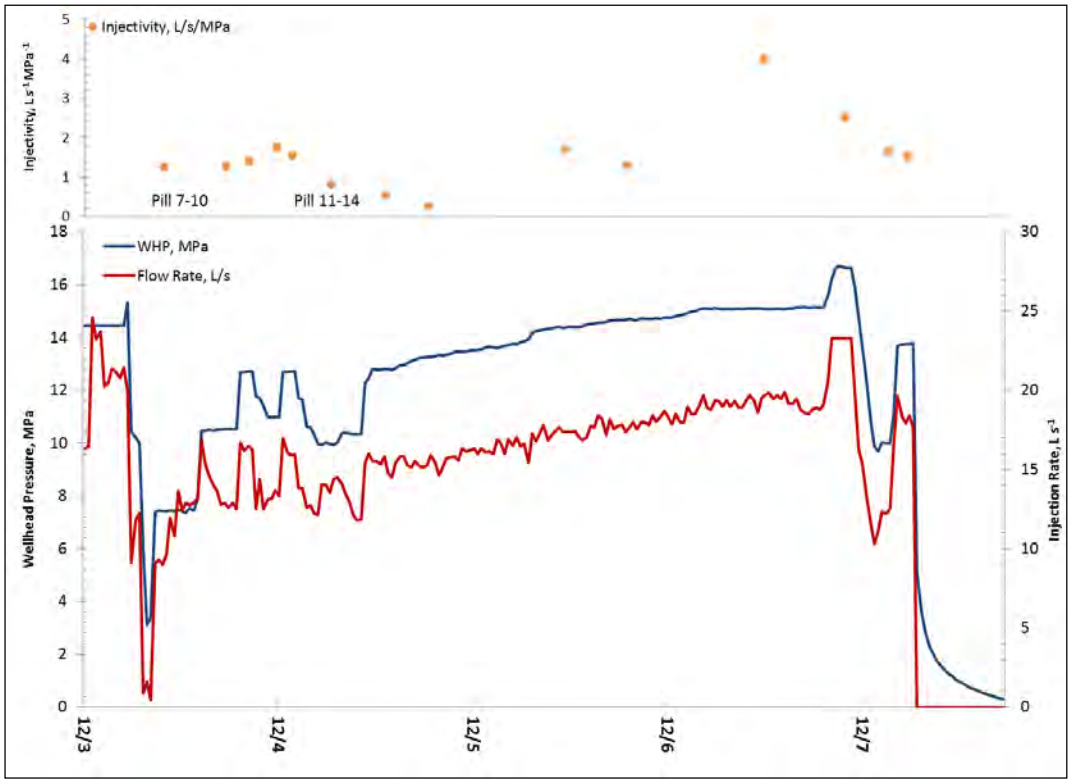

Figure 3-13. Second TZIM injection and Stage 3 stimulation: pressure (blue), injection rate (red) and calculated injectivity (orange).

Table 3-2. Diverter pill injection mass size and timing.

Pill Number	Stimulation Stages	Amount Injected (pounds)	Date and Time of Injection
Pill 1	1-2	200	11/25/2012 19:20
Pill 2	1-2	450	11/26/2012 12:17
Pill 3	1-2	500	11/27/2012 18:00
Pill 4	1-2	400	11/27/2012 19:40
Pill 5	1-2	400	11/27/2012 21:00
Pill 6	1-2	1000	11/28/2012 18:00
Pill 7	2-3	400	12/3/2012 16:52
Pill 8	2-3	400	12/3/2012 17:43
Pill 9	2-3	400	12/3/2012 18:42
Pill 10	2-3	400	12/3/2012 19:29
Pill 11	2-3	400	12/4/2012 12:11
Pill 12	2-3	400	12/4/2012 12:55
Pill 13	2-3	400	12/4/2012 13:35
Pill 14	2-3	400	12/4/2012 14:10

3.6.5 LESSIONS LEARNED

During the stimulation the power to the ultrasonic flow meter went out and the calibration for the meter was reset automatically. For a period of time the flow was not matching the flow being registered by the manual flow gauges on the pump inlet side. Once this was discovered the flow meter was recalibrated and checked by redirecting by-pass flow from the sump to the weir box to validate the values being measured. Going forward, flow should always be validated by using the weir box flow at regular time intervals; on the order of once a day.

3.7 TRACER INJECTION

Conservative and reactive tracers were injected in three distinct episodes, each following a period of hydraulic stimulation. Lithium chloride (LiCl) and cesium bromide (CsBr) were used as reactive tracers because they will adsorb to the rock surfaces at these temperatures. These tracers are stable at reservoir temperatures, and once they have reacted with the rock surfaces the excess tracer material should remain in the geofluid until a flow test can be initiated. Three different naphthalene disulfonic acids (NDS) were used as conservative tracers because they will not react with the rock surfaces and they do not thermally degrade. These tracers are also stable at reservoir temperatures, and the tracer material should remain in the geofluid until a flow test can be initiated. Tracers were injected following at the end of each stimulation Stage, and TZIM diverter materials were injected immediately after tracer injection in the first two stimulation Stages.

3.7.1 FIRST TRACER INJECTION

On October 21, 120 kg (264.6 lbs) of LiCl and 25 kg (55.1 lbs) of the disodium salt 1,5-naphthalene disulfonate(1,5-NDS) were added to 1,892.7 L (500 gal) of water. The solution was recirculated to ensure complete dissolution of the tracer salts. At 22:30, injection of the solution was initiated into the intake of the booster pump and maintained at a rate of 4.5 L/min (1.2 gpm) for the next 7 hours. The flow rate through the booster pump and into NWG 55-29 was approximately 295 L/min (78 gpm). By 05:30 on

October 25, all 1,892.7 L (500 gal) of tracer solution had been pumped into the wellbore. Several wellbore volumes of water were then used to flush the well before pumping the first diverter pill down hole.

3.7.2 SECOND TRACER INJECTION

On December 3, 25 kg (55.1 lbs) of the disodium salt of 1,6-NDS was added to approximately 6,057 L (1,600 gal) of water, which was recirculated to insure complete mixing. The solution was then injected into NWG 55-29 between 14:45 and 15:30 at a rate of approximately 132 L/min (35 gpm). After flushing with the equivalent of one wellbore of fresh water, the second diverter pill was pumped down hole.

3.7.3 THIRD TRACER INJECTION

Following the third stimulation episode, a third tracer injection was conducted. On December 7, 40 kg (88.2 lbs) of CsBr and 25 kg (55.1 lbs) of the disodium salt of 2,6-NDS were added to 1,892.7 L (500 gal) of water. The solution was recirculated to ensure complete dissolution of the tracer salts. At 15:50, the tracer solution was pumped into the injection line at a rate of approximately 45 L/min (12 gpm). By 16:30, the tank had emptied and was immediately flushed with an additional 1,892.7 L (500 gal) of fresh water. During the tracer injection, the total flow rate into NWG 55-29 was approximately 871 L/min (230 gpm).

3.7.4 BOREHOLE FLUORIMETER DEPLOYMENT

An obstruction has developed in NWG 55-29 at approximately 2,103 m (6,900 ft) which prevents the deployment of not only the DTS capillary tubing but also any wireline tools, including the borehole fluorimeter. In addition, harsh weather conditions ended the stimulation campaign prematurely, and an opportunity to clear the obstruction and deploy the borehole fluorimeter was not presented.

3.7.5 LESSONS LEARNED

The tracer injection process went smoothly and coordination with the teaming partners went well.

3.8 MICROSEISMICITY

Injection into NWG 55-29 began October 17 and the first micro-earthquake located in the EGS stimulation zone occurred October 29. Micro-seismicity in the EGS zone continued for 4 months, with the last confirmed event February 18, 2013. Preliminary locations were determined for 174 micro-seismic events, usually within 8 hours of the event's occurrence. Twelve seismicity reports, discussing the locations and depths of seismic events and performance of the MSA were prepared and emailed during the stimulation (Appendix D). The *Interactive Map of Earthquakes at the Newberry Caldera* hosted at LBNL (LBNL, 2013) and the *Volcano Seismicity* site hosted by the Pacific Northwest Seismic Network (PNSN, 2013) also displayed the locations of Newberry Volcano EGS induced events, usually within 12 hours. The speed and accuracy of these two public sites reduced the need for AltaRock-issued seismicity reports.

The summary results discussed below are shown in Figure 3-14. Prior to November 25 the changes in WHP were due to stimulation pump issues. After November 25, WHP changes were intentional. The vertical bars delineate the begining (green) and end (dark red) times for the two TZIM batches.

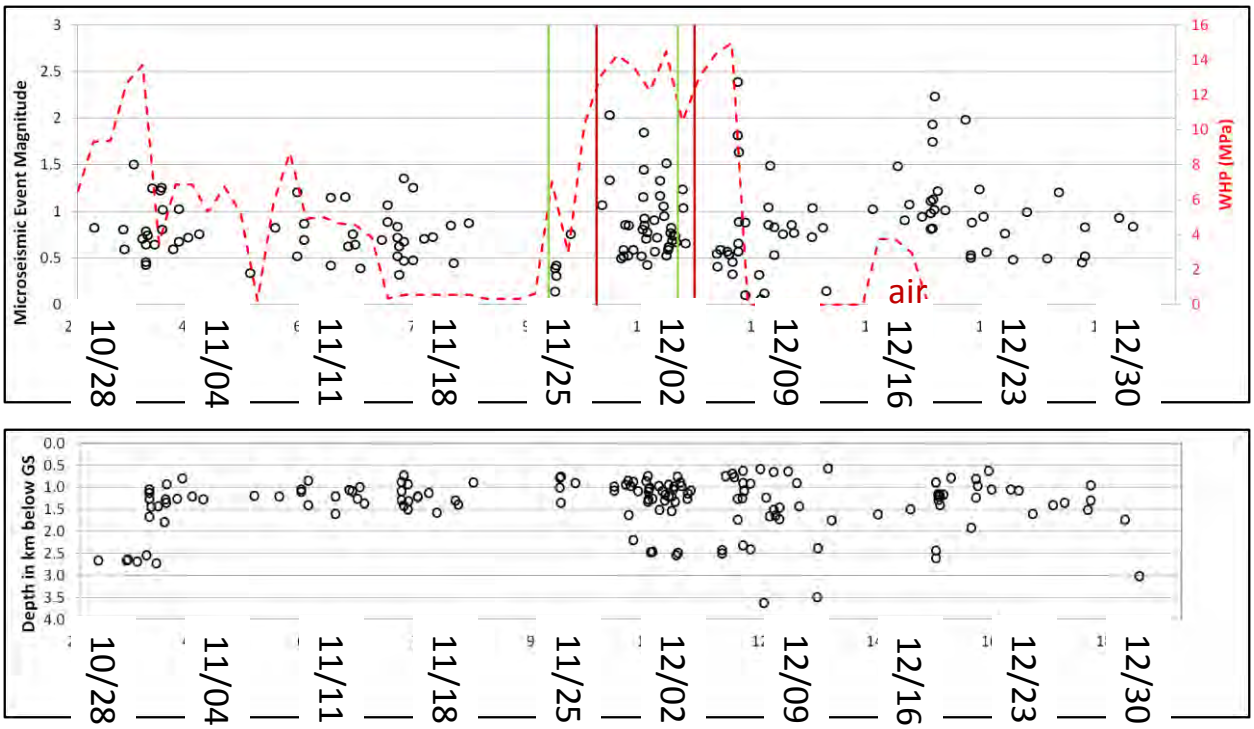

Figure 3-14. Magnitudes (top) and depths (bottom) of microseismic events with time compared to WHP (dashed red line).

3.8.1 WELL HEAD PRESSURE AND HYDROSHEARING

During step-rate testing October 18-20, the well head pressure (WHP) exceeded 12 MPa (1,740 psi) for 3 hours. This was insufficient time or pressure to initiate hydroshearing. Due to stimulation pump problems, the WHP did not exceed 9 MPa (1,305 psi) again until October 28. After 12 hours at 9.3 MPa (1,349 psi), the first definite micro-earthquake in the EGS stimulation zone occurred near the injection well bore at a depth of approximately 2.4 km (7,874 ft), consistent with a temperature deflection on the DTS (Petty et al., 2013). Forty-two hours passed until the next event occurred, by which time the WHP had been increased to 12.5 MPa (1,813 psi). Six events followed, indicating that sustained pressure over 12 MPa (1,740 psi) is required to cause sustained hydroshearing at depth in this well.

After November 1, problems with one of the stimulation pumps necessitated lower pressures, approximately 5 MPa (725 psi) for two weeks and approximately 0.5 MPa (72.5 psi) for 10 days (Figure 3-14). During the lower WHP period, micro-seismicity continued for 19 days after WHP dropped below 12 MPa (1,740 psi). When the stimulation pumps were fully repaired, November 25, seismicity re-initiated at the lower pressure of 7 MPa (1,015 psi).

A maximum WHP of 16.7 MPa (2,422 psi) was reached December 7, and the well was shut-in that same day. The seismicity rate dropped over the following week. After the well was pressured up to 3.9 MPa (565.6 psi) with an air compressor on December 16, in an attempt to flow the well, seismicity increased, similar to the re-initiation of seismicity on November 25.

3.8.2 LOCATIONS

Seismic events during stimulation were located automatically in real time by software that detected seismic signals observed from all the seismometers simultaneously, and that had clear enough P- and S-waves in order to locate them in proximity to the well. The MSA network functioned well during

stimulation and post-stimulation, although borehole stations returned significantly higher quality P- and S-wave data than surface stations. This is likely due to waveform attenuation by unconsolidated material (typically volcanic cinders, ash and pumice) surrounding the shallow surface stations. Further discussion of MSA performance is provided in Section 3 of Appendix G. Events automatically detected by the software were then reviewed by seismologists in order to qualitatively adjust the P- and S-wave arrival times as an initial analysis of the event locations. Figure 3-15 shows the events that were qualitatively located during stimulation for various stages of injection/diversion.

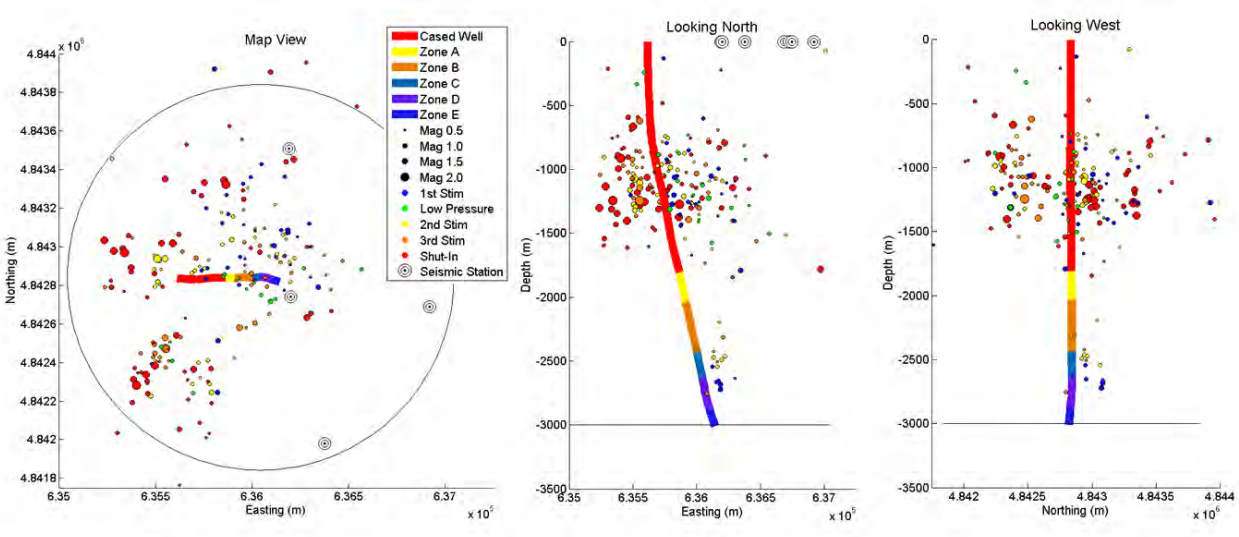

Figure 3-15. Located seismic events from seismic signals in real time.

Initial seismicity from stimulation (blue dots) was observed near the bottom of the wellbore, and was quickly followed by multiple events that occurred at shallow depths that would spread further away from the well over time. Over the next several weeks, shallow events would continue to occur sporadically, including while pumping at low pressure when the stimulation pumps were under repair (green). Instances of shallow seismicity also occurred after pumps were re-started following both stages of diversion (yellow and orange dots), and would continue to spread shallow. The largest events observed (Mw>2) occurred near or after shut-in (red dots) all of which were observed above a depth of 2,000 meters.

The events shown in Figure 3-15 are preliminary locations, and represent our observations during the stimulation operations. Observations of real time seismicity helped guide the pumping strategy to maximize increases in injectivity, and also aided in compliance to the ISMP. Further analysis of seismicity and its implications for a reservoir model are presented in Section 4 of this report.

3.8.3 INDUCED SEISMICITY MITIGATION PLAN

AltaRock developed a project-specific ISMP (AltaRock, 2011b; BLM, 2011) for the Newberry EGS Demonstration that satisfied the requirements of the Induced Seismicity Mitigation Protocol adopted by the DOE (Majer et al., 2008, 2011). This included predicting the largest possible induced micro-earthquake and developing predefined thresholds of event magnitudes and ground motion accompanied by appropriate mitigation actions.

The most relevant ISMP guideline during stimulation was related to *unwanted vertical growth: "[a]ny seismic event with M > 1.0 or that is picked on 6 or more stations of the MSA that is located shallower than 6000 feet (1.8 km) below the ground surface at NWG 55-29 will result in use of diverter to shift stimulation*

to another zone. Any planned increase in flow rate will be postponed until after the diverter is applied (AltaRock, 2011b)."

The first shallow seismic event with a magnitude greater than 1.0 occurred on November 3, just after the WHP had exceeded 12 MPa and pump problems that dropped the WHP down to ~6 MPA (Table 3-3). At this time, there was uncertainty about whether the shallow events were being well-located or were an artifact of incorrect phase picks or a poor velocity model. In any case, the WHP and flow rates were kept low during most of November while pumps were repaired. Shallow seismicity with smaller magnitude (M_w<1) did continue to occur even at low WHP. At the time, we surmised that thermal expansion of previously injected water was causing the seismicity, thus we did not expect that diversion at the well bore could cause the shallow events to cease.

In mid-November, after the seismologists (Ernie Majer at LBNL and Bruce Julian at Foulger Consulting) determined that the shallow depths were likely *real*, AltaRock planned to pump diverter as soon as the pumps were repaired and brought back online (e.g. see November 18 seismic report, Appendix D). When the stimulation pumps were brought back on line, diverter was injected before returning to higher WHP (see Figure 3-12). Although, the microseismicity did seem to initially deepen, the shallow events soon returned during Stage 2 of stimulation. After two stronger shallow events occurred on December 1, the decision to proceed to Stage 3 was made and the mixing unit personnel were called back to the site. After TZIM treatment, Stage 3 did not have any shallow events (Mw > 1.0) until the last day of stimulation, December 7.

Table 3-3 Shallow seismic events, those with depths less than 1.8 km (6,000 ft) below ground surface with M greater than 1.0 and mitigation actions taken. Based on LBNL catalogue.

Date	# of Seismic events with M>1.0 and depth less than 6000 feet bgs	Response	Phase
11/3	1	Low Pressure	Pump Repairs
11/29	1	More Diversion	Stage 2
12/1	2	Held WHP	Stage 2
12/3	1	Diverted	Stage 2 - 3
12/7	2	Stimulation Halted	Stage 3
12/9	2	None	Shut-in
12/15	1	None	Shut-in
12/19	5	None	Shut-in
12/20	1	None	Shut-in
12/27	1	None	Shut-in
Total	17		

The strongest seismic event occurred on the last day of stimulation (12/7/2012) and had a moment magnitude (Mw) of 2.39 which exceeded the initial Mw limit of 2.0. The mitigation action for this limit was to wait 24 hours before increasing well head pressure or flow rate. Since the event occurred on the last day of planned stimulation, no modification to operational plans was necessary, and the well was shut-in later that day.

Ground motion at the NNVM SMS due to the Mw 2.39 event was estimated PGA of 0.1% g, far below the action threshold set in the ISMP (AltaRock, 2011b) of 1.4% g. From the seismometer closest to the event, a borehole seismometer at NN17, a PGA of 0.3% g was estimated. That level of ground motion would not necessarily have occurred at the surface, due to the highly attenuating cinders blanketing the volcano flanks. In any case, there were no reports of any felt seismicity from the field crews on-site for this or any other micro-earthquake. Due to winter conditions, no visitors were near the site.

3.8.4 LESSONS LEARNED

While it is possible to see events occurring in real time it is not practical to also find a location and magnitude for those events in real time. There is at least a one or two day delay on location and magnitude estimates. The quality of locations improves as a function of the number of events that have been recorded. Borehole seismometers returned higher quality data than surface seismic stations. Initial locations will likely contain significant error.

3.9 ATTEMPTS TO FLOW THE WELL

3.9.1 FLOW TEST ATTEMPT 1

On December 15, the first attempt to create flow back from the well began. Weatherford air jammers were used to pressure up the well to 5.3 MPa (770 psi; Figure 3-16). Air was pumped through a 7.63 cm (3 in) wing valve located on the wellhead. This wing valve was then closed and the well quickly equilibrated to a pressure of 3.8 MPa (550 psi), and the well was then allowed to warm for 3 days. WHP remained constant during this time at 3.8 MPa (550 psi). On December 17 well was pressurized to 5.3 MPa (770 psi) and an attempt was made to flow the well. The flow line valve froze and had to be defrosted (Figure 3-17) and opened as quickly as possible. WHP decreased rapidly to zero, but no water flowed from the well.

An additional attempt to flow the well was done by injecting air mixed with soap down the well's parasitic aeration string (PAS) line to a depth of 550 m (1,800 ft). The air soap mixture, injected soap at 19.8 m^3/min (700 ft^3/min), was intended to lighten the water column above 550 m (1,800 ft). However, the wellbore did not pressurize, flow was not induced, and it was suspected then that the PAS line was leaking.

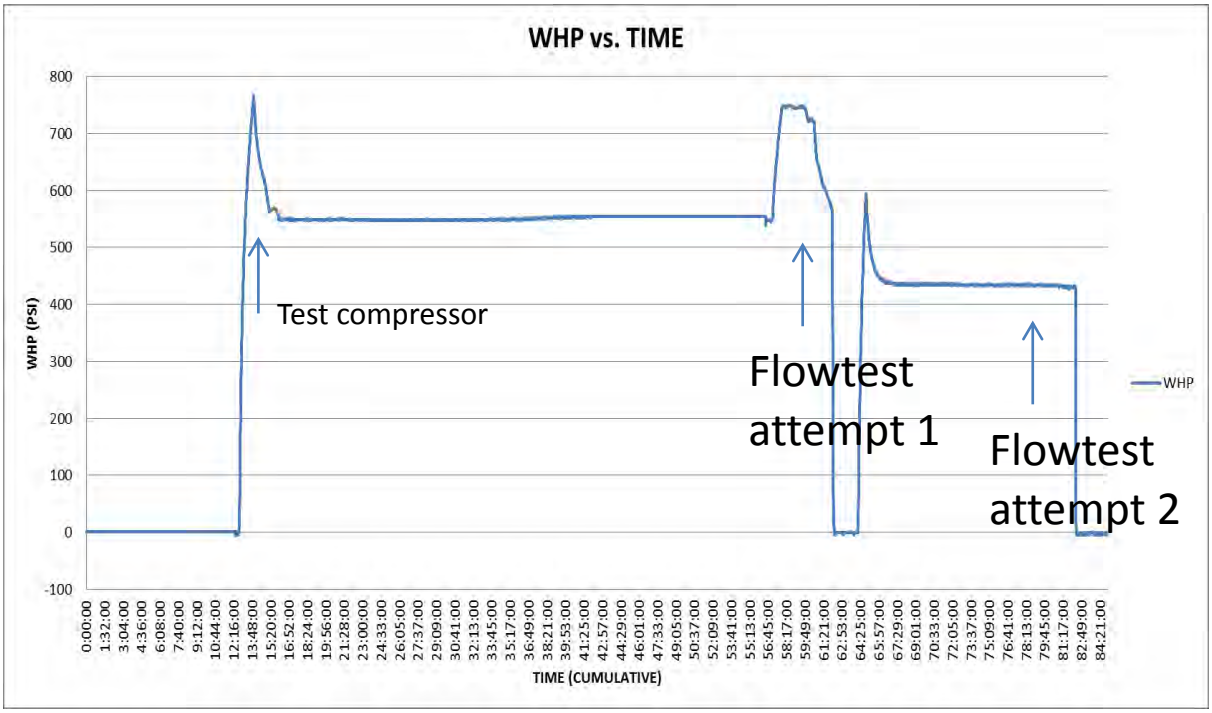

Figure 3-16. WHP during both flow test attempts.

Figure 3-17. Defrosting the frozen flow line valve.

3.9.2 SECOND FLOW TEST ATTEMPT

The well was again pressurized to approximately 5.3 MPa (770 psi) and allowed to heat up. An air and soap mixture was pumped through the 7.62 cm (3 in) wing valve to lighten the water column. The maximum pressure reached was 4.1 MPa (600 psi) during the second attempted flow test. When the wing valve was closed the pressure quickly equilibrated to 2.97 MPa (432 psi), over 0.69 MPa (100 psi) less than the previous equilibrated pressure. The well was allowed to heat up for a day and another attempt was made to flow the well on December 18. This attempt was also unsuccessful.

3.9.3 LESSONS LEARNED

Have a plan to unfreeze valves in case of cold weather. If using a PAS line, pressure up well head and record pressure on PAS line valve to check for leaks.

3.10 ENVIRONMENTAL MONITORING

A groundwater monitoring program is being operated to characterize local water resources before, during, and after the stimulation of the NWG 55-29 injection well, as described in the Newberry Volcano Enhanced Geothermal System Demonstration Project Environmental Assessment (BLM, 2011). The intent of the program is to confirm that the stimulation process did not have any significant impact on the surface and groundwater resources of the region. Hydrologic features considered and evaluated for potential effects from the Demonstration include:

- East Lake and Paulina Lake in the Newberry Caldera;
- Thermal springs around the lakes;
- Regional and local groundwater systems;
- Surface outflow from Paulina Lake into Paulina Creek; and
- Surface outflow from the Little Deschutes River.

3.10.1 BACKGROUND – REGIONAL HYDROLOGIC FEATURES

The Newberry Volcano is located in the southern edge of the Upper Deschutes River Basin which is bounded on the west by the Cascades range and on the east by an artificial boundary based on low data availability and on the low likelihood of significant groundwater exchange between this east boundary and the Deschutes Basin (Gannett et al., 2001). The Newberry EGS Demonstration site is adjacent to several distinct hydrologic features of the basin.

3.10.1.1 CALDERA LAKES

East and Paulina lakes are situated within the Newberry Caldera. The lakes recharge almost exclusively by precipitation and infiltration, with approximately 0.89 m (35 in) of rain and snow falling into the caldera annually. East Lake does not have a surface water outlet, while Paulina Lake discharges through a dam and outlet structure into Paulina Creek and is used for irrigation purposes. The level of Paulina Lake and outflow volume to Paulina Creek have been controlled and managed at the dam since the early 1900s. Lake levels fluctuate seasonally, and the level of East Lake is generally 12 to 15 m (40 to 50 ft) higher than Paulina Lake. The hydraulic gradient from East Lake toward Paulina Lake indicates appreciable groundwater flow from East Lake toward and into Paulina Lake. Nearby groundwater levels relative to East Lake further support evidence of flow from East Lake toward Paulina Lake.

The groundwater system within the caldera appears to be structurally-controlled by faulting and a series of ring-fractures around the caldera. These faults and ring-fracture structures create groundwater flow boundaries, impeding the vertical and/or horizontal flow of groundwater out of the caldera, although some groundwater flow from the caldera to regional and local aquifer systems does occur.

3.10.1.2 THERMAL SPRINGS

Thermal springs and diffuse seeps are found along the northeast shore of Paulina Lake and the southeast shore of East Lake. These are considered to be fumaroles (gas vents) covered by the lakes and are not the result of deep geothermal fluid, nor are they connected to a deep geothermal system outside the caldera. Surface expression of the fumaroles is due to recirculation of heated groundwater and/or mixing with steam as it migrates up through a network of subsurface cracks within the caldera ring fractures.

The recharge volume from thermal springs and diffuse flows to the caldera lakes has not been quantified, but it has been described as many small diffuse flows and is relatively small compared to recharge from precipitation (Sammel and Craig, 1983). A deeper geothermal system consisting of higher temperatures and depths greater than 396 m (1,300 ft) is also present at Newberry Caldera.

3.10.1.3 GROUNDWATER SYSTEMS

Groundwater underlying the west flank of Newberry volcano and the La Pine sub-basin is divided into regional and local systems based on geology, areal extent, and flow characteristics. The prolific regional aquifer is of wide areal extent. Host rocks include basaltic lavas, volcaniclastic rocks, and sedimentary units of the Deschutes Formation. These overlie low permeability basement rocks of the Clarno and John Day Formations. The depth to the top of the regional aquifer varies with elevation, generally ranging from 30 to 152 m (100 to over 500 ft) below ground surface.

Local aquifers are unconfined and of lesser areal extent than the regional aquifer. Host material consists of unconsolidated, glaciofluvial sediments below the water table. Host rock includes well-graded sand and gravel with minor interbeds of low permeability silt and clay that overlie clay-rich marsh and lacustrine deposits associated with the damming of the ancestral Deschutes River. These materials blanket most of the La Pine sub-basin and were deposited as glacial outwash from the High Cascades Range to the west. Domestic wells in the La Pine sub-basin are typically completed in this shallow aquifer at depths usually less than 15 m (50 ft). Water levels in wells installed at various depths within the local system generally show similar water levels of 1.5 to 4.5 m bgs (5 to 15 ft bgs), suggesting no significant vertical movement of water in the local aquifer (Century West, 1982). Below this depth, decreasing permeability caused by increased clay content forms a basal aquiclude, defining the base of the local aquifer. The top of the aquifer likely fluctuates several meters or more depending on seasonal precipitation. Pressure transducers were installed in water wells NN-17 and NN-18 prior to stimulation.

The groundwater system is recharged primarily by infiltration of precipitation (rainfall and snowmelt), and to a lesser extent by canal leakage, infiltration of applied irrigation water, and stream loss. A strong correlation between recharge rate and elevation exists. The mean recharge to the upper Deschutes Basin between 1962 and 1997 has been estimated at 28.9 cm/yr (11.4 in/yr), which is equivalent to 3.39 km^3/yr (2,750,000 acre-feet/yr) (Gannett et al., 2001). Groundwater recharge ranges from less than 2.5 cm/yr (1 in/yr) at lower elevations to greater than 330.2 cm/yr (130 in/yr) in the High Cascade Range. Precipitation ranges from less than 30.5 cm/yr (12 in/yr) to greater than 5 m/yr (200 in/yr) in these areas, respectively. About 84 percent of recharge from precipitation infiltration occurs between November and April (Gannett et al., 2001). Recharge to the groundwater system from the west flank of Newberry volcano may approach 0.28 km^3/yr (224,000 acre-feet/year) (Dames and Moore, 1994). The Fort Rock Basin to the southeast also contributes approximately 0.04 km^3/yr (36,200 acre-feet/yr) to the upper Deschutes Basin (Gannett et al., 2001).

Groundwater flows eastward from the High Cascade Range and west-northwest from Newberry volcano toward the La Pine sub-basin where it enters the regional and local aquifers. From the La Pine sub-basin, groundwater flow is generally to the north within basalt bedrock and overlying volcanic and sedimentary deposits of the Deschutes Formation. The Clarno and John Day Formations underlie the regional (Deschutes Formation) aquifer and include low permeability stratigraphic units that inhibit the horizontal and vertical flow of regional groundwater (King, 1991). The shallow, local aquifer extends north approximately 29 km (18 mi) to the Benham Falls area where the ancestral Deschutes River was dammed by Newberry lava flows erupted from a cinder cone in the northwest rift zone (Lava Butte), approximately 7,100 years ago. There is an abrupt topographic gradient north of Benham Falls at the contact between Newberry lavas and those of the High Cascade Range with source areas to the west.

Correspondingly, the Deschutes River gradient increases from approximately 0.8 m/km (2.6 ft/mi) in the La Pine sub-basin to 9.5 m/km (50 ft/mi) between Benham Falls and Bend. The slope of the water table also increases north of Benham Falls. The depth to water near the river at Benham Falls ranges from approximately 1.5 to 7.6 m (5 to 25 ft). Approximately 12.9 km (8 mi) to the north beneath Bend, the depth to the regional aquifer increases to over 91.4 m (300 ft) (Sherrod et al., 2004).

The northward-increasing depth to groundwater has implications for the interaction of the groundwater system and surface water. Within the La Pine sub-basin south of Sunriver, the Deschutes River system experiences slight gains due to groundwater discharge and significant gains from several major spring complexes. North of Sunriver, the Deschutes system begins to lose water as groundwater levels drop far below stream levels. Between Sunriver and Bend, the Deschutes River loses an estimated 3.2 m^3/s (113 ft^3/s) as it flows through permeable volcanics of Lava Butte and the north rift zone (Gannett et al., 2001).

3.10.1.4 PAULINA CREEK

Paulina Creek flows west for over 21 km (13 mi) from Paulina Lake (elevation 1.9 km or 6,330 ft) to the confluence with the Little Deschutes River at an elevation of 4,180 feet. A concrete spillway built in the early 1900s controls the flow of Paulina Creek. A one-lane concrete bridge allows traffic to pass over Paulina Creek above the spillway. Gauge records indicate peak seasonal flows between March and June of 0.4 to 0.7 m^3/s (15 to 25 ft^3/s), primarily due to snowmelt. Outflows of 0.3 to 0.4 m^3/s (10 to 15 ft^3/s) are generally sustained through the irrigation season from April through October. There are six senior water rights for Paulina Lake and Paulina Creek irrigation water dating back to 1911 and 1918. These senior water rights total approximately 0.23 m^3/s (8 cfs). Above the Paulina-East Lake Road (also known as Highway 21 and Forest Road 21) crossing at river mile (RM) 5.2, the stream loses approximately 0.01 $m^3/s/km$ (0.75 $ft^3/s/mi$) to groundwater (Morgan et al., 1997). Below RM 5.2 Paulina Creek does not appear to lose flow to groundwater and may receive some minor recharge as the stream intersects groundwater levels of the near-surface, local aquifer.

3.10.1.5 LITTLE DESCHUTES RIVER

Paulina Creek joins the Little Deschutes River near Little Deschutes RM15. In this portion of the La Pine sub-basin, the water table elevation is near land surface. Stream gains and losses along most of the Little Deschutes River are small and related to local changes in streambed morphology. There is relatively little net exchange between groundwater and surface water in the Little Deschutes River between RM15 and its confluence with the Deschutes River.

3.10.2 SCOPE AND OBJECTIVES

The groundwater monitoring program is designed to characterize local water resources before, during, and after the stimulation of NWG 55-29. Ambient conditions were first monitored weeks before stimulation of the reservoir began to provide baseline conditions to assess whether any changes to water quality have occurred. The monitoring plan, particularly its assumptions and methodology, was reviewed by certified hydrologists (Kleinfelder, 2011) and modified based on their recommendations. The results will be made available to AltaRock Energy (ARE) staff, project collaborators, stakeholders, and/or the public as necessary.

Newberry Caldera is situated along a hydrogeologic divide from which regional groundwater flows east and west away from the edifice. Stimulation well 55-29 is located on the west flank of the volcano, and groundwater flows from the caldera, through the well site and on into the Deschutes River watershed system. Nine groundwater monitoring sites were established at locations up-, down-, and cross-gradient to the stimulation well. The areal distribution of sites is intended to provide the best possible monitoring

of groundwater conditions throughout the Demonstration based on hydrologic and geologic parameters. Monitoring sites include:

- Thermal seep/spring waters – up gradient and hydraulically unconnected to the shallow groundwater system at NWG 55-29
  - *East Lake and Paulina Lake hot springs*
- Groundwater in the caldera – up gradient
  - *Paulina Lake Visitor Center water well*
- Groundwater on the caldera flanks
  - *Microseismic (MSA) borehole NN-18* – up gradient
  - *MSA borehole NN*-17- down gradient
  - *Pad 55-29 water well* – at source
  - *Pad 46-16 water well* – cross gradient
- Groundwater and in the La Pine sub-basin
  - *Prairie Campground Water Well* – a domestic water supply well located several miles down gradient at Prairie Campground
  - *Newberry Estates water well #1* – down gradient (La Pine)

3.10.3 METHODS

3.10.3.1 MONITORING FREQUENCY AND DURATION

All groundwater monitoring sites were sampled twice before stimulation, weekly during stimulation, and will continue to be monitored for six months following stimulation (Table 3-4). Not all sites are monitored with the same frequency or duration, as noted in the table. The schedule was revised due to winterization of several wells originally planned for sampling throughout the winter months (Pad S-16, Pad S-29, Visitor Center water well and Prairie Campground water well). These wells will be sampled again in the spring pending accessibility.

3.10.3.2 WATER LEVEL MONITORING

Pressure transducers were installed at wells NN-17 and NN-18 in order to continuously monitor the depth to groundwater. These transducers were intended to be incorporated into the MSA digitizing and transmission system via an auxiliary channel. The transducer installed in NN-18 with MSA equipment had numerous breakdowns and has been replaced by a transducer supplied by Oregon Water Resources Department (OWRD). Data from this transducer is not transmitted and must be downloaded periodically. During the time between the original transducer failing and installation of the new transducer, a sonic depth sounder has been used to monitor the water level at both wells. Transducers were previously installed in the Pad S-29 and Pad S-16 water wells, and have been fitted with appropriate data loggers.

SAMPLE COLLECTION

Groundwater samples are collected in a 3.79 L (1 gal) high-density polyethylene container. Hot springs at Paulina and East Lakes are collected at the surface by dipping the container into the pool while minimizing sediment and surface disturbance as much as possible. Well samples are either collected at surface spigots from sealed production wells (i.e., domestic and campground wells), or by low flow sampling methods from wells NN-17 and NN-18 accordance with ASTM Standard D 6771-02, “Low-Flow Purging and Sampling for Wells and Devices.”

Table 3-4. Completed groundwater monitoring events.

Event	Date	Pad 29 Well	Pad 16 Well	NN-17	NN-18	Paulina Lake Hot Springs	East Lake Hot Springs	Newberry Estates Well #1	Visitor Center Water Well	Prairie Campground Well
Background Samples	July, 2012	-	-	-	-	7/27/12	7/26/12	7/26/12	7/26/12	7/26/12
Background Samples	August, 2012	-	8/16/12	-	-	-	-	-	-	-
Background Samples	October, 2012	-	-	10/5/12	10/5/12	-	-	-	-	-
Stimulation begins 10/16/2012	October, 2012	10/18/12	-	10/18/12	10/18/12	-	-	-	-	-
1st tracer 11/24/2012	November, 2012	11/26/12	11/26/12	-	-	11/27/12	-	-	-	-
2nd tracer 12/7/2012	December, 2012	-	-	-	-	-	11/29/12	-	-	-
Well shut in 12/7/2012	December, 2012	12/10/12	-	-	-	-	-	-	-	-
1st month	January, 2013	-	-	1/7/13	1/7/13	1/6/13	1/6/13	1/18/13	-	-
2nd month	February, 2013	**W**	**W**	2/10/13	2/10/13	2/9/13	2/9/13	2/28/13	**W**	**W**
3rd month	March, 2013	**W**	**W**	3/14/13	3/14/13	3/12/13	3/12/13	3/22/13	**W**	**W**
4th month	April, 2013	**W**	**W**	4/11/13	4/11/13	4/10/13	4/10/13	-	**W**	**W**
5th month	May, 2013	**W**	**W**	5/15/13	5/17/13	5/15/13	5/15/13	-	**W**	**W**
6th month	June, 2013	**W**	**W**	-	-	-	-	-	6/22/13	6/22/13
7th month	July, 2013	7/18/13	-	7/23/13	7/19/13	7/19/13	7/19/13	-	7/13/13	7/23/13
8th month	August, 2013	-	-	-	-	-	-	-	-	-
9th month	September, 2013	9/11/13	9/12/13	9/3/13	9/3/13	-	-	-	-	-

Note, sampling was interrupted at NN-17 and NN-18 during stimulation due to sampling pump malfunctions.
W indicates well was winterized and no sample was taken.

3.10.3.3 FIELD MEASUREMENTS

Temperature, pH, oxidation-reduction potential (ORP), conductivity, and turbidity are measured in the field at the time of sample collection. These parameters are measured directly in the 3.79 L (1 gal) HDPE container. Groundwater from the wells is allowed to flow until the field parameter values stabilize within 10% prior to samples being bottled for lab analysis. Field measurements are conducted with a hand held PHH224 Intelligent Meter, which is calibrated prior to each field visit. Turbidity is measured in the field with a handheld LaMotte 2020we turbidity meter, calibrated prior to each sample analysis.

3.10.3.4 CHEMICAL ANALYSES

Hot spring samples are collected once turbidity has decreased following clearing of the hot spring areas. Well samples are collected after surface readings of temperature, pH and conductivity values have stabilized within 10%. Water collected in the gallon container is filtered through a 0.45-µm cellulose acetate membrane using a vacuum Erlenmeyer flask. Filtered water is distributed among 4 containers as follows:

- 950 mL bottle without preservative sent to SEM
- 500 mL bottle with HNO_3 sent to SEM
- 250 mL bottle with H_2SO_4 sent to SEM
- 30 mL HDPE bottle without preservative for $\delta^{18}O$ and $\delta^{2}H$ analysis, sent to UC Davis
- 60 mL amber bottle (tracer analyses) sent to University of Utah

Samples are labeled with date, time, sample location, and name of field technician. These are refrigerated until shipment to analytical facilities. Analytical samples shipped to SEM are packed in coolers on ice and shipped with Chain-of-Custody forms. The types of analyses and facilities where they are conducted are listed in Table 3-5.

Table 3-5. Geochemical analytes and facilities responsible for analysis.

Analyte Type	Analyte	Sample Bottle and Preservative	Analytical Laboratory
Field Parameters	Temperature, pH, conductivity, ORP, turbidity	none	ARE personnel operating calibrated field meter
Water chemistry	alkalinity, Al, NH_3, As, Ba, B, Ca, Cs, Cl, Cr, F, Fe, Li, Mg, Mn, Hg, NO_3, pH, K, Rb, SiO_2, Na, Sr, SO_4, TDS	950 mL bottle without preservative; 500 mL HDPE bottle with HNO_3; 250 mL HDPE bottle with H_2SO_4	SEM
Stable isotopes	$\delta^{18}O$, $\delta^{2}H$	30 mL HDPE bottle without preservative	UCD
Geothermal tracers	Naphthalene sulfonates	60 mL amber bottle unfiltered	EGI
Rare earth elements	REEs	4 L HDPE bottle with HNO_3	INL

EGI – Peter Rose
Energy and Geoscience Institute
University of Utah
423 Wakara Way, Suite 300
Salt Lake City, Utah 84108
phone: 801-585-7785
email: prose@egi.utah.edu

SEM – Sierra Environmental Monitoring
1135 Financial Blvd.
Reno, NV 89502
phone: (775) 857-2400
email: jnava@sem-analytical.com

UCD – Emily Ngo Schick
U.C. Davis Stable Isotope Facility
One Shields Avenue, Mail Stop #1
Davis, California, 95616
phone: 530-752-8100 | fax: 530-752-4361
email: sif@ucdavis.edu

INL – Travis McLing
Idaho National Lab
PO Box 1625
Idaho Falls, ID 83415-3553
phone: 208-526-7269 | cell: 208-520-1968
email: travis.mcling@inl.gov

3.10.3.5 DATA ANALYSIS AND REPORTING

Field parameter data were reviewed against background conditions after every sampling event during the simulation period. Laboratory analytical reports are received approximately two weeks after each sampling event. Once these data are confirmed to be within acceptable limits, they are compared with the established background conditions. Potentially significant deviations in water quality are considered to be a change of 10% or more of any constituent value outside its background condition.

3.10.4 RESULTS

Table 3-6 summarizes the average background water chemistry at each monitoring location and results from the first monitoring event following stimulation of the reservoir; full collected results to date are presented in Appendix E. Of particular interest are the results for water wells closest to the stimulation site, notably the water supply well at Pad S-29 and boreholes NN-17 and NN-18.

3.10.4.1 PRE-STIMULATION BACKGROUND GROUNDWATER CONDITIONS

Of the groundwater monitoring sites, the water well at Pad S-29 and MSA boreholes NN-17 and NN-18 have the poorest water quality. Results to date show these three sites have higher alkalinity, arsenic, boron, fluoride, magnesium and total dissolved solids (TDS) relative to the nearest up-gradient site (Pad S-16) and down-gradient wells (Prairie Campground water well and Newberry Estates water well #1). Furthermore, the chemistry of the water at the hot springs is significantly different than groundwater chemistry in any of wells, which supports the interpretation that the lakes and the regional groundwater are not connected hydrologically.

Water from the well at Pad S-29 is elevated in alkalinity, arsenic, boron, fluoride, and magnesium relative to up-gradient and down-gradient sites. The nearest up-gradient sites are NN-18 and Pad 46-16. Borehole NN-17 and the water wells at Prairie Campground and Newberry Estates are the four down-gradient sampling sites from Pad S-29.

Total alkalinity ranges from 230-250 mg/L $CaCO_3$ at Pad S-29. Alkalinity decreases distally from Pad S-29. Data ranges from 171-190 mg/L and from 39-42 mg/L at up-gradient sites NN-18 and Pad S-16, respectively. Total alkalinity at the nearest down-gradient site, borehole NN-17, ranges from 240-241 mg/L. Further down-gradient sites include the Prairie Campground and Newberry Estates water wells; data from these three sites ranges from 48-57 mg/L.

Arsenic concentration data ranges from 0.032-0.034 mg/L at Pad S-29. This is highest level detected at any monitoring site to date. Arsenic concentration decreases with distance from Pad S-29, with values of 0.028 mg/L at NN-18 and less than 0.004 mg/L at Pad S-16. Paulina Lake and East Lake hot springs, the two furthest up-gradient sampling locations, range from <0.002-0.015 mg/L. Results from all four down-gradient sites (NN-17, Prairie Campground and Newberry Estates wells) were less than 0.011 mg/L, with most of these under 0.002 mg/L.

Boron concentration ranges from 0.55-0.59 mg/L at Pad S-29; values range from 0.86-0.96 mg/L at NN-18 and 0.55-0.56 mg/L at NN-17 to less than 0.005 mg/L at all other down-gradient sites. Paulina Lake Hot Springs data ranges from 0.76-0.90 mg/L and East Lake Hot Springs data ranges from 0.61-1.0 mg/L in comparison.

Fluoride concentrations are higher at Pad S-29 than at all other monitoring sites, with the exception of Paulina Lake Hot Springs (0.6-0.9 mg/L). Data ranges from 0.05-0.08 mg/L at Pad S-29. Similar values were recorded at NN-17 (0.7 mg/L) and the Visitor Center well (0.8 mg/L). Fluoride concentrations at all other sites including East Lake Hot Springs are lower than those measured at Pad S-29, ranging from <0.01-0.05 mg/L.

Magnesium concentrations are highest at Paulina Lake and East Lake hot springs, where data range from 41-48 mg/L and 37-54 mg/L, respectively. Pad S-29 and borehole NN-17 have similar concentrations to one another: 24-26 mg/L and 24 mg/L, respectively. Up-gradient data range from 2.5-2.6 mg/L at Pad S-16 to 3 mg/L at the Visitor Center well and 6.4-17 mg/L at borehole NN-18. Down-gradient sites range from 3.5 mg/L and 4.3-4.7 mg/L at the Prairie Campground well and the Newberry Estates wells, respectively.

Total dissolved solids at all sites range from 70 mg/L at several sites to 900 mg/L at East Lake Hot Springs. Water at Pad S-29, boreholes NN-18 and NN-17 have similar TDS concentrations, ranging from 270-280 mg/L to 190-240 mg/L and 260-270 mg/L at NN-18 and NN-17, respectively. The furthest down-gradient wells at Newberry Estates range from 92-110 mg/L TDS.

In summary, the most notable results from geochemical analyses to date indicate that with few exceptions, the water well at Pad S-29 has higher alkalinity, arsenic, boron, fluoride, magnesium and total dissolved solid concentrations relative to the surrounding monitoring sites. Paulina Lake and East Lake hot springs have much higher alkalinity, magnesium and TDS levels on average than other sites. The hot springs also have higher boron concentrations than other sites, although the difference is not as pronounced as with alkalinity, magnesium and TDS levels. The fluoride concentration at Pad S-29 is lower than at Paulina Lake Hot Springs, but higher than that measured at East Lake Hot Springs. Borehole NN-18 has higher boron concentration than the water well at Pad S-29 and borehole NN-17. Pad S-29 and borehole NN-17 also have similar magnesium levels, although all other sites except for the two hot springs locations have much lower magnesium concentrations. Together, these data indicate that the area around Pad S-29 tends to accumulate these elements more than other sites in general.

Paulina Lake and East Lake hot springs present unique hydrologic, geologic and thermal regimes relative to the seven other monitoring sites. These are not likely connected to the surrounding shallow aquifer sampled by the wells at other sites. Heated flow at the hot springs is most likely due to lake water recirculation and interaction with gas and steam from the caldera system. The higher alkalinity, arsenic, boron, magnesium and TDS concentrations detected at the hot springs are not surprising considering that the caldera system is likely responsible for their formation.

Table 3-6. Average background and post-stimulation water quality results.

Monitoring Location	Sample Type	Number of Samples	Field Parameters					Laboratory Analytical Results										
			Temp, (°C)	pH (SU)	Cond. (mS/m)	ORP (mV)	Turbidity (NTU)	pH (SU)	Temp. (°C)	TA (mg/L CaCO3)	Al (mg/L)	NH_4 (mg/L N)	As(mg/L)	Ba (mg/L)	B (mg/L)	Ca (mg/L)	Cs (mg/L)	Cl (mg/L)	Cr (mg/L)
PLHS	BG	4	49.8	6.6	324.6	133.3	0.1	7.34	19.0	653	<0.05	<0.1	0.014	0.213	0.86	51.5	0.004	6.1	<0.002
	P	6	42.8	6.6	70.6	112.3	0.4	7.71	21.3	524	<0.05	<0.1	0.0	0.051	0.77	47.2	0.0	6.6	<0.002
ELHS	BG	8	52.6	6.3	1.0	47.0	14.1	7.43	19.2	424	<0.05	0.15	0.0045	0.013	0.96	72	<0.002	1.8	<0.002
	P	6	31.8	7.0	43.7	81.5	1.1	7.51	20.4	238	<0.05	0.2	<0.002	0.016	0.96	42.8	<0.002	1.7	<0.002
NEWW	BG	9	9.3	7.4	0.1	143	0.55	7.87	19.1	55	<0.05	<0.1	<0.002	0.003	<0.05	7.2	<0.002	2.1	<0.002
	P	3	8.4	7.3	0.3	122	0.1	7.77	20.5	59	<0.05	<0.1	<0.002	0.004	<0.05	7.9	<0.002	2.4	<0.002
PAD-16	BG	2	6.9	7.7	0.0	146	0.2	7.86	19.2	41	<0.05	0.1	<0.004	0.002	<0.05	5.1	<0.002	0.8	<0.002
	P	1	6.88	8.2	-65	–	0.84	7.83	20.7	40	<0.05	<0.1	<0.002	0.003	<0.05	5.1	<0.001	0.8	<0.002
PAD-29	BG	5	16.3	7.6	0.4	136	0.1	7.92	20.0	242	<0.05	0.2	0.0314	0.008	0.57	19.2	<0.002	3.6	<0.002
	P	4	18.0	7.3	-41.3	23.9	0.0	7.77	19.8	250	<0.05	0.1	0.0	0.008	0.57	19.0	<0.001	3.6	<0.002
NN-17	BG	2	10.6	7.4	0.4	NA	68.1	8.35	20.4	241	<0.05	0.2	0.0105	0.005	0.56	18	<0.002	3.1	<0.002
	P	7	7.1	8.3	-6.9	-41.5	4.2	8.20	20.9	233	<0.05	0.2	0.0	0.006	0.52	17.7	<0.002	3.3	<0.002
NN-18	BG	2	10.2	7.2	0.3	NA	9.8	8.48	20.3	181	<0.05	0.1	0.028	0.010	0.91	10.7	<0.002	6.6	<0.002
	P	7	7.2	8.9	10.1	87.6	3.8	8.27	21.1	181	<0.05	0.1	0.0	0.013	0.85	9.8	<0.002	6.0	<0.002

Monitoring Location	Sample Type	Number of Samples	Laboratory Analytical Results																
			F (mg/L)	Fe (mg/L)	Li (mg/L)	Mg (mg/L)	Mn (mg/L)	Hg (mg/L)	NO_3 (mg/L N)	P (mg/L)	K (mg/L)	Rb (mg/L)	SiO_2 (mg/L)	Na (mg/L)	Sr (mg/L)	SO_4 (mg/L)	TDS (mg/L)	δ^2H	$\delta^{18}O$
PLHS	BG	4	0.7	0.13	0.20	49	1.733	<0.0002	<0.5	0.16	14.5	0.036	187.33	122.7	0.19	3.1	723	-105.85	-14.07
	P	6	0.8	<0.1	0.19	43	0.702	<0.0001	1.3	0.14	11.9	0.033	157.6	101.6	0.17	8.9	642	-107.66	-14.32
ELHS	BG	8	0.2	0.39	0.025	32	0.428	0.0003	<0.5	0.12	8.55	0.034	126.5	54.3	0.21	57.2	587	-103.08	-13.27
	P	6	0.2	0.1	<0.1	21	0.203	<0.0001	<0.5	0.12	5.6	0.0	67.3	37.3	0.15	45.3	348	-85.12	-9.43
NEWW	BG	9	0.2	0.1	<0.1	4	0.002	<0.0002	1.4	0.24	1.4	0.002	43	9.7	<0.05	1.4	101	-119.53	-15.89
	P	3	0.2	<0.05	<0.1	5	0.002	<0.0002	1.2	0.18	1.4	<0.002	46	10.0	<0.05	1.5	98	-120.98	-15.68
PAD-16	BG	2	0.2	0.07	<0.1	3	0.002	<0.0001	<0.5	0.12	1.04	0.003	40	6.6	<0.05	0.3	73	--	--
	P	1	0.2	<0.05	<0.1	3	0.003	<0.0001	<0.5	0.10	1.6	0.002	39	6.2	<0.05	0.3	74	-113.96	-15.58
PAD-29	BG	5	0.7	0.085	<0.1	25	0.003	<0.0001	0.21	0.18	4.78	0.0132	60	44.2	0.08	2.5	278	-110.80	-14.70
	P	4	0.6	<0.05	<0.1	25	<0.002	<0.0001	<0.5	0.17	5.0	0.0	58	44.3	0.07	2.5	280	-110.38	-14.72
NN-17	BG	2	0.7	<0.05	<0.1	24	0.091	<0.0002	<0.5	0.09	4.1	0.013	52	39.5	0.07	2.0	265	-111.95	-14.89
	P	7	0.7	0.2	<0.1	24	0.031	<0.0001	<0.5	0.11	4.2	0.0	53	38.6	0.09	1.9	251	-111.68	-14.97
NN-18	BG	2	0.5	0.09	<0.1	10	0.012	<0.0002	2.2	0.08	6.95	0.015	56	47.0	<0.05	9.0	215	-113.41	-15.13
	P	7	0.4	0.2	<0.1	13	0.009	<0.0001	<0.5	0.11	6.2	0.012	69	45.7	<0.05	4.7	243	-112.36	-15.21

BG – background chemistry
Cond. – Conductivity
ELHS – East Lake Hot Springs
PLHS – Paulina Lake Hot Springs
< – constituent was not detected above the laboratory reporting limit
P – post-stimulation chemistry
TA – Total Alkalinity
Temp. – Temperature
– – constituent not analyzed

3.10.4.2 POST STIMULATION GROUNDWATER CONDITIONS

Comparison of the post-stimulation results with the background water quality results did not show any significant change following stimulation of the reservoir around the injection well (Table 3-6). Significantly, the cesium and lithium-based tracer compounds injected into the reservoir during stimulation were not detected at any of the monitoring locations, further evidence that there is no hydraulic connectivity between the newly stimulated reservoir and the shallow aquifer.

3.10.5 LESSONS LEARNED

Challenges specific to groundwater monitoring during this phase of the Demonstration included breakdown of the pressure transducer originally installed at borehole NN-18; bladder pump system malfunctions at boreholes NN-17 and NN-18; and winterization of wells originally planned for sampling at Pads S-29 and S-16 as well as the NNVM Visitor Center and Prairie Campground water wells.

The pressure transducer originally installed at NN-18 during borehole seismometer deployment was replaced by OWRD in mid-December. The bladder pumps installed at NN-17 and NN-18 malfunctioned during stimulation, delaying sampling at both sites. The pumps were likely blocked with silt which later settled off and freed enough surface area for the pumps to operate; both are currently in working order and were removed from the wells after final sampling was completed. Water wells at the NNVM Visitor Center and Prairie Campground were originally planned for sampling during stimulation but the wells were winterized by Forest Service staff in October, preventing sampling at these two sites. Generators powering the well pumps at water wells on Pads S-16 and S-29 were removed from the site and wells were winterized in December.

3.11 ROAD CROSSING REMEDIATION

During the 2012 operating season, a 0.25 m (10 in) water line was installed between Pad S-16 and Pad S-29 to provide backup water for stimulation and flow-back capacity. Three road crossings were built for the pipeline, each with approximately 1.5 m (60 in) road base coverage, and each including CRP piping with aluminum water pipe inside. In August 2013, these crossings were excavated, pipe materials were removed, and the road base rebuilt and graded to match existing road grade (Figure 3-18) illustrates the project area and road crossings.

Figure 3-18. Pad locations and road crossings.

4 COLLABORATORATIVE WORK

Five grant sub-recipient research groups carried out collaborative investigations during Phase 2.1:

- NETL/Oregon State University
- Lawrence Berkeley National Laboratory, Earth Sciences Division
- Energy and Geoscience Institute, The University of Utah
- Texas A&M University
- Lawrence Livermore National Laboratory

4.1 4D IMAGING OF FLUID MIGRATION BY COMBINED MT/CSAMT, GRAVITY, INTERFEROMETRIC RADAR, MICROSEISMICITY

During Phase 2.1, the National Energy Technology Laboratory (NETL) oversaw a project exploring techniques to monitor fluid injection, changes in permeability, porosity and mineral reaction products during stimulation. This project seeks to improve low-cost monitoring capabilities through integration of newly emerging, surface-based techniques. The field work was completed by Oregon State University (OSU) and Zonge International from Tucson, Arizona, between October and December, 2012. Research focused on overlaying three monitoring techniques to reduce ambiguity: portable interferometric radar, wideband magnetotelluric (MT)/controlled source electromagnetic (CSEM) surveys, and gravity surveys.

4.1.1 PORTABLE INTERFEROMETRIC RADAR

The study used a portable field-based interferometric synthetic aperture radar system, as opposed to a typical satellite or aircraft based approach, which allows for detection of sub-centimeter ground surface deformations. The system employed an array of 100 radar reflectors installed in the projected stimulated zone to monitor ground surface deformation during the stimulation. An initial visualization of radar system using TerraSAR-X satellite data is shown in Figure 4-1. This aspect of the project is overseen by Paul Vincent at OSU, and results are pending.

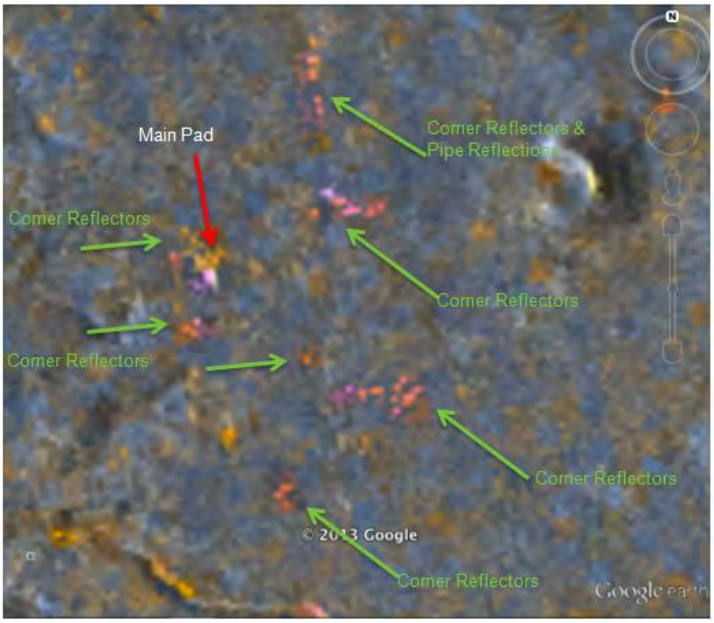

Figure 4-1. Image of TerraSAR-X satellite data highlighting position of radar reflector array at Newberry.

4.1.2 WIDEBAND MAGNETOTELLURIC (MT)/CONTROLLED SOURCE ELECTROMAGNETIC (CSEM) SURVEY

The MT/CSEM survey was designed to study the electrical resistivity within the reservoir. Resistivity is affected by the presence or absence of fluids, fluid and rock composition, temperature variations within the reservoir, reservoir porosity, and permeability. MT/CSEM surveys were conducted by Zonge International in coordination with OSU. Pre-stimulation MT/CSEM data were obtained over a 75 station grid, and Figure 4-2 illustrates the three dimensional contour map of resistivity based on MT data. MT data were obtained from 29 stations of that grid during stimulation. Additionally, continuous MT profiling data were obtained before and during stimulation. Weather made running continuous MT survey stations difficult because the solar power sources for the stations were inhibited by snowfall. Fuel cell systems were brought to the site to provide additional power. Currently, data gathered before and during stimulation are being processed and results are pending.

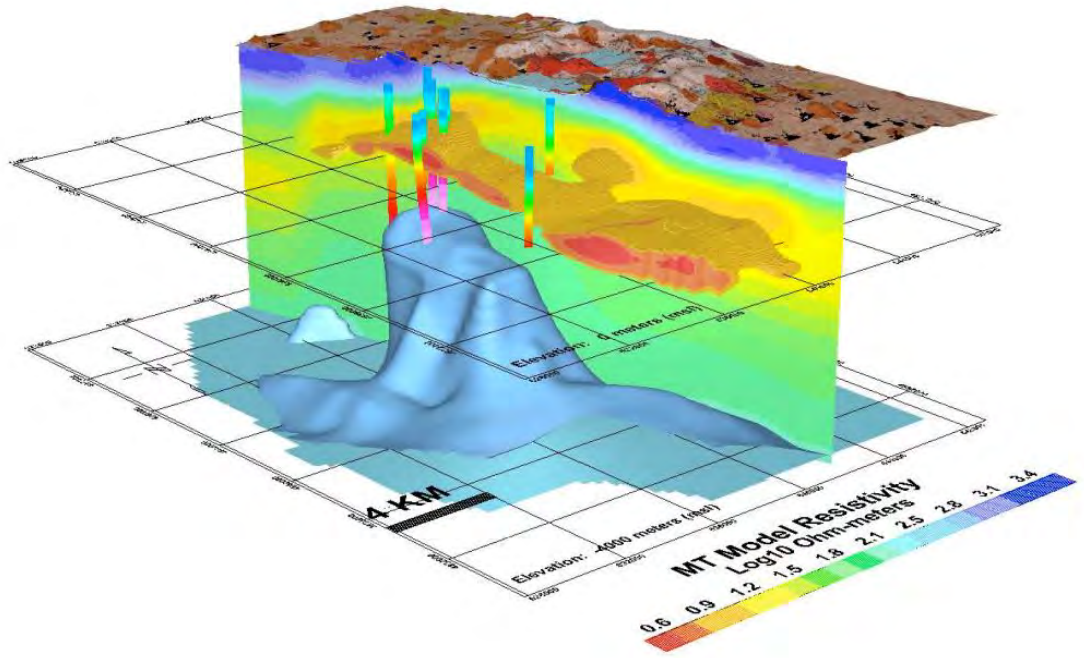

Figure 4-2. Data analysis of previous MT survey performed at Newberry Caldera

4.1.3 GRAVITY SURVEYS

Gravitational acceleration was measured as an indicator of rock density below and surrounding the points of measurement. Density is related to rock composition, mineral structure, and porosity of the rock. A pre-stimulation survey of variations in absolute and relative gravity over the stimulation zone was measured across a 400 point survey grid. Gravity surveys that were planned to be conducted during and after stimulation were abandoned because of extreme winter weather conditions. Figure 4-3 shows an example of one of the gravity stations employed in the survey.

Figure 4-3. Absolute gravity gravimeter survey site preceding stimulation.

4.2 THERMAL-HYDROLOGICAL-MECHANICAL (THM) SIMULATIONS

The research group of Dr. Eric L. Sonnenthal at in the Geochemistry Department at Lawrence Livermore National Laboratory (LBNL) has modelled the thermal response of the reservoir around well NWG 55-29 in response the stimulations. The purpose of these analyses was to evaluate the potential locations and magnitudes of leaks from the cased well bore during the 2012 stimulation work. Locations of the potential leaks are constrained by comparing modeling results with observed DTS temperature measurements and wellhead pressures. Modeling results are also compared to micro-earthquake (MEQ) locations in order to better evaluate the fluid pressure changes that led to fracture slip or propagation in the rock mass. A series of sensitivity scenarios were performed with leaks in different parts of the cased interval. In this analysis, changes in fracture permeability owing to mechanical deformation are not considered, other than simple effects from pore compressibility and thermal expansion/contraction. Although THM effects are certainly important in understanding changes in permeability in the reservoir accompanying microseismicity, the focus of this analysis is to model the temperatures and pressures in the wellbore. Dynamic mechanical effects on permeability can be better understood if temperatures and pressures are constrained at the wellbore.

4.2.1 STUDIES PERFORMED PRIOR TO THE STIMULATION TEST

A native-state 2-D numerical model and a 2-D radially symmetric model were developed to constrain the hydrological and thermal properties of the main hydrogeologic units. Steady-state temperature and pressure distributions were then developed within these models and used as the initial conditions for the native-state Thermal-Hydrological-Chemical (THC) model (Figure 4-4). The static temperature profile measured in 2010 was used to estimate thermal conductivities along the length of the wellbore for both models. At steady-state, the pressure and temperatures profiles generated by the models closely match the static survey data. The models capture many of the major high-temperature alteration minerals and their distributions determined through analysis of cuttings from the NWG 55-29 well (Sonnenthal et al., 2012).

a.

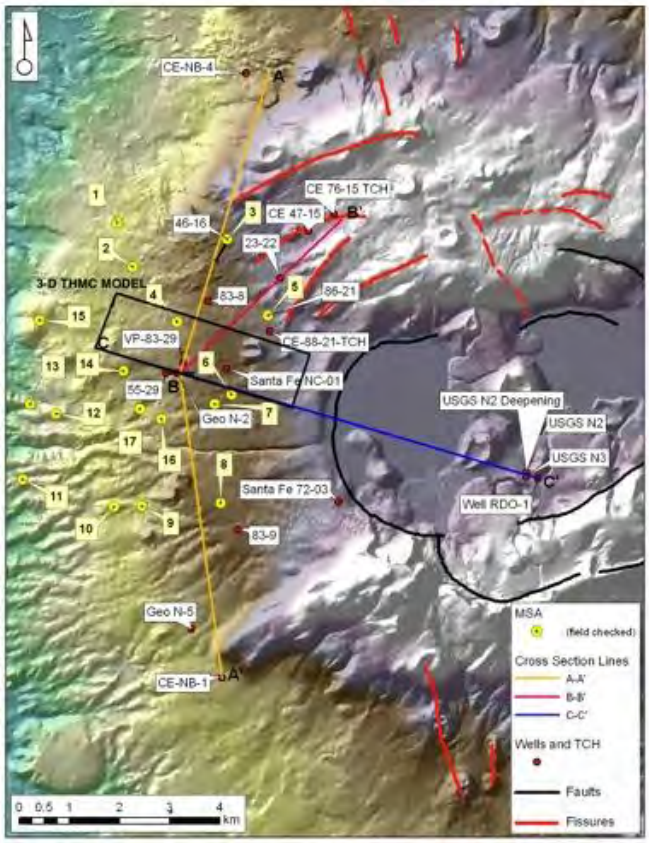

b.

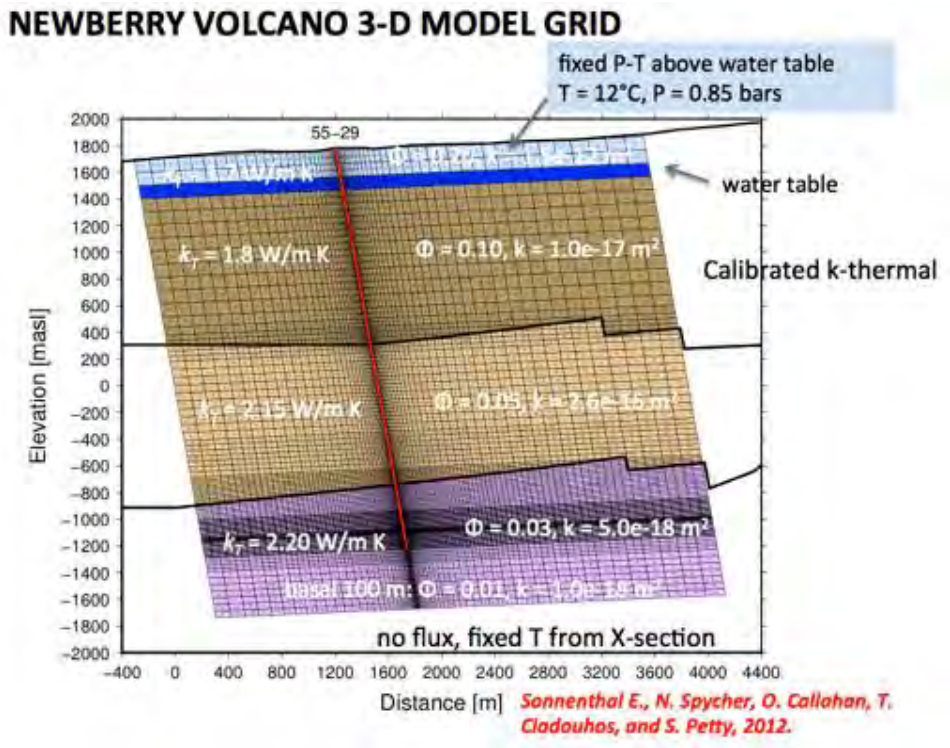

Figure 4-4. a) Plan View of 3-D THC Model of Newberry Volcano Stimulation. b) Cross-section of model mesh along C-C' with base-case thermal and hydrological properties for large-scale units.

The predictive thermal-hydrological-mechanical (THM) simulations were performed prior to the stimulation using the TOUGH-FLAC simulator code and thermal-hydrologic properties from the native-state THC model. The simulation results showed significant increases in permeability (approximately two orders of magnitude) in the rock surrounding the uncased borehole (Rinaldi et al., 2012). This region extended up to about 500 m (1,640 ft) from the wellbore, and was confined to the deeper hydrogeologic units below the casing shoe. However, these simulations were based on a simplified plan of the stimulation experiment prior to the test, and assumed an intact well casing.

4.2.2 MODELING APPROACH

The approach to analyzing the stimulation experiment was to extend a 2-D model to a 3-D model, refine the well design and rock hydrologic properties, and implement the detailed injection rate history. Simulations were performed assuming different possible leak locations, leak permeabilities, host rock permeabilities, and local fracture permeability differences.

The numerical mesh was modified from the 2-D mesh used in Sonnenthal et al. (2012) by extending it about 1.2 km to the northeast to make it a fully 3-D model (Figure 4-4). The southwestern domain of the system was considered to be identical by symmetry. Revisions were made to more accurately reflect the well design (i.e., areas, volumes, and effective Darcy permeabilities, Table 4-1). The designations of the rock units (i.e., Newberry-Deschutes, John Day, etc.) are based on the initial geologic conceptual model for the system by AltaRock, but may not be directly correlated to these specific geologic formations found in Central Oregon. However, the model does not use any data collected elsewhere for these formations, and so the names are merely convenient designations. The values of the hydrologic parameters were determined primarily by starting with the base case values and then making adjustments by comparison to temperature profiles and wellhead pressures, keeping them in reasonable ranges. These adjustments are discussed later.

Calibrated rock thermal conductivities (Sonnenthal et al., 2012), along with heat capacities and densities of the steel and cement are given in Table 4-2. Thermal conductivities for shorter segments in the wellbore, calculated by David Blackwell, are shown in parentheses for comparison.

Injection in the field was performed by adjusting the pumping rate to achieve specific wellhead pressure targets, with measured injection rates that were the result of flow into and out of the wellbore. For systems where the boundary conditions vary over time, with TOUGH2 or TOUGHREACT we typically assign a time-dependent injection rate and enthalpy schedule, since time-dependent pressure boundary conditions cannot be easily implemented. To calculate the TOUGHREACT inputs, injection rates measured at the wellhead during the stimulation were filtered to create a table of injection rates. The filtering for the injection rate schedule was based on a 2-hour boxcar mean, averaged over a 4-hour window (Figure 4-5) using the *filter1d* routine in the GMT5 software package (Wessel & Smith, 1998). The 2-hour boxcar mean captures many of the spikes and drops in injection rate thus leading to a fairly close approach to the test measured values. Because some of the spikes in the measured data are very short in duration (minutes), numerically it would be difficult to consider the raw data directly, and their inclusion would not significantly change the overall amount of fluid injected. However, some of the spikes could be important as indicators of changes in hydrologic properties or problems with the pumps.

Table 4-1. Base-case and revised (red) hydrological properties for the wellbore, rock units, and simulated leaks.

Hydrogeologic Unit	Porosity	k_x (m^2)	k_y (m^2)	k_z (m^2)
Newberry-Deschutes (upper 300 m)	0.20	1.5×10^{-12}	1.5×10^{-12}	1.5×10^{-12}
Newberry-Deschutes	0.10	1.0×10^{-17}	2.0×10^{-17}	2.0×10^{-17}
	0.02	**2.0×10^{-15}**	**4.0×10^{-15}**	**4.0×10^{-15}**
John Day	0.05	2.6×10^{-16}	5.2×10^{-16}	5.2×10^{-16}
	0.05	**5.0×10^{-18}**	**1.0×10^{-17}**	**1.0×10^{-17}**
Intruded John Day	0.03	5.0×10^{-18}	1.0×10^{-17}	1.0×10^{-17}
Intruded John Day (lowest 100m)	0.01	1.0×10^{-18}	1.0×10^{-18}	1.0×10^{-18}
PAS/Casing (initial leak)	0.95	1.0×10^{-17}	1.0×10^{-17}	2.0×10^{-7}
PAS/Casing (leak 10/21)	0.95	1.0×10^{-11}	1.0×10^{-11}	2.0×10^{-7}
Casing (13 in)	0.95	0.0	0.0	2.0×10^{-7}
Casing (9 in)	0.95	0.0	0.0	1.0×10^{-7}
Uncased Interval	0.98	1.0×10^{-7}	1.0×10^{-7}	1.0×10^{-7}

Table 4-2. Calibrated and Calculated Thermal Properties

Hydrogeologic Unit	Calibrated/Calculated Thermal Conductivity (W/m-°K)	Heat Capacity (J/kg)
Newberry-Deschutes (upper 300 m)	1.70	1000
Newberry-Deschutes	1.80 (1.46-1.85)	1000
John Day	2.15 (1.85-2.30)	1000
Intruded John Day	2.20 (1.99-2.26)	1000
Intruded John Day (base)	2.20	1000
Well Casing & Cement	4.00	1635

Calibrated rock values from Sonnenthal et al. (2012). Values in parentheses are the range of calculated values from Dave Blackwell, which reflect a finer discretization along the wellbore. Combined well casing and cement values calculated by AltaRock.

Enthalpies of the fluid were calculated using the measured temperature of water before it was pumped into the wellbore. Owing to large differences in air temperature during the test due to a transition from summer to winter weather, the injected water temperature varied by over 20 °C during the stimulation at the wellhead. Temperatures measured at the wellhead by DTS often differed by as much as 20 °C, but these values were not measured at the same frequency as the injection rates. There were no systematic differences in temperatures between water going into the pumps and the wellhead temperature, so it is not straightforward to correct the injection water temperature such that it always matched the wellhead temperature. While this did not appreciably affect temperatures below 1000 m depth, the shallow temperatures cannot be directly captured at all times, particularly at later times. Future revisions of the enthalpy inputs may be improved by using average measured wellhead temperatures over short time intervals to calculate enthalpy input values.

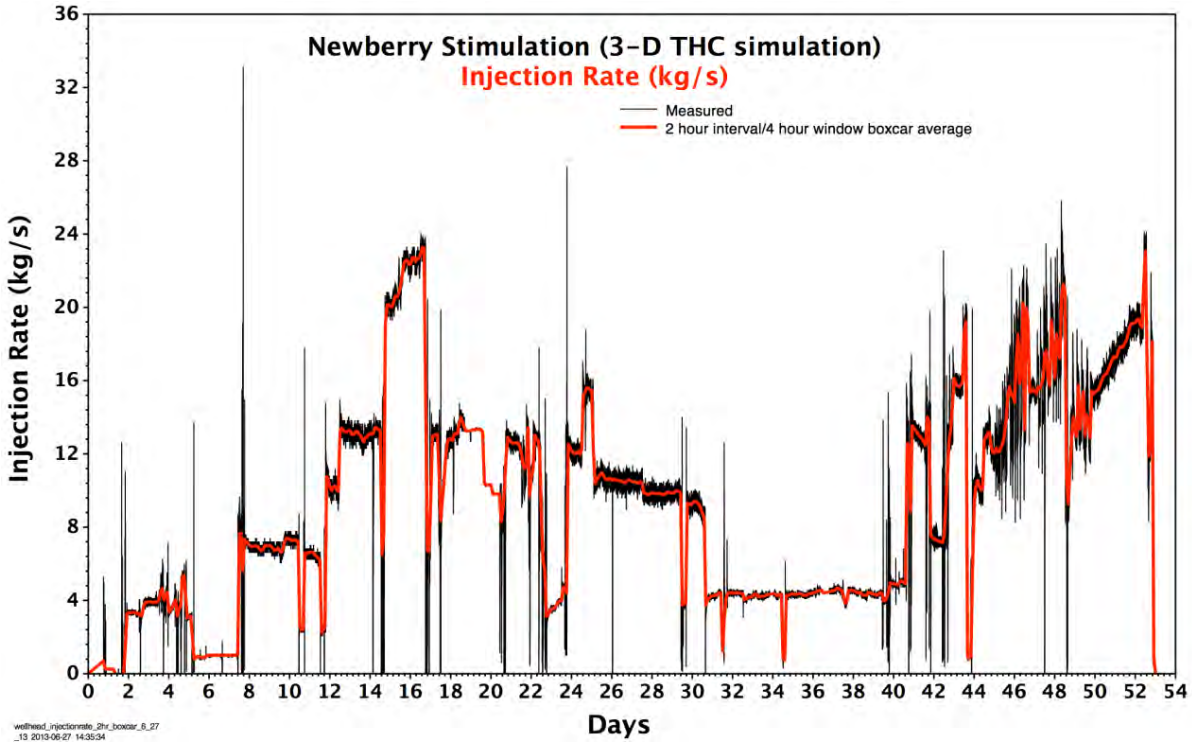

Figure 4-5. Filtered injection rates (kg/s) over time in red (2-hour boxcar average with a 4 hour window), and measured rates in black.

Simulations were performed using a new parallel version of TOUGHREACT (Sonnenthal et al., in prep.) based on Version 2 (Xu et al., 2011). The simulations include full coupling for thermal and hydrological processes with a very simplified chemical system (quartz, $SiO_{2(aq)}$, H^+, LiCl, and CsBr tracers), and permeability changes owing to quartz dissolution/precipitation. This simplified chemical system was included primarily as a basis for visualizing fluid transport and for later inclusion of the full chemical system from the native-state model. The only mechanical effects considered are pore compressibility (uniformly 3.2×10^{-9} Pa^{-1}) and rock thermal expansion/contraction (uniformly 3.0×10^{-5} K^{-1}).

Several dozen simulations were performed with different combinations of parameters, some of which were described in an earlier draft report. This analysis focuses mostly on the latest most complete simulations, with some of the intermediate results for comparison. Compared to early results presented in the first draft of the Phase 2.1 Stimulation report and at the DOE Peer Review, simulations described in this report have a better description of the wellbore geometry, hydrological, and thermal parameters.

Earlier simulations showed significant fluid flow into the "John Day" unit and into observed fracture zones below the casing shoe. In addition to the casing leaks, four features in the open cased section were considered: one high permeability dike-like feature near the base of the well, and three features closer to the casing shoe that were observed in the borehole televiewer which had noted loss zones during borehole completion. All three features were initially given permeabilities two orders of magnitude higher than the surrounding rock (based on THM results on shear fracture permeability changes; Rinaldi et al., 2012). Early simulations showed that the features near the casing shoe must have relatively low permeabilities, because DTS measurements do not show significant perturbations in the temperature gradient. Simulations using high local permeabilities result in strong temperature perturbations (Figure 4-6).

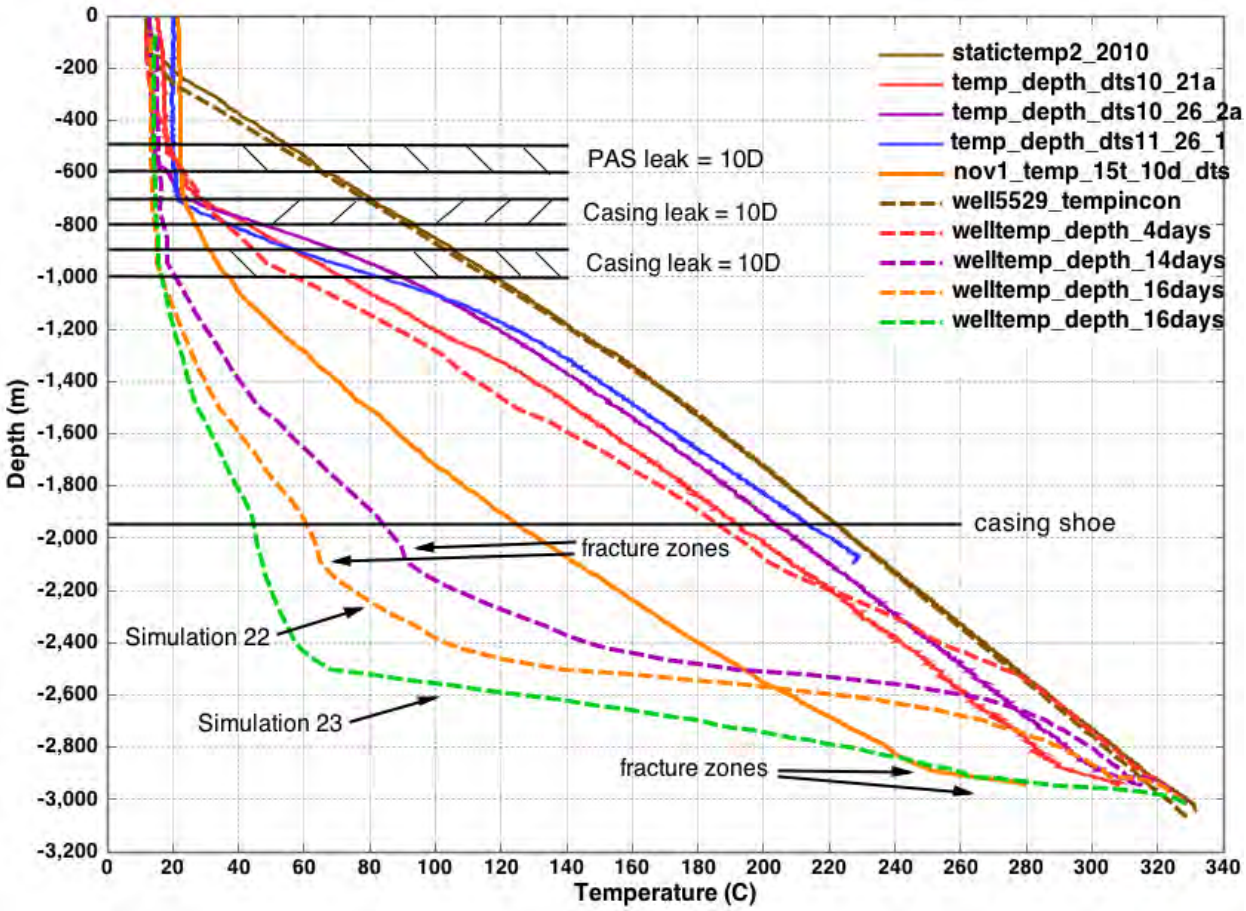

Figure 4-6. Temperature profiles for earlier simulations using base case permeabilities and fracture zones near the casing shoe. Note the strong depression in simulated temperatures (dashed lines) compared to DTS measurements (solid lines) below the casing shoe indicating excessive flow into deeper units.

4.2.3 STIMULATION MODEL RESULTS – TEMPERATURE AND PRESSURE

Simulated temperature profiles using these parameters could not match DTS measurements, regardless of the leak permeability value used (Figure 4-6). Because observations of the temperature gradients and the lack of fluid losses during drilling did not show any significant differences between the "John Day" unit and the lower "Intruded John Day" unit, the permeability of the former was adjusted to match the latter unit. Simulations with the permeability of the Newberry-Deschutes hydrogeologic unit set to about 2.0 x 10^{-17} m^2 showed that leaks in the casing alone were not sufficient to allow significant water to exit the casing. Therefore, in the latest simulations, the permeability of the "Newberry-Deschutes" unit was increased by about two orders of magnitude (Table 4-1). Since it was necessary to increase the permeability of this unit prior to the leak event and before any observed seismicity at this depth, it is unlikely that the increase in permeability was solely a result of fracture slip or propagation associated with the shallow leaks.

In the latest simulations, only the deeper features were retained, and hence modified to an initial permeability of 3 x 10^{-16} m^2, which is only about a factor of three to six higher than the average permeability. However, these grid blocks have vertical dimensions of 10 meters, which is larger than the actual fracture thicknesses; such increases reflect averaging of larger localized features. The permeabilities used for the leaks were estimated based on simulations using a range of values. The ranges

of values for each leak were not based on leak rates or wellbore crack sizes, but were instead artificially chosen and used to provide potential bounding combinations for the observed DTS profiles.

Figure 4-7 shows the measured wellhead pressure (MPa) over time (blue curve) with the results from Simulations 16 (red), 18 (green), and 22 (purple). These simulations used successively higher permeabilities for the Newberry-Deschutes unit, all with 3 leaks (500-600 m, 700-800 m, and about 1230 m depth), which were originally thought to be the possible leak locations. The leak permeability was held constant through the simulation. Permeability effects from the expansion, compressibility, and dissolution/precipitation were small, did not result in significant changes to pressure or temperature, and are not discussed here.

It is clear that the modeled pressure is higher than the measured pressure for most simulations, yet during the first five days the modeled pressure is less than half the measured pressure. This reversal of modeled vs. measured wellhead pressures between the early aseismic periods (2-5 days) and after about 7.5 days suggests significant changes to injectivity in the wellbore. The measured injection rate between 2-5 days is about 4 kg/s, while after eight days injectivity is about 7 kg/s (Figure 4-5). The measured wellhead pressure drops from roughly 12 MPa to about 3 MPa, which translates roughly to about a seven-fold increase in injectivity. No observed microseismicity was associated with this change. One question is whether this sharp change was due to a leak in the well or some aseismic permeability increase in the uncased section.

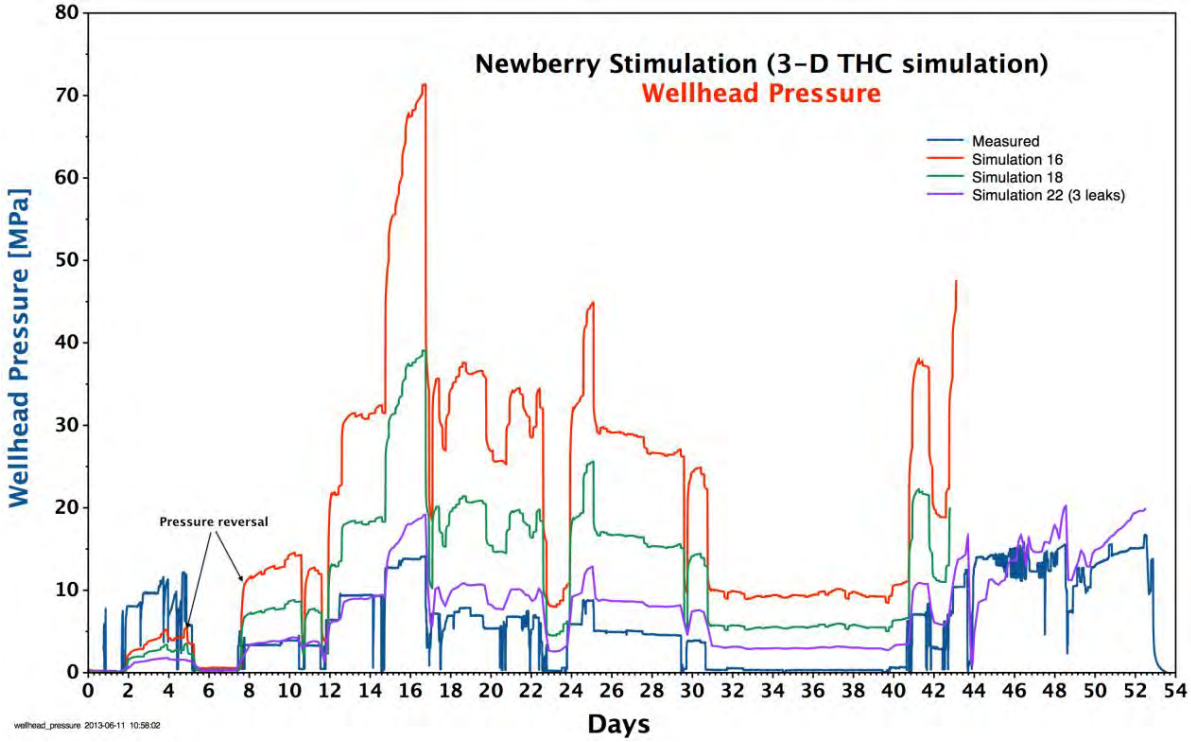

Figure 4-7. Measured (blue) and modeled wellhead pressures (MPa) over time (red, green, and purple curves are simulation results). Note reversal in modeled/measured pressures between approximately 4.5 days and 7.5 days, indicating about a 7-fold increase in injectivity.

Owing to this observed rapid reversal in wellhead pressures, the latest simulations considered a stepwise increase in leak permeability from 1 x 10^{-17} m^2 to 1 x 10^{-11} m^2. However, if there were no leaks over the first 4.5 days, then the wellhead pressure would far exceed that which was observed. Sensitivity studies showed that with a leak permeability of 1 x 10^{-17} m^2 at two locations (500-600 m and 600-700 m depth),

the wellhead pressures roughly match those observed in the first three days (Figure 4-8). The difference between measured and modeled pressures increases by a little after about three days, possibly indicating that the well casing leaks opened as pressures increased. However, the large increase in leak permeability must have taken place around 4.5-5 days when the pressure peaked and one pump was abruptly shut down. When the pumps were both operational and pressures increased again at around 7.5 days (October 23), the injectivity was about seven times higher. From 7.5 days to just over 14 days the difference between modeled and observed pressures was consistently about 1.5 MPa. At 14.5 days (October 31), when the pressures increased to their highest level and the deep microseismic events started, the pressure difference rose to about 4 MPa, and then to about 5 MPa at 16 days. On November 1, the highest injection rate (~23.5 kg/s) was reached at a pressure difference of 6.4 MPa. This consistent increase in the pressure difference between measured and modeled pressure indicates a significant increase in permeability, either at the leak points, in the deeper section of the well, or both.

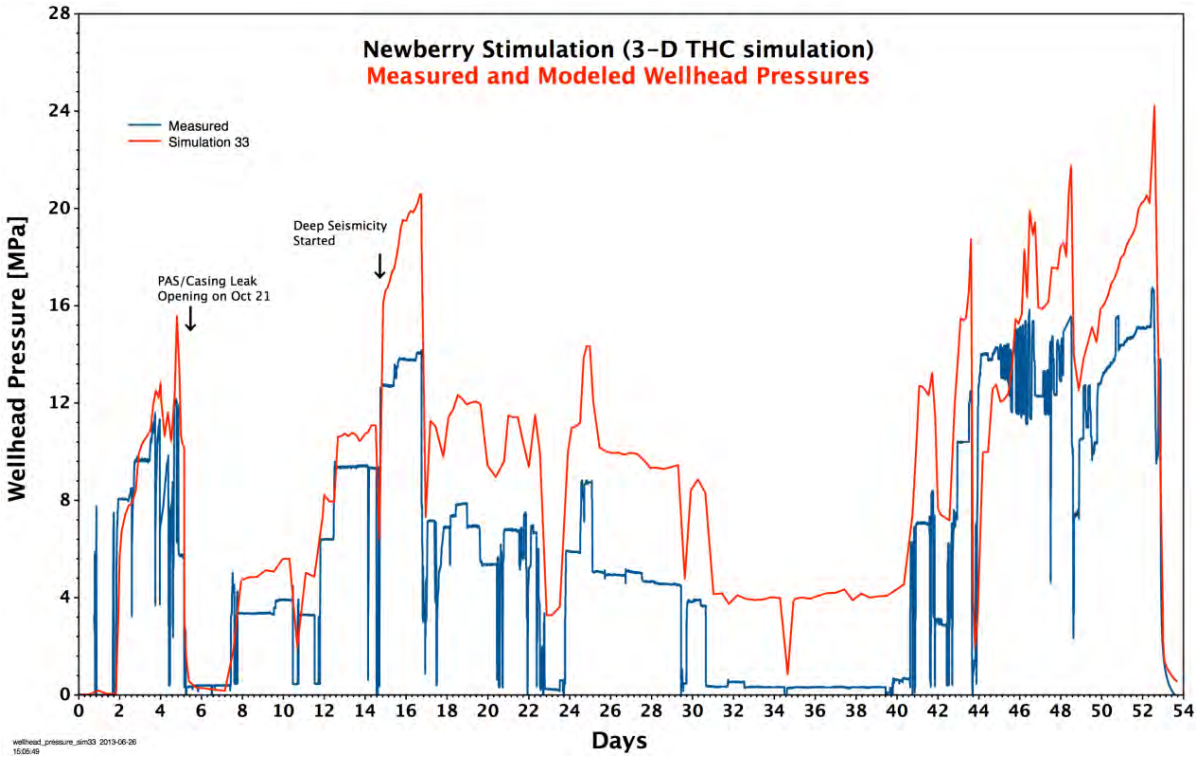

Figure 4-8. Measured (blue) and modeled wellhead pressure (MPa) over time (red - Simulation 33).

After the peak injection rate, and before the diverter injection after 44 days, the pressure differences ranged from about 3.5 MPa at the lower wellhead pressure periods, and about 5.5 MPa, at the times of higher pressure, with only a small increase in injectivity. The effect of the diverter is very obvious between 44 and 46 days, where the modeled pressures (with no diverter added) are significantly lower than the measured pressures. At the end of the stimulation, the pressure difference increased to about 7.5 MPa, suggesting a further increase in injectivity after the second set of diverters were added. Due to the injection of cold water, the diverters would not have begun to thermally degrade until after the injection ceased, so there should be no pressure signal of diverter degradation apparent.

The distribution of flow out of the well is best assessed using temperatures from the DTS measurements. Figure 4-9 shows comparisons for temperatures measured by DTS and for the simulation shown in Figure 4-8. Most of the DTS curves were averaged over 15 measurement times (30 minutes) and 10 meters of depth. These are designated as "Averaged". Raw data are shown for November 30. Comparisons of

averaged and raw data have shown that they are coincident, with the raw data just showing some noise around the mean (not shown).

Except for the earliest period of stimulation (October 19), which was likely when the leaks were starting to open given the cooler shallow observed vs. simulated temperatures, all other curves match nearly perfectly below about 1000 m depth. Even after the diverters were added on December 6, the curves continued to match. As discussed previously, later in the simulation experiment it was difficult to predict the wellhead temperatures given the measured injection temperatures (prior to going through the pumps) because they differed by as much as 20 °C, and there were no consistent trends.

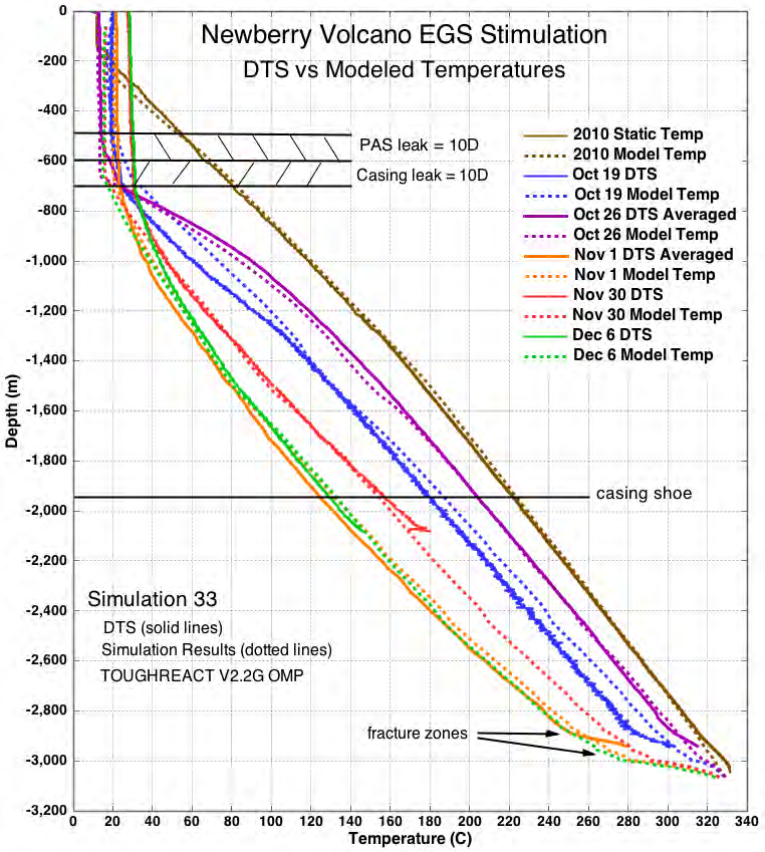

Figure 4-9. Temperatures from DTS measurements (solid lines) and simulation 33 (dotted lines of the same color) at selected times vs. depth in meters.

Given that measured temperature profiles below 1000 m match very closely after leak permeability was increased on October 21, it is clear that some small additional increase in both casing leak loss and deep fluid loss are necessary to match the wellhead pressures while preserving the temperature profile match. Further tweaking of the model to accurately match both pressure and temperature profiles would not likely yield more realistic results because of the dynamic, non-linear thermal-mechanical permeability increases due to both tensile fracture propagation and shear slip.

4.2.4 STIMULATION MODEL RESULTS – WELLBORE FLUXES

Since the latest model results matched measured temperatures quite well and showed a consistent although slightly offset wellhead pressure response, the effect of leaks on flow out of the wellbore can be assessed. First, it is instructive to look at the effect of the leaks on the temperature profiles. Figure 4-10 shows the temperature distributions at the start of the test (based on the October 2010 static survey),

and on October 26, 10 days after the injection began and after the large leaks apparently opened up. The curves show a match in the simulation just described (purple dotted curve) for a constant leak permeability of 1 x 10^{-17} m^2 (purple broken dotted curve), and for no leaks (purple dashed curve). It is clear that even the small initial leak considered at the start of the simulation, if unchanged, results in strong flow to the uncased section and a large change in the temperature profile. The simulation without any leaks allows all flow to exit the uncased part of the well, particularly in the deep fracture zones.

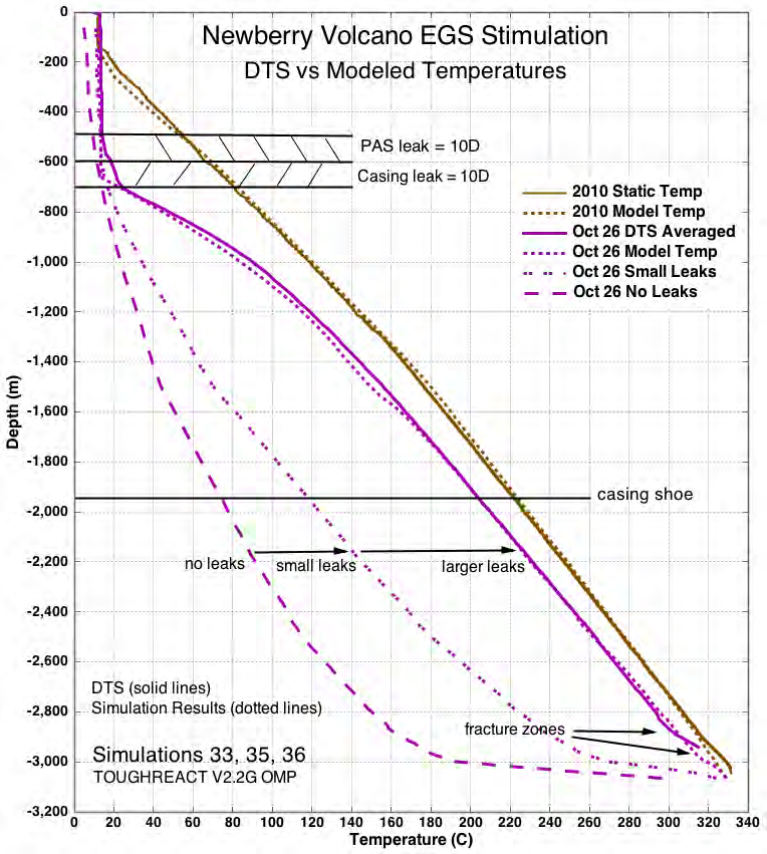

Figure 4-10. Temperatures from DTS measurements (solid lines) and simulated (dotted/dashed lines of the same color) at selected times vs. depth in meters.

The percentages of fluid exiting the two leak points and for the entire cased interval in Figure 4-11 are shown as a function of time for specific days. The percent exiting the casing is calculated according to Equation 5.1:

$$\% \text{ Exiting fluid} = (\text{Injection rate} - \text{Flux out of the casing})/\text{Injection Rate} \times 100 \qquad (5.1)$$

The percent of fluid loss out of the leaks is about 50% for the first four days and prior to the simulated increase in leak permeability. After the leak permeability was increased, there was a large drop in wellhead pressure owing to pump breakdown which resulted in flow back up the well and out of the leaks and yielded a greater than 100% fluid loss. After that temporary increase, the total leak loss stayed at about 90% until the end of the experiment. The loss out the second slightly deeper leak (600-700 m) was only slightly higher than at the PAS (500-600 m). No other leaks were necessary to match the temperature profiles, though it is possible other very small leaks were present.

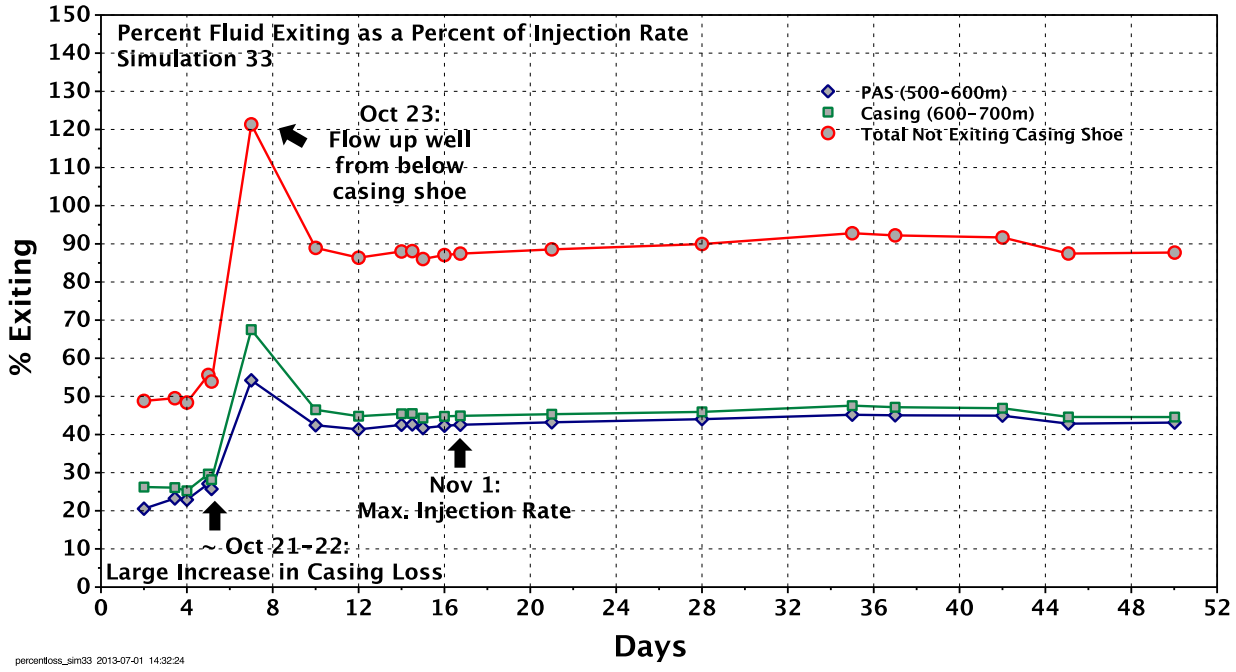

Figure 4-11. Percent of fluid exiting the two leak points and for the entire cased interval shown as a function of time for specific days.

4.2.5 SIMULATED PRESSURE FIELDS AND MEQS

This section compares the simulated pressure fields to the location of MEQs from Cladouhos et al. (2013). Pressure differentials (P_{fluid} - $P_{hydrostatic}$ > 0.05 MPa) from the simulation that best matched temperatures (Simulation 33 shown in Figure 4-7) are plotted in 3-D in Figure 4-12 at 16.7 days (peak injection rate) and at 50 days. Because the model assumes symmetry for the region to the southwest of the wellhead, the model results are plotted for the full volume and the southwest half is a mirror image. The pressure cutoff of 0.05 MPa is arbitrary but successfully captured the area of all MEQ locations. All relocated (red) MEQ events are shown for comparison. While there are systematic errors in the calculations used to relocate the MEQs and measurement errors in the locations themselves; that discussion is beyond the scope of this report. Therefore, only the relocated events for a qualitative comparison are plotted.

The most significant aspect of the simulated pressure fields include:

1) The umbrella-like shape of the upper zone around the cased well, with a sharp cutoff at the contact between the lower permeability "John Day" unit below the "Newberry-Deschutes" unit. This seems to capture the overall distribution of shallow MEQs.

2) The limited zone of increased pressure in the deeper uncased section, roughly coincident with the deeper MEQs.

3) The large gap in increased pressure between the casing shoe and the unit contact above, where no MEQs are located.

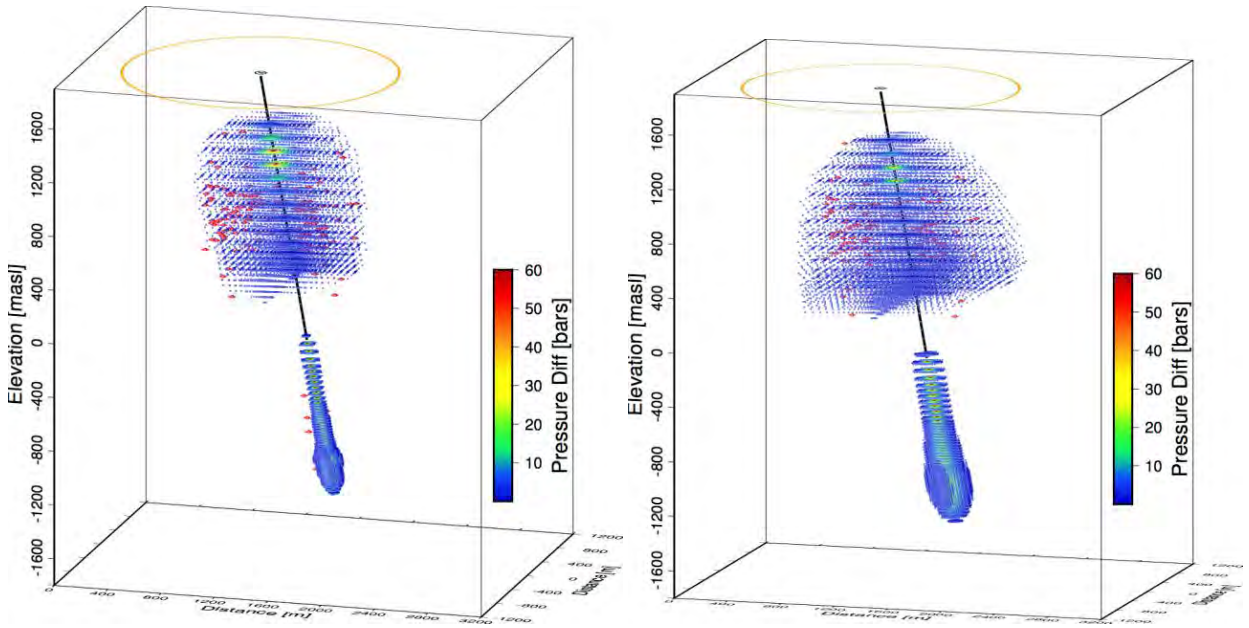

Figure 4-12. Pressure differential (P_{total} - $P_{hydrostatic}$ > 0.05 MPa) plotted at 16.7 days and 50 days for simulation 33. View is from the southeast toward the northwest. Yellow circle outlines a region having a 1 km radius from the wellhead (black circle at top). Cased interval is in black. Red symbols are relocated MEQs (Cladouhos et al., 2013).

4.2.6 EFFECTS OF STIMULATION ON PERMEABILITY

Here we evaluate potential permeability changes from stimulation and fracture geometries constrained by earthquake magnitudes. A simple percolation approach for a narrow distribution of 2D cracks (Gueguen & Dienes, 1989) can be used to evaluate the size and connectivity of the fracture network. This model assumes a narrow fracture size distribution, and therefore calculated connectivity and permeability changes are higher than if a broad distribution is considered; such as the fracture density and mean diameter given in Charlaix et al. (1987).

A block size where most of the earthquakes took place is approximately 1.5 km on each side. It may be a little more oblong in the northeast-southwest direction, but this size gives about the right volume for the events. The number of events in the shallow region was roughly 200.

Case 1:

The first case looks at whether the density of events and their mean rupture diameter exceeds the percolation threshold, assuming the events are associated with planar 2-D cracks. For the probability of connectedness to exceed the critical value, the fracture radius would need to be at least 66 meters. Because the mean radius of rupture is only about 40 meters (based on calculations from the seismic moments, Ernie Majer, pers. comm.), the fracture slip events alone are not enough to exceed the percolation threshold.

Case 2:

Assuming the fracture spacing is 30 meters, which approximates the scale of the layer thickness and observed fracture spacing, then:

$$\text{Number of fractures} = (\text{block length/spacing} - 1)^3 = 117649 \qquad (5.2)$$

To exceed the percolation threshold in this case, the fracture radius must be at least about eight meters. A permeability of 2.9 x 10^{-16} m^2 is achieved if the aperture is 100 microns (µm), which is roughly an order

of magnitude higher than the inferred permeability of 2-4 x 10^{-15} m^2. If the fracture radius is 10 meters, then the aperture can be about 10 µm to get a permeability of 1.6 x 10^{-16} m^2. These fracture sizes are smaller than the sizes determined from the seismic moments, so there must be much larger fractures in the distribution of fractures that are slipping.

Case 3:

This scenario assumes fracture sizes as calculated from the seismic moments (40 m radius average). Also assumes there are more fractures that have not slipped. How many more? About 900 fractures are needed to exceed the percolation threshold (roughly 4.5 times the number of events). To obtain a permeability of 3.2 x 10^{-16} m^2, with an aperture of 10um, 3000 fractures are needed, which yields a fracture spacing of just over 100m.

The permeability needed to simulate the pressure and temperature data measured in the well after leakage began was k_x = 2 x 10^{-15} m^2, $k_y = k_z$ = 4 x 10^{-15} m^2. To increase the permeability from 3.2 x 10^{-16} m^2 to near that value (2.6 x 10^{-15} m^2) requires doubling the fracture aperture from 10 µm to 20 µm, assuming no increase in the fracture size or density.

4.2.7 SUMMARY & CONCLUSIONS

In summary, THC simulations were performed to give insight into the potential range of properties for different possible leaks in the wellbore. Modeled effects on temperature and pressure for different leak values were compared to observed data recorded in the 2012 stimulation. Detailed injection rates from the stimulation measurements and wellbore properties, including casing and cement thermal properties, were used in conjunction with a newly developed 3-D model of the site extending about 1.2 km to northeast of the stimulation well. The simulations were not meant to model the MEQs, but nevertheless the TH-induced pressure changes were used to evaluate shear failure in a continuum THM model. The results indicate that a significant change in injectivity took place between 5 and 7.5 days into the stimulation period which caused about a seven-fold increase in injectivity. Modeling showed that it is unlikely that a significant leak exists at the liner overlap, but one is likely at the PAS connection between 500 and 600 m depth, and in the casing between 600 and 700 m depth.

After adjusting the base case permeabilities estimated from the native-state THC model, simulated temperatures matched DTS measured values closely for a simulation scenario having the two small leaks at the start of the simulation, followed by a large increase in the leak permeability (six orders of magnitude) on October 21. Fluid losses out the casing for this simulation are about 50% for the first few days, and about 90% for much of the period after the leaks opened up and injection pressures increased. A short period of time after the leak permeability increased, a pump failure may have resulted in flow up the well and out the leak. After deep seismicity was observed on October 30th, the difference between modeled and measured pressures became larger which indicated some increased permeability throughout the well bore. This can be further inferred because temperatures profiles match well for the entire simulation.

Pressure differences in 3-D from the latest simulation roughly capture the overall distribution of relocated MEQs. Therefore, given a better incorporation of geologic heterogeneities from core logs and wellbore fracture distributions for well NWG 55-29 (Davatzes & Hickman, 2011), as well as from the nearby well N-2 (Fetterman, 2011; Fetterman & Davatzes, 2011), it seems possible that the MEQs may be able to be simulated directly by THM models by manipulating changes in fluid pressure-driven stress on the rock.

Simple calculations/speculations based on percolation theory and rough estimates from MEQ data analysis suggest that the initial fracture network in the shallow zone where most of the MEQs were observed may consist of fractures having a mean radius of 8 to 10 m. Given that estimated slip areas for

MEQs correspond to mean fracture radii of about 40 m, the observed MEQs represent events on the larger end of the fracture size distribution, which by themselves would not form a connected network. Therefore, it is likely that smaller events, ones below the detection threshold of the Micro-Seismic Array, play an important role creating a connected fracture network.

4.3 BOREHOLE FLUORIMETER PROTOTYPE

A borehole fluorimeter has been designed at the Energy and Geoscience Institute at the University of Utah to identify newly created fractures down the wellbore. The location of these fractures would be confirmed in real-time downhole through the measurement of fluorescent tracers emerging from the newly created fractures. These tracers are injected into the wellbore immediately prior to running the tool; injection also cools the wellbore to which protects the tool from thermal damage. The fluorimeter is rated for 3 hours of exposure at 275 °C, and so deployment of the tool will work within these limits.

A bench-test unit of the prototype fluorimeter was fabricated, including the printed circuit boards that control the operation of the LED and photo-diode. Shown in Figure 4-13 is a sketch of the tool, showing the LED light source, the photodiode detector, and the various lenses, prisms, and fiber optics that are key to the design of the tool.

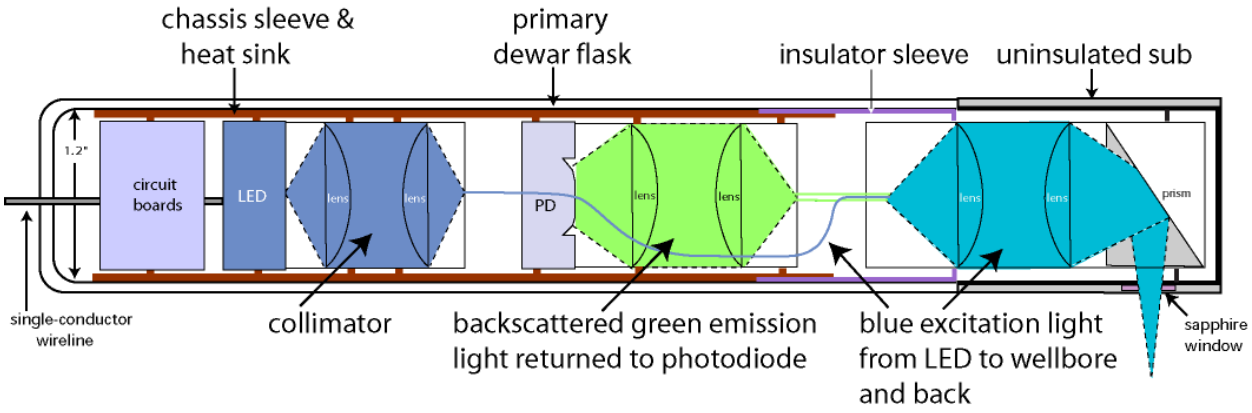

Figure 4-13. Schematic of the borehole fluorimeter tool design.

Shown in Figure 4-14 is a picture of the portion of the borehole-fluorimeter prototype that includes the LED light source and the photo-diode detector (with accompanying optics and electronic controls) inside its protective heat-sink chassis. Not shown are the collimator lens and prism that deliver the excitation light signal and return the backscattered light signal. Also not shown is the protective thermally insulating flask that will seal the sensitive components in the prototype.

Fabrication of a field-deployable prototype of the fluorimeter is waiting on funding.

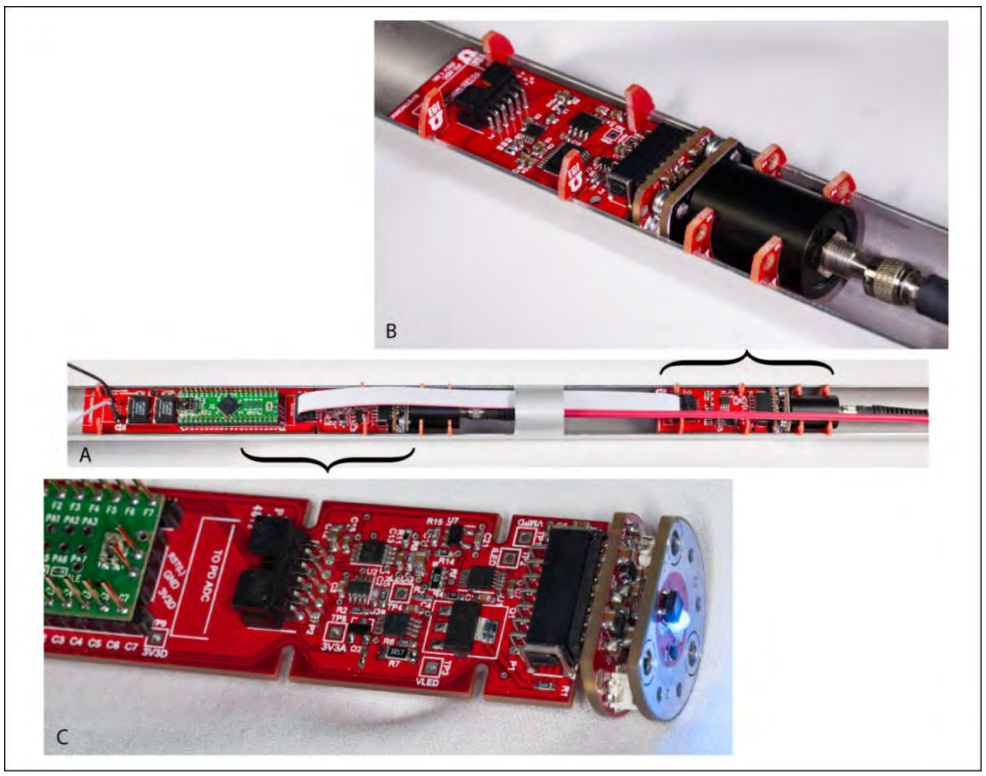

Figure 4-14. Photographs of a portion of the borehole-fluorimeter prototype, showing (A) the assembled LED light source and photo-diode detector with accompanying fiber-optics, collimators, and electronic controls, (B) an expanded view of the photo-diode detector with the associated circuit boards, collimator, and fiber-optic, and (C) an expanded view of the blue LED light source and associated circuitry.

4.4 MECHANICAL PROPERTIES OF INTACT ROCK AND FRACTURES IN NEWBERRY WELDED TUFF

The research group of Dr. Ahmad Ghassemi at Texas A&M University has been actively studying the mechanics of Newberry Volcano rock (Li et al., 2012); Ghassemi is now at the University of Oklahoma. This work characterized the mechanical properties of welded tuff samples collected from three boreholes completed on the western flank of Newberry Volcano. Multistage triaxial compression tests were performed to determine Young's modulus, Poisson's ratio, and failure envelope. Multistage triaxial shear tests were performed to determine the mechanical properties and shear strength of the fractures developed in the compression tests. Joint Roughness Coefficient (JRC) and Joint Wall Compressive Strength (JCS) were obtained through back-analysis of the shear tests. The results of the report are provided in Table 4-3. It was found that the JCS of tested joints are larger than the intact rock Uniaxial Compressive Strength. The joint surfaces were characterized by a laser profilometer to correlate the surface roughness profile to the JRC from back-analysis of experimental data. Joint normal stiffness and shear stiffness were estimated and it was observed that a higher confining pressure results in higher joint shear stiffness. The stiffness is gradually reduced as the contact surfaces become smoother with additional shear displacement.

Table 4-3. Mechanical properties obtained from compression

Sample ID	Young's Modulus (psi); Poisson Ratio	UCS (psi)	Cohesion (psi)	Friction angle	Joint Roughness Coefficient	Joint Wall Compressive Strength (MPa)
N1-4103 (1H)	3,945,273; 0.42 (P_c = 4500 psi)	17,676	3,586	45.1°	0.236	188.8
N1-4383 (2H)	2,402,227; 0.28 (P_c = 4500 psi)	10,811	3,376	26.3°	0.353	170.2
N2-4219 (2H)		8,270	2,211	33.8°	0.127	181.3
Oxy-4395 (5V)	6,822,836; 0.41 (P_c = 4500 psi)	17,247	3,955	39.1°	0.372	196.9

4.5 MICRO-SEISMIC INTERPRETATION VIA MATCHED FIELD PROCESSING

Dennise Templeton at Lawrence Livermore National Lab (LLNL) has performed new micro-seismic interpretation using the empirical Matched Field Processing (MFP) technique to enlarge and improve the seismic catalog (Wang et al., 2011; see Appendix F). MFP differs from the established earthquake detection techniques and is an adaptation of a signal processing technique originally developed to locate continuous underwater acoustic sources (Bucker, 1976; Baggeroer et al., 1993). LLNL calculated the wave field structure across the array by estimating the structure directly from field calibration data, i.e., previously observed seismic events (Figure 4-15). Then they steered the array explicitly in the frequency domain using the complex phase and amplitude factors obtained from the field data (Harris and Kvaerna, 2010). They refer to this strategy as empirical MFP, in which the master templates created from the seismograms of previously detected micro-earthquakes contain contributions from direct and scattered seismic energy.

Empirical MFP largely eliminates the sensitivity of correlating operations to source time history variations by processing the observed data stream in a large number of narrow frequency bands. This makes MFP sensitive to the spatial structure of the signal at the observing aperture (controlled by mechanism and propagation), but not the temporal structure (controlled, in part, by source time history). In this way MFP can identify previously undiscovered events even if they bear little resemblance to the master event in the time domain.

Using the empirical MFP method, LLNL was able to identify 240 additional events (Figure 4-16) occurring between September 2012 and December 2012 at the Newberry EGS site. There were 207 events in the original catalog during this same time period. The new events were primarily located in the shallow seismic swarm. Combining the original and newly detected event catalog, possible seismic planes in the subsurface become further illuminated. One such plane is shown in (Figure 4-17).

Future work will include an extension in time of the above MFP earthquake detection method to identify more microearthquakes post-December 2012. The last observed event in the original catalog occurred in late February. LLNL will determine how long the "crackling" will continue after the last known event occurs and which seismic lineations are the most active.

LLNL will run a standard earthquake detection routine to verify the suitability of the AltaRock automatic STA/LTA parameters. All seismic studies that AltaRock initiated were based on the original automatically triggered catalog. Verifying the routine will be relatively straight-forward and provide evidence that no larger-events were originally missed.

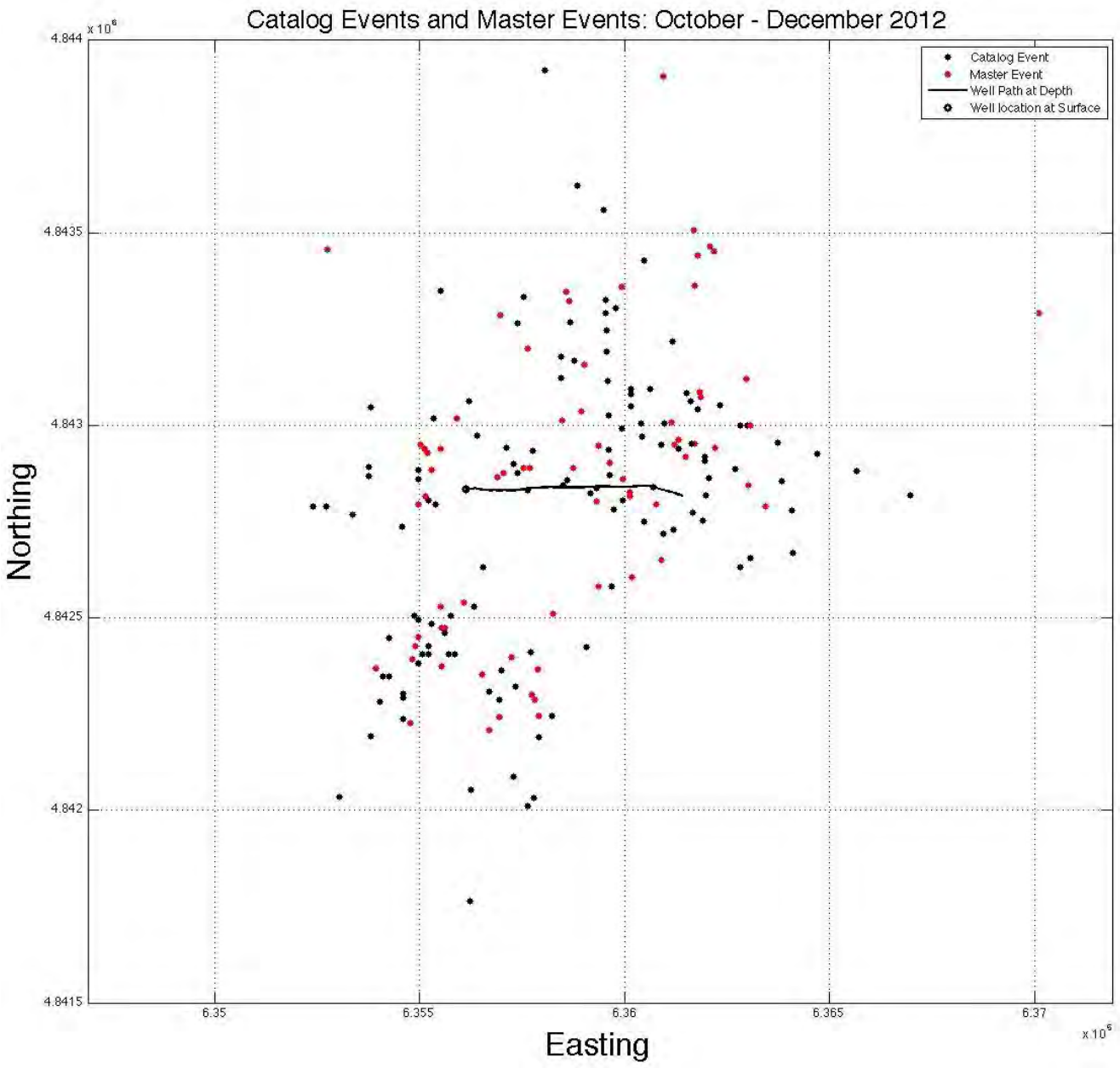

Figure 4-15. Map view of seismic events detected by Foulger Consulting. Events highlighted in red were used as field calibrated data.

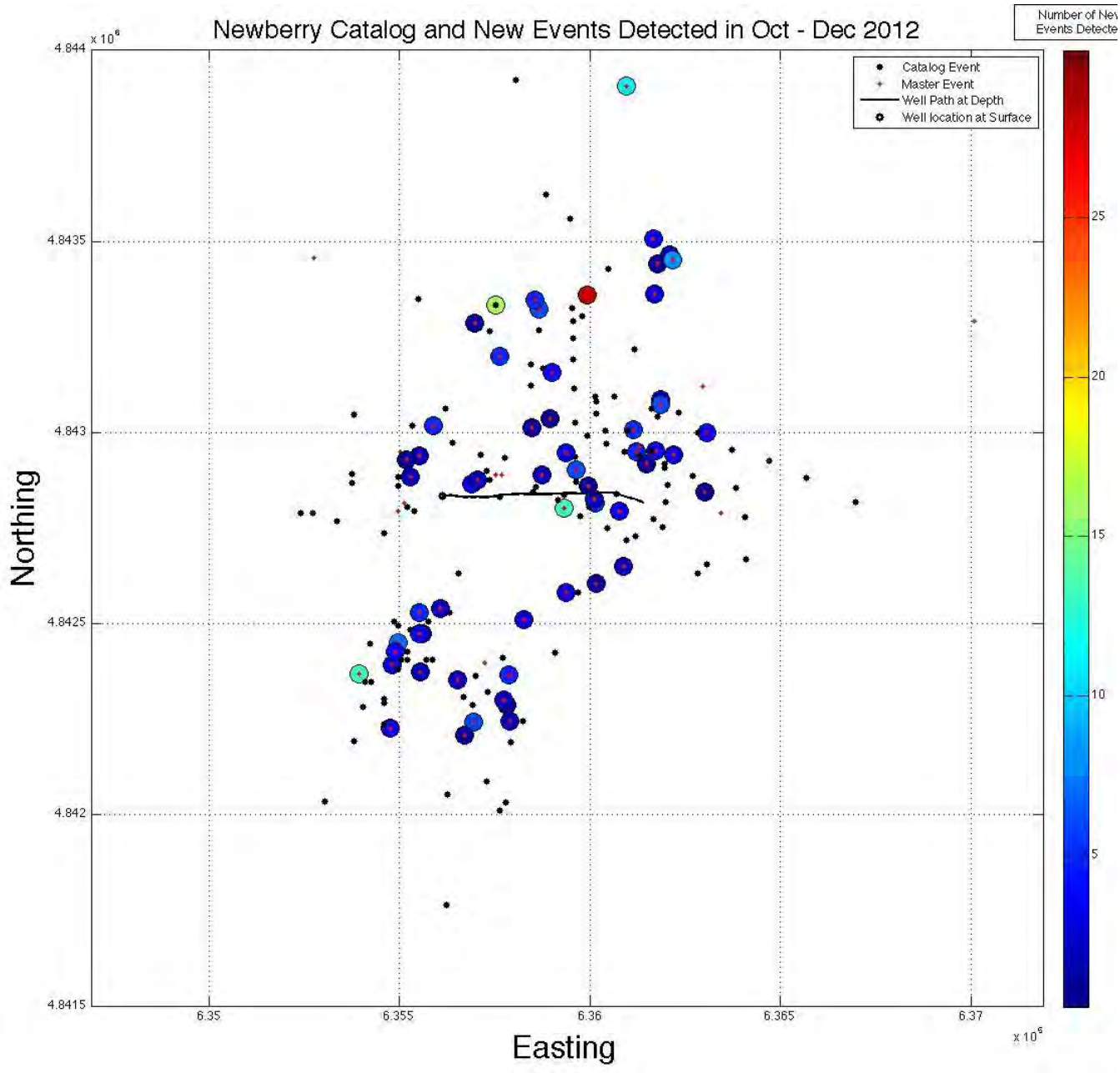

Figure 4-16. Map view of additional seismic events located by the MFP method. The circles are color coded to indicate the number of new events the master events detected. Catalog events that were designated as a master event are plotted as red dots. Catalog events that were not used as master events are plotted as black dots.

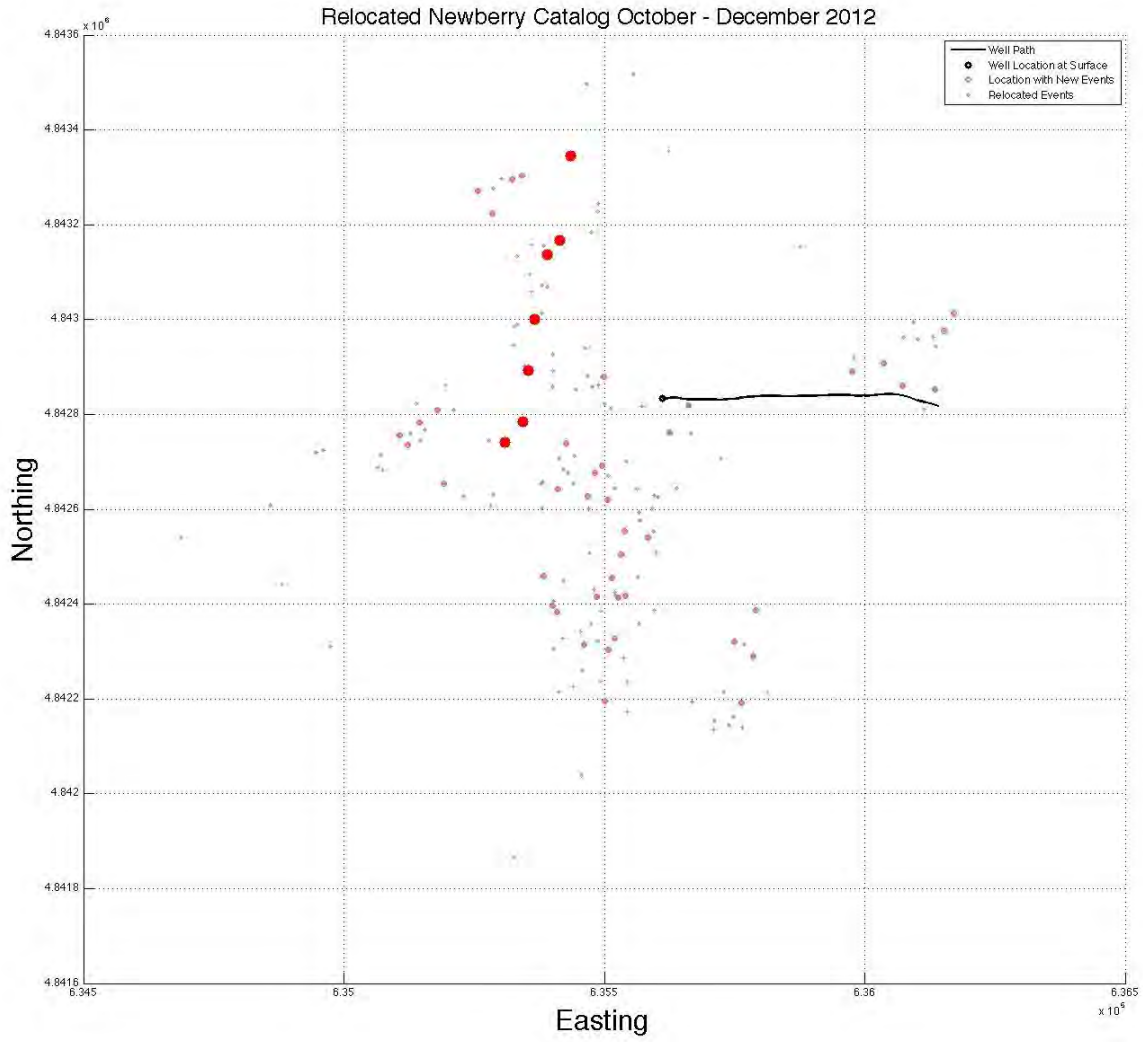

Figure 4-17. Map view of a fracture illuminated by the newly detected events. Newly detected events are in general much smaller than other events in the original catalog. The lineation indicates a small fracture.

Researchers at LLNL are currently applying the ambient noise correlation technique to the surface and subsurface seismic data to obtain an improved 3D velocity model of the subsurface. They will use this improved model to relocate the larger of the newly detected MFP events using an advanced earthquake location technique. The proposed technique can determine the Bayesian errors in the locations. A previous study showed that new events in a traditional geothermal field were within the error bars of their master events. They aim to prove that the same is true in an EGS as well.

Additionally, LLNL will use the improved 3D model to apply the model-based MFP technique to the Newberry site to determine if any small events occurred in the aseismic zone between the deep and shallow seismically active areas. The ability of the model-based method to produce robust results will depend on the resolution of the 3D velocity model.

These data will be shared with Dr. Ernest Majer at the Earth Science Division's Subsurface Geosciences, Geophysics/ Geomechanics Department at the Lawrence Berkeley National Laboratory. Subsequently, the

data will be made publically available to interested investigators through Majer's induced seismicity monitoring program.

4.6 DATA SHARING – NATIONAL GEOTHERMAL DATABASE SYSTEM

One of the terms of the DOE grant is submittal of various data sets pertaining to the Newberry EGS Demonstration collected before, during, and after the stimulation. Table 4-4 itemizes each data set, data type, file format, and a brief description of the data submitted to the Geothermal Data Repository (GDR; http://gdr.openei.org/) on December 4, 2013; the data is currently in curation. Once it is finished being curated, it will be available to researchers from the National Geothermal Database System (NGDS; http://geothermaldata.org/).

Table 4-4. Description of data submittals made to the NGDS

Data Set	Data Type	Data Format	Description
Geochemistry	Report	PDF	Geochemical analysis from flow testing of well 55-29
			Gas analysis of Newberry wells
Temperature	Raw	CSV	Static profile – Oct 2008 PT survey
		Tab Delimited	*1st DTS -Temperature and signal loss
			*2nd DTS - Temperature and signal loss
WHP & Flow	Raw	CSV	*Well head pressure and flow through system
	Interpreted/ Graphs	Excel Spreadsheet	*Well head pressure and flow through system compared to temperature data and annotated with operational changes.
Seismic	Spatial	CSV	Micro seismic array installation information
	Map	JPEG Image	Micro seismic array station map
	Map	PDF	*Micro seismic event map in
	Map	JPEG Image	*Micro seismic event map in 1km radius from 55-29 wellhead
	Signal - Interpreted	Power Point	*Daily seismic wave pattern recorded from station NN19
	Raw	DAT & Tab Delimited	*Raw seismic event locations
	Interpreted	DAT & Tab Delimited	*Relocated seismic event locations
	Interpreted	CSV	*54 Event moment tensor components and source type components
Lithology	Interpreted	Excel Spreadsheet	Generalized mud logs and lithology with identified mud loss zones
	Analysis Results	Tab Delimited	Mineralogy by weight percent at depth (XRD analyses)
	Image	JPEG	Graphic representation of mineralogy, natural gamma, bulk density, neutron density and mud loss
	Analysis Results	PDF	Heat conductivity values for different zones of the well
	Image	Bitmap Image	Borehole televiewer image log
	Interpreted	Excel Spreadsheet	Borehole televiewer image log interpreted for fracture population and lithology attitudes
Well Construction	Detail Image	PDF	Wellbore schematic with casing and open hole depths and sizes
	Field Report	PDF	Details of each string used during well casing
	Field Data	CSV	Well bore deviation data with survey points in UTM
		PDF	Directional survey report
	Analysis Results	Excel Spreadsheet	Thermal properties of well bore casing and cement
Diverter Injection	Field Data	CSV	*Diverter Injection dates and times
Tracer Injection and groundwater monitoring	Field Data	Excel Spreadsheet	*Groundwater and gas chemistry data
		CSV	*Tracer injection dates and amounts
Geophysical Logs	Field Data	LAS	Geophysical logs of various parameters collected during drilling of borehole
		Text File	Units of parameter values in geophysical logs and ranges of values collected in the open hole
Daily Reporting	Field Data	PDF	*Daily reports of field operations before, during, and after stimulation
Publications	Interpreted	PDF	Papers and presentations given about stimulation

*Data collected during stimulation, including metadata files in .txt format.

5 EGS RESERVOIR CHARACTERIZATION

This section characterizes the EGS reservoir using micro-seismic data and Distributed Temperature Sensing (DTS) data. Micro-seismic data provides information about the locations of presumed permeability-enhancing seismic events and the failure mechanisms generated during hydraulic stimulation. The complete micro-seismic data set provides the best estimate of the shape and size of the EGS reservoir and the nature of the stimulated fracture system. Time series DTS data gives insight into the development and evolution of stimulated fractures intersecting the wellbore and provides a mechanism for relating stimulated fractures in the wellbore to the seismic cloud generated during stimulation.

5.1 INDUCED SEISMICITY

The microseismic array and seismic data collected during the stimulation were presented in Sections 2 and 3, respectively. The post-stimulation data processing summary and analysis presented here is based upon final seismic results delivered by Foulger Consulting in October 2013 (Appendix G).

5.1.1 SIZE DISTRIBUTION AND CUMULATIVE MOMENT

The size distribution of 114 events located during the stimulation period (October 29 – December 7) is shown in Figure 5-1. The curvature away from a linear fit at small magnitudes indicates that most events down to a moment magnitude (M_w) of 0.5 were located. The rest of the curve is remarkably linear (especially given that the data set is small) with a negative slope, or b-value, of approximately 1.2. The b-value for the entire catalog of events (October 29 – February 18) has a much lower b-value of 0.8 which indicates that most of the events which occurred after stimulation were much larger in magnitude than those generated during stimulation (Figure 5-1).

The cumulative injected volume and cumulative seismic moments are positively correlated on a logarithmic scale (Figure 5-2). The M_w 2.39 event at the end of the Stage 3 stimulation accounted for 29% of the total seismic moment. The total cumulative moment of 37.0 x 10^{12} N m (Table 5-1) would correspond to a single M_w 3.0 event. Compared to predictions (AltaRock, 2011) and EGS projects in Basel, Switzerland (Häring et al., 2008), and Soultz, France (Dorbath et al., 2009), the cumulative moment is at least an order of magnitude lower for similar injected volumes. The Newberry site appears to have a much lower seismogenic index (Shapiro et al., 2010) than other sites. We speculate that this could be due to the much higher temperatures at Newberry compared to other projects and/or less competent bedrock; the Basel and Soultz projects both injected into Mesozoic granites.

Given the fact that we now know there was a leak in the casing, a similar plot of injected water to cumulative moment was made for the deep events in order to characterize the potential reservoir created around the bottom of the well (

Figure 5-3). The amount of water injected deep follows the results of the THM modeling of the wellbore, that is, 50% of the injected water leaked from the casing, followed by pump shutdowns which caused flowback and a temporary 120% loss through the leak, and then a 90% loss for the rest of the stimulation (Sonnenthal et al., 2012). The accumulated seismic moment for the deep events is still much lower than Soultz and Basel projects considering similar injected volumes, and it is about one fourth the total seismic moment for all the events to the total injected volume of water. This is probably due to the fact that the deep loss zones were fractures with incipient failure, as indicated by prior low pressure injection temperature logs which allowed water to escape from the wellbore aseismically. Therefore, the initiation of a deep EGS reservoir in this well was accompanied by very low levels of seismicity when compared to EGS in granitic environments.

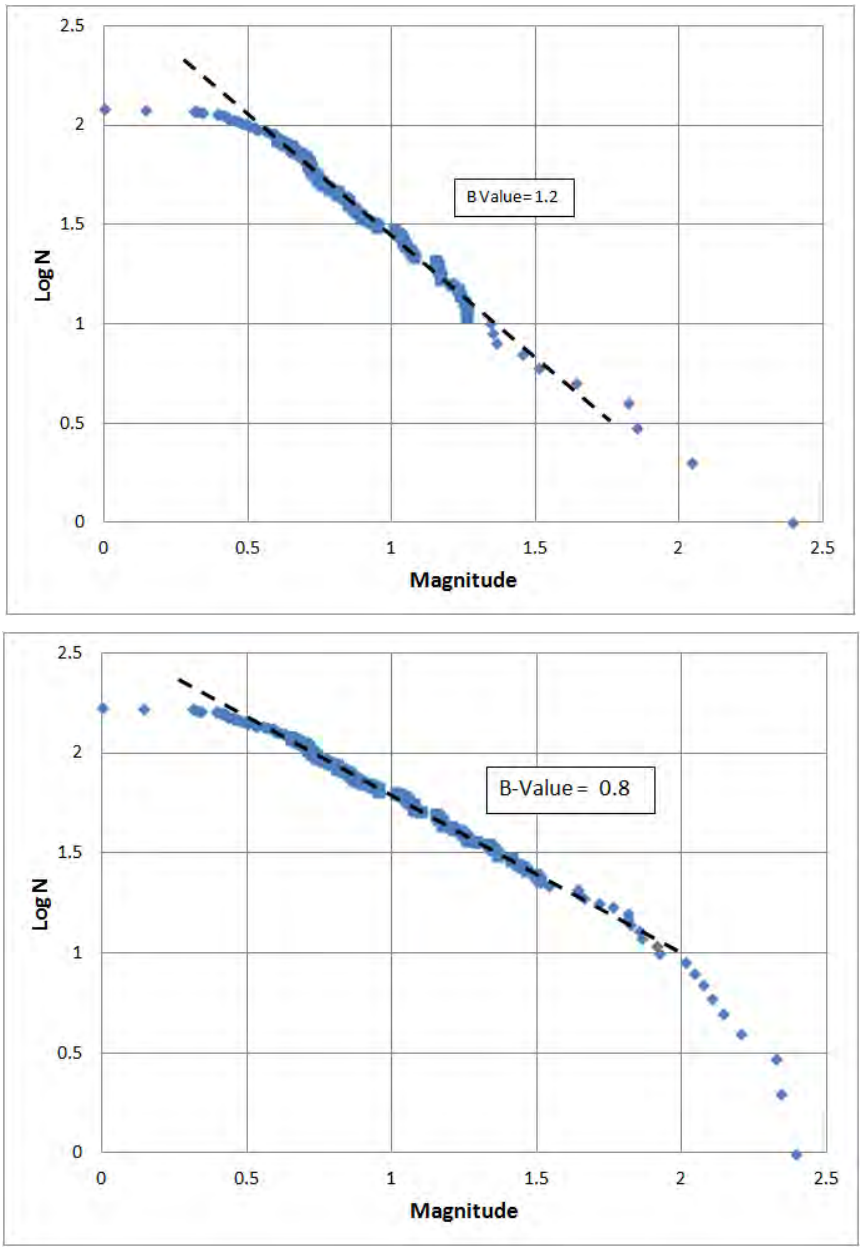

Figure 5-1. Size distribution of events during stimulation only 10/16-12/07 (top) and the full data set (until February 18, 2013) showing a decrease in B-value and a relative increase in larger events.

Table 5-1. Injected volume and seismic moment, by Stage.

Phase	Injected volume (m^3)	Cumulative Injected Volume (m^3)	Cum. Moment (10^{12} N m)	Max. mag. (M_W)
Stage I	26,225	26,225	1.5	1.51
Stage II	9,795	36,020	4.7	2.04
Stage III	5,305	41,325	10.4	2.39
Shut-in	0	41,325	37.0	2.23

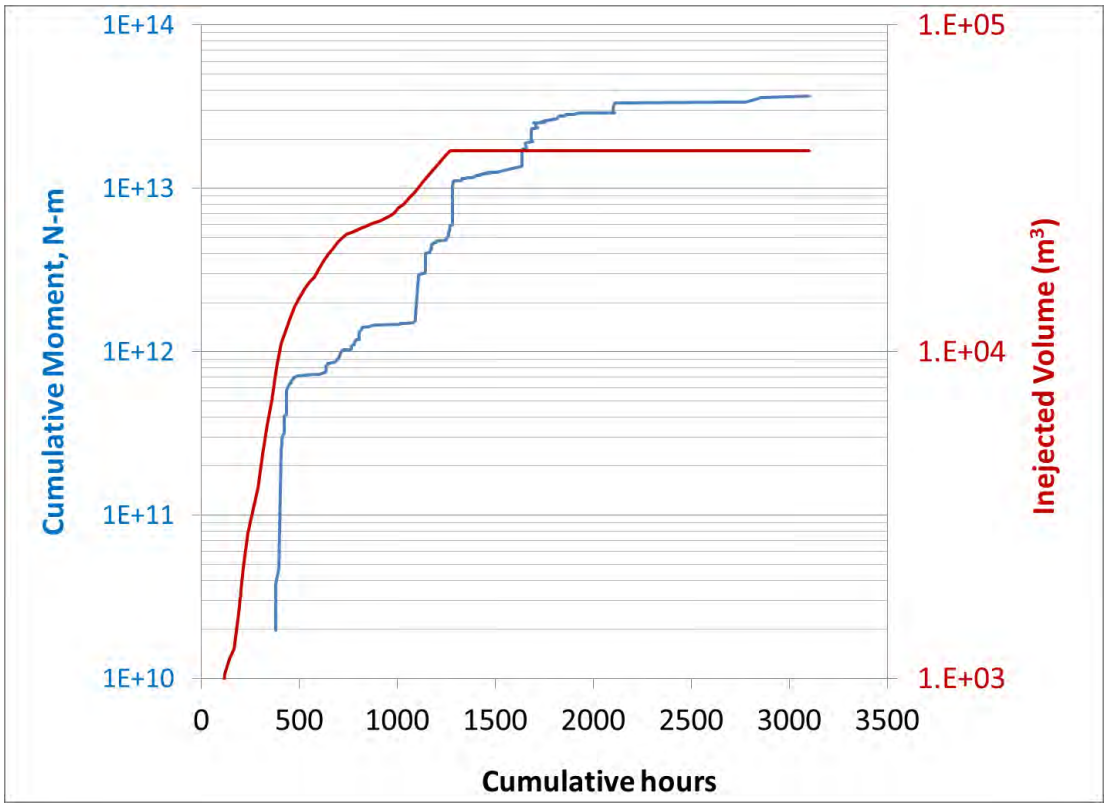

Figure 5-2. Cumulative injected volume and cumulative seismic moment.

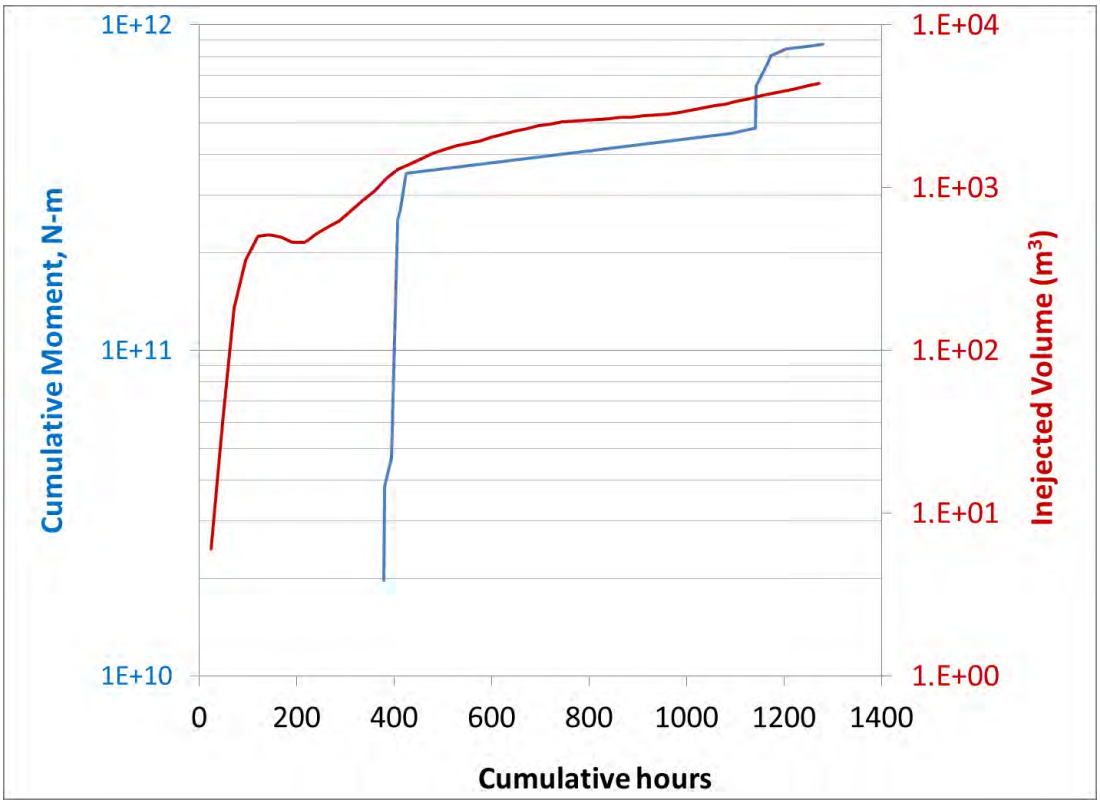

Figure 5-3. Cumulative injected volume and cumulative seismic moment for deep events.

5.1.2 RELATIVE EVENT RELOCATIONS

Figure 5-5. illustrates the individually determined locations of 172 seismic events that occurred during and after stimulation. These are the locations that the AltaRock team had access to during the stimulation to make operational decisions (see Section 3 for more details). Figure 5-5. b shows the micro-seismic data set after quality control and relative relocations were performed that became available on March 18 after Foulger Consulting provided a draft of their report (Appendix G). Event relocations were calculated using the program HYPOCC, a program that improves upon the relative location approach of Waldhauser and Ellsworth (2000). This method groups the entire event catalogue into discrete clusters and locates multiple events simultaneously within each cluster based on the relative arrival times of seismic waves to each individual seismic station. The relative relocations can help to interpret the seismicity as indicators of structures and fluid pathways created during stimulation. A detailed analysis of relocated events is presented below during each stage of stimulation in order to better understand how the TZIM treatments caused multiple zones of seismicity, and opened up fluid flow pathways around the injection well.

Stage 1 (10/17/2012-11/25/2012): Microseismicity initiated near the well bore at a depth about 2.4 km bgs (Figure 5-5. a). With time the events became shallower and occurred mostly in the northeast quadrant (relative to the well head).

Stage 2 (11/25/2012-12/3/2012): Following the first injection of TZIM, fewer seismic events occurred in the areas northeast and south of the well, and a small cluster of larger events occurred directly to the northwest of the wellhead (Figure 5-5. b).

Stage 3 (12/3/2012-12/7/2012): After injection of the second TZIM batch, the majority of microseismicity occurred in the southwest quadrant (Figure 5-5. c), indicating enhanced reservoir connectivity to the southwest. During this stage, there was an approximate 300 m (984 ft) gap in seismicity between the southwest cluster of events and the well bore.

Stage 4 (12/7/2012-present): After well shut in, significant seismicity continued to occur in all the areas that had been stimulated during the previous three stages. Small clusters of larger events were observed in the northeast, northwest, and southwest quadrants (Figure 5-5d).

The overall pattern of seismicity (Figure 5-6) is 1.5 km x 0.7 km with a NE-SW long axis and an area of approximately 1 km^2. The depth range is currently uncertain but appears to be at least 1 km and could easily be 1.5 km. Thus the total subsurface volume over which the seismicity occurred is between 1 and 1.5 km^3.

Lineaments within the cloud form a conjugate set with similar trends as the boundaries of the overall cloud, trending north-northeast to south-southwest and west-northwest to east-southeast (lower half of Figure 5-6). These lineaments appear to be sub-vertical and would be oblique normal faults and strike-slip faults in the stress regime, E-W S_{hmin}, determined from regional studies and borehole breakouts in NWG 55-29 (Davatzes and Hickman, 2011). Since this region is in a normal faulting stress regime, some of these structures which would otherwise be inactive appear to have been stimulated from the high levels of fluid pressure induced on them, creating fluid pathways with a broader range of orientation relative to the injection point.

The spatial and temporal distribution of the relocated events, along with analyses of moment tensors and source mechanisms provide the basis for a conceptual structural model. This model will provide insight into flow paths away from the well bore and into the stimulated rock volume. A refined structural and flow path model will be used in the location and routing of production wells.

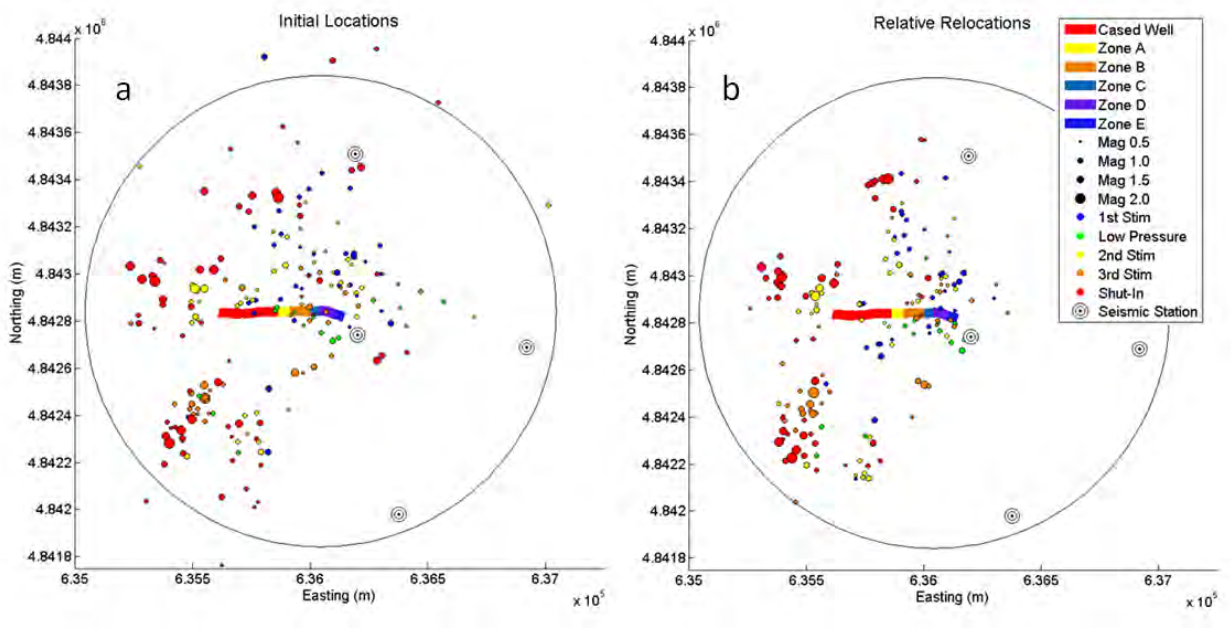

Figure 5-4. Events initially located during stimulation (a) and relative relocations (b).

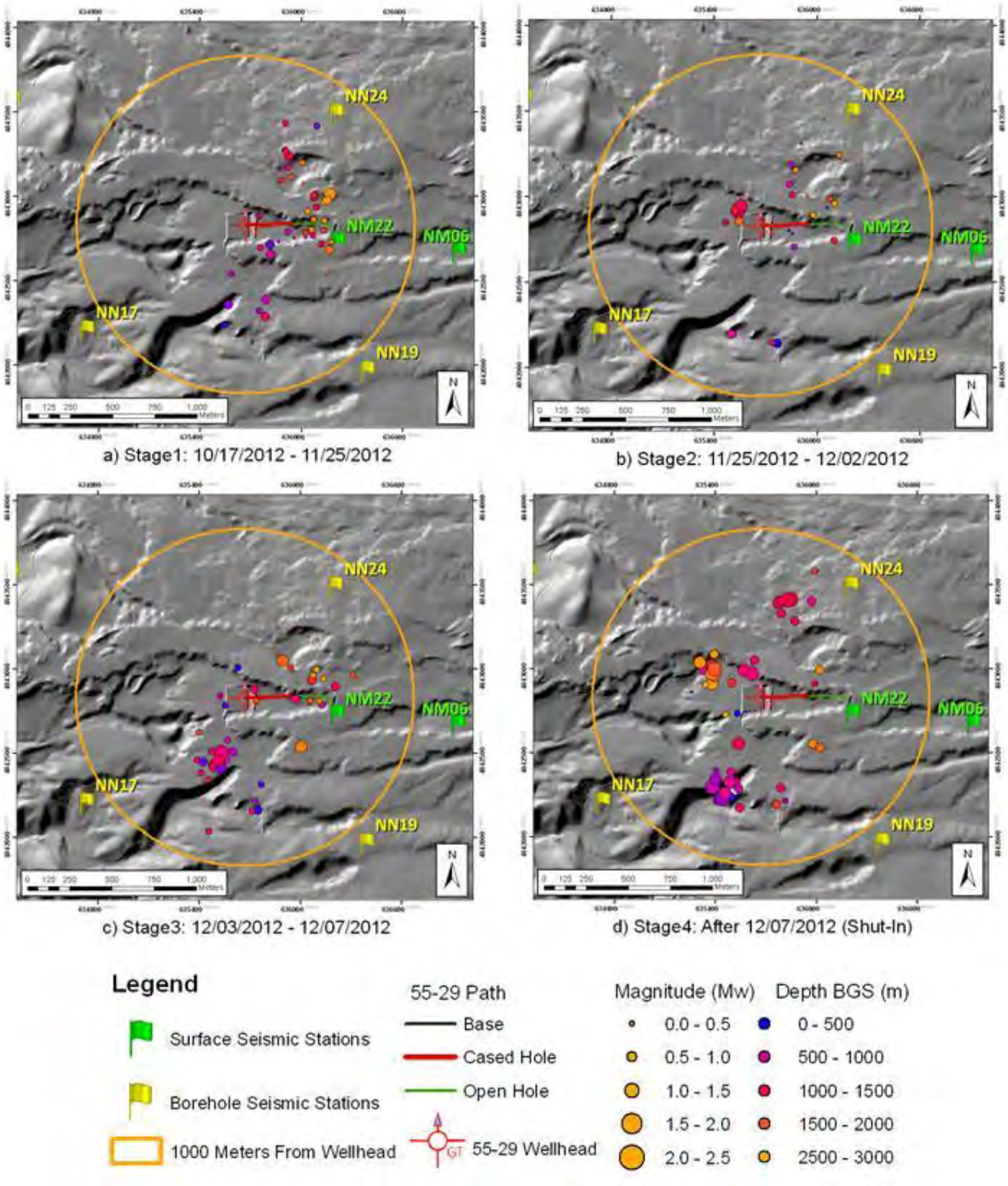

Figure 5-5. Maps of microseismicity during EGS stimulation; locations have been relatively relocated.

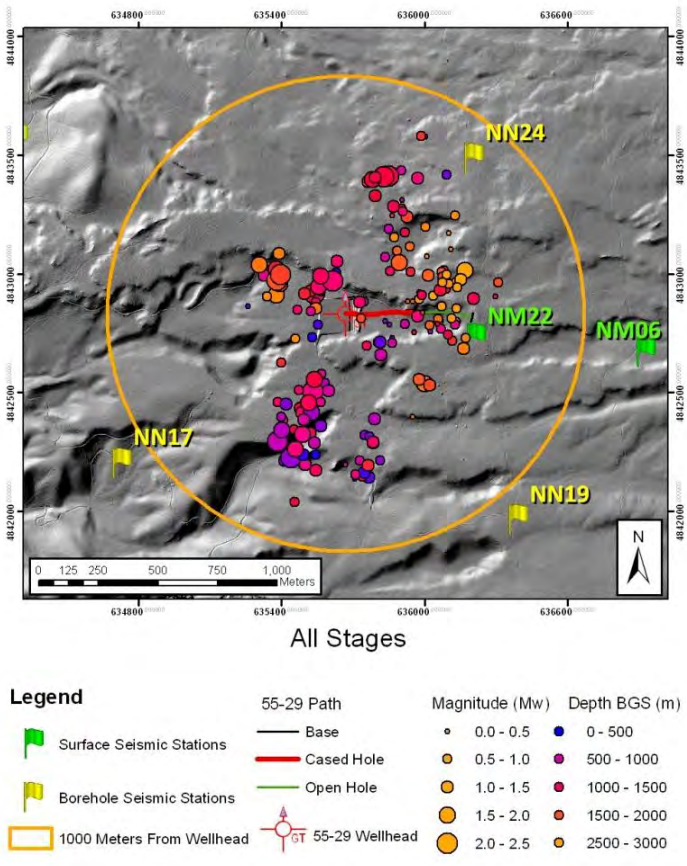

a.

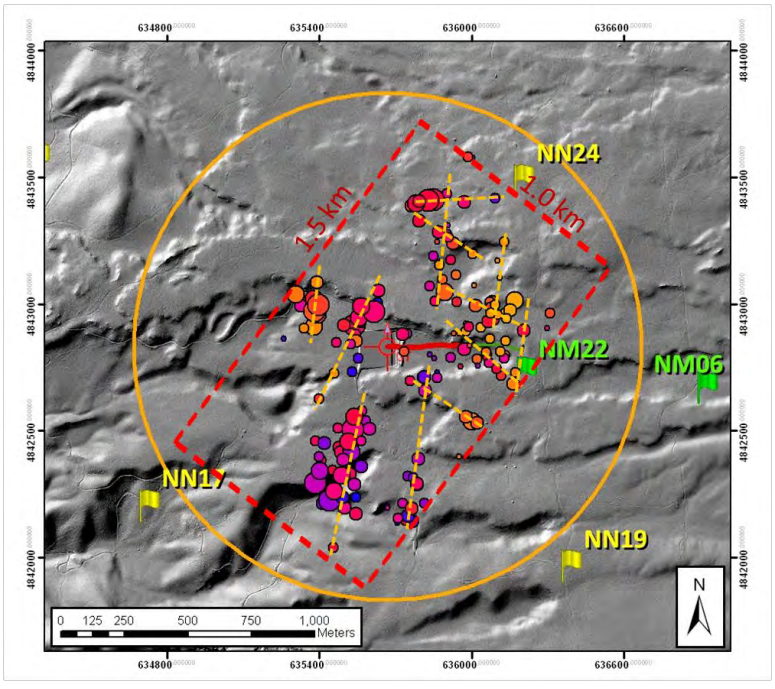

b.

Figure 5-6. a) Map of microseismicity for all stages of EGS stimulation; locations have been relatively relocated. B) Map with lineaments and reservoir boundaries marked.

5.1.3 MICROSEISMIC EVENT DEPTHS

The depth distribution of seismic events is bimodal: 1) a deeper set of events (n = 14) with a median depth of 2600 m (8,530 ft); and 2) a shallow set of events (n = 185) with a median depth of 1,100 m (3,595 ft) (Figure 5-7). Between these two clouds of seismic events there is a 600 m (1,970 ft) thick aseismic zone between 1700 m (5,580 ft) and 2300 m (7,545 ft) (Figure 5-7). Temporal analysis shows that at the beginning of each stage of stimulation seismic events first occur at depth near the wellbore at a radial distance of up to 200 m (656 ft) from the well path, followed by events occurring shallow at a median radial distance of 450 m (1476 ft) from the well path. This pattern is repeated for each Stage of stimulation (Figure 5-8, Figure 5-7). During Stage 1, shallow seismicity occurred northwest of the well. During Stage 2, shallow seismicity occurred west-northwest of the well. During Stage 3 shallow seismicity occurred west-southwest of the well. After shut-in, each of the shallow sub-clusters continued to grow (crosses in lower part of Figure 5-7); no seismicity was recorded at depth.

Initially two hypotheses were retained to explain the bimodal distribution: 1) a permeable vertical fluid conduit that connects the two clusters without causing detectable seismicity, and 2) a leak in the casing in the 700-1,100 m range. The injection tests and casing integrity evaluation performed in August 2013 and described in Section 6 confirmed a leak in the casing is present at a depth of 695 m (2244 ft) which is the top of the shallower seismic zone.

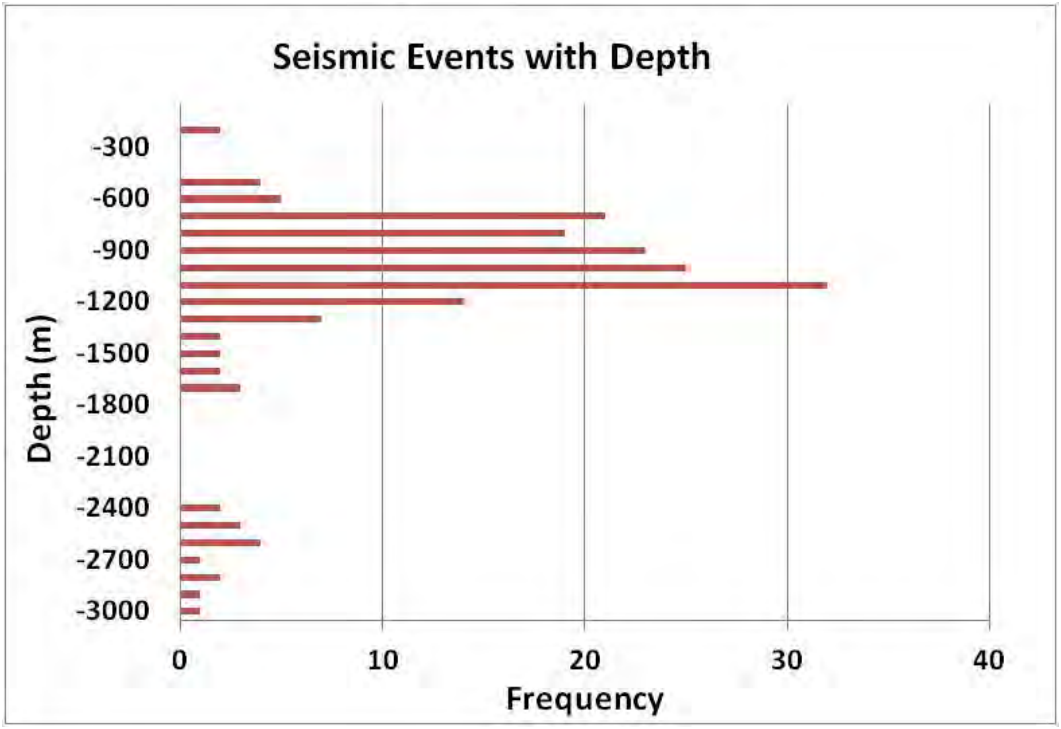

Figure 5-7. Distribution of seismic events with depth.

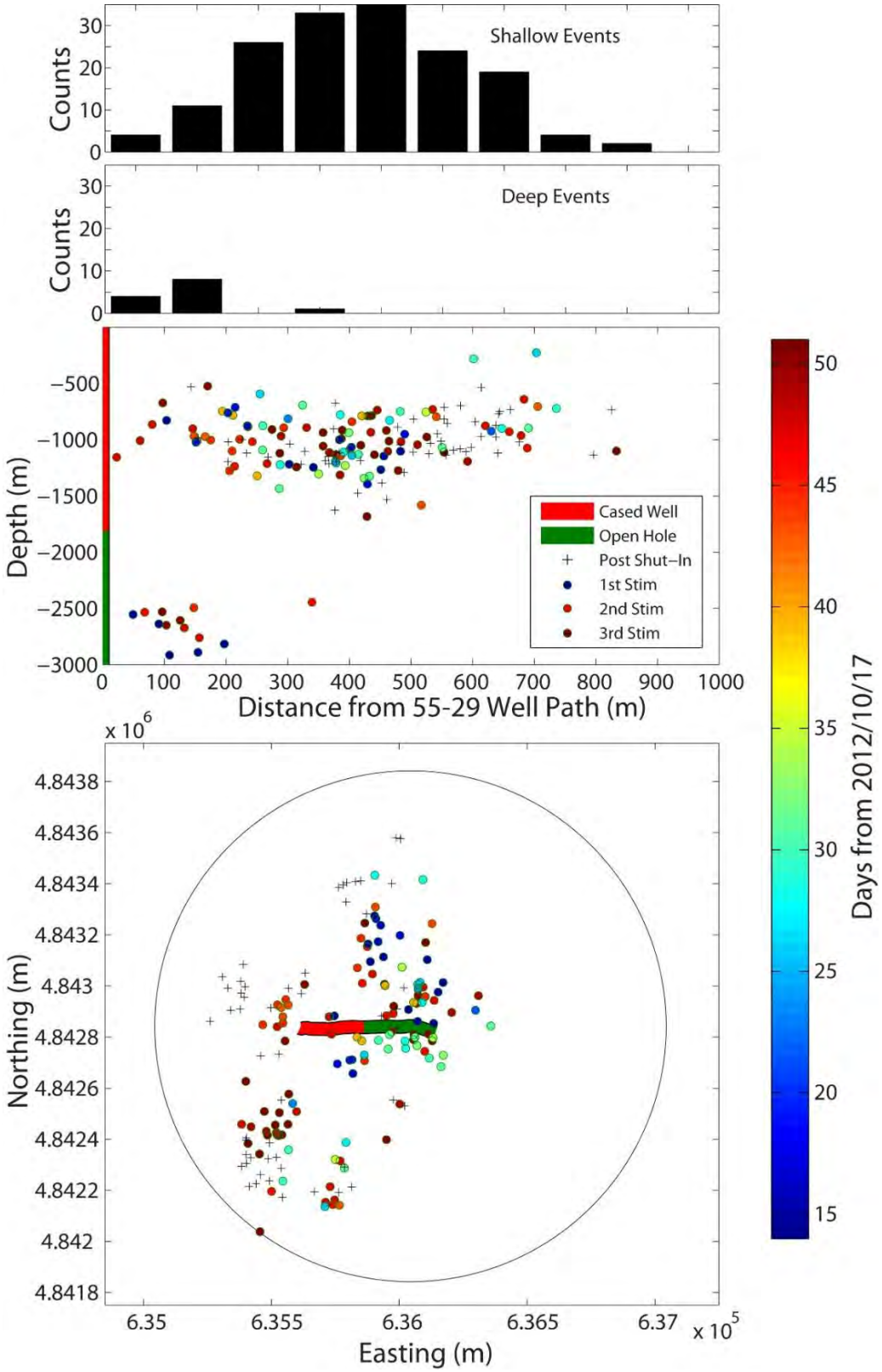

Figure 5-8. Microseismic events with depth and time. Top: Histogram of horizontal distance of events from well path for shallow and deep clusters. Middle: Radial distance from well path versus depth, with events color coded by time. Bottom: Map view of events, with same color coding and connecting lines as middle figure.

The extent of the reservoir at depth as indicated by the 14 deep events (except for the one outlier ~350 meters from the wellbore) is 250 by 250 meters in in areal extent spanning a depth of 600 meters, making up a volume of 0.0375 m^3, which is only 5% of the volume occupied by the shallow events alone, and 2.5% of the volume over which all the seismicity occurred (Figure 5-9).

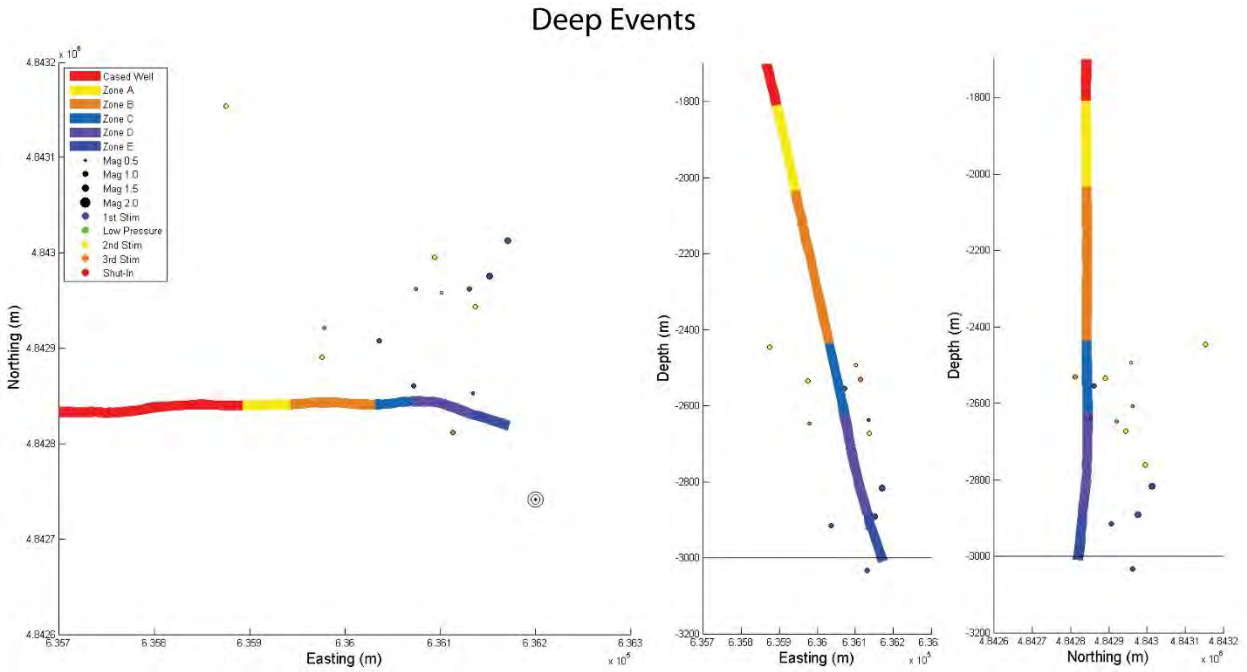

Figure 5-9: Map and cross section of deep events.

5.1.4 MOMENT TENSORS

Microseismicity in geothermal reservoirs can involve several different physical processes (Julian et al., 1998; Miller et al., 1998a), including:

1. Simple shear slip on planar faults
2. Tensile cracking
3. Rapid fluid motion

Understanding these processes is critical to understanding hydroshearing mechanics in EGS projects. Traditional 'fault-plane solutions' assume only simple shear slip occurs which ignores both processes associated with opening and closing cracks and fluid flow. For this reason, a moment-tensor approach should be used which requires more information than just P-wave polarities. The most effective and readily obtained information is P- and S-phase amplitudes (Julian and Foulger, 1996).

Moment tensors are displayed graphically using source-type diagrams (Hudson et al., 1989). This has been applied to many natural and industrially induced micro-earthquake sequences, including geothermal and hydrocarbon reservoirs and EGS stimulations (Julian and Foulger, 1996; Julian et al., 1997; Julian et al., 2010a; Miller et al., 1998). A source-type diagram (Figure 5-10) illustrates the deviation from a pure earthquake double-couple (DC) source at the center in terms of a volumetric component; explosion on top and left or implosion on bottom and right. Tectonic earthquakes typically fall near the center point of the plot (labeled DC). Injection-induced seismicity, which involves an underground change in volume, may require non DC source-types.

Moment tensor solutions have been calculated for 54 Newberry events. The source-type plot (Figure 5-10) indicates a wide variety of source mechanisms ranging from double couple to opening cracks (+Crack) to closing cracks (-Crack). This variety may be due to a relatively low differential stress and stimulation of variable volcanic features (e.g., dikes, flow boundaries, ring fractures). Interestingly, a source-type plot of seismic events occurring in the Geysers geothermal field shows a similar range of source mechanisms (Julian and Foulger, 2004). Figure 5-11 illustrates the corresponding P, I, and T axes which are approximate indicators of the principal stresses, for the 54 events assessed at Newberry. The highest density of T-axes, usually considered to represent the direction of the minimum principal stress axis, has a trend of 32° (NNE) and plunge of 61° (Figure 5-11, left). The highest density of P-axes, usually considered to represent the direction of the maximum principal stress, has a trend of 179° (South) and plunge of 30° (Figure 5-11, middle). The expected stress directions, based on borehole breakouts (Davatzes and Hickman, 2011) and recent structures (Cladouhos et al., 2011a, 2011b) were EW and horizontal for the minimum principal stress and vertical for the maximum principal stress. Thus it appears that fluid injection changed the stress regime locally enough the cause the principal axes to flip.

Although overall trends of the moment tensors can be seen for the entire Newberry event catalog, there is significant spatial variation in source types that can be seen locally around the site (Figure 5-12) (Appendix G). Many of the source types that resemble a DC, with equal areas of dilation (white) and compression (black), create a lineation from the WNW to ESE (red dots) that is also reflected in the apparent slip plane orientation in this area (events # 29, 25, 51, 31, 54, and 34).

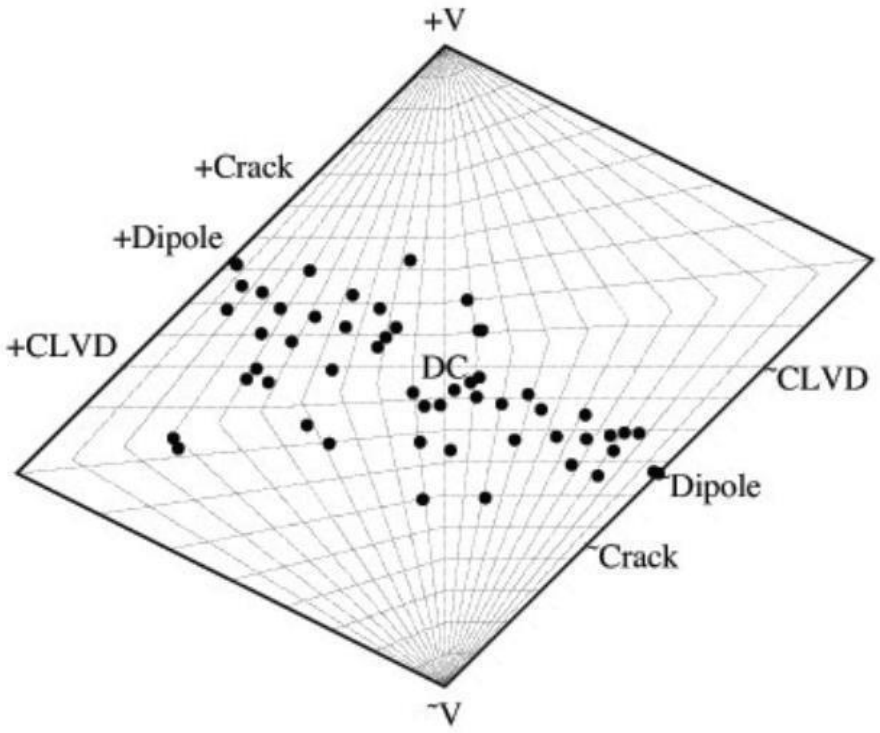

Figure 5-10. Source-type plot of 54 Newberry EGS events.

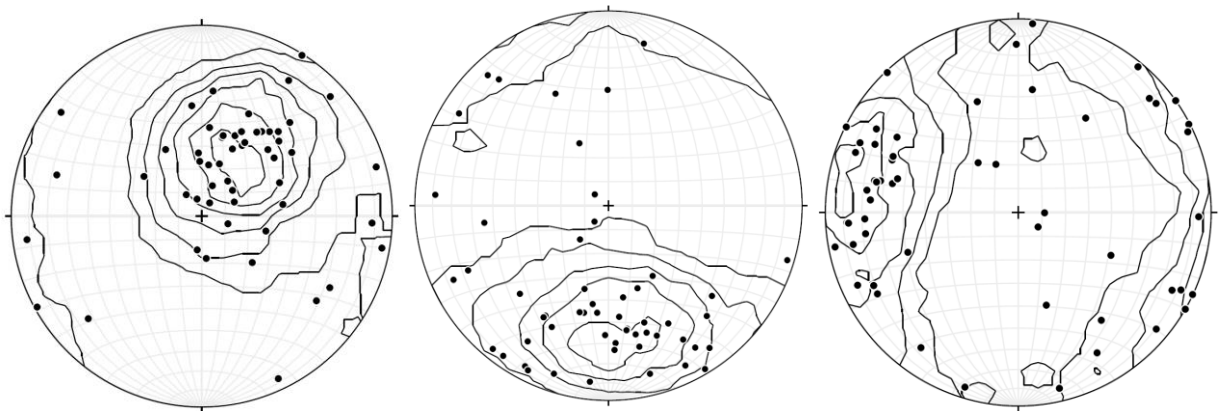

Figure 5-11. Principal axes of moment tensors for (left) T-axes, (middle) P-axes, and (right) I-axes with 2 sigma Kamb contours on equal area lower-hemisphere stereonets for all 54 moment tensors.

Source types that have unequal areas of white and black represent events with more significant isotropic components of volume change, and would stray from the DC point in the middle of Figure 5-10. Since the majority of the moment tensors have significant volume changes, the spatial distribution of volume loss/gain can be seen more clearly by plotting the k-values for the source types, which represent the isotropic component of the moment tensor, and are also the vertical axis on the source type plot (Figure 5-10). Positive values indicate a relative volume gain and negative values indicate a relative volume loss (Figure 5-13). The vertical distribution of the source types (Figure 5-13b and c) further reveals where similar source types are grouped at depth, which may indicate individual structural features. The small grouping of positive k source types just to the west of the well head, and located near where the well begins to deviate to the east at depth, all have T-axis that are nearly vertical (Figure 5-13b). These are also within the west-northwest to east-southeast lineation created by the apparent shear planes from the DC P-wave polarity plots ("beach balls", red dots, Figure 5-12), which have associated minor volume losses. Another planar grouping of similarly oriented moment tensors can be seen to the north of the well in the N-S cross section (Figure 5-13c).

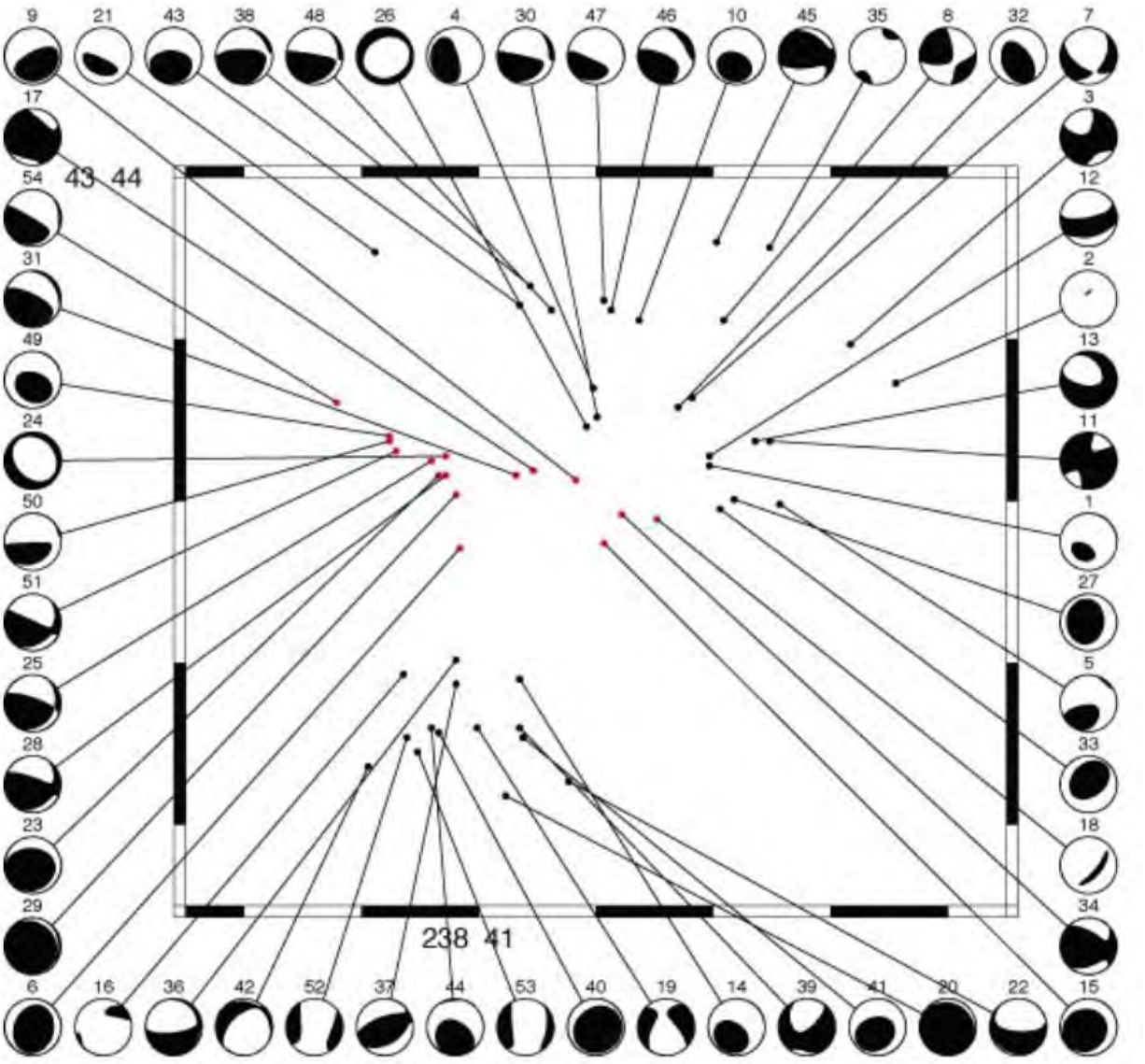

Figure 5-12. Spatial distribution of moment tensors for each event. The individual events are shown spatially with their P-wave arrival polarities on equal area, upper-hemisphere projections ("beach balls"), with areas of compression in black (T-axes) and areas of tension in white (P-axes). Events in red indicate an alleged fault zone that separates more randomly oriented moment tensors to the northeast and southwest.

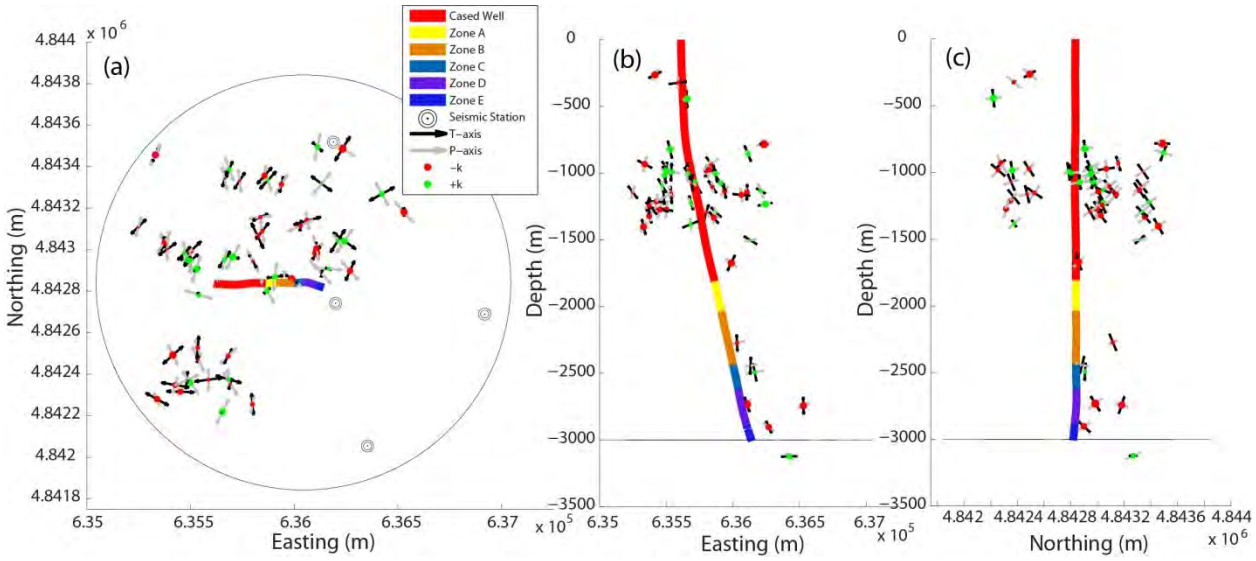

Figure 5-13. Spatial distribution of volume losses shown in red and volume gains shown in green for (a) map view, (b) looking north and (c) west, with the corresponding T- and P-axis as black and gray vectors respectively.

Locations of volume gain and loss can be used as an indicator of the extent of the reservoir created during stimulation. Figure 5-14 shows an iso-surface between positive and negative volume gain from a 3 dimensional grid that has a linear fit to the volume changes of the moment tensors. The geometry of the volume gain zone is complex and does not clarify the extent of the shallow stimulated volume. Figure 5-15 also shows an iso-surface between volume gain/loss, but the grid has been weighted by the inverse distance between the grid points and the data points. This causes the regions with more data density to be more favorable. This image provides a better indication of where the volume gain is at shallow depths, and is a better indicator of the potential extents of the stimulated reservoir.

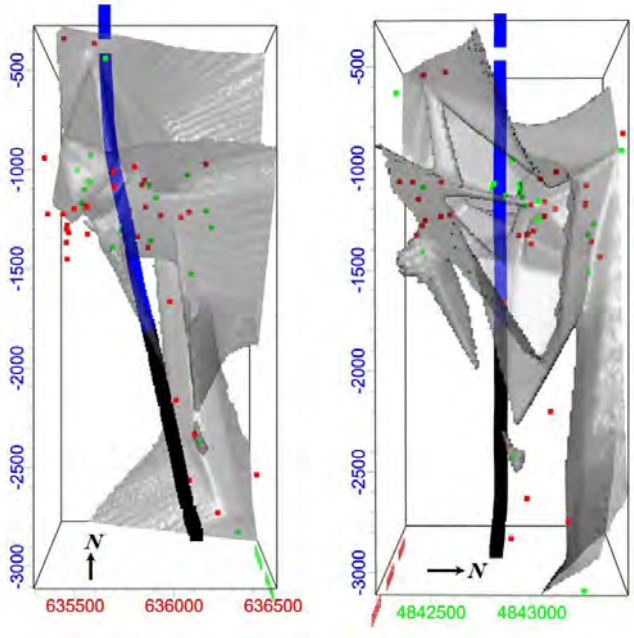

Figure 5-14. Iso-surface between positive and negative volume gains from a 3D linearly fit grid. Green events have volume gain and red events have volume loss. Distances in meters.

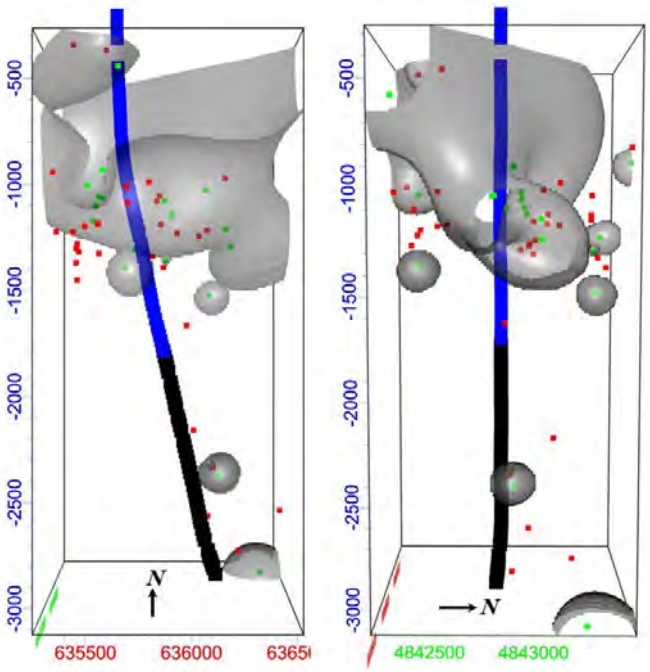

Figure 5-15. Iso-surface between positive and negative volume gains from a 3D grid with inverse distance weighting. Green events have volume gain and red events have volume loss. Distances in meters.

5.1.5 RESERVOIR DIFFUSIVITY

In order to hydraulically characterize the seismically active stimulated region around the well, an underlying mechanism of pore-pressure diffusion is applied to the temporal distribution of events around the point of injection. This is done by assuming a point source of pressure from the bottom of the well and measuring the distance of each event from the point source for the length of the stimulation. The spatial distribution of the events over time has a triggering front with a parabolic signature (Parotidis, et al., 2004):

$$r = \sqrt{4\pi D t} \qquad (6.1)$$

Where r is the distance of the triggering front, t is time, and D is the hydraulic diffusivity of the surrounding rock. After pumping of the well has ceased, and the well is shut-in, seismicity continues to spread from the point source of pressure, but develops a parabolic back front from the point source:

$$r = \sqrt{6Dt\left(\frac{t}{t_0} - 1\right) ln\left(\frac{t}{t-t_0}\right)} \qquad (6.2)$$

Where t_0 is the shut-in time. The event distances with time were fit to parabolic triggering (Equation 6.1) and back fronts (Equation 6.2) using a hydraulic diffusivity value of 0.015 m^2/s, and is shown with the wellhead pressure and flow curves in Figure 5-16. This is a reasonable value for hydraulic diffusivity and it is in the range of observed diffusivity values for fractured and unfractured igneous rocks (Figure 5-16).

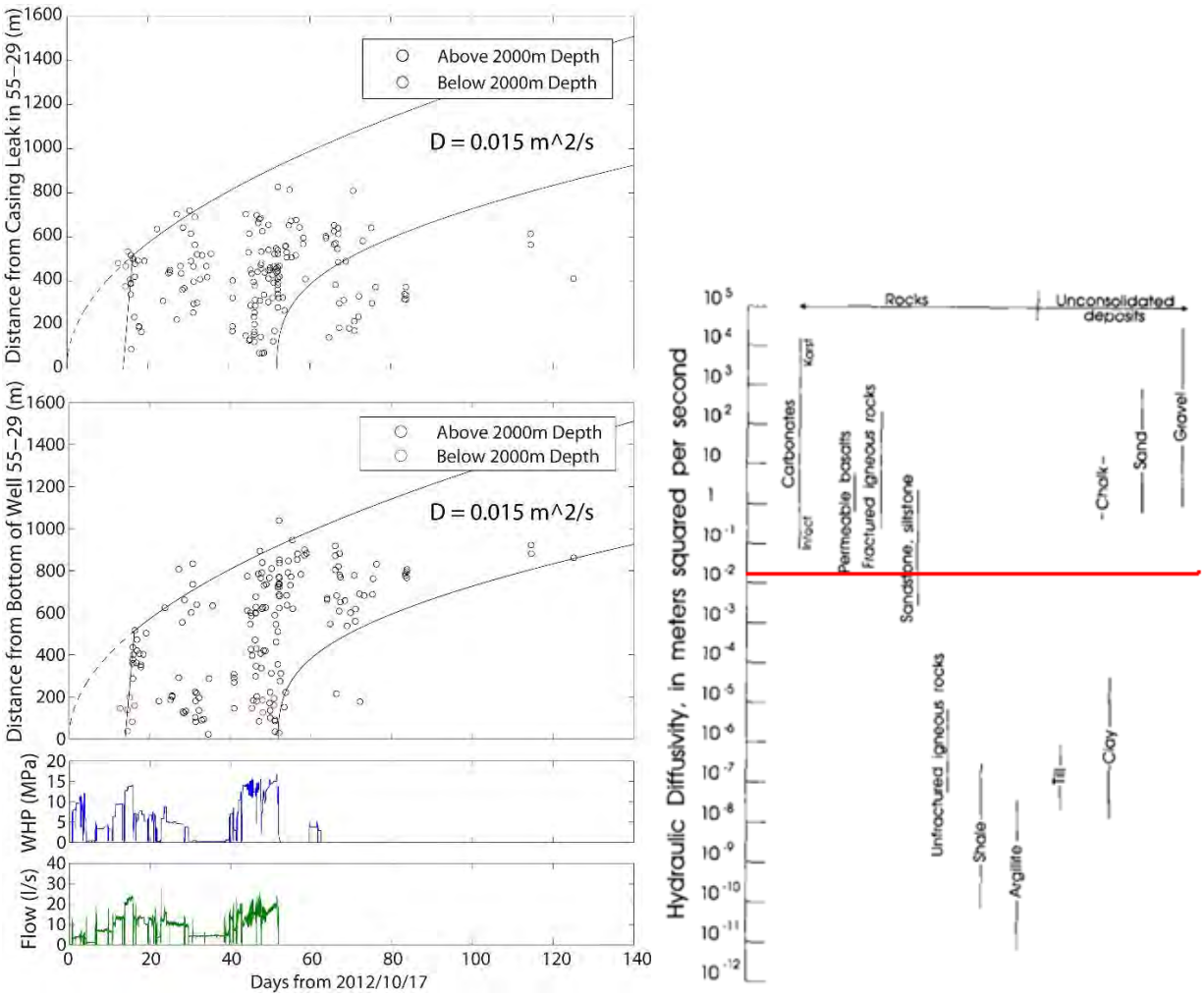

Figure 5-16. Event distances from the bottom of the well and the casing leak at 682 m over time fitted to the parabolic triggering and back fronts using the same value of hydraulic diffusivity of 0.015 m^2/s. Deep events are shown in red and shallow events in black. Diagram on the right showing observed ranges of hydraulic diffusivity as determined from field and laboratory studies (Roeloffs, 1996) with 0.015 m2/s marked in red.

For the first 12 days of stimulation no events were observed. Once the wellhead pressure approached 14 MPa (2000 psi), seismicity was first observed near the bottom of the well. Over the next five days seismicity was observed deep as well as shallower at a horizontal distance of up to 500 meters from the bottom of the well. This may be explained by the fact that the fluid stresses and/or thermal cooling after 12 days of injection had reached critical values that initiated the opening of fluid pathways. The onset of seismicity has been fitted with a linear triggering front that is characteristic of hydraulic fracture propagation (Figure 6-14) (Shapiro and Dinske, 2009).

$$r_f = \frac{Q_I t}{2 h_f w} \qquad 6.3$$

Where r_f is the distance of fracture propagation from the well which reached 450 m, Q_I is the flowrate which was held constant at 200 gpm during this time, h_f is the height of the fracture which was modeled as 250 m, and w is the aperture which was modeled as 1 cm. This is either 1) a clear indication that a hydraulic fracture was initiated at shallow depths or 2) pathways that breached the relatively permeable rocks overlying the open-hole source at depth, and initiated upward fluid flow in what is assumed to be a 'fast-path' that hydro-mechanically behaves like a hydraulic fracture. The alignment of the linear front

with the deep and shallow events for the deep exit point indicates that two event clusters may be hydro-mechanically interacting even though they are separated by a 600 m thick aseismic layer. For the shallow exit point near the casing leak the shallow events alone resemble a hydraulic fracture, and the deep events occur 400 m horizontally from this point, even though we know that they were the first events that occurred near the wellbore. This is an indication that these two clusters of events represent two hydraulically separated zones, and therefore are two separate reservoirs.

5.1.6 ALTASTIM MODEL PREDICTION/INITIAL INDUCED SEISMICITY

As part of Phase I of the Newberry Volcano EGS Demonstration project, data was collected and simulations were run to plan and predict EGS stimulation and productivity using AltaStim, a proprietary software model developed by AltaRock. One of the model predictions was to determine the WHP required to initiate hydroshearing at depth and which geologic formations at depth are most likely to stimulate first. The model was created based on observations of fracture intensity in the wellbore, and rock types encountered in the well and assumptions of their frictional strengths to define five separate zones (A-E) along the length of the open hole. The properties of the zones defined in the model setup predict that zones A and B were the least likely to stimulate, and that zones C, D and E were likely to stimulate first. Zone D in particular was predicted to be the initial fluid exit zone because temperature surveys taken before and after a prior injection test (max. WHP 1153 psi/7.95 MPa) indicate fluid exit points in that zone, and because of its lithology, it was assumed to have a lower frictional strength. The numerical model simulated the propagation of seismicity around the well through a discrete fracture network with a given horizontal stress orientation, both derived from the observed fractures in the well, and reasonable assumptions of horizontal stress magnitudes. The model predicted that significant seismicity would initiate at a WHP of 9.31 MPa (1350 psi) and that over 13.44-15.17 MPa (1950-2200 psi) was required to reach the required reservoir volume goal (Cladouhos et al., 2011).

The first detected seismic event during the stimulation occurred at a WHP of 9.40 MPa (1,364 psi), followed by a greater frequency of events detected after 13.18 MPa (1,912 psi) was reached, which is consistent with the AltaStim model prediction (Figure 5-23).

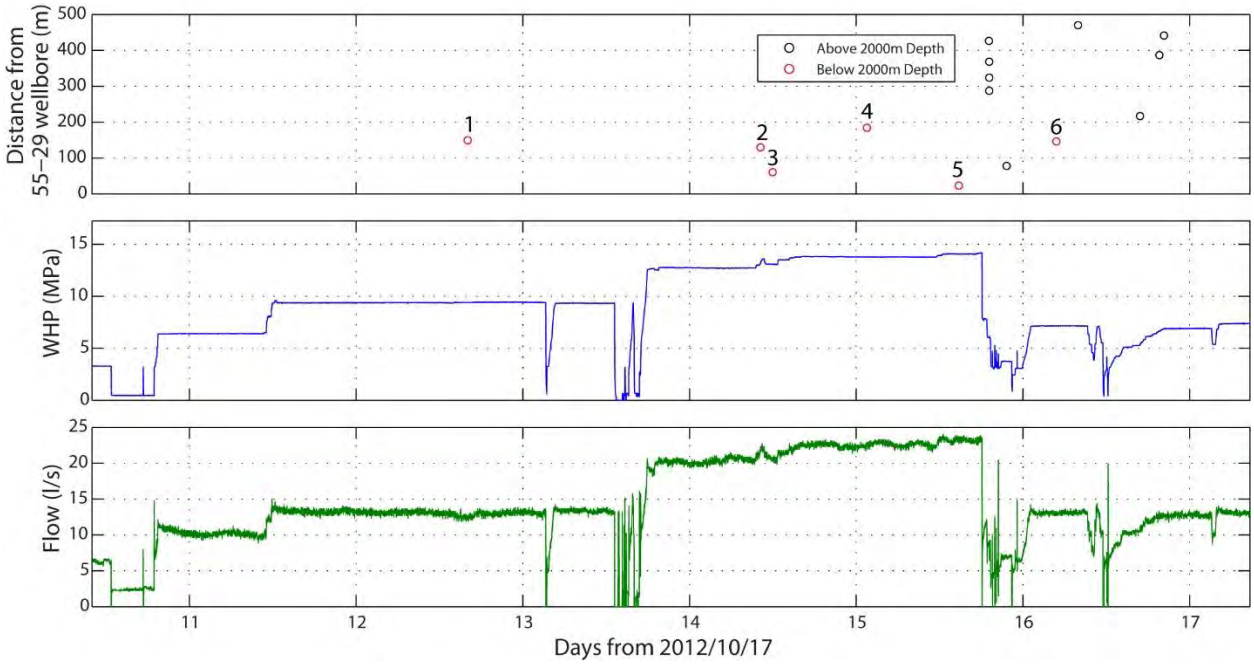

Figure 5-17. Event distances from the wellbore, WHP and flow during the initiation of seismicity during stimulation. The first six deep events during Stage 1 are numbered according to their locations shown in the next figure.

A total of 6 deep events were produced during Stage 1, and their locations and order of occurrence are shown in Figure 5-18. The events extend north of the wellbore, and are spatially and temporally distributed fairly evenly with depth around Zone D. Since Zone D was assumed to be in incipient failure during the lower pressure injection test, this Zone was most likely taking water aseismically during the injection test and during the stimulation, which explains why the first events occurred above and below this depth.

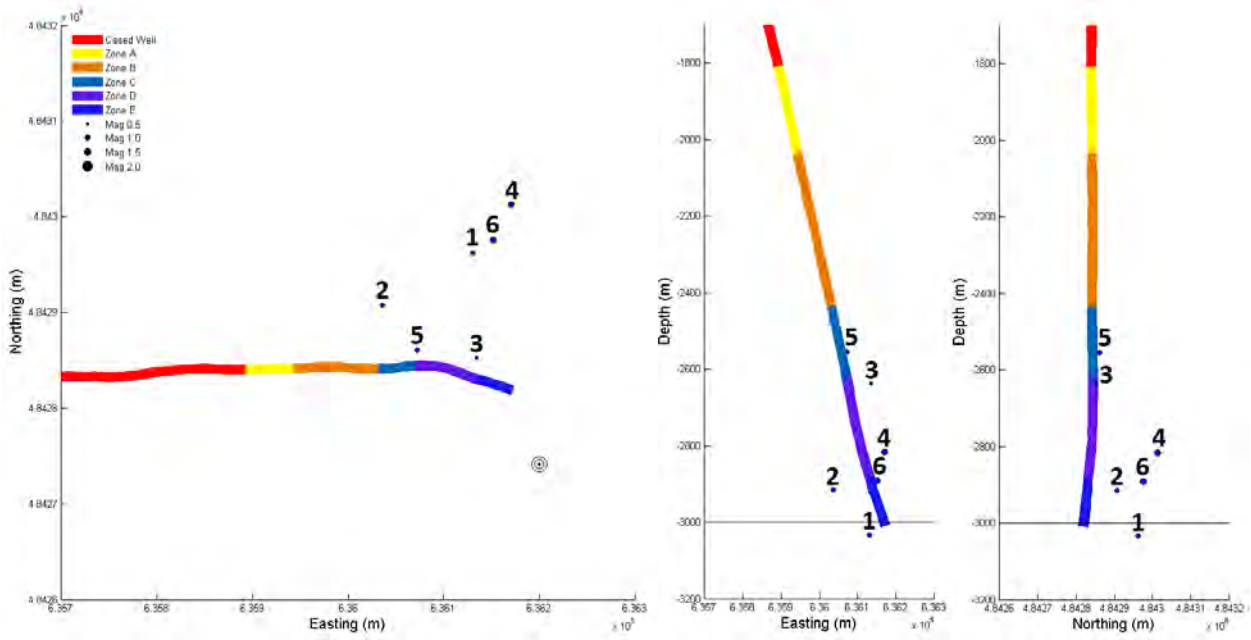

Figure 5-18. First six deep events during stimulation, numbered 1-6 in the order they occurred.

About 1 hour after the stimulation pumps shut down after reaching a WHP of 14.17 MPa (2,055 psi) the first four shallow events occurred within 36 seconds of each other. After these four events, small spikes in WHP were accompanied by increasingly higher surges of flow into the well. The cause of this highly erratic pressure and flow behavior may have been caused by mechanical failure of the pumps, but it is clear that it also occurred after these four nearly simultaneous seismic events (Figure 5-175). The fact that we now know that the casing had a leak at 547 m and 693 m (1,767 ft and 2,240 ft), and possibly at other depths, these four events may indicate the initiation of a hydrofracture, since the water pressure at this depth was 19.4 MPa (2820 psi) which was more than double an S_{hmin} of 8.5 MPa (1237 psi) from the assumed fracture gradient of 14.9 – 15.8 MPa/km (0.66 – 0.70 psi/ft).

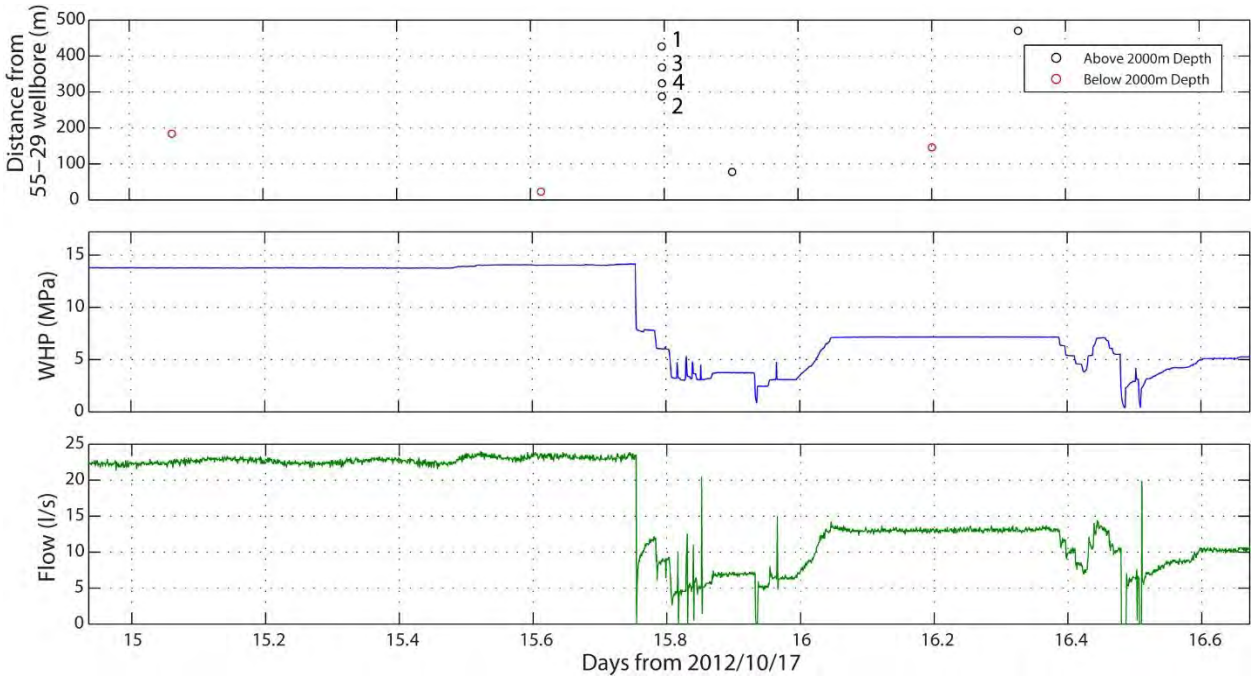

Figure 5-19. Event distances from the wellbore, WHP and flow during the initiation of seismicity during stimulation. The first four shallow events during Stage 1 are numbered in the order they occurred, and also with their locations shown in the next figure.

The locations of the events are all about 300-400 meters (984-1640 ft) north of the well, and form an E-W striking plane that steeply dips to the south (Figure 6-18). This apparent structure also resembles the lineation indicated by the moment tensors shown in Figure 5-12 (red dots). This indicates that while hydrofracturing may have been occurring shallow it probably connected to this primary shallow structure which experienced mostly normal failure during the stimulation. The fact that this structure was nearly perpendicular to the greatest principal stress, and that these four events all occurred at the same time, indicates that this is most likely a pre-existing shallow fault that was slipped during the stimulation.

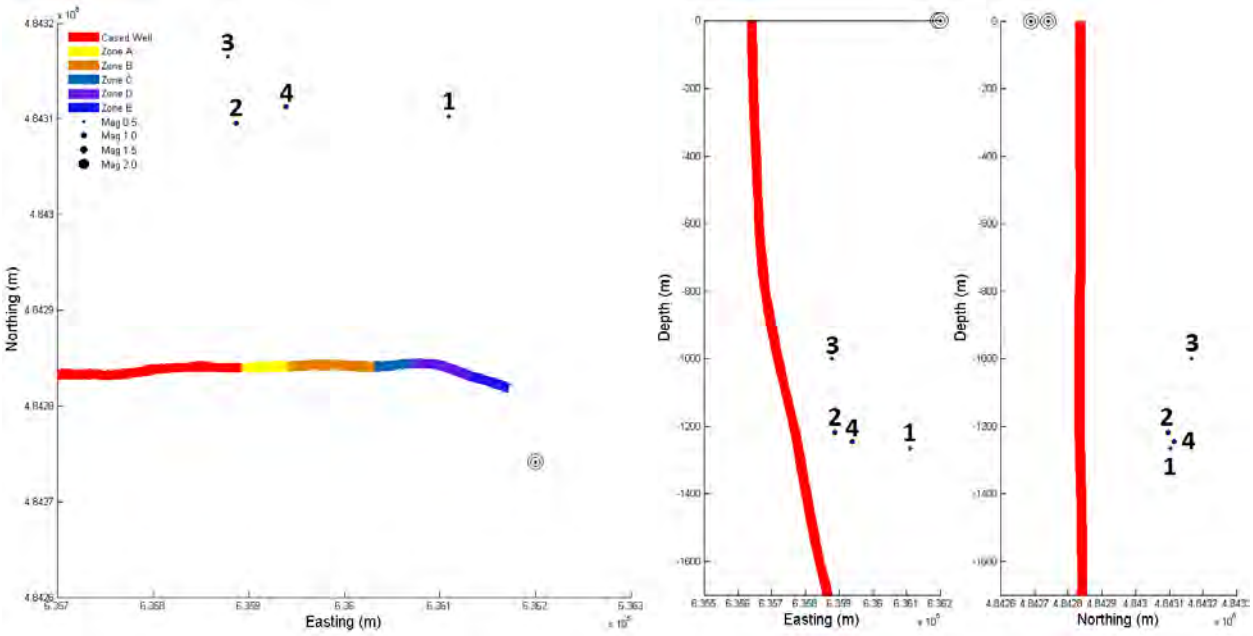

Figure 5-20. First four shallow events during stimulation, numbered 1-4 in the order they occurred.

5.2 SEISMIC RISK AND MITIGATION

The ratio of seismic energy to volume of injected water at Newberry was significantly lower than other sites that have experienced seismicity due to volume changes in the earth due to injection/extraction of fluid. They fall far below the line plotted from the empirical formula developed by McGarr (1976) on a plot of maximum seismic moment to Injected volume (Figure 5-21). The largest magnitude of all the events created during the stimulation was M_w 2.39, which caused 0.1%g ground shaking at the strong motion sensor, and corresponds to a total injected volume of ~11 million gallons. In the deeper formations of the open hole, where the bulk of the EGS reservoir is assumed to be created, the largest magnitude event was M_w 1.51, which corresponds to one tenth of the total injected volume, and a seismic energy to injected volume ratio of less than one half (Figure 5-21).

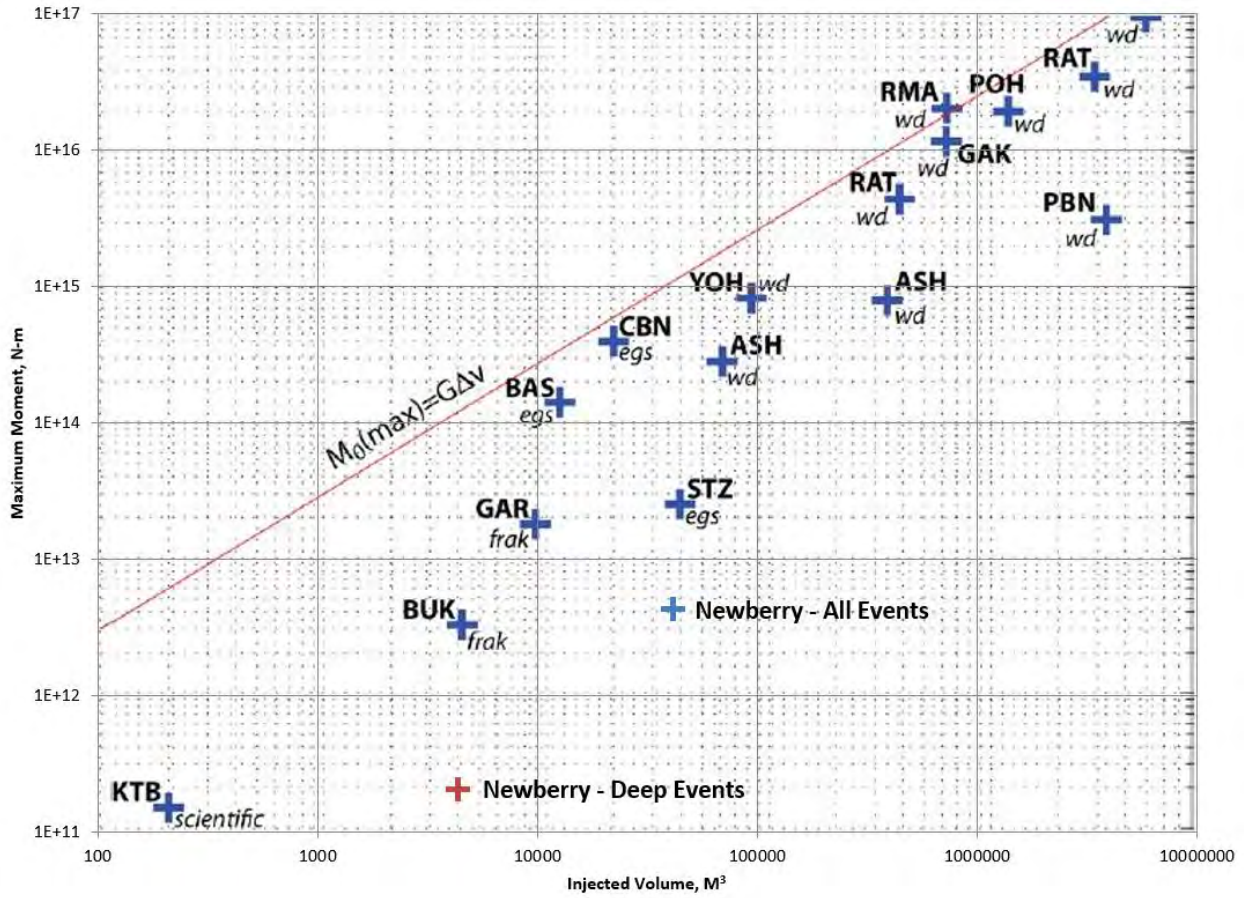

Figure 5-21. Largest seismic events at Newberry For all events/injected water (blue) and deep events/injected water (red) compared to other EGS, hydraulic fracking, and wastewater disposal sites (McGarr, 2014).

The M_w 2.39 event was not felt on the surface or in the surrounding communities around Newberry, and created only a small signal on the surface seismic stations. The seismogram that was placed at nearby LaPine High School as part of the AltaRock community outreach program and ISMP experienced far more ground shaking from the passing of nearby trains than from the largest event created during the injection (Figure 5-22).

The hardware and software of the microseismic array performed very well, apart from some limited downtime on non-critical stations during cloudy periods in December. Most importantly, the borehole seismometers were far more effective than the surface seismometers. Continuous monitoring of the microseismic array during the stimulation allowed for important operating decisions to be made to stay in compliance with the ISMP. Continued use of this monitoring equipment is recommended for any further stimulations at Newberry because of its effectiveness at determining event locations and magnitudes in near real-time.

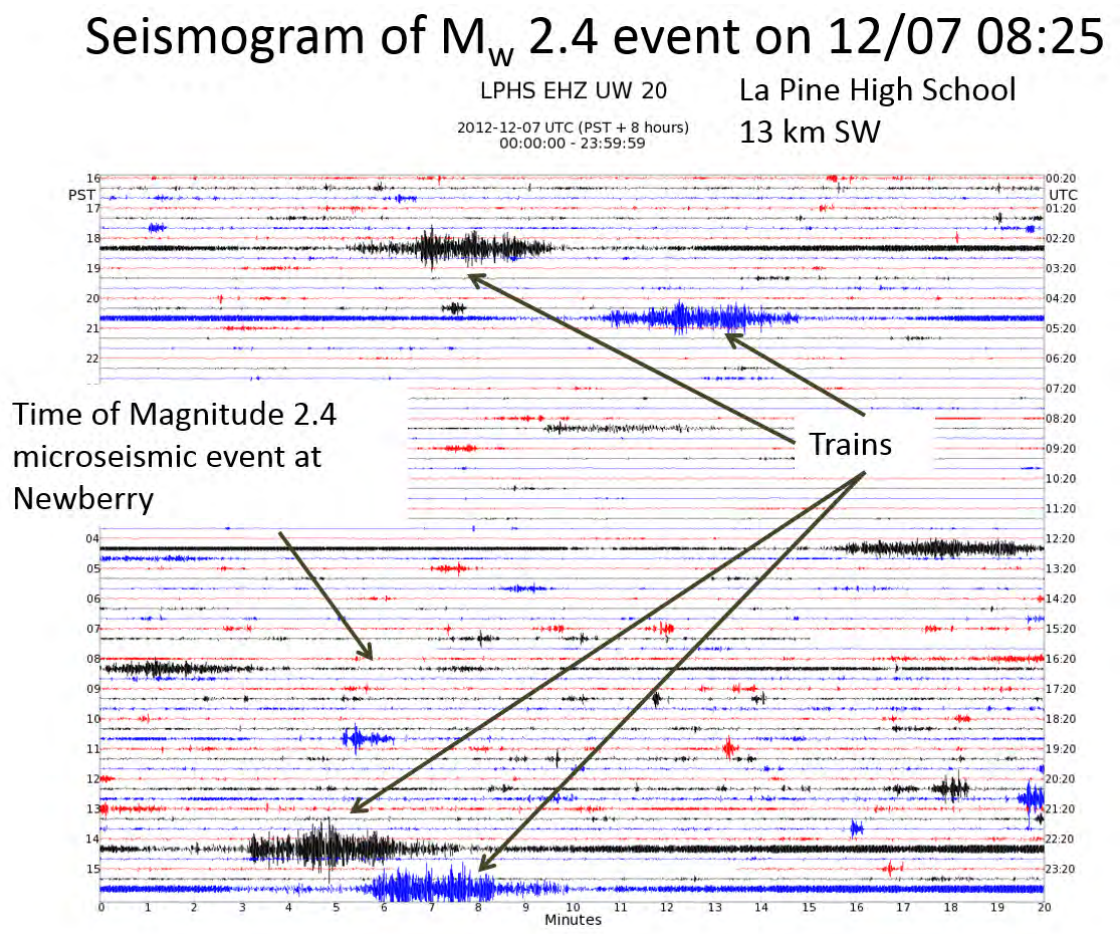

Figure 5-22. Seismogram located at Nearby La Pine High School on the day of largest Event (M 2.39) during stimulation.

5.3 DISTRIBUTED TEMPERATURE SURVEY

The first Distributed Temperature Sensor (DTS) cable was obtained and then deployed on October 17. It lasted until November 24, when signal loss was significant enough that it needed to be pulled from the well. The second deployed DTS cable did not make it through a washout zone at 2,088 m (6,850 ft), and DTS monitoring only occurred to that depth during Stage II and Stage III. Therefore, identification of stimulation fractures must concentrate on data gathered during the first stage of stimulation.

Figure 5-23 displays the change in temperature gradient along the wellbore over time. Displaying the DTS data in this way is an efficient means of identifying fluid exit points along the wellbore. Fluid exit from the wellbore can be detected when the data is displayed in this way due to the temporary increase in gradient at the point of exit. Flow rate inside the well decreases below an exit point because of a loss of energy and pressure to the fracture above. The contrast between the fast moving water above the exit point and the slower moving water below the exit point creates a gradient spike as the slower moving water has more time to heat up. This theoretical exit point may actually be distributed over an exit zone in some cases. If this is true one would expect an isothermal zone over where water is flowing out, followed by a gradient spike. Conversely, when pressure in the well is quickly brought down, heated over-pressured water from the open fracture system will flow back into the well causing a gradient spike. Based on this basic concept there are seven different features clearly evident from the DTS graph in Figure 5-23.

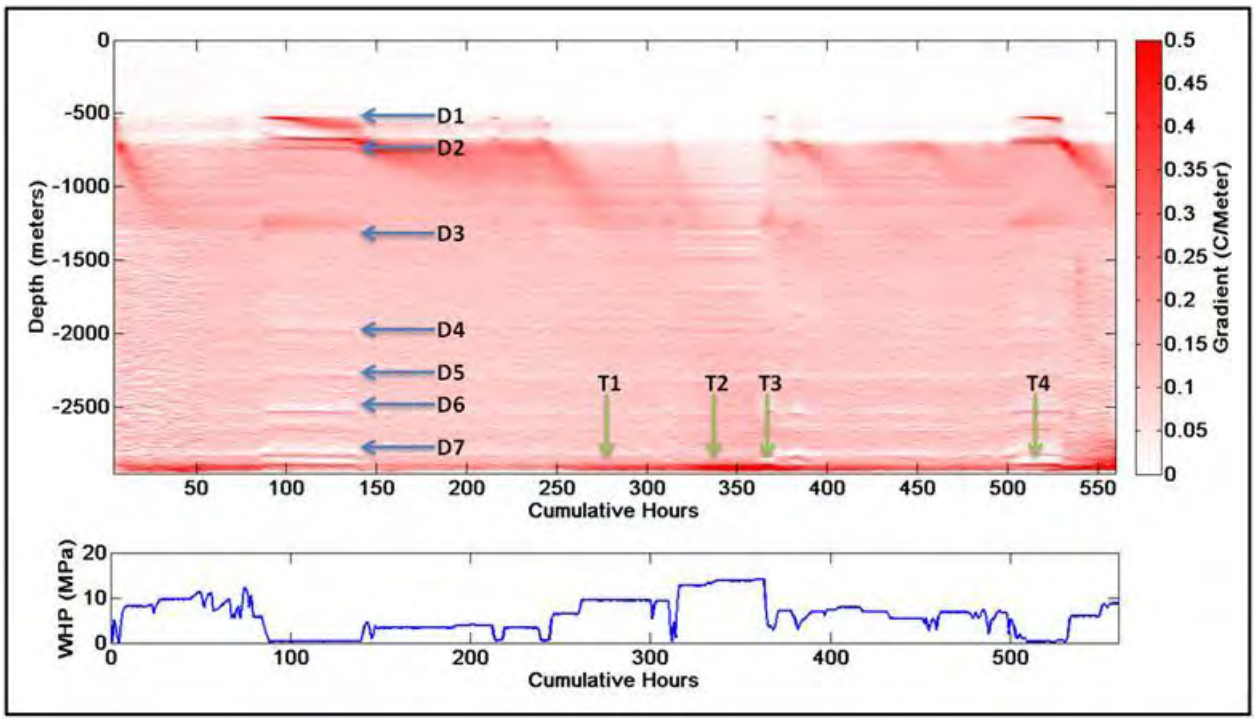

Figure 5-23. Contour map displaying temperature gradient as a function of time and depth; well head pressure for this time period is displayed on the bottom section of the graph. D number values stand for depth where there is apparent fluid flow. T number values stand for times where the effect of well head pressure on flow into the bottom of the well is apparent.

5.3.1 INSIDE THE CASING SECTION

D1 (550 m; 1804 ft) is the location of the PAS, used for lifting cuttings during drilling and flow testing the well. Because this thermal anomaly shows most prominently during low-pressure episodes, the current hypothesis is that the PAS line check valve leaks, allowing water to flow into the PAS line. When pressure in the well was reduced, a pressure differential between the PAS line and the well-bore caused heated, trapped water in the line to flow back and mix with the colder water in the well bore.

D2 (685 m; 2246 ft) **is the depth where the temperature profile consistently transitions from isothermal to a geothermal gradient (**

Figure 5-24). Above this depth, the water is nearly the same temperature as the water injected at the surface, and below this depth the water begins to heat up due to the approximate 50 °C differential between the temperature of the reservoir rock and the injected fluid.

This is the depth at which what appears to be a crack in the casing was identified in the DHTV (Section 6). Furthermore, between the depths of 610 and 1070 m (2000-3500 ft), the well bore's inclination increases from 3° to 13° and at 712 m (2334 ft) and the directional survey (Appendix H) shows a high dogleg severity (1.752). Thus the potential for a casing leak due to casing stress or drilling pipe wear would be increased at a depth of 700m. This depth is also the location of some of the highest degree of hematite/clay alteration in the shallow part of the bore-hole (Figure 5-25).

D3 (1294 m; 4245 ft) is the depth of the liner lap. The cross sectional area of the casing below the liner lap is roughly half that of the casing above the liner lap (casing inside diameter (ID) goes from 33 cm (13.375 in) to 24.4 cm (9.625 in). This means that the velocity of the water will nearly double past the liner

lap. Increasing the velocity of the water should lead to a reduced gradient below the liner lap, which is what we see.

D4 (2000 m; 6562 ft) is the depth of the shoe. At this depth water is going from contact with the insulated wellbore to direct heating from the rock wall. This would likely cause a small initial gradient spike. The disappearance of this signal as injection continued supports this interpretation.

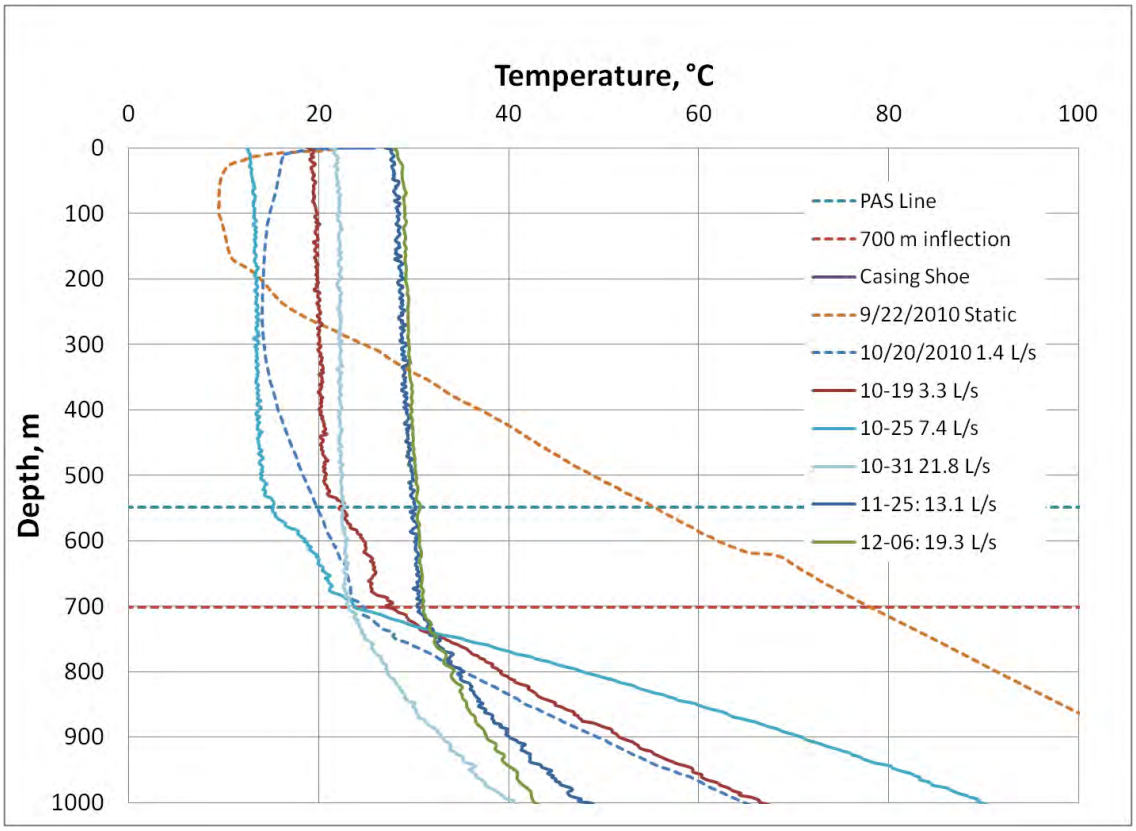

Figure 5-24. Temperature profiles at various times and pumping rates in upper cased portion of bore hole, with inflections at PAS line (550 m) and 700 m marked.

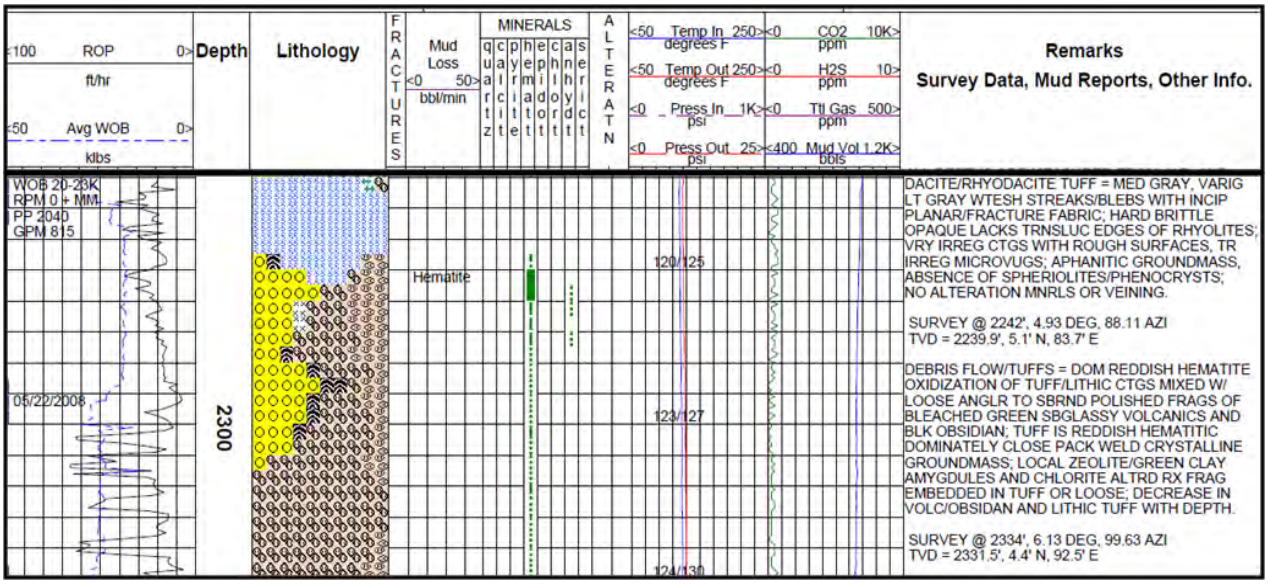

Figure 5-25. Mud log at depth of D2, which is located at 700 m (2300 ft)

5.3.2 OPEN HOLE SECTION

D5 (2360 m; 7462 ft): This lineation is an example of water flowing from the formation into the wellbore during a period of low wellhead pressure. This depth marks the first stimulated fracture intersecting the wellbore and is clearly defined in both the borehole televiewer (Figure 5-26) and mudlog (Figure 5-27). Borehole televiewer data indicate multiple minor fractures in the area of the perceived gradient spike, which are shown as the purple lines in Figure 5-27.

The mudlog shows significant mud losses and mud gains at this depth, indicating an open fracture filled with preexisting fluid. Furthermore, the mudlog shows unusually high levels of H_2S, which also indicate an open fracture. Mud gains, mud losses, and high levels of H_2S indicate that the section is connected to a system outside of the wellbore. The smaller aperture of these fractures indicates that flow into this section would have been minimal unless it was stimulated.

D6 (2512 m; 8241 ft): On the borehole televiewer log this section of the wellbore is characterized by high-angle minor fractures (purple lines) and associated high-angle lithological bedding planes (green lines) (Figure 5-28). From the mud log it appears that high-angle bedding is associated with a small isolated felsic dike, shown as a green crosshatched pattern in the lithology column (Figure 5-29). There does not seem to be any significant mud loss associated with this zone during drilling, and it is probable that this zone has been hydraulically sheared.

D7 (2815 m and 2885 m; 9236 ft and 9465 ft): This location defines two separate gradient spikes that are found fairly close together. At these depths the temperature exceeds the 176 ˚C (350 ˚F) which is the operational threshold of the borehole televiewer, so no high resolution image data has been gathered on fractures at these depths. However, there is sufficient data within the mudlog to determine a generalized model for these exit zones. Figure 5-30 shows the mudlog at the first zone. It appears that the fracture system at this depth is associated with the base of a felsic dike. No mud loss is shown at this depth because the drillers pulled out of the hole for a new bit, masking any possible signals recorded in the well. During the pipe trip 450 bbls were lost; meaning although it is hard to say where fluid was being lost it is likely

that this zone was taking fluid. Elevated CO_2 levels also support the hypothesis that fluid is likely exiting in this section of the wellbore.

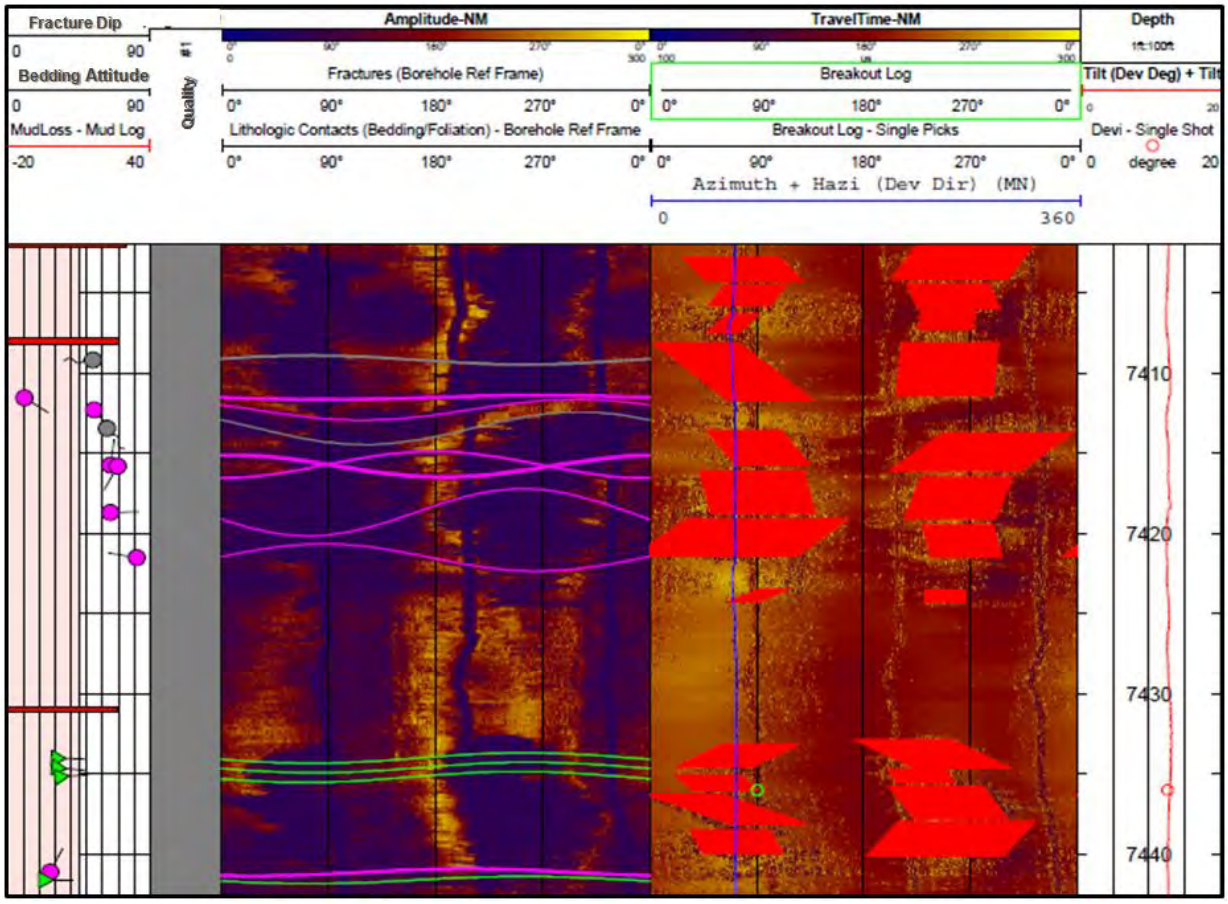

Figure 5-26. Data from the borehole televiewer at depth D5, which is located at 2264 m (7428 ft). Purple lines indicate the locations of multiple minor fractures intersecting the wellbore.

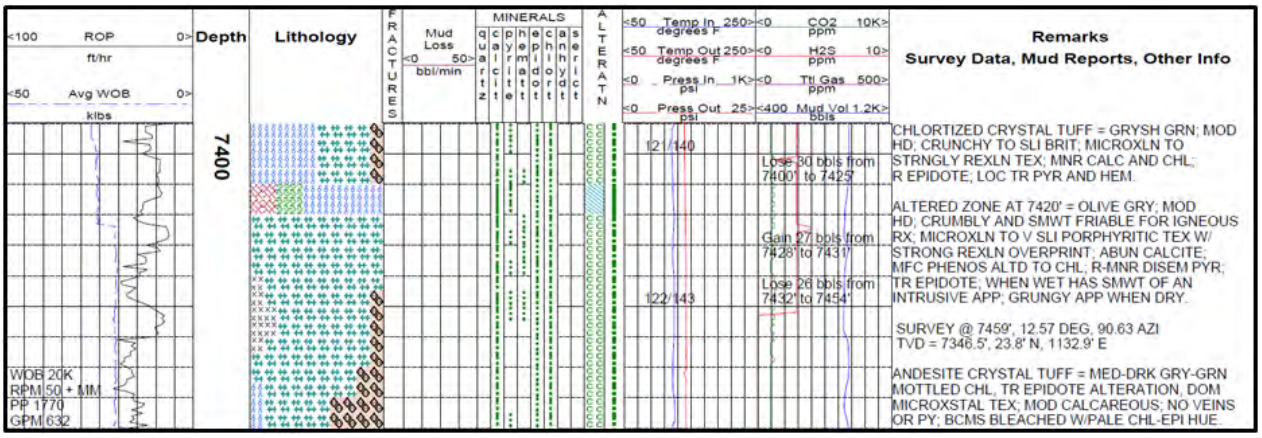

Figure 5-27. Data from the mudlog at depth D5, which is located at 2264 m (7428 ft).

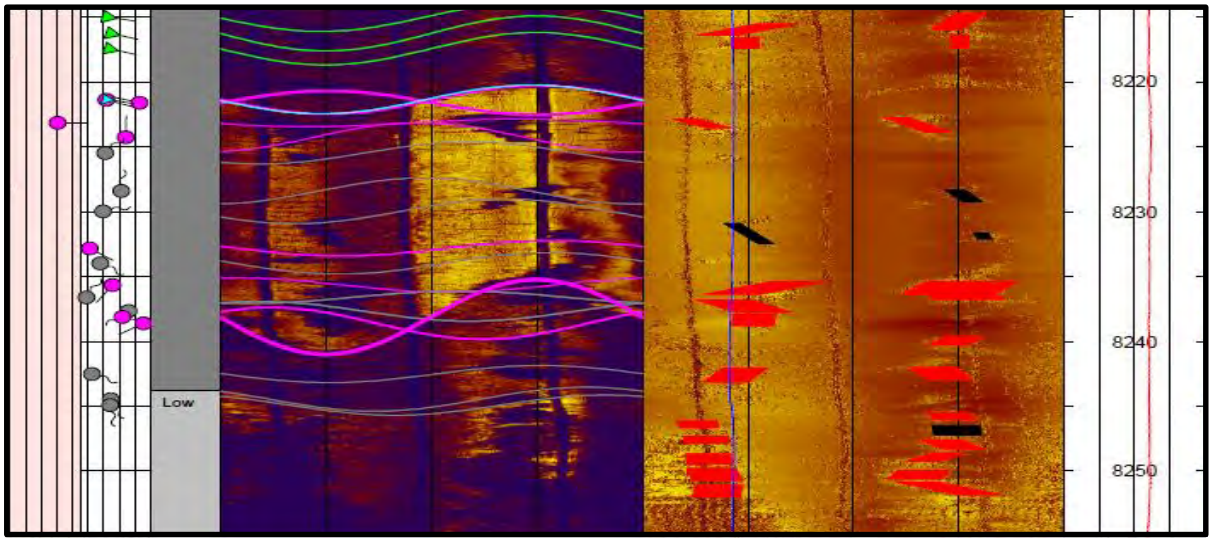

Figure 5-28. Borehole televiewer data for depth D6, which is located at 2512 m (8240 ft). Purple lines indicate high-angle minor fractures and green lines indicate associated high-angle lithological bedding planes.

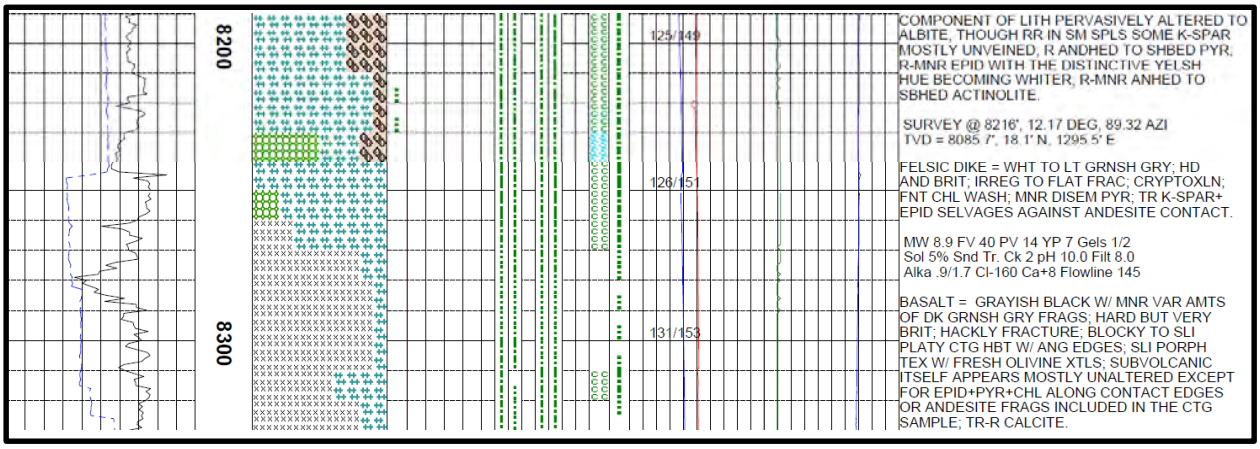

Figure 5-29. Mudlog data for depth D6, which is located at 2512 m (8,240 ft).

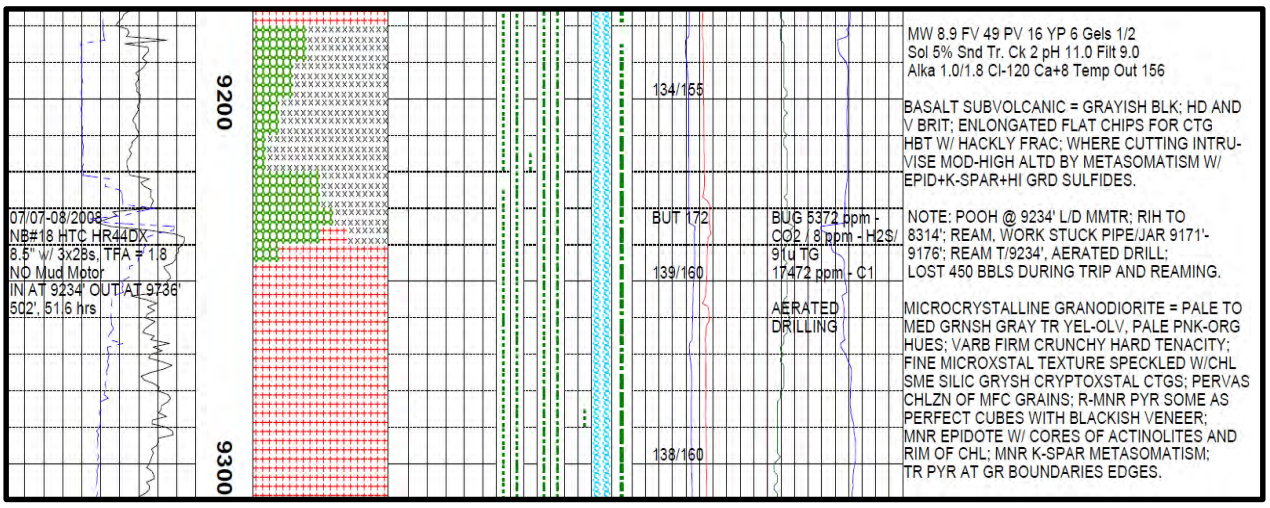

Figure 5-30 Section of the mud log characterizing the first zone D7.

The second zone of D7, located at 2875 m (9430 ft) is heavily altered, has high associated H_2S values and elevated mud temperatures. According to the mudlog there appeared to be some mud losses associated with this zone as well, however, losses were masked by dumping the sand trap, which temporarily drops the mud volume recorded in the mud tanks. Fracturing seems have occurred along the contact between granodiorite and basalt subvolcanic material. This zone is characterized by significant epidote and silica alteration as well as the presence of pyrite and other sulfides. Alteration provides evidence for a connected fracture system undergoing alteration by a hydrothermal system. Both locations within the D7 zone have the largest gradient changes within the wellbore, indicating substantial fluid flow out the wellbore and into these zones.

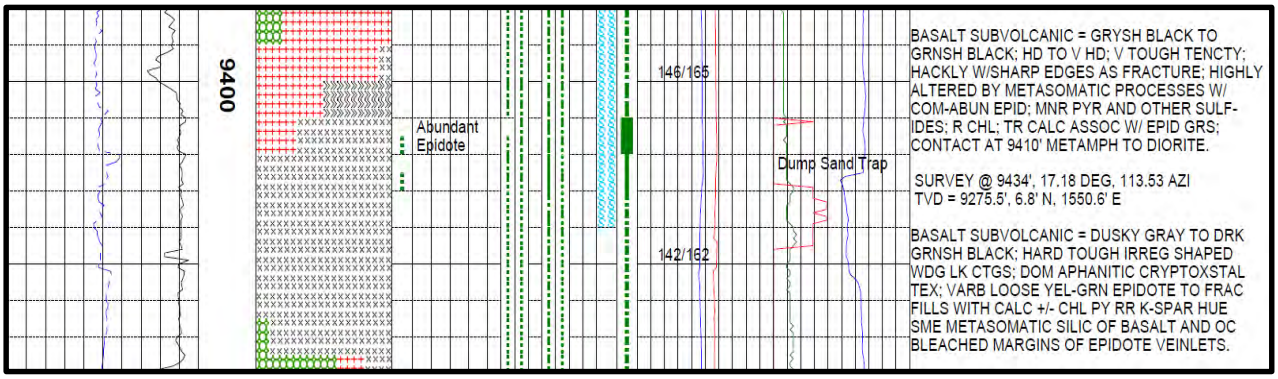

Figure 5-31. Section of the mud log characterizing the second zone D7.

Time Evolution of D7 Zone:

Evolution of the temperature gradient at 2875 m (9430 ft) is shown in Figure 5-32. Increases in wellhead pressure appear to correlate to a rise in temperature gradient. As discussed before, the increase in gradient describes the contrast between fluid velocity before and after a fluid exit point. Time events T1 and T2 show an increase in thermal gradient as a function of pressure, which provides evidence that the fractures found near the bottom of the well were successfully stimulated.

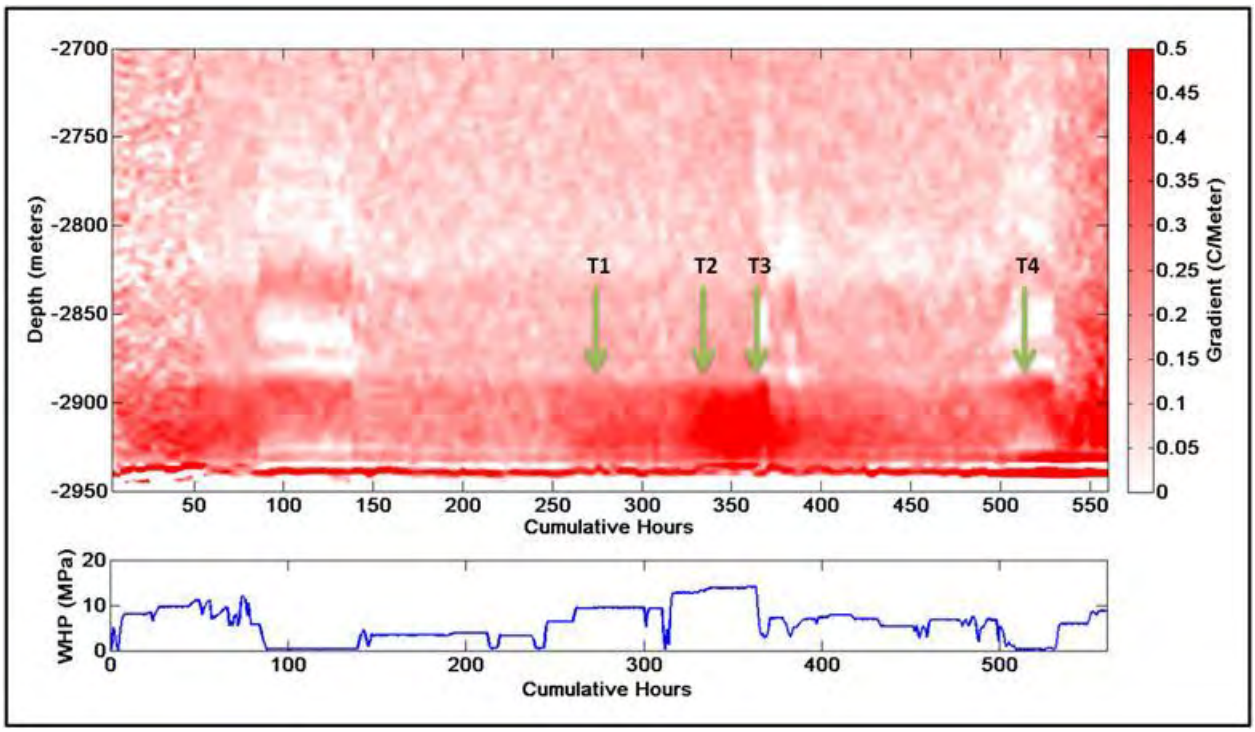

Figure 5-32 Close up of gradient contour map for the bottom of the well, see Figure 5.10.

Event T3 shows a bump in the elevated temperature gradient immediately following a period of high pressure. This immediate response indicates that there is fairly good communication between the fracture plane or interconnected network and the wellbore. Event T4 shows a temperature gradient increase during a period of low pressure, which is most likely an indication that water is coming out of the formation into the well. While fluid exiting from the formation into the wellbore is not ideal, it provides valuable insight into the nature of the fracture system. This suggests that, given fairly good communication, the stimulated fracture or interconnected network extends a significant distance away from the wellbore.

5.4 THM MODELING OF STIMULATION

The modeling results by Eric Sonnenthal at Lawrence Berkeley National Lab are presented in Section 4. Modeling has focused on exploring the implication of potential leaks within shallow zones of the wellbore. Here we comment on how the modeling results compared to the results observed in the field.

Modeled temperature profiles were generated by a wellbore simulator module in TOUGH2 that used the same initial conditions as defined for a specific Thermal-Hydrological-Chemical (THC) native state model. Model uncertainty is defined by variance associated with permeability and thermal conductivity values for the casing and surrounding rock volume. Modeled temperature profiles are most sensitive to changes in permeability for different points within the wellbore.

Figure 4-6 compares the simulated temperature profile results, using native state values from sensitivity test 18, are shown with observed DTS data. Dashed lines represent modeled temperature profiles and solid lines represent observed temperature profiles. At first glance temperature profiles seem to diverge significantly, however, they are closer than they appear. There are two things that contribute to this perceived divergence. The first is that the initial surface temperature in the model is less than the observed values. Secondly, the significant cooling shown by the dashed purple and orange lines

correspond to times where wellbore observations are limited to a depth of 2088 m (6850 ft). The best comparison available is the dashed light blue line with the solid purple line. The dashed light blue line models 6.2 days of stimulation and the purple line is modeling 8-9 days of stimulation. If one were to change the initial surface temperature and reduce the permeability at the exit point located at 2500 m (8200 ft) then the profiles would likely be closer. According to simulation results it is likely that the shallow leak and the exit point at the bottom of the well are the dominant permeable features during the first phase of stimulation.

Figure 4-12 shows the pressure propagation from the well, and has been modeled using initial inputs from sensitivity test 18. In this model leaks are located at the PAS line and at 685 m (2245 ft). The pressure diffusion cloud is thinner near the bottom of the well because there are significant lithological changes which occur at approximately 2590 m (8500 ft), Figure 4-12.The assumption has been made that this rock is more competent and has lower permeability than the overlying rock. Another assumption which is made is that there are no large conduits transporting water rapidly across discrete intervals in the wellbore; this model assumes that rock behaves as a porous media to reduce computational complexity.

Further model updates are planned and budgeted for Phase 2, including development the coupled THC (TOUGHREACT), Thermal-Hydrological-Mechanical THM (TOUGHFLAC), and Thermal-Hydrological-Mechanical-Chemical THMC numerical models of the EGS system for the purpose of assessing reservoir capacity, and for planning and optimizing reservoir management (production and injection). This will include simulation of injection/pumping tests, tracer tests, and potential alteration and mechanical deformation of newly created and/or stimulated fractures. TOUGH-FLAC simulations will evaluate well spacing for placement of the production wells. The final THMC models will use the newly developed parallel TOUGHREACT with temperature and mineral-dependent coupling of thermal properties, using permeability fields generated by TOUGH-FLAC.

5.5 MINERALOGY/ALTERATION OF MICROSEISMIC DEPTHS

Alteration minerals give further insight into events seen during stimulation. Smectite and calcite alteration dominate between 360 m (1180 ft) and ~1400 m (4600 ft) (Figure 5-34). This clay alteration material is dominantly hydrophilic and in some cases expands in the presence of water. Significant transport of water through fractures in this alteration zone is unlikely. Core samples from N-2 and drill cuttings from NWG 55-29 show that altered clays are found along intersected fracture planes within this zone (AltaRock, 2011a). Calcite is first seen at 500 m (1640 ft) and is primarily found along fracture surfaces. The disappearance of calcite at 2600 m (8450 ft) is fairly sudden and suggests a significant change in alteration histories from above and below this depth (Figure 5-33). The first instance of silica and pyrite veining begins at 1100 m (3595 ft) and is found in a rhyodacite crystalline tuff below a 33 m (100 ft) thick obsidian/debris flow. The onset of silica and pyrite filled fractures correlates with the highest concentration of seismic activity. At depths below 1100 m (3595 ft) smectite appears less often in the observed wells. Epidote first appears at a depth of 1785 m (5850 ft) along the fracture surface found within basaltic andesite flow. It does not become common until about 2000 m (6560 ft). Chlorite first appears at a depth of 1250 m (4100 ft) but does not become prominent until 1525 m (5000 ft).

Figure 5-34 shows that the shallow seismic zone is within this clay (smectite) altered zone. The frequency of seismic events is highest along the lower portion of the clay alteration zone. Thus, this zone may be an area of preferential fluid flow for water which leaked from the casing at 695 m depth. The lateral distribution of the shallow seismicity and its relationship to the volcanic rocks and alteration can be examined using lithological data from GEO N-2 (Bargar and Keith, 1999), a temperature core hole (TCH) drilled in 1985 (Figure 5-35). In the top 600 m (1967 ft) of these two holes, where no microseismicity occurred, the lithologies can be fairly well-correlated. Below about 600 m (1900z ft), depths at which

seismic events did occur, the correlation is more difficult to make. Perhaps past volcanic processes and associated deformation such as previous caldera-forming events, created a complex permeability and alteration structure below 600 m (1967 ft). In this case the units above 600 m may form a more continuous and impermeable cap rock.

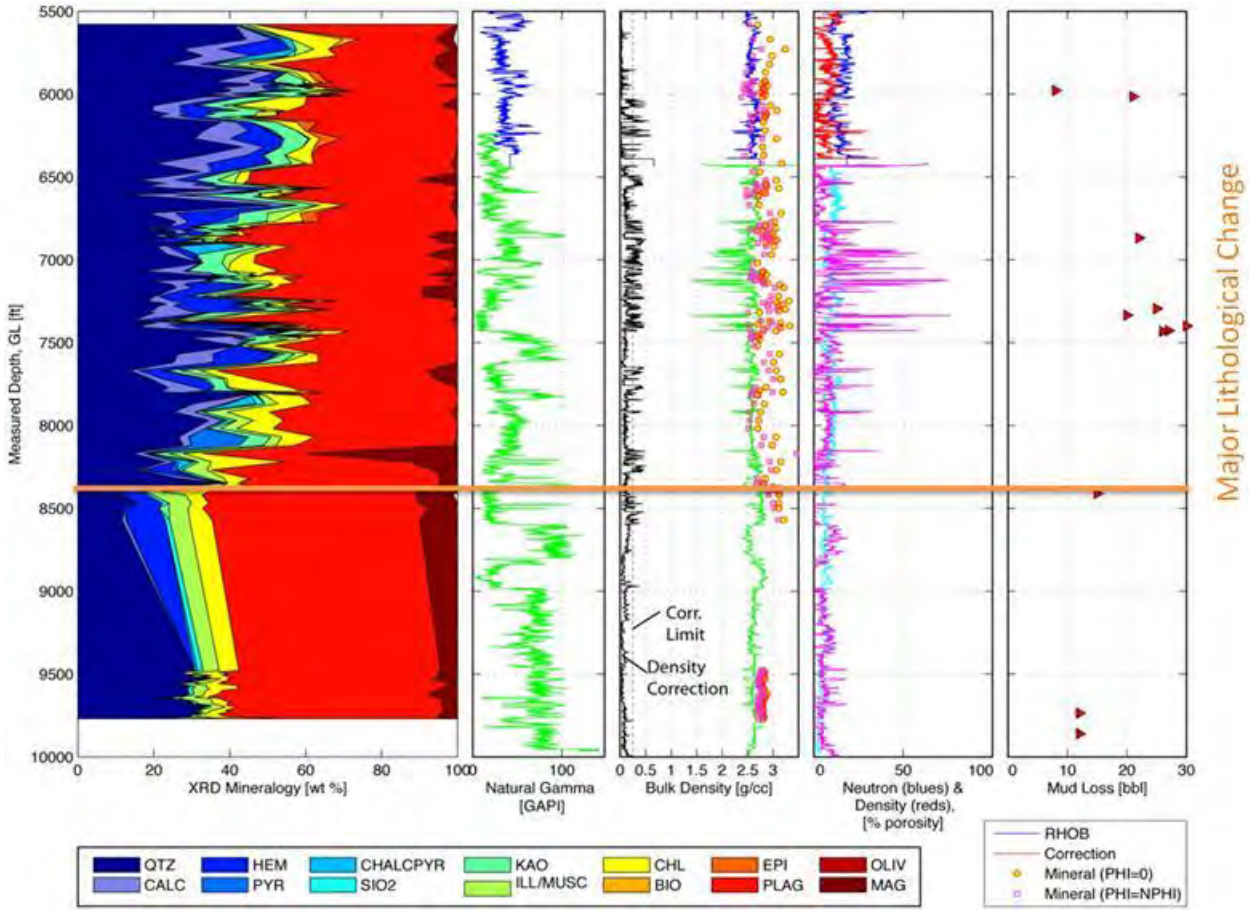

Figure 5-33 XRD Mineralogy data plotted with gamma ray, density and mud loss data. Data shows significant lithological changes at 2590 m (8500 ft), going from quartz rich material to feldspar rich material.

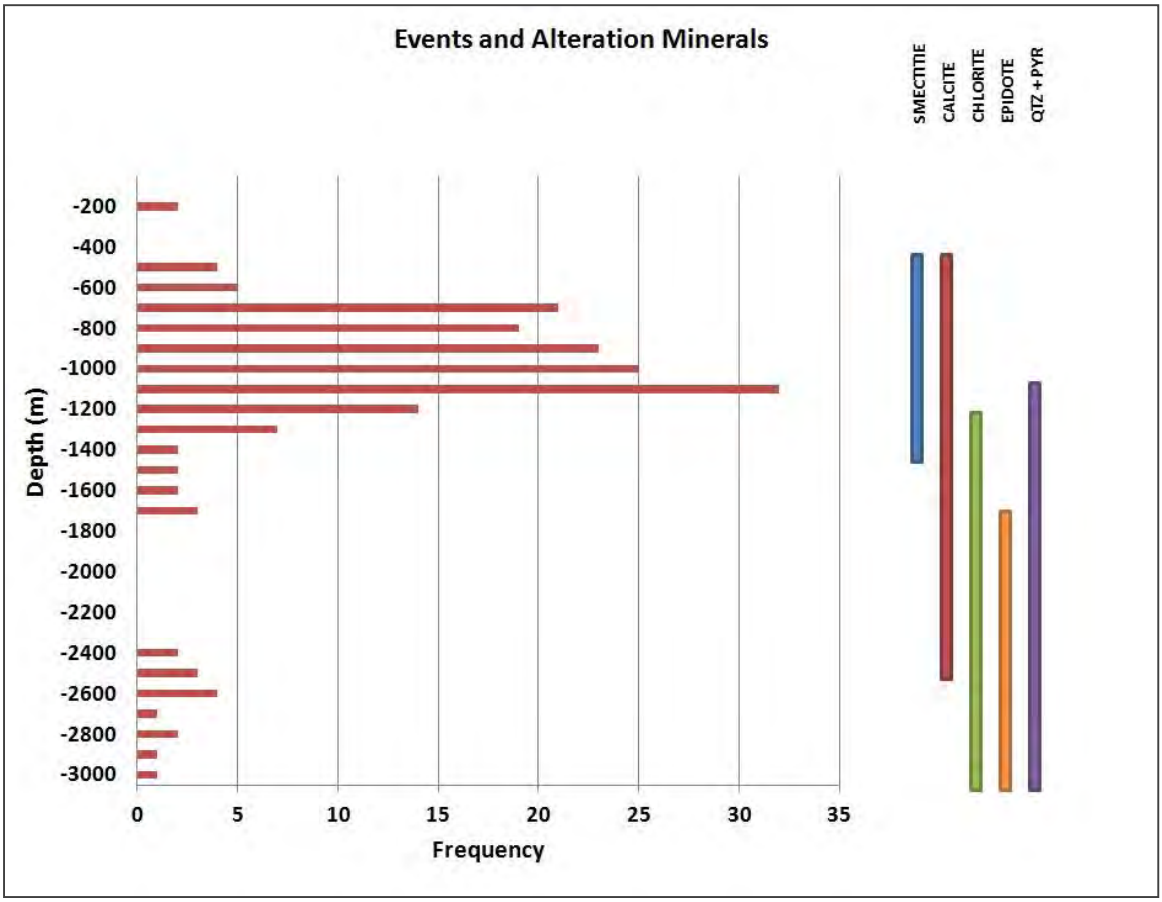

Figure 5-34. Presence of alteration minerals (mud log) compared to distribution of events with depth.

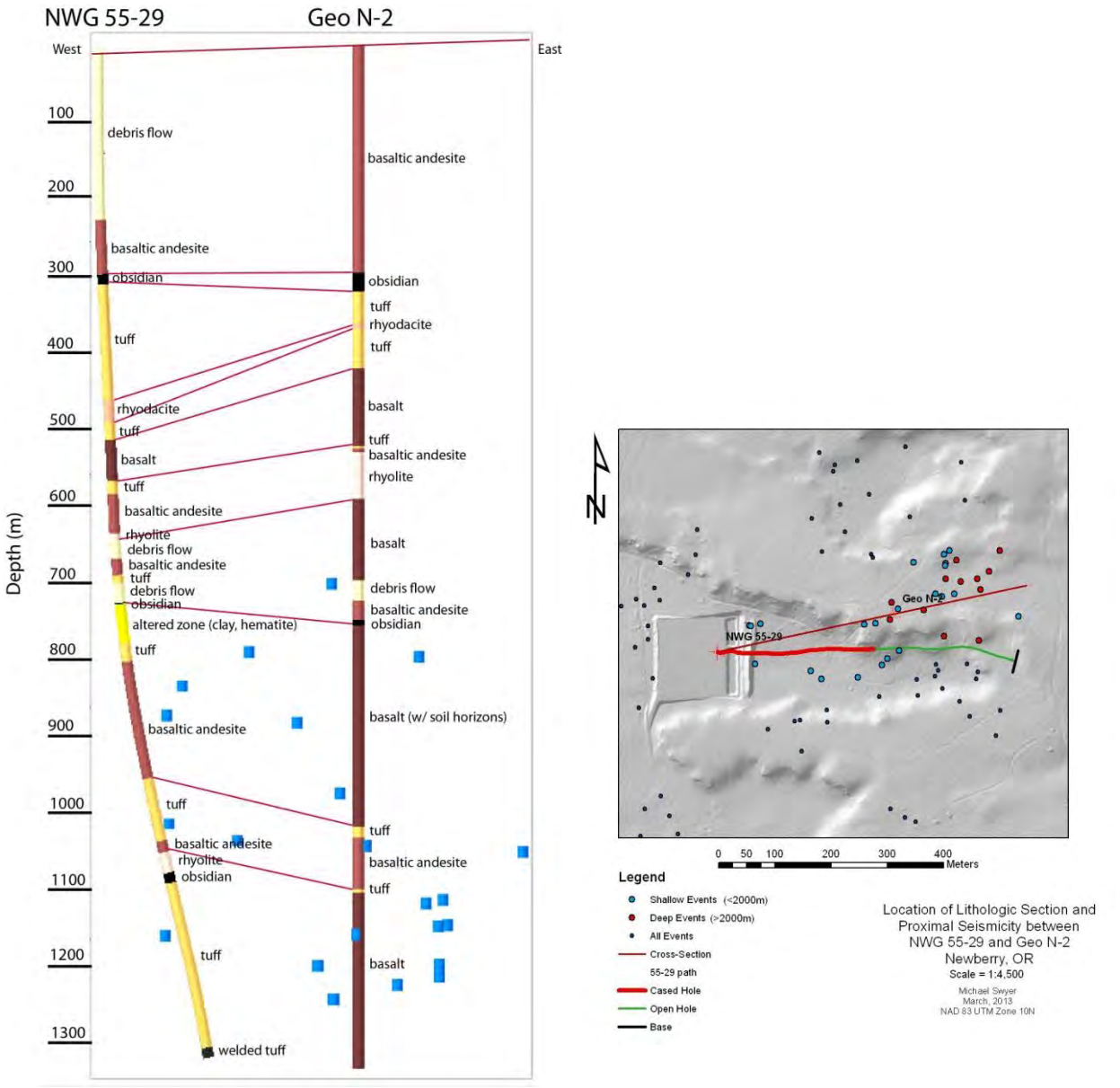

Figure 5-35. Left: cross section showing lithological comparison between NWG 55-29 and GEO N-2 with MEQ's (blue squares) that occurred within 100 m of the cross section line between the holes. Right: map view of cross section line. Red dots on map are below the cross section line.

5.6 CONCLUSION

Analysis of the microseismicity and temperature profiles supports the conclusion that stimulation of NWG 55-29 created a multi-zoned, EGS reservoir with a volume of up to 1.5 km^3. The bimodal distribution of seismic event depths resulted from stimulation of the reservoir within the open bore hole interval and leakage from the surface casing at measured depths between 500 and 700 meters (1,640-2,297 ft). The casing will have to be repaired in order to performing any additional work. Despite an estimated loss of over 90% of the fluids injected through the casing leak, the lower, open section of the hole was successfully stimulated at depths of 2512-2885 m (8246-9465 ft). Furthermore, the use of TZIM was successful in diverting injection fluids and stimulating different parts of the well bore.

6 2013 FIELD WORK

6.1 CASING INTEGRITY EVALUATION AND INJECTION TEST

Field work performed in August 2013 was designed to measure the increase in permeability achieved during the 2012 stimulation program and to assess potential casing leaks, particularly at depths between 500 to 700 m (1640 to 2297 ft). The likelihood and importance of casing leaks was elevated during the preparation and then review of the first draft of this report. Thus, finalization of this Phase 2.1 report was put on hold and a program to evaluate the integrity of the casing developed. The results are presented in this new section.

Several well bore surveys were performed to evaluate the casing and open hole. Figure 6-1 provides a flow chart and details of the survey activities. A dummy tool was first run to make sure the wellbore was clear and safe for additional logging tools. Multiple Pressure-Temperature-Spinner (PTS) surveys were run both under static conditions and during the step rate injection test. A 30-finger caliper log was run to measure the inner diameter of the well bore and assess casing integrity. A caliper log was run in the 34 cm (13 ⅜ in) portion of the well bore (depth of 0 – 1280 m; 0-4200 ft). A down-hole camera survey visually inspected for the potential leaks (one of which was confirmed) and help to identify whether sinker bars dropped in December 2012 (the ”fish”) was located at a potential ledge at 2,090 m depth (6,880 ft) just below the casing shoe.

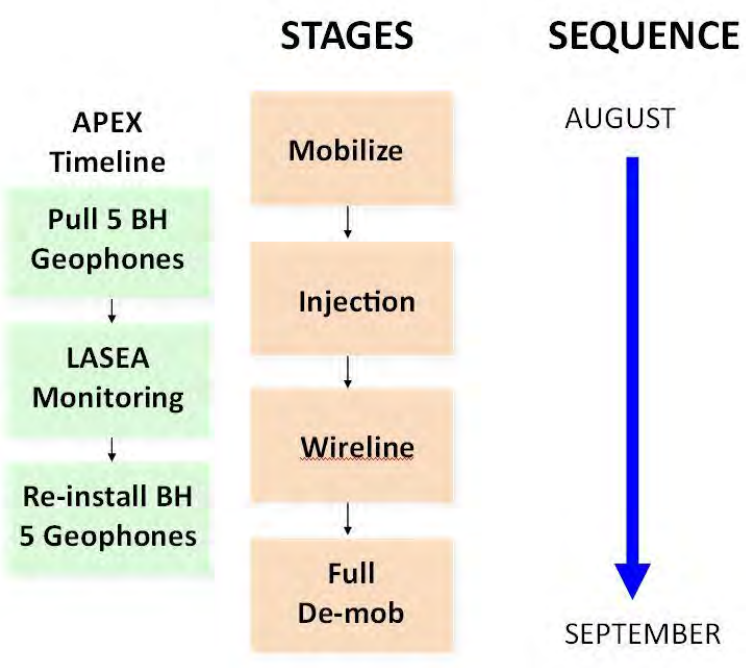

Figure 6-1. Flow chart of summer 2013 activities.

6.2 CASING INTEGRITY EVALUATION

During the week of August 26, 2013, several logging methods were deployed down NWG 55-29 to assess the integrity of the 34 cm (13-⅜ in) casing. The combined results from a Pressure Temperature Spinner (PTS) survey, multi-finger caliper tool and a downhole video camera all provided valuable information regarding the current casing condition.

Prior to running any logging tools downhole, a dummy run using sinker bars was conducted to make sure the cased hole section did not have any obstructions. The tungsten sinker bar diameter was $1^{11}/_{16}$ in and weighed approximately 330 kg (150 lbs). A tapered bull nose was connected at the end of the sinker bar to minimize chance of sticking the tool downhole. After a successful dummy run, a PTS tool was lowered to 2,000 m (6,462 ft) under static conditions. When the PTS tool reached the bottom of the 9⅝ in casing, the water well pump and booster pump was turned on and injection begin to cool the wellbore. Three injection rates were used during the injectivity test, and injection lasted overnight. Results of the injectivity test are discussed in Section 6.3. Both pumps were shut off the morning of August 27, the PTS tool first recorded pressure fall off at 2,000 m (6,462 ft) and then was returned to surface.

On the last day of logging, August 28, four PTS runs were conducted inside the 13-⅜ in casing and two were conduct inside both the 34 cm (13-⅜ in) casing and the 24 cm (9-⅝ in) casing. The temperature plots for all the runs are shown in Figure 6-2. Similar temperature deflection at 683 m (2,240 ft) depth was noticed on the DTS data set in the fall of 2012.

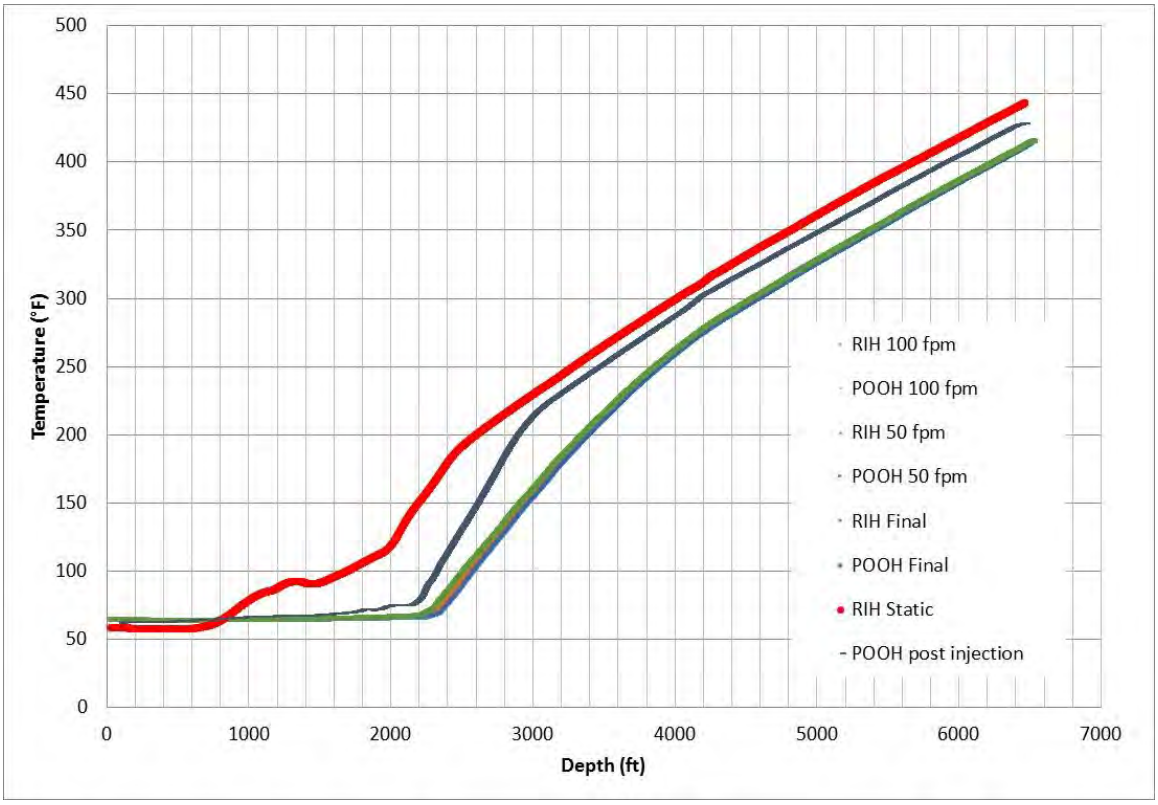

Figure 6-2. Temperature survey of 2013 logging efforts.

Figure 6-3 summarizes the spinner survey conducted with the PTS tool. The spinner tool consists of a rotating propeller. Pulses are generated with each revolution of the propeller, and changes in revolution per second (rps) signals flowrate changes downhole. The positive data represent the tool running in the hole and the negative data represent the tool pulling out of the hole. The injection rate was held constant

during all spinner surveys. The multi-pass method was used to ensure the most accurate and repeatable conditions were recorded, this involved three up and three down logging passes at two different speeds. When compared with the temperature surveys similar deflections were observed at 547 m and 693 m (1,767 ft and 2,240 ft) depth in all the spinner runs (Figure 6-3).

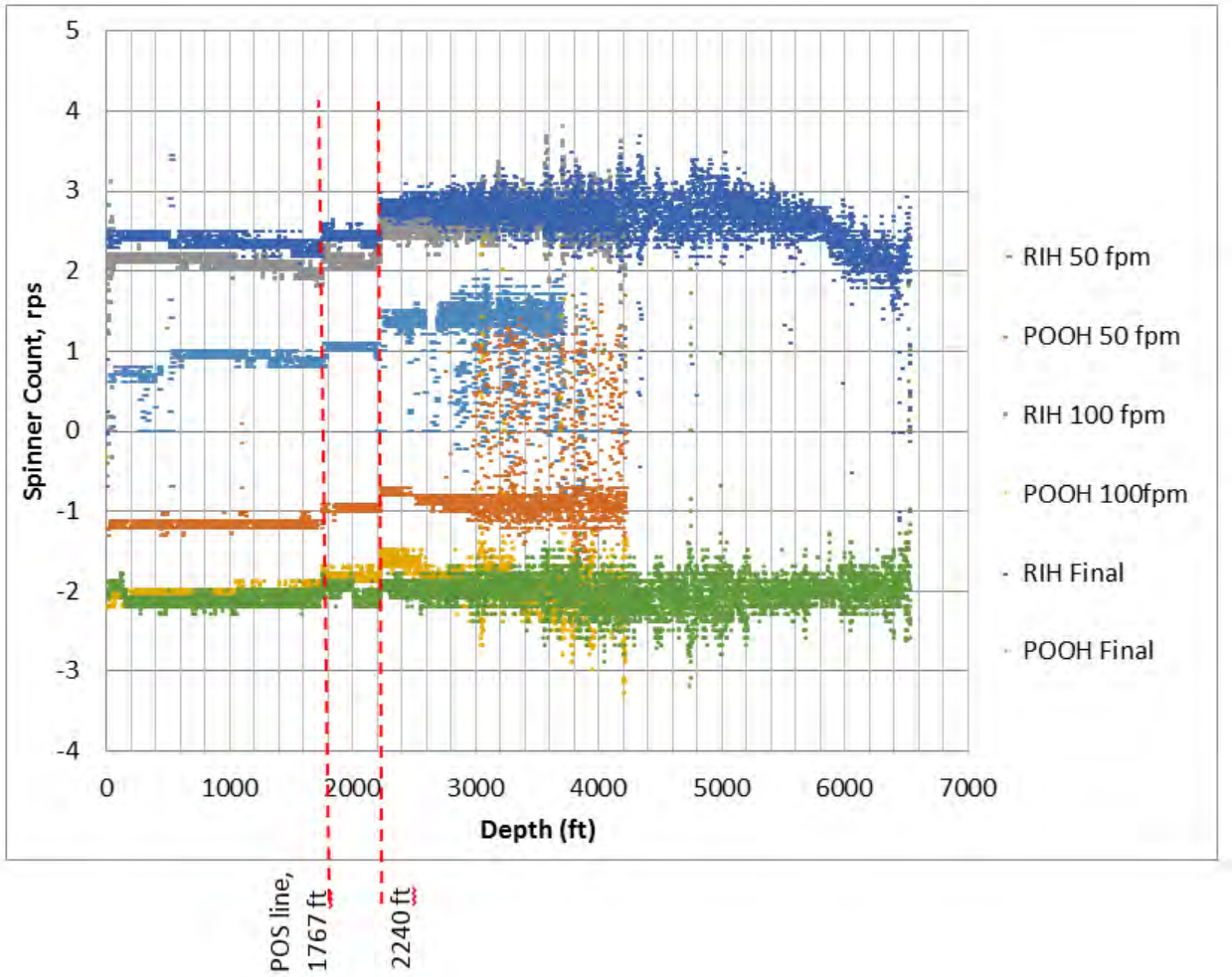

Figure 6-3. Spinner data recorded on August 29, 2013. Three up and down passes were made in the 13-⅜ in casing. All passes showed consistent spinner revolution changes at 547 m and 693 m (1767 ft and 2,240 ft) depth.

When compared with the temperature survey, the spinner results and changes in the temperature profile both indicate flow out of the well at depths of both 547 m the depth of the POS line, and 693 m (1,767 ft and 2,240 ft) depth.

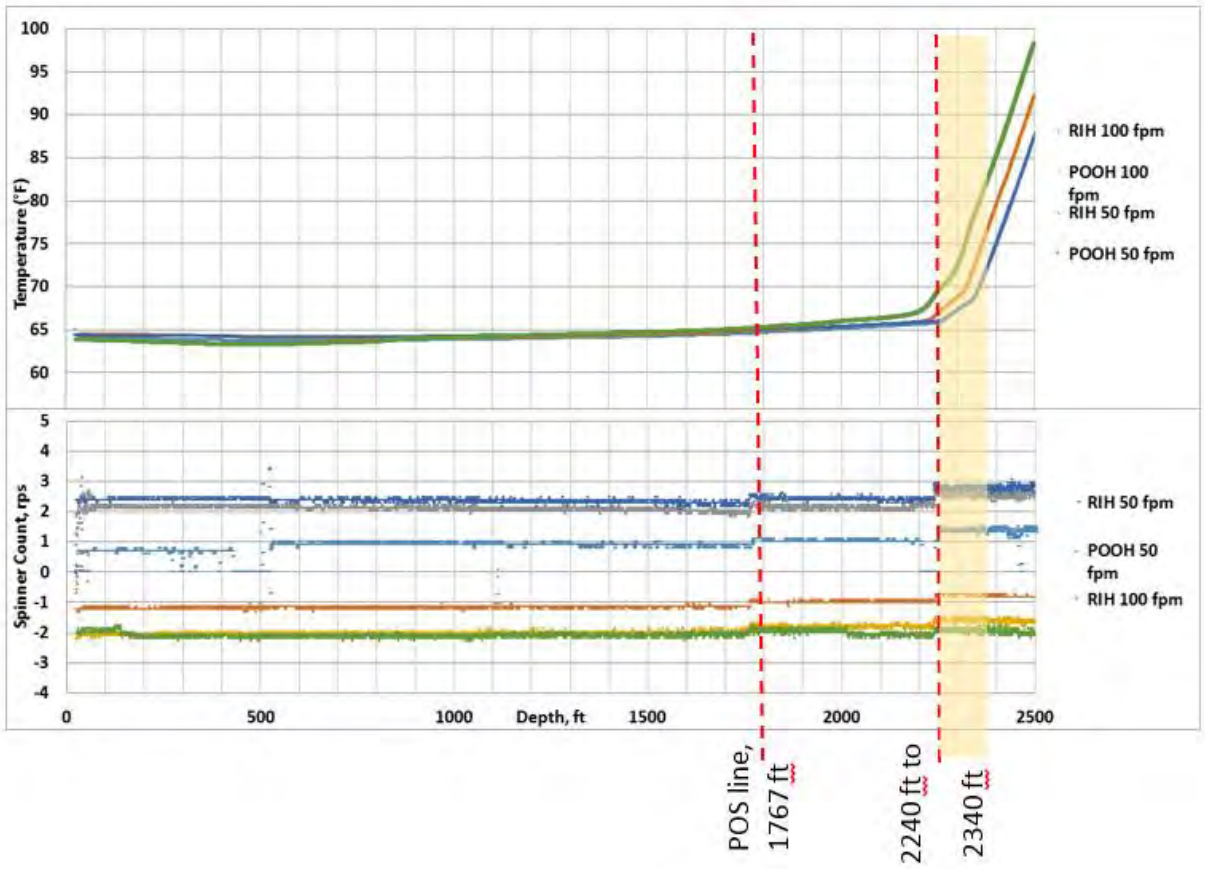

Figure 6-4. Spinner and temperature data, August 29, 2013 - an expanded view of the data shown in Figure 6-3.

A Kinley Megadata Caliper tool was run from surface to 1,772 m (3,788 ft) on August 27 to access the 34 cm (13-⅜ in) casing. This tool offers fully mechanical, simultaneous, and continuous readings from 30 feelers for temperatures up to 600 °F. The tool is centralized with an array of 30 feelers that reach out to the inside of the 13-⅜ in casing. The tool is run in hole fully collapsed, and the feelers extend to the size of the casing on the trip out of hole. Feeler position data are recorded continuously on a copper cylinder inside the tool joint. The recorded downhole data is converted to electronic data at the surface using Expro's scanning technology. Prior to running the caliper tool, a dummy run was run through with 10 ¼ inch 25 gauge rings to make sure tool could pass through the casing free of obstructions.

The survey noted scattered pits, partial rings of reduction and areas of corrosion. The deepest penetration recorded is a 0.71 cm (0.28 in) pit, or 51% of the wall thickness, in a line of pits located in the lower part of joint #57 (Figure 6-5). The condition of the casing surveyed appears good with respect to mechanical damage, with only one joint showing 10-20% metal loss (Figure 6-6). Based on the maximum penetration results of the caliper survey, the probability of a hole in the casing was calculated to be 2.34% with a 99.4% correlation. This confirms that caliper surveys alone cannot provide accurate predictions regarding holes in the casing. A high temperature bore hole camera provided by Expro was also deployed to further visualize the problematic areas. The camera was deployed August 28 under injection conditions to cool the hole and allow it to be deployed more deeply. There was a difference in the joint lengths recorded by the caliper survey vs. the casing collar counter used in the PTS tool, thus the caliper survey depth reference differs from the actual depth. The caliper survey on average displayed shorter casing joint length. Casing sections are here referenced by the corresponding casing joint number in the order installed.

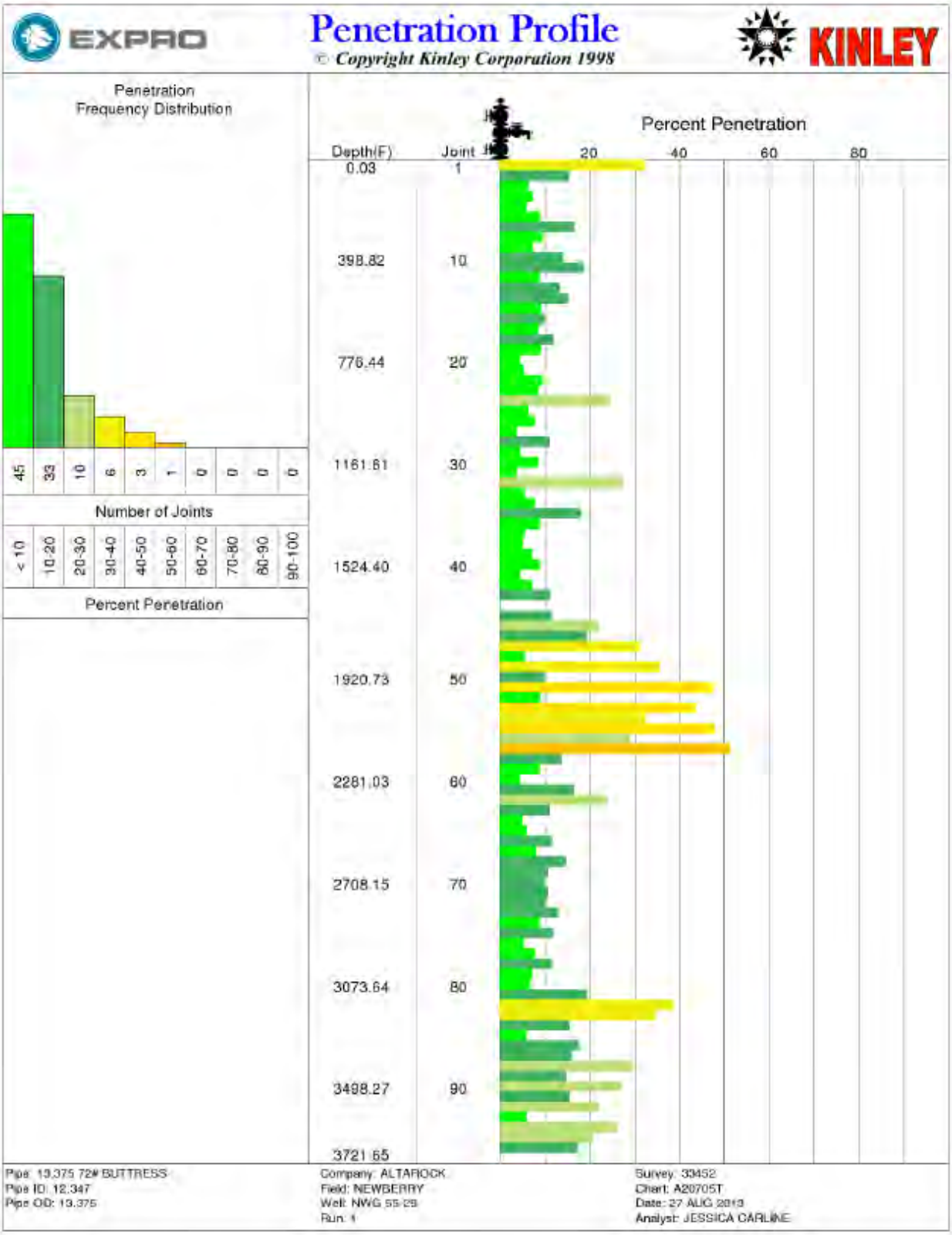

Figure 6-5. Corrosion damage summary. Results show percent penetration noted with caliper.

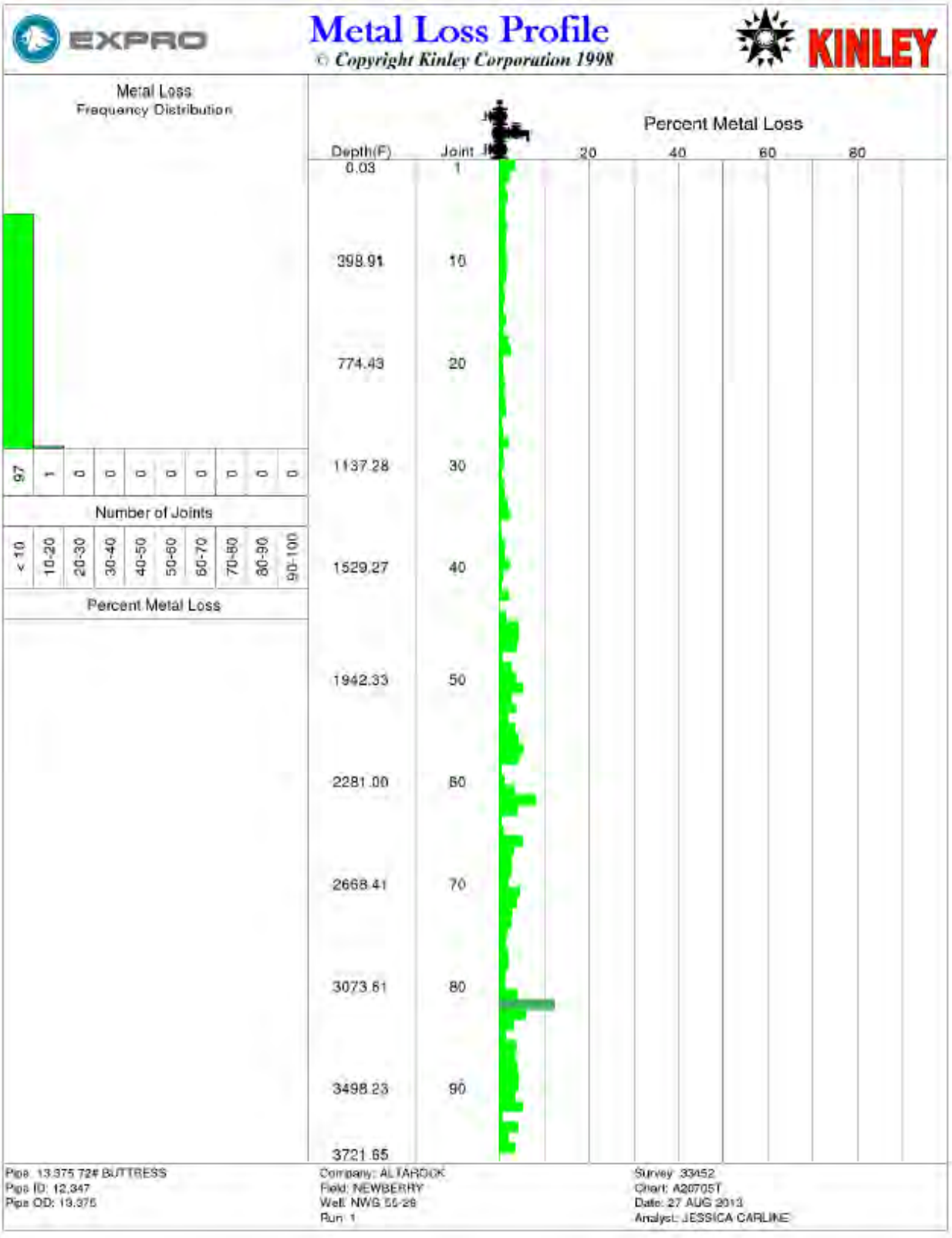

Figure 6-6. Mechanical damage summary. Percent metal loss noted.

A sample of the caliper results and camera view at the POS line near 539 m (1,767 ft) is displayed in Figure 6-7. The caliper tool picked up two signals, similar to a casing collar above and below the PAS line connection in casing joint 44. The connection can be clearly seen from the video camera run. The tool was left static at this depth to observe any fluid exit points. Under injection conditions, a small amount of scale is mixed with the injection water and falls downhole consistently. During our observation, the scale was seen exiting the PAS line, indicating fluid loss.

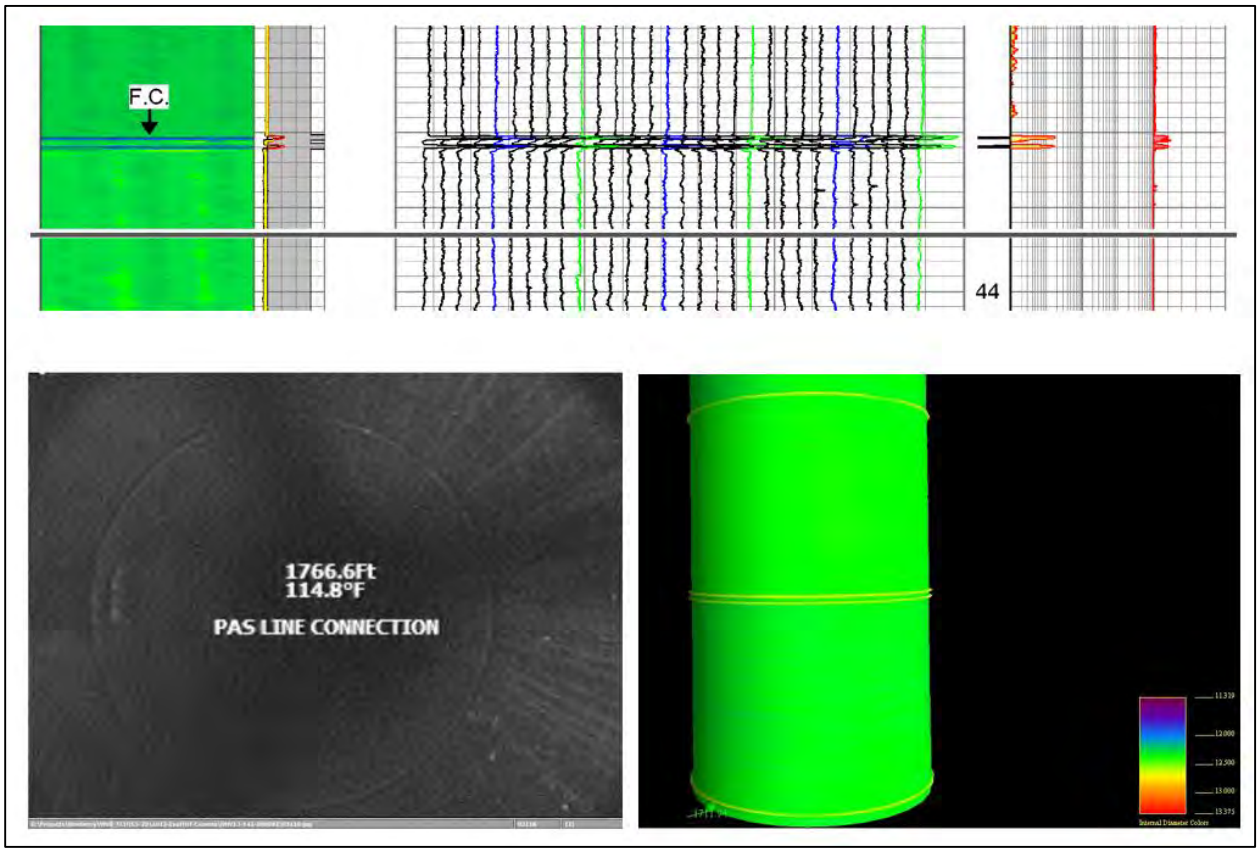

Figure 6-7. Caliper results of the casing joint containing the PAS line. Down view of the bore hole camera run at the PAS line shown in the lower left. 3D view of the caliper results for casing joint 44 shown in the lower right.

The summary of the caliper results and camera view near 683 m (2,240 ft) is displayed in Figure 6-8. This same depth correlates to casing joint 55 in the caliper survey. The video camera run noted a structure similar to a casing collar at this depth, while both CCL and casing run history showed no collar connection should be found at this depth. Further caliper and camera results showed the actual casing collar for joint 55 to be located at 685 m (2,246 ft). This ring could potentially be a gap in the casing and explain the temperature and spinner deflections observed.

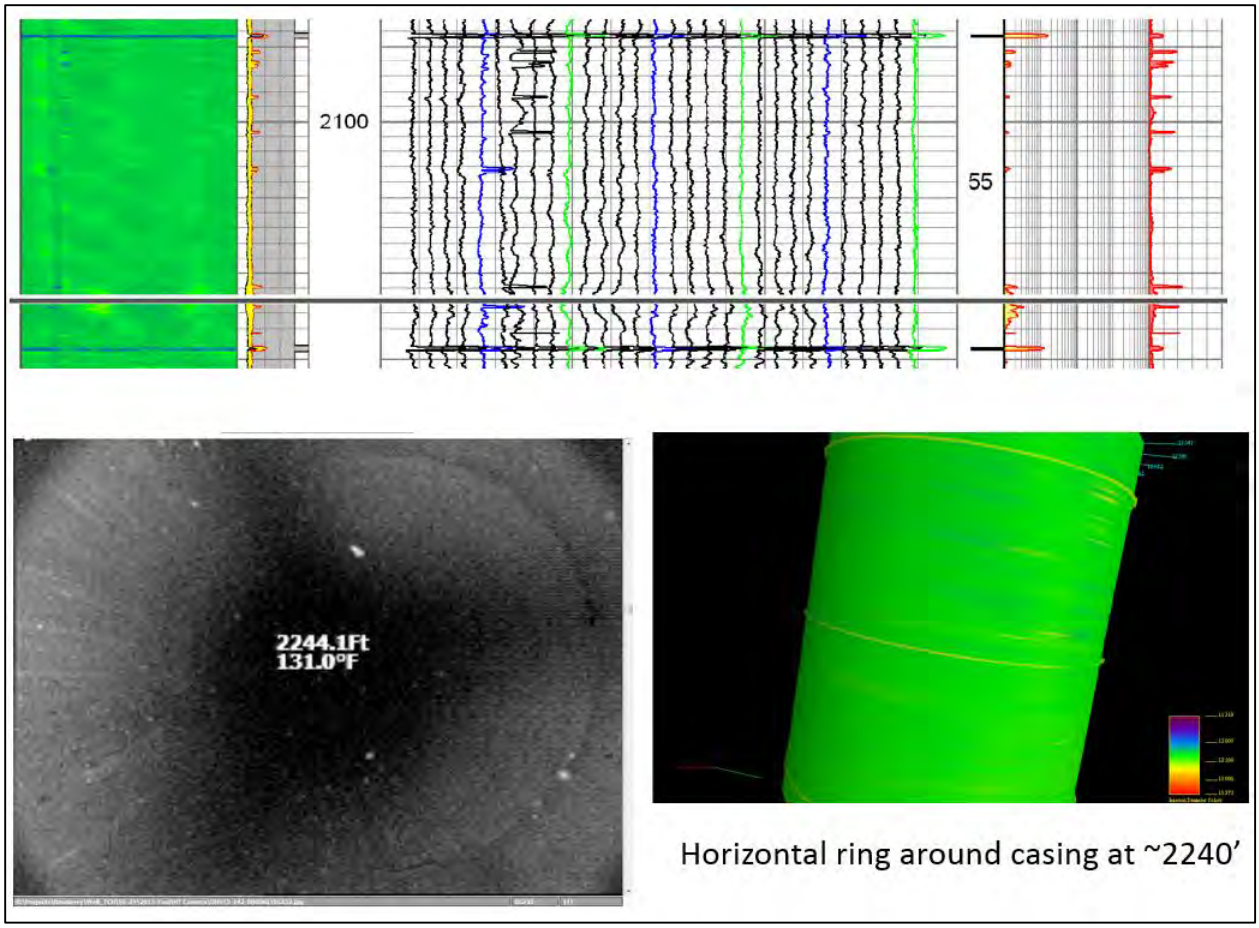

Figure 6-8. Caliper results of casing joint 55. Down view of the bore hole camera run at 2240' with ring like structured shown in the lower left. 3D view of the caliper results shown in the lower right.

The deepest penetration pit noted in joint 57 is displayed in Figure 6-9. The video camera view showed the pit to be series of grooves, possibly as a result of rotational wear during drilling. A schematic of the potential groove caused by drill pipe is shown in Figure 6-10. Drill pipe damage has the potential to be 9.47 cm (3.73 in) wide, registering 1 to 3 caliper arms and usually observed on the low side of the casing. Both caliper and video camera results do not indicate a leak at this depth.

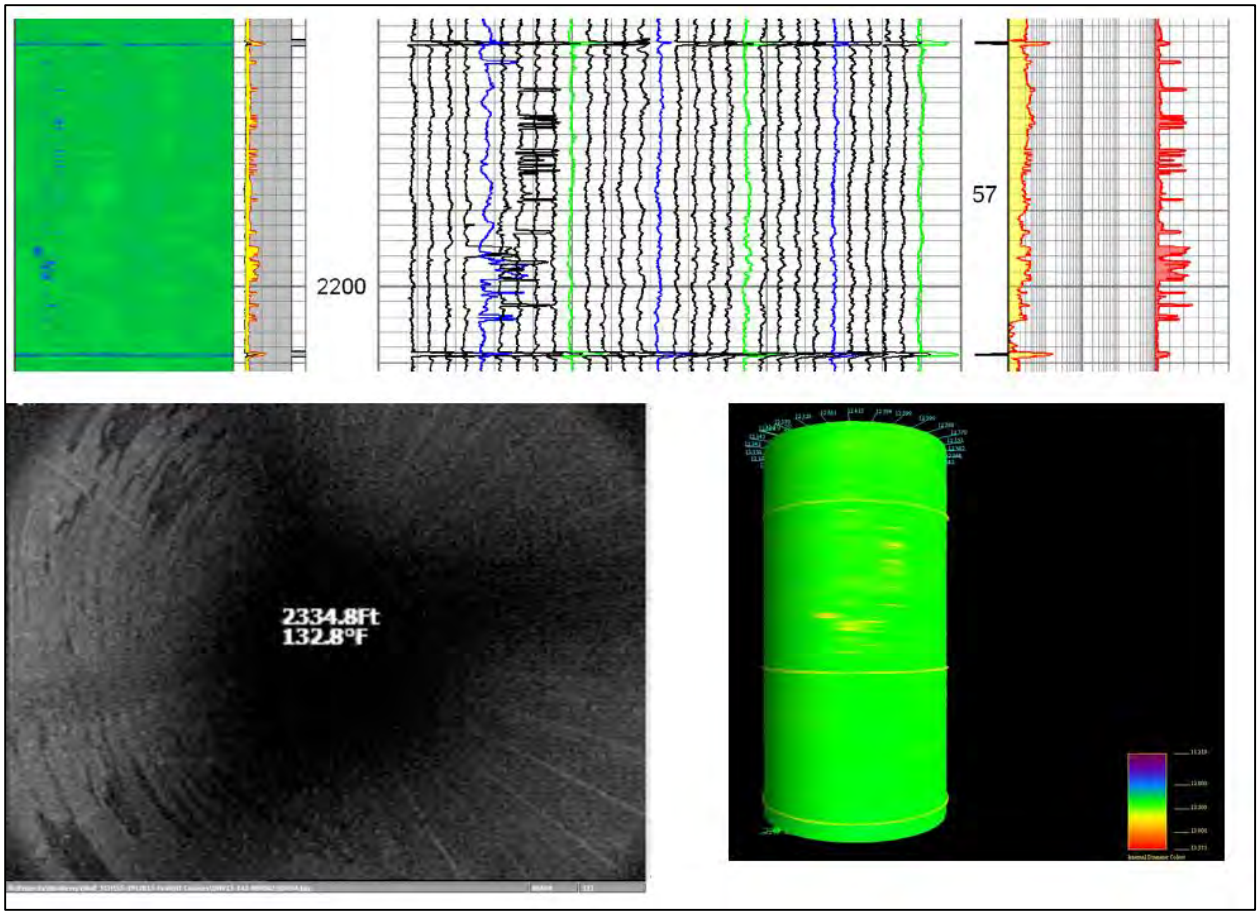

Figure 6-9. Caliper results of casing joint 57. Down view of the bore hole camera run at 711 m (2,335 ft) with grooves shown in the lower left. 3D view of the caliper results shown in the lower right.

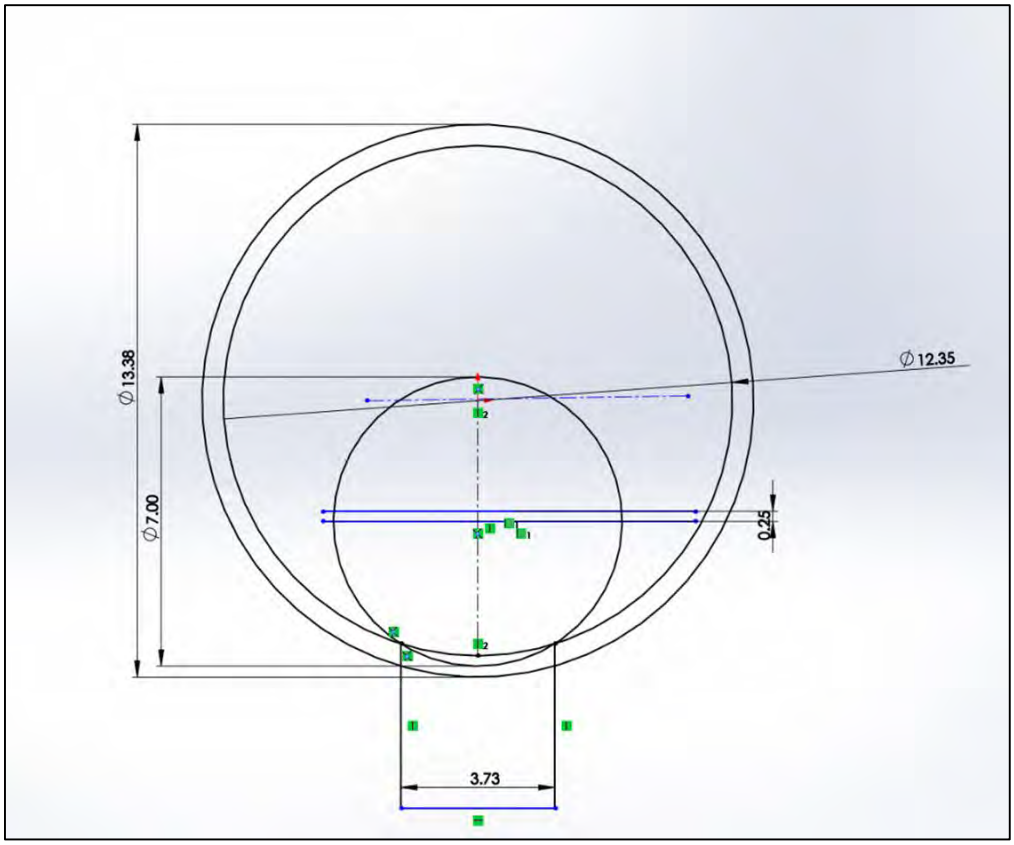

(Source: Steve Knudsen, Sandia National Laboratory)

Figure 6-10. Schematic of potential groove caused by drill pipe.

6.3 INJECTION TEST

Injection test on NWG 55-29 began on 8/26/2013 at 13:25 and ended on 8/27/2013. The Pad S-29 water well and a booster pump combination was used to delivery water through both wing valves via 4 in piping. The magnetic flow meter on the water well discharge end was used to monitor flow rates, and a pressure transducer was installed on the wellhead to record WHP. A PTS tool was lowered to 6462' and stayed at depth to monitor downhole pressure during step-rate injection test and the subsequent pressure fall-off period. The injectivity and fall-off test data are shown in Table 6-1 and Figure 6-11. The post-stimulation injectivity showed results ranging from 0.1-0.15 gpm/psi. This is an improvement when compared with pre-stimulation injectivity of 0.05 gpm/psi. The injectivity calculated here does represent the post TZIM degradation injectivity, though a portion of the fluid lost contributes to the leak in the casing. The modeled results of this leak is further discussed in Section 4.2.

Table 6-1. Results of the 2013 Injection Test

	Flow, gpm	Pressure, psi	Injectivity, gpm/psi
Step 1	77.76	2604	
Step 2	120.82	2896	0.15
Step 3	142.67	3112	0.10

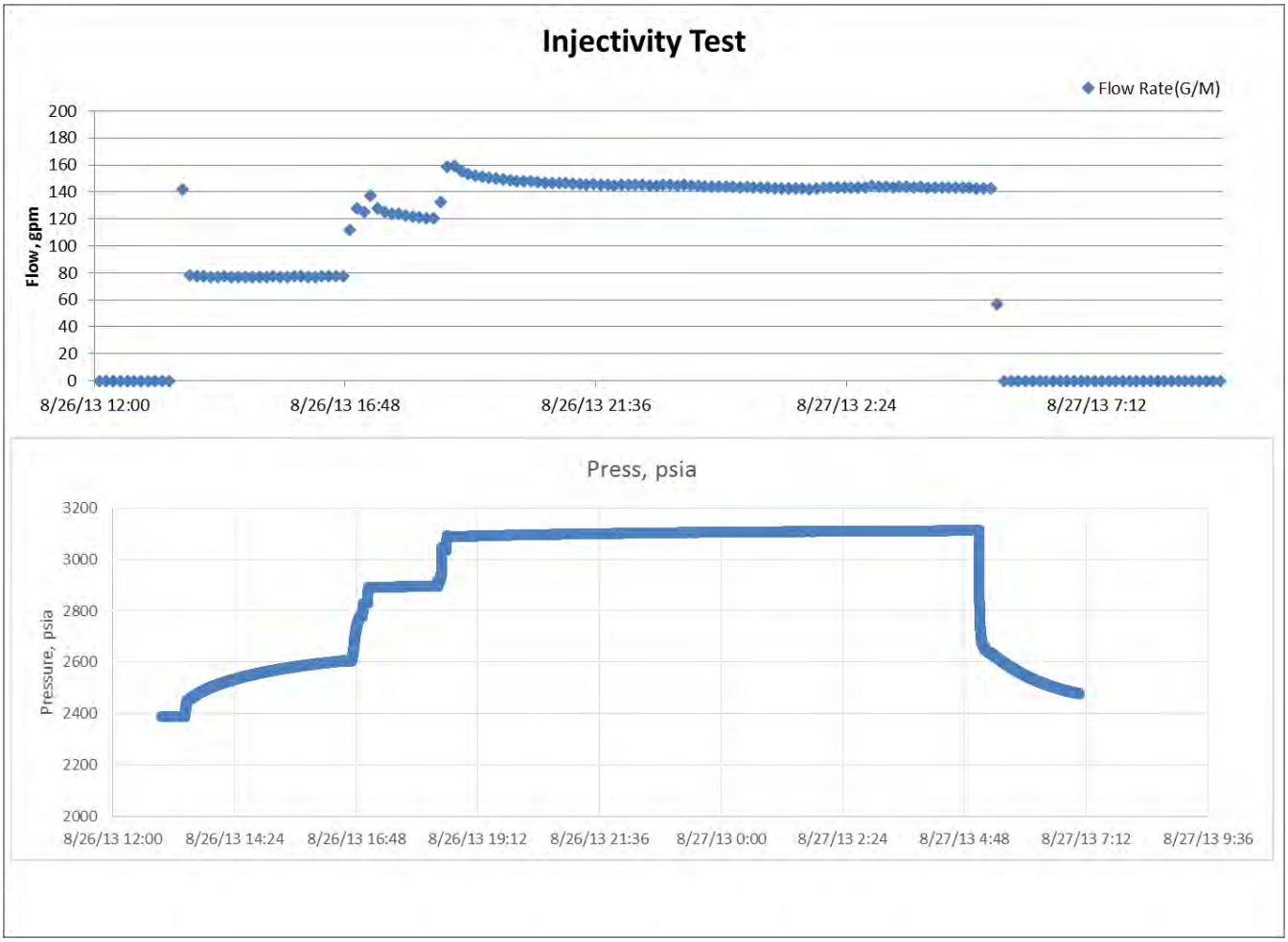

Figure 6-11. 2013 step-rate injection test and fall-off test results

The pressure fall-off data collected were used to create a Horner plot for estimating post-stimulation transmissivity and permeability. The Horner plot is shown in Figure 6-12. Similar results of transmissivity and permeability are presented in Section 3.6.4, calculated using the Stage 3 stimulation fall-off data. By using the same reservoir and fluid parameters, the 2013 fall-off data resulted in a calculated transmissivity of 2.63E-12 m^3 (8727 mD-ft) and permeability of 1.31E-14 m^2 (13.3 mD). The increase in transmissivity and permeability when compared to 2012 results (Transmissivity: 6.46E-13 m^3 or 2,147 mD-ft. Permeability: 3.23E-15 m^2 or 3.27 mD) is another indication of TZIM degradation since the 2012 stimulation.

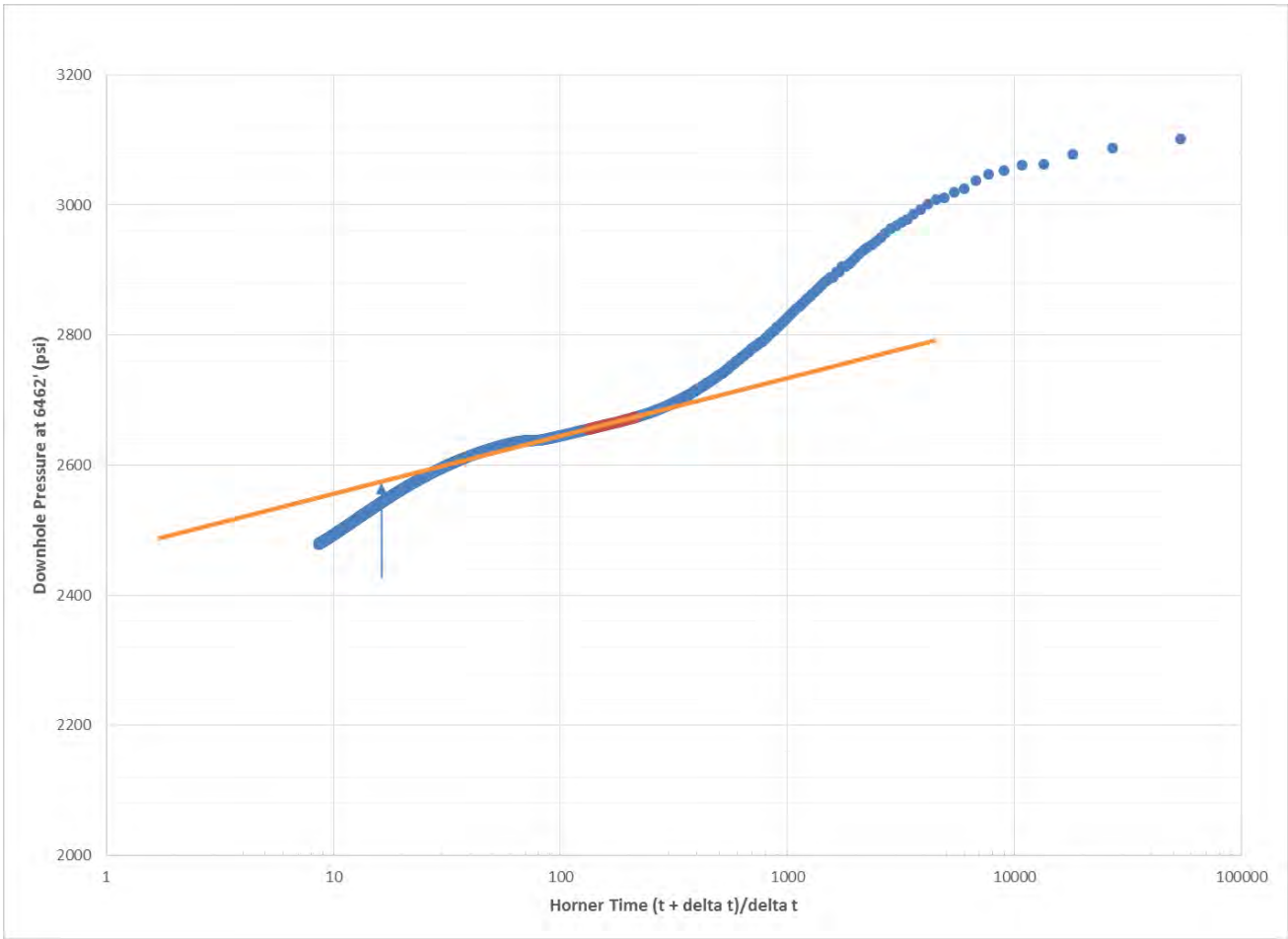

Figure 6-12. Horner plot based on 2013 fall-off test results

6.4 SURPLUS CASING EVALUATION

Starting on 12/9/2013 and ending on 12/13/2013, casing inspection determined that of the 139 pieces of casing stored in the Davenport storage yard, 116 had no apparent defects. The length of acceptable casing contained in the storage yard was 1473 m (4,834 ft), which is more than the 1277 m (4,189 ft) needed to complete the tie-back. The casing inspection was carried out by Tuboscope, a company which specializes in these types of inspections. Despite some initial start-up trouble, no significant problems were encountered during the casing inspection. All pieces of casing were thoroughly analyzed and a sufficient number of them were determined to be suitable for the proposed tie-back of NWG 55-29.

The casing inspection was carried out in five parts:

Step 1: Number each piece of casing

Each piece of casing was spray painted with all-weather paint in two different places with a specific number to allow for better note taking and identification.

Step 2: Check for Stencils

Rocky Mountain Steel stenciled each piece of casing delivered to Davenport with a stencil showing: that the steel came from their mill, the weight of the steel, the date that it was produced and the hardness. Pipe threading vendor Hunting Boss stenciled each piece of casing with the type of threads that were

added on to the casing as well as the date the work was done. Each piece of casing was thoroughly checked for both these stencils.

Step 3: Running a Special and API drift

A special drift, a 45.7 cm (1.5 ft) long metal cylinder 21.6 cm (8.5 in) in diameter, was run through every piece of casing to ensure that a 21.6 cm (8.5 in) bit and the associated BHA would not get stuck in any part of the casing. If the pipe did not pass the special drift then it was tested to see if it would pass the API drift, which is the more standardized measure. In most scenarios 24 cm (9 ⅝ in) casing would pass an API drift, but the casing at Newberry requires a wider interior diameter (ID).

Step 4: Washing and Inspection of Threads

Once the 8½ in drift was passed through each piece of casing, the treads were then cleaned of pipe dope and inspected by Tuboscope personnel for any potential defects. Defects include: burrs, dents, pitting etc.

Step 5: Pitting Inspection

The inside of the casing was visually inspected by Tuboscope personnel to check for any potential pitting. Much of the pitting near the end of the casing had been ground by Hunting Boss, and an example of which can be seen in Figure 6-13c.

a)  b) 

c)  d) 

Figure 6-13 a) Picture of the inside one of the pieces of casing. b) Casing threads cleaned of all pipe dope. c) Pit on the inside of a piece of casing. d) Pipe was spray painted with pink marking to designate a specific casing number. Stencils can also be seen in this picture as white markings along the length of pipe.

After five days of inspection it was determined that there was a sufficient amount of acceptable casing to complete the 55-29 tie-back. All inspection details were cataloged and summarized below:

- **139 Casing joints** were inspected over 3 full days. There was a miscount by two to reach the previous 141. In addition, one joint was of dissimilar threading (buttress) and was set aside from the larger lot.
- **116 Joints** (**4,834.1 ft**) of the 9.625 in OD/53.5#, L-80 seal lock boss connection casing passed all visual and dimensional inspections.
- **20 Joints** (**866.05 ft**) of the 9.625 in OD/53.5#, L-80 seal lock boss connection casing were found to have ID grinding in the non-pin ends. These were not necessarily rejects but needed further examination if placed into service due to the location of the grinding damage.
- **3 Joints** (**126.75 ft**) of the 9.625 in OD/53.5#, L-80 seal lock boss connection casing were found to not pass the non-API (larger) 8.500 in Drift test. These did pass the API Drift test for 9.625 in Casing (all casing was drifted with both sizes.
- **139 Joints (5,826.9 ft)** of the 9.625 in OD/53.5#, L-80 seal lock boss connection casing were passed for Hardness Testing with values deviating by no more than 10%.
- **2 Joints** where stencil was still apparent but weathered enough that lettering was not conclusive.
- **3 joints** with no apparent stencils on the casing.

7 PHASE 2.2: 55-29 WELL REPAIR AND RESTIMULATION

After having completed the well assessment work for NWG 55-29, it has been determined that the best means of fixing the compromised casing is to complete a tie-back of the well. A detailed plan for repairing and restimulating the well is presented in Appendix I, and the work will be overseen by AltaRock's Director of Wellfield Services. The tie-back will involve running and cementing smaller diameter casing inside the existing casing to isolate leaks in the existing casing. This repair will allow AltaRock to restimulate the deep section of NWG 55-29 and improve the EGS reservoir. Well repair work has been planned for late spring or early summer of 2014 to be followed by restimulation. The original stimulation program design will be improved based upon lessons learned from the 2012 stimulation work.

7.1 PERMITTING

United States Forests Service (USFS):
Two notification need to be made in order to proceed with future work. One is notification and Road Use Plan describing activities for the existing Road Use Permit. The other is a notification and description of temporary irrigation piping to 46-16 if still needed, which is still covered under existing permit. However, this work will not likely require irrigation piping.

United States Bureau of Land Management (BLM):
To move forward with the casing repair plan for the existing GDP for NWG 55-29 a Geothermal Sundry Notice (GSN) will be submitted.

Oregon Department of Environmental Quality (DEQ):
To move forward with the drilling and stimulation processes a modification to the Simple Air Contaminant Discharge Permit will be made to match up gen-set for new rig. This modification may or may not be needed depending on DEQ determination and emission estimates from new gen-set.

Oregon Water Resources Department (OWRD):
The limited use license for groundwater set up during the initial stimulation is still active. All that is left to be done for the upcoming work is to estimate water usage and purchase the mitigation credits required from the Groundwater Mitigation Bank.

Oregon Department of Geology and Mineral Industries (DOGAMI):
Modification of the current Geothermal Drilling Permit will be required. Work to be accomplished is similar to the sundry notice for the BLM, but it will require a lengthier time frame. One of the reasons for this are public notice requirements. This is the long lead permit item and an application must be started as soon as the final plan and budget are approved.

7.2 CASING REPAIR

In order to isolate the leaks within the 13 ⅜-inch diameter casing section, a tie-back will be installed from the 9 ⅝-inch liner lap at 4,189 ft depth (1,268 m) to the surface. Inspection of the casing stored in the Davenport storage yard was carried out in December, 2013, and casing was found suitable for completing the tie-back (see Section 6.4). An adequately experienced cementing service company, drill rig, and drilling contractor will be identified by that meets the requirements of the job. Testing of the casing and the wellbore after the tie-back is installed will be required to adequately plan for the subsequent stimulation, per Appendix I.

7.3 INTEGRITY TEST

An integrity test will be conducted to ensure that the casing has no apparent flaws and that it meets the manufacturer's specifications. Before the shoe is drilled out the casing will be pressured to no less than 3000 psi, and the well head will be shut in. Wellhead pressure will be monitored to confirm that the wellhead pressure does not fall more than 10% over 30 minutes in accordance with the federal regulations:

> *Prior to drilling the plug after cementing and in the cases of plugs in production casing strings and liners not planned to be subsequently drilled out, all casings, except the drive or structural casing, shall be pressure tested to 70 percent of the minimum internal-yield pressure of the casing or as otherwise approved or required by the District Supervisor. If the pressure declines more than 10 percent in 30 minutes or if there is another indication of a leak, the casing shall be recemented, repaired, or an additional casing string run and the casing pressure tested again. Additional remedial actions shall be taken until a satisfactory pressure test is obtained. The results of all casing pressure tests shall be recorded in the driller's report.* (30 CFR 250.1609)

7.4 AFTER THE CASING INTEGRITY PRESSURE TEST, A CEMENT BOND LOG (CBL) WILL BE RUN TO MAKE SURE THAT THE CASING IS PROPERLY CEMENTED INTO PLACE. SURFACE WATER INJECTION CAN BE APPLIED IF COOLING IS NEEDED DOWNHOLE TO PREVENT THE CBL TOOL FROM EXCEEDING ITS OPERATING TEMPERATURE LIMIT.REAM HOLE AND SET LINER

During the stimulation and the running of multiple tools down hole, ledges were encountered in the open hole. Based on reinstallation of the DTS in November 2012 and follow-up logging in August 2013, AltaRock is confident that it has identified a ledge at 2,097 m (6,880 ft) measured depth and that there may be additional ledges further down hole. To insure that downhole tools such as the DTS and BHTV will be able to log deeper than 2,097 m (6,880 ft), this ledge, as well as other potential ledges down hole, will have to be cleaned and remedied with a drill rig. This will require that the drill rig run the bit through these problem areas multiple times until the ledges and irregularities in the well are smoothed out. Any fish encountered above the bottom of the borehole will be milled through and pushed to the bottom of the wellbore and is not expected to cause any problems. A liner will then be set over the problem section of the well so that further ledges or bridges are not recreated during restimulation of the well.

7.5 WELL RESTIMULATION

Following the well repair and liner set, well NWG 55-29 will be restimulated using essentially be the same as the process described in Section 2. AltaVert 154 of the same grain size will again be used to allow multistage stimulations. A detailed stimulation procedure which will be provided to project stakeholders and associated vendors is presented in Appendix I. Adjustments to the original stimulation plan were be made based upon the lessons learned from the 2012 work (including edits to the Induced Seismicity Mitigation Plan presented in Appendix J):

1. If any stimulation work continues past September 15, physical plant equipment (e.g., pumps, piping, sensors, instruments) will be both passively and actively winterized (i.e., application of insulation and heat tape wraps).
2. The field instruments selected to monitor the stimulation system will be more environmentally robust than the ones used in 2012 so they can withstand colder weather.

3. On site control system require wireless communication infrastructure as well as a host of sensors which can be run indefinitely and withstand severe weather conditions. During the 2012 stimulation setting up all these systems took roughly three weeks. However, given the lessons learned from the previous effort the set up time should be reduced.
4. Temporary water storage tanks will not be needed, and water storage will be provided by the northern sump located on the pad.
5. A backup pipeline to Pad 46 will not be necessary as the Pad 29 sump will be adequate for the stimulation volumes that will be used (Appendix J).
6. The original (pre-2012) seismic mitigation protocol design was to flow back 10% of the injection volume when seismic criteria were exceeded. 2012 results showed that the formation did not hold pressure after stimulation, and thus the risk of seismic impacts is lower than had been originally anticipated. Therefore, we suggest that a flow back of 5% of the injected water volume will be sufficient to mitigate seismic risk during restimulation (Appendix J).
7. The DTS coiling trailer will remain onsite in case of prolonged pump failure, in which case the DTS will be removed from the borehole to protect it from heat damage.
8. The micro-seismic array monitoring system was extremely effective in 2012. However, a more expedited data analysis methodology will be developed to provide near real-time event analysis.
9. One unique tracer will be injected following each diverter pill injection, however only conservative NDS tracers will be used. Three species of NDS will be used which were not used in 2012.
10. We will be prepared for self-initiated flow from well NWG 55-29, however, the current plan and budget do not include the costs for a coiled tubing rig and air compressor to actively air lift the well. It is possible that the well repair rig (if still onsite) or the production well rig could be used to initiated flow of 55-29.

7.6 RISKS, LESSONS LEARNED AND MITIGATION

As part of the Stimulation Plan specified in the Phase I Report (AltaRock. 2011a), potential project risks were identified which were monitored during the 2012 stimulation work. Following the stimulation work, the results of these risks were assessed, as described below, and future stimulation procedures were modified to further mitigate these risks if needed:

1. RISK: MSA may not be not sensitive enough to detect microseismic events caused by hydroshearing, preventing visualization of the treatment.

   2012 RESULT: The MSA proved to be capable of detecting many small microseismic events.

2. RISK: Stress model has underestimated coefficient of sliding friction - underestimation of rock strength prevents results in failure to induce shear at ≤20.7 MPa (≤3000 psi) WHP.

   2012 RESULT: Hydroshearing was achieved in the deep part of the hole; initiating at 1350 psi WHP, with robust hydroshearing at 1800 psi WHP.

3. RISK: Tensile failure occurs near the casing shoe - temperature monitoring indicates that a fracture has opened or been created within 152 m (500 ft) of the casing shoe before deeper zones have been stimulated.

   2012 RESULT: Tensile failure likely occurred in the formation at the casing leaks. There was no pressure or flow evidence of tensile failure at the shoe or in the open hole, although it is possible

that the ledge at 6880 feet was caused by tensile failure. To further protect this zone, a liner will be installed in the upper ~500 feet of the open hole.

4. RISK: Development of a 'short-circuit' - the creation of a high permeability fracture path from injection to production well, or a 'short-circuit', is undesirable because the injected water will not have enough residence time in the reservoir to be sufficiently heated before reaching the adjacent production well, resulting in rapid thermal breakthrough and low production enthalpy. If microseismic data shows that reservoir growth is following a linear structure, as was the case in Soultz GPK3, a fluid short-circuit may be present.

   2012 RESULT: The deep events were near the well-bore. There was no evidence that an unknown fracture or fault zone was stimulated in 2012.

5. RISK: Diverters fail to effectively seal fracture network - diverters may fail to block fracture networks due to rapid degradation of diverter due to excessive temperature, or due to the diverter particle size being too large or too small.

   2012 RESULT: The effectiveness of the diverter in the deep part of the open hole is uncertain based on the 2012 results, when much of the diverter may have gone out the shallow casing leaks. Therefore, this risk and mitigation still exist.

   MITIGATION: If premature degradation occurs, a diverter with higher temperature rating will be applied. Multiple diverters will be on-hand to handle the wide range of temperatures that we expect to encounter during the treatment. If high temperature diverters fail to effectively block fractures, the well will be sanded back so that the upper intervals can be stimulated. If the diverter particle size does not effectively block the fracture set, a diverter of a smaller or larger size will be on on-hand to cover a wide range of fracture apertures. Lab testing is currently underway to develop the ideal particle size distribution for the higher temperature diversion chemicals.

6. RISK: The failure of stimulation pumps, transfer pumps, valves, piping or instrumentation could severely delay the stimulation process.

   2012 RESULT: Failure to maintain positive inlet pressure to the stimulation pump caused several weeks of delay. The best practice developed at the end was to use the north side of the Pad S-29 sump as a buffer reservoir and submersible water pump to transfer water to booster pumps. This method eliminated the pressure drop caused by using multiple tanks and small diameter piping and minimized chance of air leaking into the system. The delay of stimulation start-up resulted in conducting the stimulation in late September/October. An unusual cold snap caused pump instrumentation to malfunction, which lead to eventual breakdown and damage of the stimulation pumps. Additional pump damage were caused by debris being sucked into the pump body and clogging the impellers.

   Furthermore, when the pumps failed and cold water could not be injected for several weeks, water in the borehole reheated which damaged the DTS and prevented collection of temperature data in the deeper sections of the borehole. The DTS could not be removed because the coiling trailer had been demobilized from the site to save budget.

   MITIGATION: The 2014 stimulation will still include appropriate levels of redundancy for critical equipment such as pumps, instrumentation and power generation equipment. Generators will be rotated in and out of service for scheduled maintenance, including oil changes, to ensure that they can last the duration of the stimulation and flow-back. Mechanics will be on-call during the entire stimulation event. Spare parts, such as oil filters and fluid ends, will be on location. Heat-traces will be used to prevent freezing and malfunctioning of instrumentation. More robust,

industrial grade sensors will be used. A filter will be installed on the pump inlet to catch any debris on the stimulation pump suction side. All rental pumps will be the same model and year to ensure compatibility. Furthermore, the coiling trailer will remain onsite so long as the DTS remains deployed.

7. RISK: If induced seismicity mitigation requires relief of reservoir pressure by flowing the well, or the liquid production rate is relatively high during flow-back testing, the Pad S-29 sump could be filled to capacity.

   2012 RESULT: The well did not flow by itself when it was depressurized, and water levels continued to fall for several weeks after the stimulation was completed.

   MITIGATION: Flowing back this well is not considered necessary or expected to be even possible. Therefore, the ISMP has been modified so that a sump capacity to contain a flowback of 5% of the injected volume is all that is necessary (Appendix J).

8. RISK: Exceeding casing design limits could result in breach or failure of casing. In 2012, the weakest point in the wellbore was at 1277 m (4189 ft), which is the deepest point at which the 13-⅜ in casing was exposed.

   2012 RESULT: A defect in the casing caused a failure and leakage below 2000 psi WHP at a depth of 2342 ft.

   MITIGATION: The foam cemented 9 ⅝ in casing will be much stronger. The tie-in depth at 4189 may still be a weak point, but with the tie-back the weakest point will be the well head, which is rated to 3750 psi. More attention will be paid to the shallow deviations in the DTS. Tie-back casing has been inspected to ensure quality and strength.

9. RISK: Thermal cycling may cause the open-hole well bore to fracture and spall, causing a blockage in the well. If the open-hole has collapsed or bridged, it would not be possible to effectively continue reservoir stimulation would prevent the removal of the DTS or installation of wireline survey equipment.

   2012 RESULT: A blocking ledge appears to have developed at a depth of 2090 m (6,880 ft) by what appears to be spalling of the wellbore.

   MITIGATION: Liner or expandable casing will be installed from the shoe at 6450 to about 7000 ft. This risk still exists below 7000 feet.

10. RISK: Induced seismicity could result in shaking that is felt in the NNVM and surrounding communities. Shaking, though not dangerous or damaging, could disturb and cause concern to some residents in surrounding home sites.

    2012 RESULT: The strongest event had a magnitude of 2.4 event and was felt neither at the site nor anywhere outside of it. Outreach and education was also successful in allaying most of the public's fears about induced seismicity.

    MITIGATION: Detailed plans to educate and inform stakeholders, especially visitors and local residents, are discussed in detail in the Induced Seismicity Mitigation Plan (AltaRock, 2011b). These efforts will continue, building on the public outreach and education since 2011. We will again have monthly public meetings.

11. RISK: The reservoir grows vertically such that the top of the reservoir is shallower than 1829 m (6000 ft) below the surface, as would be indicated by microseismic results. In order to maintain an approximately 1524 m (5000 ft) buffer between the top of the stimulation zone and the bottom

of the groundwater-bearing intervals, the top of the reservoir will not be allowed to grow shallower than 1829 m (6000 ft).

2012 RESULT: Shallow seismicity did occur due a casing leaks. However, there was no geochemical evidence of mixing of injected water and groundwater. Based on the seismic locations, the stimulation in the open part of the hole did not grow upward; therefore the same mitigation steps should still be effective.

MITIGATION: Use diverters to seal off the flow path and divert the stimulation treatment to a deeper zone. The fiber optic and subsequent microseismic data will tell us if the diverters have been successful. This mitigation is discussed in detail in AltaRock (2011b).

12. RISK: The reservoir grows horizontally east as indicated by the microseismic data and threatens to cross over into NNVM.

    2012 RESULT: This was not an issue in 2012. However, the same mitigation plan will be used in 2014.

    MITIGATION: Use diverters to seal off the flow path and divert the stimulation treatment to another interval. The fiber optic and subsequent microseismic data will tell us if the diverters have been successful.

13. RISK: Geothermal field operations involve the use of heavy equipment and rotating machinery, and work with very hot pipe and related materials, sometimes in adverse weather conditions. Accidents can occur without proper training and other precautions.

    2012 RESULT: Two safety incidents occurred. The first was slip/trip and fall which resulted in a facial laceration requiring stitches. The second was a car accident due to snowy conditions on the access forest road with no resulting injuries.

    MITIGATION: All field operations will include detailed written procedures, including provision for health and safety. Safety meetings will be conducted every morning and at the start of each new event (e.g., stimulation, flow-back testing) to remind on-site personnel of job procedure and hazards, wind direction, evacuation plan and personal protective equipment. Safety conditions will also be reviewed following any unexpected changes in conditions (e.g., heavy snowfall).

    An emergency response plan accompanies the operating procedures for the stimulation. A copy of these procedures will be given to a representative of each vendor on-site. The emergency response plan will also be posted on-site in the data trailer. BLM will be notified immediately of any safety incident that occurs on the well pad, and BLM and FS will be immediately notified of any incident that occurs off the well pad. A speed limit of 30 mph will be communicated to all staff, if the roads are icy the speed limit will be reduced to 20 mph.

    No staff member will be left alone on-site; management will schedule appropriate staff for all phases of operation. All on-site vehicles (ARE and contractors) will be equipped with an appropriate first-aid kit and emergency response binder with contact list and emergency procedures. Also, the helicopter coordinates sign at the pad will be replaced.

14. RISK: Geothermal field operations involve work around hot water, steam, noncondensable gases and industrial chemicals. The Newberry EGS Demonstration is occurring on a geothermal lease in the Deschutes National Forest. Without adequate precautions, harm to the environment could occur due to spills or chemical release.

2012 RESULT: The environmental protection protocols were followed and no environmental releases occurred. No changes in those protocols will be made.

7.7 EMERGENCY RESPONSE PLAN

Call 911 for immediate aid. Vehicles should be parked upwind of the wellhead and pointed toward the pad exit for quick evacuation. All personnel should meet at the designated safe area in the event of an emergency. If an individual sustains a life-threatening injury, then 911 should be called and LifeFlight requested. The GPS coordinates below are provided for all emergency responders. All emergencies, leaks, tank or sump overflows and equipment failures should be reported IMMEDIATELY to the AltaRock Energy on-site supervisor. A contact list will be available on site (Table 7-1).

Coordinates for emergency vehicles and Life Flight

Pad 55-29:

43°43'33" N 121°18'58" W
UTM: 635603.01 Easting, 4842799.79 Northing, UTM Zone 10T

Pad 46-16:

43°45'05" N 121°18'04" W
UTM: 638306.18 Easting, 4770559.49 Northing, UTM Zone 10T

Hospital

The closest and largest hospital in the area is St. Charles Hospital located at 2500 NE Neff Road, Bend, OR (approximately 48 km (30 miles) north of La Pine).

Driving directions to 2500 NE Neff Rd, Bend, OR 97701 - 35.6 mi – about **1 hour**

1. From Pad 55-29: Exit via FS Rd 300 to 300A/300B split. Turn left and follow to green gate.
2. At green gate, turn left onto FS Rd 9735. Continue 7.5 miles to intersection with US-97N/The Dales-California Hwy.
3. Turn right onto US 97N/The Dales-California Hwy for 16.9 miles
4. Take Exit 143. Turn right onto Knott Rd.
5. Knott Rd continues onto SE 27th St. Follow SE 27th St for 3.9 miles.
   Turn left onto NE Neff Rd. St. Charles Medical Center on the right at 2500 NE Neff Rd, Bend, OR 97701

Fire - The La Pine Rural Fire Protection District, located at 51590 Huntington Road, La Pine, OR, can be contacted via phone at 541-536-2935.

Police - Deschutes County Sheriff's office is located at 51340 Highway 97 #G, La Pine, OR. Their phone number is (541) 536-1758.

HazMat - The Hazardous Materials Response Team for Deschutes County is located at City of Redmond Fire: 341 West Dogwood, Redmond, OR.

Potential Hazards for the Operation:

Vandals and unauthorized personnel
Aerial work (boom lifts, ladders, etc.) above 1.8 m (6 ft) off the ground
Heavy manual lifting
Automobiles and heavy machinery
Wireline winches
Cranes and crane trucks
Hydrogen sulfide and carbon monoxide gases

High pressures (equipment will be tested to 24.1 MPa [3500 psi])
Wildlife
Hazardous driving conditions
Deep water in sumps

Table 7-1. Responsibilities and Contact Information

Contact Name	Telephone Number	Responsibility
Yini Nordin	206-883-6561	AltaRock Energy, Production Engineer, contact for questions about the procedure and well operations. Onsite company representative during stimulation.
Michael Moore	541-410-1795	AltaRock Energy, Project Manager, onsite company representative during stimulation.
Kyla Grasso	541-410-9538	AltaRock Geologist and Office Manager of Bend Office

7.8 BUDGET AND SCHEDULE

Table 7-2. Budget for 2014 stimulation work

Item	Cost	Description
NON-ARE Equipment Costs		
By-pass line from stimulation pump to Baker Tank	$10,000	2 in Schedule 80 line and valves from stimulation pump discharge to Baker Tank
Line & isolation valves from By-pass tank to return pump	$1,400	4 valves ($350/month each) 8" Line/Hose from tanks to 8 inch pump inlet
100 psi bypass return transfer pump (electric or diesel)	$11,000	2 pumps (1 in service, 1 backup) - $2,500/month rental (each) + $1,500 mobilization + $1,500 demobilization; Pump from Baker tank back into inlet filter line
Line & isolation valves from return pump to stimulation pump inlet	$1,500	8 in line/hose from pump to 8 in inlet line (up stream of meter run)
Electric submersible pump	$14,000	Subcontracted, 1 Month rental turbine pump, inlet and discharge lines and assembly
1MW Stimulation Pump Generator	$40,000	2 Generators @ $20,000 month rental each
Mob/Demob	$10,000	$2500 mobilization + $2500 demobilization each
Site Trailer	$7,500	5th Wheel Equivalent; 1 month rental
Delivery & Set-up	$2,500	
Tear-Down & De-MOB	$2,500	
50KW Site Trailer Generator	$5,000	1 month rental
Mob/Demob	$1,500	
Misc Rain4Rent fittings	$10,000	Fittings/reducers/isolation valves
Sani-Hut	$2,000	Monthly Rental & Service (per unit)(2 Units)
Light-Towers	$3,000	4 Units @ $750/month
Non ARE Equipment Subtotal	$121,900	
Seismic Monitoring		
Seismic Monitoring Equipment		Utilize existing 20-Station seismic network
Data Analysis	$25,300	ARE Subcontracted - Foulger
Seismic Monitoring Subtotal	$25,300	
DTS		
DTS Installation	$13,750	ARE Sub-Contracted - Pacific Process Systems
Boom Truck and Operator	$1,600	To constrain top sheave; $800/day for truck; Operator 8 hr @ $100/hr
Man lift / Extenda-boom forklift	$2,400	Set tubing in sheave; attach to lubricator; $800/day + mob/demob
DTS Removal	$15,400	ARE Sub-Contracted - Pacific Process Systems (Includes 1 week Lubricator rental)
Boom Truck and Operator	$1,600	to constrain top sheave; $800/day for truck; Operator 8 hr @ $100/hr
Man lift / Extenda-boom forklift	$2,400	Set tubing in sheave; attach to lubricator; $800/day + mob/demob
DTS Subtotal	$37,150	

Stimulation Pump Set up cost (per Well)		
Pump Site/Pad Preparation	$10,000	$2,500 road base + $2,500 grader & Operator + $1,500 Backhoe & Operator $1,000 equipment mob + 2 Man-Crew with Compactor/hand tools
Stimulation Equipment Mob/DeMob @ Job Site	$40,867	per job
Boom truck (no operator)	$2,000	$1500/week + mob/demob
Fork lift - extending boom (no operator)	$2,000	$1500/week + mob/demob
Diesel fuel use & storage (@ $4.50/gal delivered)	$450	100 gallons
Pump Assembly crew (1 Welder, 1 Electrician, 2 General)	$16,000	4 men, 5 days [3 assembly; 2 Travel], $100/hour, 8 hour day
Pump Dis-Assembly crew (1 Electrician, 3 General)	$16,000	4 men, 5 days [3 Dis-assembly; 2 Travel], $100/hour, 8 hour day
Electrical / Software Engineer	$4,840	ARE Sub-contracted - Bandt Consulting; 5 days [3 assembly, 2 travel]
ARE Contracted Mechanical/Electrical Support Staff	$16,800	21 days [19 Operations, 2 Travel], $100/hour, 8 hour day - Cascade Pump
Diesel fuel use & storage (@ $4.50/gal delivered)	$174,079	per week ($4,145/day/pump)
Diverter	$0	Sufficient diverter remains from the 2012 work
Material Cost	$45,000	Diverter Plan dependent (Est $15K/Zone) - Bill actual amount used
Blending Truck	$56,485	Sub-Contracted - ThermaSource Cementing (Mob/De-Mob, 3 Pump Days, 3 Standbye Days, 6 Travel Days)
Travel	$4,000	Round-Trip Airfare (2 People, 2 Round-Trips ea.); Direct Bill (Est. $1,000 each)
Per Diem	$18,600	$150/Day/Person - (24 Person Days)
Stimulation Pump Setup & Operation Subtotal	**$407,120**	
Mob/demob Flow Test Equipment	**$20,000**	Separators, valving and piping
Flow Injection Well	**$50,000**	May need nitrogen assist
Conduct Wellbore Survey	**$115,000**	Including BHTV
Tracer Testing	**$25,000**	
GW Monitoring	**$60,000**	
STIMULATION TOTAL	**$861,470**	

Table 7-3. Newberry 2014 Repair and Restimulation Schedule

Operation	Start Date	End Date
Repair 55-29	05/08/14	06/27/14
Mobilize Rig	05/08/14	05/23/14
Ream out hole	05/26/14	06/02/14
Install Liner (6500-8000?)	06/03/14	06/10/14
Run Tie-back (0-4100)	06/11/14	06/18/14
Rig Test Tie-back	06/19/14	06/27/14
Restimulate 55-29	05/26/14	08/19/14
Set Up Stimulation Pumps and Accessories	05/26/14	06/23/14
Modify/Increase Concrete Pad Size & Cure	05/26/14	06/06/14
Inspect/Repair 10 in Flow Valves (WH and Silencer)	05/26/14	06/23/14
Re-Commission 55-29 Well Pump (Gen-Set)	06/09/14	06/11/14
Install Stim Pumps, Piping, Elec, GenSets	06/09/14	06/20/14
Clean Sump of Cuttings & Repair Sump Liner	06/09/14	06/20/14
Build Sump Booster Pump, Install & Test	05/26/14	06/12/14
Hookup DTS	06/30/14	07/04/14
Stimulate 3 weeks	07/07/14	08/04/14
Flow Back and Test Well	08/05/14	08/13/14
Seismic Relocations		
Target Production Well	08/05/14	08/08/14
DOE Approval	08/11/14	08/19/14

8 PHASE 2.2: DRILL NEW PRODUCER 55-29B

8.1 LOCATING THE NEW WELL

Location of a new well must satisfy three criteria to be considered a viable target:

1. It must be found in proximity to micro-seismic events
2. It must be a sufficient distance away from the stimulated well to generate sustainable power for the planned power plant
3. It must be at sufficient depth to obtain the production temperatures needed for the planned power plant

These three criteria will be determined by modeling the created reservoir using data gathered from the original stimulation as well as the upcoming stimulation. Tracer recovery will be highly valuable in characterizing the created reservoir. All attempts will be made to retrieve this data. An initial characterization of the reservoir will be completed using the micro-seismic data, DTS data, pressure and flow data, and any tracer information that is obtained. Scenarios will then be run in Tough2 using the resultant reservoir characterization. The well placement with the highest probability of success will be chosen as the target. For an overview of the current reservoir characterization model please refer to Section 6 of this report.

8.2 DRILLING SCHEDULE

After a final decision has been made to drill the production wells, there will be several long lead time items that must be procured before drilling can begin. These are outlined in Table 8-1. The drilling schedule for the production well is outlined in Table 8-2.

Table 8-1. Long-lead time items prior to drilling.

Item	Lead Time
Mobilization of rig	60 – 90 days
Special drill bits	60 days
Wellhead equipment	
600 and 900 series wellheads	120 days
1500 series wellheads (if needed)	150 days
Permits	
BLM Geothermal Drilling Permit	60 days
DOGAMI Permit	60 days
Air Permit (modified existing permit)	60 days

Table 8-2. Drilling stage durations (days)

Operation	Case No.1 Base	Case No.2 Liner	Case No.3 Shallow	Case No.4 Deep	Case No.5 Large
Pre-Spud Activities	7	7	7	7	7
Mobilization of Rig	8	8	8	8	8
Drill and complete Interval 1 – 20”casing	10	10	10	10	11
Drill and complete Interval 2 – 13-⅜ in casing	21	21	21	21	23
Drill and complete Interval 3 – 9-⅝ in liner	17	17	14	17	18
Drill Interval 4 – 8.5 in open hole to total depth[1]	23	22	20	31	24
Total Time	**86**	**86**	**80**	**95**	**91**

[1] Slotted liner may be installed in Interval 4 if required to keep hole open during well operation.

8.3 DRILLING AND CASING PLAN

This section is taken from the Phase 1 report (AltaRock, 2010a). The field work performed in 2012 and 2013 did not give cause to make any changes to the well design.

8.3.1 WELL DESIGN

Reservoir dimensions and drilling targets will be determined based on final stimulation and testing results. Therefore, we have developed well designs, schedules and budgets for five different cases that provide for variations in top of the EGS reservoir, depth of completion, well productivity and mode of production. The casing sizes and depths of the model cases are shown in Table 8-3.

Table 8-3. Production well casing designs

Case No.	Base 1	Liner 2	Shallow 3	Deep 4	Large 5
Conductor (ft)	50	50	50	50	50
Surface (ft)	1000	1,000	1000	1000	1000
Intermediate (ft)	4500	5500	4500	4500	4500
Production – top (ft)	0	5200	0	0	0
Production – bottom (ft)	7500	7500	6000	7500	7500
Open Hole Diameter (inch)	8.5	8.5	8.5	8.5	10.625
Total Depth (ft)	10000	10000	8000	12000	10000

The casing points were chosen in the following manner:

- Surface casing will be set at 305 m (1000 ft) to ensure that the most severe lost circulation zones are sealed behind pipe and groundwater aquifers are protected by two or three layers of casing and cement.
- Intermediate casing set at 1372 m (4500 ft), about midway between 1000 and 2286 m (7500 ft) casing points. The intermediate casing will be run just into the top of the John Day formation, estimated to occur at 4400 ft beneath Pad S-29. For Case 2, with 9-⅝ inch liner, the intermediate casing will be set at 5500 ft, and the production liner hung from 5200 ft, to minimize well flow frictional losses and provide a sufficient hole diameter for installation of a production pump. Case 5 further decreases frictional losses by increasing casing diameters through the total depth of the well.
- Production casing set at 7500 ft and cemented to surface to allow production from the uppermost fracture zone, while providing for relatively high production temperature. Case 3, with production casing set at 6000 ft, allows for a shallower uppermost fracture zone. If this resulted in a relatively low mass-weight production enthalpy, a hung production liner, as in Case 2, could be utilized.
- In the Base case, the open-hole interval is drilled with 8-½ inch bit to 10000 ft, similar to existing well NWG 55-29. This depth may be greater or less depending on the final target depth and will be determined from post-stimulation processing of the microseismic data. We expect fracture zones to be relatively steeply dipping, with zones deeper on one side of the reservoir and shallower on the other. Thus, Case 3 provides for a total depth of 8000 ft and Case 4 provides for deep completion to 12000 ft. Case 5 provides a larger open-hole diameter of 10-⅝ inch to maximize productivity.

8.3.2 CASING PLAN

All casing strings have been selected to accommodate the temperature, pressure and stresses that might be encountered during stimulation and production, with additional safety margin consistent with standard engineering practice and American Petroleum Institute specifications. Specific values for casing strings are given in the individual well sections below. While high stimulation pressures are not anticipated, the casing design will be planned to support higher than normal pressures. Final drilling plans, including casing configuration and engineering calculations, will be reviewed and approved by BLM as part of the drilling permit process.

Table 8-4. Production well casing size, weight, grade and connection.

Case No.	Base 1	Liner 2	Shallow 3	Deep 4	Large 5
Conductor	30", 108 lb/ft 54,000 psi mild steel welded	30", 108 lb/ft 54,000 psi mild steel welded	30", 108 lb/ft 54,000 psi mild steel welded	30", 108 lb/ft 54,000 psi mild steel welded	30", 108 lb/ft 54,000 psi mild steel welded
Surface Casing	20", 106.5 lb/ft K-55, buttress	20", 106.5 lb/ft K-55, buttress	20", 106.5 lb/ft K-55, buttress	20", 106.5 lb/ft K-55, buttress	22", 142 lb/ft 54,000 psi mild steel welded
Intermediate Casing	13-⅜" 68 lb/ft HCL 80 buttress	13-3/" 68 lb/ft HCL 80 premium	13-⅜" 68 lb/ft HCL 80 buttress	13-⅜" 68 lb/ft HCL 80 buttress	16" 109 lb/ft L-80 buttress
Production Casing	9-⅝ " 47 lb/ft L-80 premium	9-⅝ " 47 lb/ft L-80 premium	9-⅝ " 47 lb/ft L-80 premium	9-⅝ " 47 lb/ft L-80 premium	11.75" 71 lb/ft L-80 premium
Perforated Open Hole Liner – (contingent on hole stability)	7-⅝" 26.4 lb/ft K-55 buttress	7-⅝" 26.4 lb/ft K-55 buttress	7-⅝" 26.4 lb/ft K-55 buttress	7-⅝" 26.4 lb/ft K-55 buttress	9-⅝" 47 lb/ft K-55 buttress

8.3.3 DIRECTIONAL DRILLING PLAN

The EGS reservoir is expected to develop in the shape of an oblate spheroid with a radius of about 500 m (1640 ft), oriented in a north-south direction, and the vertical extent of the EGS fracture network is expected to range from 6000-12000 ft. The production wells will be directionally drilled to intercept this fracture network. The final directional drilling plan will not be determined until the stimulation of NWG 55-29 is complete and final fracture intercept targets are identified. The program has been discussed with a directional drilling vendor, and the approach has been verified as technically feasible.

8.3.4 DISPOSAL AND SPILL PROCEDURES

8.3.4.1 CUTTINGS DISPOSAL

During drilling, cuttings will initially be placed in the existing sump on Pad S-29. After drilling, the cuttings will be disposed at a site approved by Oregon DEQ based on chemical analysis conducted at an EPA-certified laboratory. Cuttings are expected to be non-hazardous, as was the case with NWG 55-29 and NWG 46-16.

ARE may apply for a solid waste beneficial use permit from the Oregon DEQ. Beneficial use is a more environmentally sustainable use of drill cuttings if analysis demonstrates the absence of hazardous constituents. If a permit is obtained, the material may be used for beneficial uses such as lining of other sumps, roads, well pads, etc. This secondary disposal method may be explored after drilling operations are complete.

8.3.4.2 EXCESS CEMENT DISPOSAL

During cementing operations it is likely that some cement slurry will be circulated out of the well at the end of cement placement. Steps will be taken to minimize the amount of excess cement that will actually be circulated out of the hole and into waste pits. The major factor that will help minimize this waste (and disposal) is the use of 'stab-in' drill pipe during circulation and cement placement. This procedure will be used on all cement jobs for all casing strings, whether or not the placement circulation method is conventional or 'reverse'. Cement will be either circulated down the drill pipe and up the annulus (conventional) or down the annulus and up the drill pipe (reverse circulation). Excess cement will be minimized when pumping conventionally by pumping 'lead' cement slurry until returns are seen coming out of the annulus or drill pipe, thus providing a positive indication that the annulus is completely full of cement. 'Tail' cement slurry will then be mixed and displaced down the drill pipe.

The use of foam cement will also decrease the excess cement requiring disposal. Because foam cement is compressible, the return flow line can be shut in while displacement of tail cement occurs at the end of the job. Instead of continuing to circulate excess cement out of the well, the return flow is shut in and the foam cement in the annulus is compressed. The compression of the foam cement actually increases the density and the compressive strength of the cement while having a minimal impact on down-hole pressure. This procedure cannot be accomplished with conventional, un-foamed cement because it is not compressible.

If conventional circulation and no inner string drill pipe are used, the job procedure will involve estimating the amount of open-hole excess that exists, pumping that large volume of cement, and then displacing the cement down the casing. The displacement volume for 1000 ft of 20 inch, 106.5 lb/ft casing is 350 bbls. The displacement volume for 1000 ft of 5-½ inch drill pipe is only 18 bbls. With the drill pipe being used as an inner string during the cement job, one can readily circulate cement back to surface, mix and pump a small volume of higher density tail cement, and then displace it down the drill pipe, thereby minimizing waste cement.

If the inner string drill pipe method is not employed, there is an increased risk of not filling the entire annulus with cement. An annulus that is not completely filled with cement increases the risk of casing failure during the life of the well, potentially leading to additional remedial repair costs or total loss of the well. To ensure that the annulus is completely filled without using the drill pipe method, approximately 350 bbls of cement would have to be circulated back to surface. Not only does this excess cement have a large environmental impact, but it also greatly increases the cost of the cement job.

8.3.4.3 SPILL PROCEDURES

ARE will adhere to the drilling contractor's spill prevention, control, and counter-measures program (SPCC) to mitigate spills during drilling operations. All operation personnel will be appropriately trained to handle spills. Safety procedures will be posted and copies given to local emergency people, daily safety meeting will occur each day, etc.

8.3.5 ADDITIONAL PERSONNEL ON LOCATION

Additional personnel, beyond those needed for well drilling activities, will be on location during specific periods of the drilling operation to provide project management, supervision and assistance. Specific operations will be witnessed and supervised by additional personnel as follows:

- All Field Operations: ARE Project Manager
- Logging supervisor
- Minifrac Test: ARE and USGS personnel

8.3.6 PRE-SPUD ACTIVITIES

8.3.6.1 SITE PERMIT

Site permits have already been obtained for this operation so there will be no delay in proceeding with site preparations.

8.3.6.2 SITE PREPARATION AND CONDUCTOR INSTALLATION

The existing well pad, S-29, is of sufficient size (5 acres) and design to easily accommodate the drilling of two or more additional wells. No additional pad preparation is necessary, and all drilling operations can be conducted on the existing location. The footprint of the rig will be considered when arranging the drill site to allow for easy access. For example, transport trucks carrying casing will require a free path to the pipe racks, so this pathway cannot be obstructed by rig equipment. Space for office trailers will be provided for the rig manager, company man, directional drilling contractor, mud logger, mud man, and shift crew operations, at a minimum.

A shallow cellar, approximately 8 x 8 x 4 feet deep, will provide for water collection and runoff through an 18 in diameter pipe pipeline installed from the cellar to the adjacent sump. A local water well driller will drill to 50 feet, then run and cement the 36 x 30 inch, ⅜ inch-wall, welded, line pipe conductor. The required cement volume of 108 ft^3 will require about 4 cubic yards of ready-mix concrete. A rat-hole driller or local water well driller will drill the relief for the mouse and rat holes as specified by the rig footprint.

8.3.6.3 RIG AND TRAILER MOBILIZATION

The drilling rig will be mobilized and rigged-up on location. The rig equipment will include three large mud tanks (800 to 1000 bbls total) to accommodate drilling fluid. Installation of office trailers and specialized equipment onto location will also occur during the drilling rig mobilization.

8.3.6.4 RIG PREPARATION

Spud mud will be mixed. Blow-out prevention equipment (BOPE) will be installed and tested for functionality. The BOPE stack will then be pressure-tested as per BLM requirements. At the conclusion of each casing and cementing job, all well control elements of the BOPE stack will be re-tested. The BOPE stack will be tested every 7 days during drilling, as per BLM requirements, and after every major change in the drilling operation. A BLM representative will be notified before every test.

8.3.7 SURFACE CASING

The surface casing interval will be drilled with a 26 inch bit and bottom-hole assembly (BHA) to 1000 feet. Existing well NWG 55-29 encountered severe circulation losses in this interval. Aerated drilling fluids will be used to mitigate lost circulation. It is important to clear the hole of cuttings in order to prevent stuck pipe, as was reported in NWG 55-29 in this interval. Foam or viscous slugs will be used to frequently clear the hole. Lost circulation material (LCM) or open-hole cement plugs will also be used minimize lost

circulation. Because rapid circulation losses can lead to insufficient mud volume and, thus, lost rig time, an additional mud tank will be used to store drilling fluid. This additional drilling fluid capacity will provide more flexibility in handling mud losses in the top section of the hole.

8.3.7.1 WELLHEAD, BHA, AND DRILLING OF THE SURFACE HOLE

- Rig wellhead top section to handle aerated fluid drilling
- Rig up banjo box and rotating head
- Drill out cement in the conductor, plus 15 ft, with a slick assembly, 26 inch bit, 3 collars and no stabilizers
- Perform leak-off test and refresh fracture gradient determination
- With 26 inch tools, drill 1000 ft to the end of surface casing interval
- Assemble 26 inch BHA and tools for drilling the surface casing interval

The BHA will consist of:

- 26 inch bit IADC Class 5
    - Using 4000 lb/diameter inch, the required collar weight is 104,000 lb
    - Considering buoyancy with a 15% margin of safety, the required drill collar weight is 119,500 lb
- 26 inch full gauge, near bit stabilizer, 6-pt roller reamer
- 30 ft x 10 inch non-magnetic drill collar
- 26 inch string stabilizer ⅛ inch under-gauge
- 30 ft x 10 inch non-magnetic drill collar
- 26 inch string stabilizer ⅛ inch under-gauge
- Drill collars
    - 5 drill collars (7 total) – 30 ft x 10 inch; 10 inch drill collar weight = 51,000 lb
    - 21 drill collars – 30 ft x 8 inch; 8 inch drill collar weight = 99,100 lb
    - Total collar weight in air 150,100 lb: Buoyed weight 128,000 lb
    - Drill collars added as depth permits
- 6 joints (5 inch – 1480 lb/joint) heavy weight drill pipe
- Shock sub
- Jars

A shock sub will be used to reduce unnecessary bit cutter damage. Jars will be run to mitigate stuck pipe problems. Single shot surveys will be taken every 60 ft (every two joints) to ensure a straight hole, with a vertical deviation of no more than 2°. A mule shoe seat will be placed at the top of the 10 inch collars.

8.3.7.2 END OF INTERVAL ACTIVITIES – LOGGING

No logging will be done in this open-hole interval after drilling. This interval was logged in NWG 55-29, which is immediately adjacent, making the additional data unnecessary. It is very likely that there will be severe lost circulation problems while drilling this interval and, thus, it will be important that this interval be cased off as quickly as possible after reaching the casing depth. Conducting a logging operation would increase the risk of losing portions of this hole to formation collapse, and the instruments used for logging.

8.3.7.3 END OF INTERVAL ACTIVITIES – CEMENTING

Foamed cement will be used to cement this interval to help ensure that the casing annulus is completely filled with cement. Reverse circulation placement may be used if extreme losses occur.

Prepare to run casing, including setting up floor post, pulleys, and a trapeze. Clean, inspect and measure the casing on the pipe racks in anticipation of running the casing. The casing collapse pressure, assuming 1000 feet of 9.6 lb/gal drilling fluid, will be 500 psi. The 106.5 lb/ft K55 casing has a collapse rating of 770 psi, providing a safety factor of 1.5. This rating is well in excess of the maximum recommended API collapse safety factor of 1.125. Run 1000 ft of surface casing. The drift of 20 inch 106.5 lb/ft casing is 18.812 inches.

The casing string will include:

- Guide shoe
- 1 joint 20 inch casing for shoe track
- Float collar with stab-in inner liner drill pipe feature
- Remainder of 20 inch casing
- Appropriate centralizers will be attached to the casing to provide a minimum of 70% standoff between the casing and the open hole. The location and number of centralizers required to achieve 70% standoff will depend on the casing size and weight, hole size, drilling fluid density, hole angle, centralizer bow strength, etc. The number and location of centralizers can be calculated along with the associated standoff using a standard program that is typically available from the major cement service companies. Centralizers will be placed on the top two joints and bottom shoe joint to ensure that casing is properly centralized at the critical locations.

After the casing has been run, rig down the casing crew equipment and rig up to cement surface casing. Circulate through the casing 2 to 4 hours to clean the hole. Circulate at least two 'bottoms-up' to lower the gel strengths of the drilling fluid, if possible, and lower the progressive gel strength development. Flat versus sharply increasing progressive gel strength of the drilling fluid is optimal. The temperature at 1,000 ft is estimated to be 110 °F. Cementing will use direct circulation foam.

Pressure test casing immediately after cement is placed and before the cement has set. By pressure-testing immediately, we will prevent damaging the cement bond, since the cement will still be liquid at this point.

Allow 4 to 6 hours for cement to firm up and check for fall back and determine if a top job is needed. Integral joint tubing (1-⅛ inch) will be used to pump a top-out cement job. Determine whether the top job was successful or whether another top job is necessary.

Wait on cement at least 24 hours total before resumption of drilling activities (i.e., drilling out the 20 inch casing shoe).

8.3.8 INTERMEDIATE CASING INTERVAL

8.3.8.1 BEGINNING OF INTERVAL – WELLHEAD, BOPE, BHA, SHOE TEST AND DRILLING AHEAD

Cut off the conductor pipe and weld on the 20 inch SOW (Slip-On-Well) wellhead. Nipple up the 21-¼ inch, 2,000 psi BOPE stack (Figure 8-1) and pressure test as per BLM requirements.

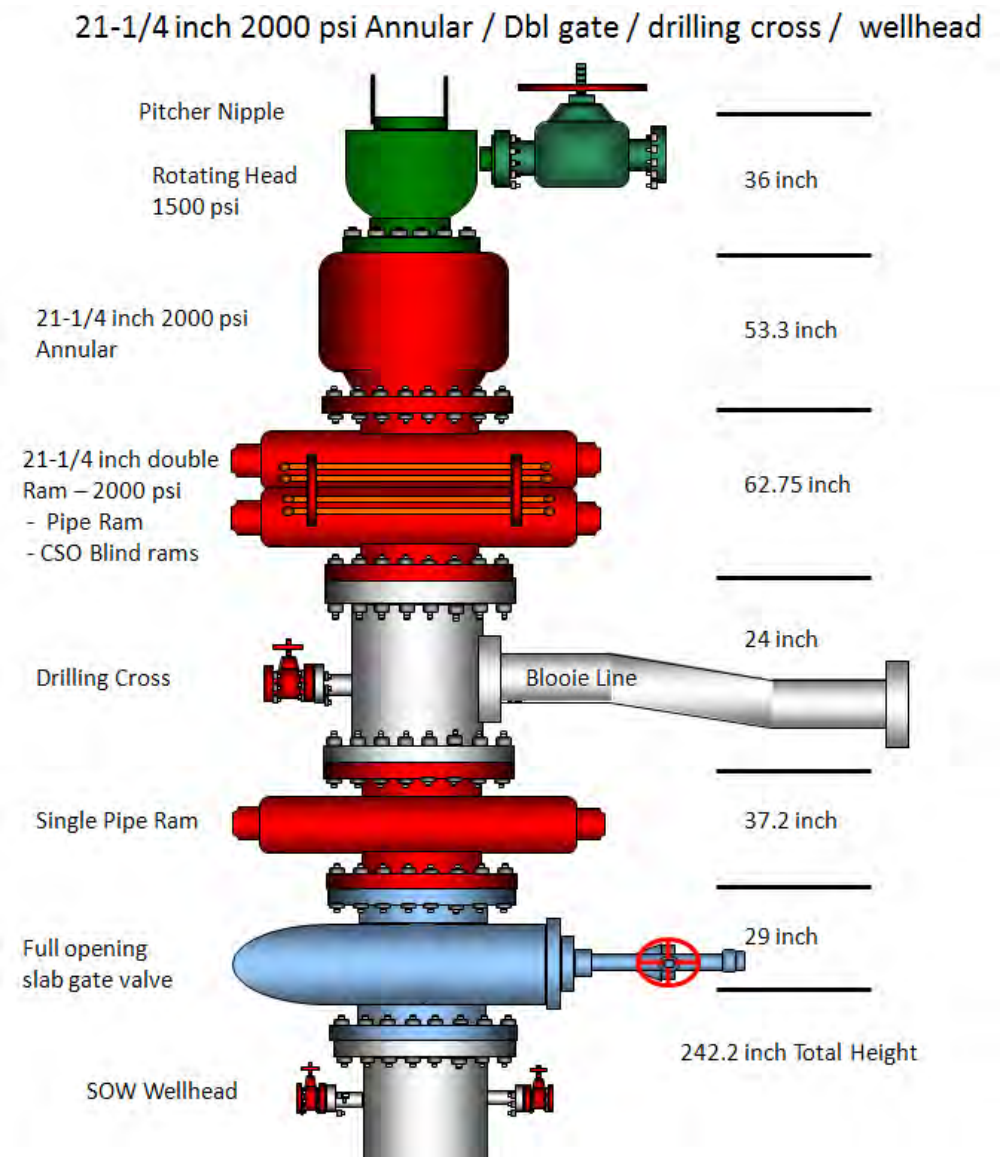

Figure 8-1. 21-¼ inch BOPE stack configuration.

The intermediate interval will be drilled from 1000 to 4500 feet with a 17-½ inch bit. The BHA assembly will include:

- 17-½ inch bit, (IADC class 5 TSI bit)
  - 5000 lb/diameter inch = 87,500 lbs
  - w/ 15% margin 100,625 lbs
- Near bit stabilizer full gauge, 6 point roller reamer
- 30 ft x 10 inch non-magnetic drill collar
- String stabilizer ⅛ inch under gauge
- 30 ft 10 inch non-magnetic drill collar
- String stabilizer ⅛ inch under gauge
- Drill Collars
  - 3 drill collars (5 total) – 10 inch – collar weight of 5 x 10 inch drill collars 36,400 lb
  - 21 drill collars – 30 ft x 8 inch – collar weight of 21 x 8 inch drill collars 99,100 lb

    - Total collar weight 135,500 lb in air: Buoyed weight 115,500 lb
- Neutral point will be in the 8 inch collars
- Geothermal rated shock sub
- 6 joints heavyweight drill pipe (5 inch 1480 lb/joint)
- 5 inch drill pipe for the remainder of the string
- Note: 9 inch slow speed drilling motor may be used in this interval. If necessary, it will be placed just above the bit.

Shock subs, jars and non-magnetic directional collars will be substituted based on the directional survey instruments to be used.

High temperature, polymer-based drilling fluids will be used in this interval. The drilling fluids engineer will specify the composition and mud check frequency, and specify operating parameters for treatment in this interval. Temperature will increase significantly in this interval, so careful attention will be paid to changes in the mud properties.

Drill out the cement, plus 15 feet, by entering the hole with a 17-½ inch bit and slick assembly of six 9-inch drill collars. Perform a formation injection test to determine the fracture gradient.

8.3.8.2 END OF INTERVAL ACTIVITIES – LOGGING

The logging program will be determined by the reservoir engineer. Equipment will be set up for running logs if required. The rig will use drilling fluid to circulate 4 to 8 hours to clean the hole; at least 2 bottoms-up. Log the well interval and then rig down the logging company. Currently, only a sonic log is planned for this interval.

8.3.8.3 END OF INTERVAL ACTIVITIES – CEMENTING

Prior to running and cementing the 13-⅜ inch casing, a multi-arm caliper survey will be run to allow estimation of the volume of cement that will be needed. The 13-⅜ inch casing pressure, assuming 4500 feet of 9.6 lb/gal drilling fluid, will be 500 psi. The use of 72 lb/ft HC L80 casing, with a collapse rating of 3470 psi, provides a safety factor of 1.5, well in excess of the maximum recommended API collapse safety factor of 1.125. A contract casing crew will be used to run the intermediate casing string. The casing string will include:

- Guide shoe
- 2 joints 13-⅜ inch casing for shoe track
- Float collar with stab-in inner liner drill pipe feature
- Remainder 13-⅜ inch casing (4500 ft, 72 lb/ft, HC L80, buttress thread)
- Appropriate centralizers will be attached to the casing to provide a minimum of 70% standoff between the casing and the open hole or the last casing string. The location and number of centralizers required to achieve 70% standoff will depend on the casing size and weight, hole size, drilling fluid density, hole angle, centralizer bow strength, etc. The number and location of centralizers can be calculated along with the associated standoff using a standard program that is typically available from the major cement service companies. Centralizers will be placed on the top two joints and bottom shoe joint to ensure that the casing is properly centralized at these critical locations.

Set up equipment to run casing. A casing crew will be employed to rig up the floor post and pulleys and trapeze for running casing. Clean, inspect and measure the casing on the pipe racks in anticipation of running the casing. Run 4500 ft of 13-⅜ inch, 72 lb/ft, K55 buttress thread casing. Remove equipment used by the casing crew equipment. Set up rig to cement casing.

Circulate drilling fluid through the casing 2 to 4 hours to clean the hole; at least 2 bottoms-up. Lower the gel strengths of the drilling fluid if possible and lower the progressive gel strength development. Flat versus sharply increasing progressive gel strength of the drilling fluid is optimal for displacement efficiency during the cement job.

Cement job placement method will be reverse circulation to minimize circulation pressure during placement, aid in minimizing retarder loading in upper-hole interval, and reduce cement set time. Pressure test of casing will be conducted immediately after cement is placed before the cement has set. This will be done to minimize damage to the cement bond, since the cement will still be liquid at this point. Allow 8-12 hours for the cement to set before performing a top job, if needed. Use Tremmie tubes to ensure that the top job cement is placed directly on the cement top. Allow 8 hours for the top job cement to set completely. Drill out the cement in the shoe track a minimum of 24 hours after the primary cement job.

Allow 4 to 6 hours for cement to firm up and check for fall back and the need for a top job. Integral joint tubing (1-⅛ in) will be used to pump top out cement job. Determine whether the top job was successful or if another is necessary.

Wait on cement at least 24 hours total before resumption of drilling activities (i.e., drilling out the 13-⅜ inch casing shoe).

8.3.9 PRODUCTION CASING INTERVAL

8.3.9.1 OPTION A: LONG STRING

8.3.9.1.1 BEGINNING OF INTERVAL ACTIVITIES – WELLHEAD, BOPE ANDFORMATION INJECTION TEST

Cut off the intermediate casing and weld on the 13-⅜ inch SOW wellhead. Nipple up the 13-⅝ inch 3000 psi BOPE stack. Pressure test BOPE stack as per BLM requirements. Stack diagrams are provided in Figures 8-2 and 8-3 below for the various cases.

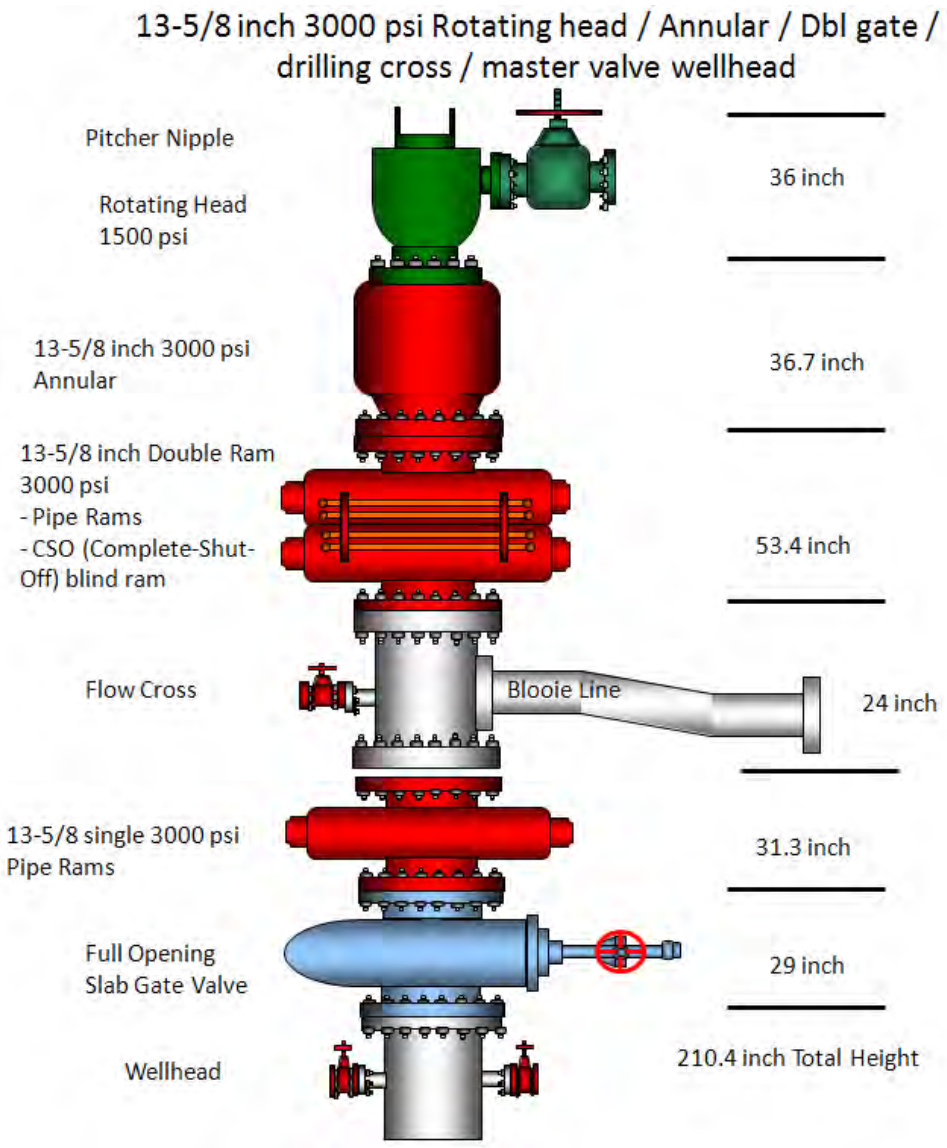

Figure 8-2. 13-⅝ inch BOPE stack configuration (Cases 1 – 4)

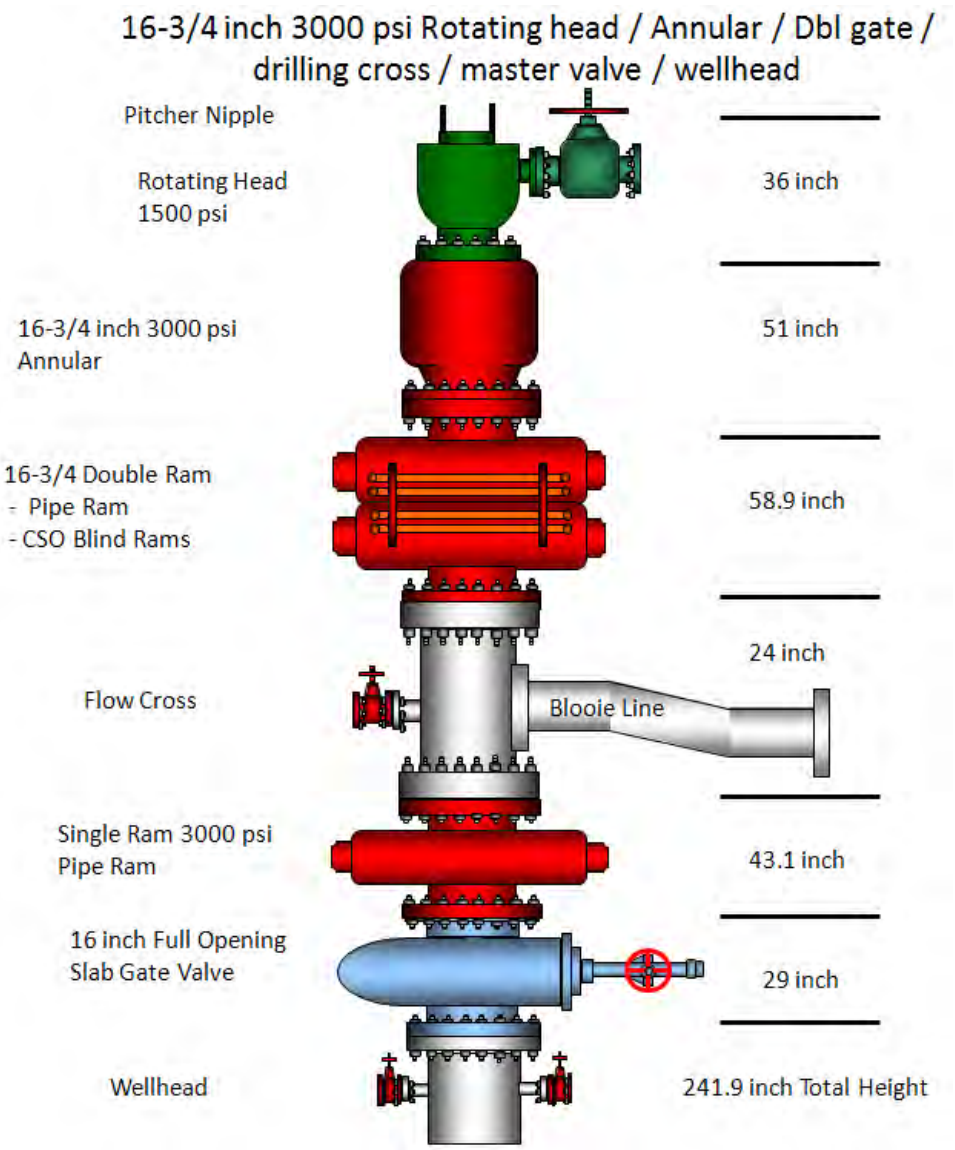

Figure 8-3. 16-¾ inch BOPE stack for Case 5

Drill 20 feet below the last joint of casing using the following assembly:

- 12-¼ inch bit
- 6 – 8 inch x 2-¾ inch drill collars

Perform a formation leak-off injection test to determine the fracture gradient.

8.3.9.1.2 INTERVAL ACTIVITIES – BHA AND DRILLING

Enter the hole with a 12-¼ inch bit and BHA and drill to 7500 feet. The BHA will include:

- 12-¼ inch bit IADC Class 5
  - 6000 lb/diameter inch = 73,500 lb
  - With 15% margin = 84,500 lb
- 12-¼ inch near bit 6 point roller reamer stabilizer full gauge
- 30 ft 9 inch non-magnetic drill collar with mule shoe seat

- 12-¼ string stabilizer ⅛ inch under gauge (non-magnetic recommended)
- 30 ft 9 inch non-magnetic drill collar
- 12-¼ string stabilizer ⅛ under gauge
- Drill Collars
    - 3 drill collars (5 total) – 30 ft x 9 inch – Drill collar weight 9 inch collars 28,830 lb buoyed
    - 21 drill collars – 7-¼ inch (x 2-½ inch bore) drill collars – drill collar weight 7-¼ inch collars 71,800 lb
    - Total collar weight 100,630 lb in air, buoyed weight 85,800 lb
- 6 joints of (5 inch 1,480 lb) heavy-weight drill pipe
- Enough 5 inch drill pipe to complete the string
- Shock sub and jars will be integrated into the string.
- An 8 inch, slow speed mud motor may be used depending on drilling progress.

8.3.9.1.3 END OF INTERVAL ACTIVITIES – LOGGING

The logging program will be determined by the reservoir engineer. Set up equipment for running logs, if required. Circulate 4 to 8 hours to clean the hole; at least 2 bottoms-up. Log the well interval, including a multi-arm caliper survey to estimate the volume of cement needed. Remove the logging equipment after logging operations. Currently, only a sonic log is planned.

8.3.9.1.4 END OF INTERVAL ACTIVITIES – CEMENTING

Run and cement the 9-⅝ inch, 47 lb/ft, L-80 premium thread casing. Premium casing threads are used on the production string to reduce the risk of joint casing failure due to excessive compressive stress loading that can occur during cyclic stress due to thermal expansion. The casing pressure, assuming 7500 feet of 9.6 lb/gal drilling fluid, will be 3744 psi. The use of 47 lb/ft, L80 casing, with a collapse rating of 4780 psi, provides a safety factor of 1.28, greater than the maximum recommended API collapse safety factor of 1.125.

The casing will be installed by a casing service company. The 9-⅝ inch casing will be stacked as follows:

- Guide shoe
- 2 joints 9-⅝ inch casing
- Float collar with stab in if long string casing is used; conventional float collar if liner is used
- Remainder of the casing string
- Appropriate centralizers will be attached to the casing to provide a minimum of 70% standoff between the casing and the open hole. The location and number of centralizers required to achieve 70% standoff will depend on the casing size and weight, hole size, drilling fluid density, hole angle, centralizer bow strength, etc. The number and location of centralizers can be calculated along with the associated standoff using a standard program that is typically available from the major cement service companies. Centralizers will be placed on the top two joints (if long string casing) and the bottom shoe joint to ensure that the casing is properly centralized at these critical locations.
- If a liner is run, an expandable liner hanger will be utilized to ensure positive seal at the top of the liner lap
- Liner lap will be a minimum of 300 ft if liner is run

A casing crew will be employed to rig up the floor post and pulleys and trapeze for running casing. Clean, inspect and measure the casing on the pipe racks in anticipation of running the casing. Run the casing. Take down the casing crew equipment. Set up necessary equipment to cement casing. Circulate 4 to 8 hours to clean the hole; at least 2 bottoms up. Lower the gel strengths of the drilling fluid if possible and

lower the progressive gel strength development. Flat versus sharply increasing progressive gel strength of the drilling fluid is optimal.

Follow procedure given in Section 8.4.3 for cementing. An inner string (stab-in drill pipe) reverse circulation foam cement job will be used to provide cement that has a reduced modulus of elasticity. The foam cement will accommodate thermal variations better than standard cement. It also reduces circulation pressure during placement, which, in turn, reduces the risk of lost circulation. Reverse circulation also provides a means of reducing retarder loading in upper stages of the cement, which results in a faster setting time for cement at the surface. Pressure test of casing will be conducted immediately after cement is placed before the cement has set. This will be done to minimize the damage to the cement bond, since the cement will still be liquid at this point. Allow 4 to 6 hours for cement to firm up and check for fall back and the need for a top job. Integral joint tubing (1-⅛ in) will be used to pump top out cement job. Determine whether the top job was successful. Repeat a top job, if necessary. Drill out the cement in the shoe track a minimum of 24 hours after the primary cement job.

8.3.9.2 PRODUCTION CASING INTERVAL – LINER OPTION

The production casing for this interval will be the same as Option A with the exception that a shorter 'liner' string will be run and cemented in place. The circulation method will be conventional, down through the drill pipe and up the annulus. Other changes will include:

- An expandable liner hanger will be used along with necessary cement dart and plugs.
- The cement at the top of the liner will be drilled out 24 hours after the cementing operation.
- There will not be a top-out-job because cement will not be circulated back to the surface.

8.3.10 OPEN-HOLE INTERVAL OR PERFORATED LINER

8.3.10.1 BEGINNING OF INTERVAL ACTIVITIES – WELLHEAD, BOPE AND FORMATION INJECTION TEST

Pressure test and check out the 13-⅝ inch BOPE tests before drilling out the cement at the shoe of the 9-⅝ inch casing. Wait on cement at least 24 hours before resumption of drilling activities (i.e., drilling out the 9-⅝ inch casing shoe).

Drill out the shoe cement plus an additional 50 ft with 8-½ inch slick drilling assembly. Perform a minifrac test to determine the maximum in-situ stress. Determine minimum horizontal stress magnitude by inducing tensile failure of the rock through high pressure, low rate and low volume injection.

8.3.10.2 INTERVAL ACTIVITIES – BHA AND DRILLING

Enter the hole with an 8-½ inch bit and BHA and drill to 10000 feet or until permeable fractures are intersected. In this drilling interval the directional program will initially determine the BHA. For conventional 8-½ inch drilling, which may occur once the direction is set, the following BHA will be used:

- 8-½ inch IADC Class 5 TCI bit
  - Using 5000 lb/diameter inch = 42,500 lb
  - With a 15% margin a drill collar weight of 48,900 lb is needed
- 8-½ inch full gauge roller reamer
- 30 ft x 7-¼ inch non-magnetic drill collar
- 8-½ inch x ⅛ inch under gauge string stabilizer
- 30 ft x 7-¼ inch non-magnetic drill collar
- 8-½ inch x ⅛ inch under gauge string stabilizer

- Drill Collars
    - 6 drill collars (8 total drill collars) – 7-¼ inch – Total 7-¼ inch collar weight is 27,300 lb
    - 12 drill collars – 6-½ inch – Total 6-½ inch collar weight is 35,700 lb
    - Total collar weight in air – 63,000 lb, buoyed weight 53,700 lb
- 6 x 4-½ inch heavy-weight drill pipe
- 5 inch or 4-½ inch drill pipe to complete the string

The drilling fluid condition will be monitored closely and the viscosity reduced in this interval. It is most desirable to drill into the fractured void with clear water to prevent formation damage from cuttings and clay-laden drilling fluids. Aerated drilling fluids can be used to drill into the fractured volumes to mitigate contamination.

No cemented casing is planned in this interval. This zone will either be an open-hole completion or a perforated liner will be installed. The decision about whether or not to use the perforated liner will be based on borehole stability encountered while drilling the interval.

8.3.10.3 INTERVAL ACTIVITIES – DRILLING THROUGH FRACTURE ZONES

The goal of drilling this well is to intersect the stimulated fractures so that fluid can be circulated from NWG 55-29 to the adjacent production wells. It is therefore critical that the well path intersect as much of the stimulated fractures as possible. To help detect when the fractures are intersected the fluid level of the drilling fluid tanks will be monitored while drilling in the open-hole interval. Adjustments will be made to the drilling program to drill this interval in an underbalanced pressure condition to minimize damage from drill cuttings and drill solids entering the stimulated fractures and plugging them off to flow. As a result, increased fluid levels are expected to occur. These changes in fluid levels will be recorded regularly to help determine when a given fracture network is intersected and when the intersection has ended. To aid in this process water will be injected into NWG 55-29 to maintain pressure in the fractures and help with drilling underbalanced in the open-hole section the these production wells.

8.3.10.4 END OF INTERVAL ACTIVITIES – DUAL STIMULATION PREPARATION AND LOGGING

To prepare the well for possible dual stimulation, the hole will be circulated with viscous sweeps and drilling fluid after drilling has reached the target depth. Drill pipe will be removed from the well, the drilling assembly removed, and the drill pipe with no drilling assembly attached to bottom will be run to the bottom of the well. The hole will then be circulated with viscous sweeps and then fresh water to remove all solids from the hole in preparation for stimulation. The hole will be circulated with fresh water for 12 hours to cool the well (Figure 8-4). The drill pipe will again be tripped out of the hole and the Bore Hole Televiewer (BHTV) will be immediately run into the well. An attempt will be made to run the BHTV as deep as possible in the well without exceeding the instrument temperature capability.

Because of the relative importance of the data, the BHTV will be run first. The other logs will be run after the BHTV. To cool the hole for the second logging run, it is likely that an additional trip to bottom with drill pipe followed by circulation of the well will be required. An open-hole log suite containing sonic, density, neutron porosity, gamma ray, and induction logs will be a part of the second logging run. For the third logging run, with the pressure and temperature surveying instruments, no additional cooling will be required because high temperature memory tools can withstand bottom hole, static temperatures in excess of 600 °F.

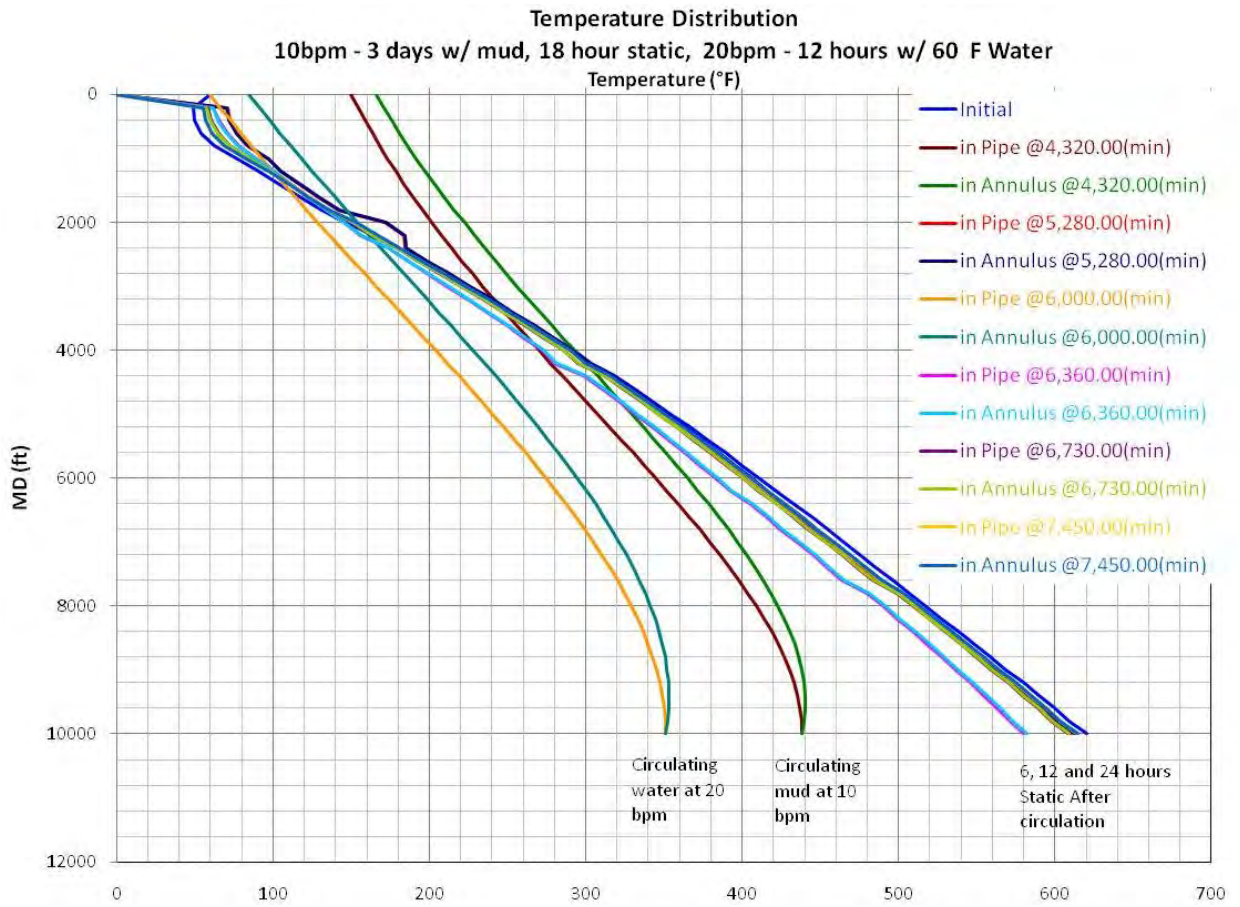

Figure 8-4. Temperature simulation of cool-down and heat-up prior to and during logging operations. The inputs include the circulation of 150°F mud for 3 days, followed by 18 hours of shut-in and by 12 hours circulation of 60°F water. The bottom-hole temperature is modeled after 6, 12 and 24 hours of static time based on injectivity test results.

Log the well interval. Remove the logging equipment after logging operations. A portion of the logging program may involve flow testing with logging equipment to monitor results. A complete suite of logs will be run in this interval, including:

- First Logging Run
  - Ultrasonic Bore-Hole Televiewer (BHTV)
- Second Logging Run
  - Fullwave Sonic
  - Neutron porosity
  - Density
  - Natural Gamma Ray
  - Induction
- Third Logging run
  - Pressure-Temperature-Spinner Survey

8.3.10.5 END OF INTERVAL ACTIVITIES – RUN PERFORATED LINER

If a perforated liner is necessary due to the instability of the open-hole formation, a casing crew will be employed to rig up the floor post, pulleys and trapeze for running casing. The casing will be cleaned,

inspected and measured on the pipe racks prior to being run in the well. The casing will be run and released at the bottom of the hole. The casing crew equipment will then be removed.

8.3.10.6 END OF RIG ACTIVITIES

- Put rig on standby
- Perform rig-on injection and production test
    - Rig up for flow test
    - Flow well for 7 days
    - Stimulate well (if necessary)
- Move the rig to the second production location or release rig

8.4 CEMENTING PLAN

The goals of the cementing operation will be to:

- Fill the annulus between the casing and open hole of a given interval completely with the given cementing system during the primary cementing operation
- Place a cement material that, when set, will support the casing and provide zonal isolation during the life of the well
- Minimize waste cement
- Minimize risk by following operational procedures and risk mitigation plans

8.4.1 SURFACE CASING CEMENTING PLAN

Well Conditions: The 20 inch surface casing will be set at 1000 ft with a bottom-hole static temperature (BHST) of 90°F and an expected bottom hole circulation temperature (BHCT) of 80°F. Lost circulation will most likely be a significant risk during placement of the cement.

Circulation Method: The circulation method will be conventional with the use of stab-in drill pipe. This will require a stab-in float collar for the 20 inch casing that will be placed one joint above the bottom of the 1000 ft-long casing string.

Cement Design: The density will be 15.6 lb/gal with 40% silica flour (fine crystalline silicon dioxide), 6.73 gallons per sack (gal/sk, where sk = 94 lb sack) mixing fluid, and 1.63 ft^3/sk. An equivalent of 1% calcium chloride will be added to the mix water to accelerate the compressive strength of the cement after placement due to the relatively low BHST across this interval. Additional calcium chloride may be added to the un-foamed cap, shoe, and shoe track cement to further accelerate the set and strength development of the cement at the top and bottom of the casing string. Foaming surfactants will be injected into the cement slurry to provide foam stability after placement while the cement sets. Foam cement has been chosen to allow for circulation of lightweight cement that has acceptable compressive strength. This will help ensure that a full column of cement will be placed even with the potential lost circulation problems. The foam cement will also have the added advantage of improved mechanical properties and long term durability over the life of the well.

Job Procedure:

- Pump 100 bbls of water
- Pump 50 bbls of chemical flush (foamed if significant lost circulation occurs during circulation).
- Pump 50 bbls of foamed water
- Pump open-hole volume of cement, plus 50% excess for wash-outs. Foam base slurry down to 11 lb/gal

- Take returns and foamed fluid returns to holding tank after all drilling fluid has been circulated out of hole
- Once foamed cement is seen at surface, indicating that the entire annulus has been filled with cement, turn off nitrogen and pump base cement (un-foamed) to provide a 200 ft of shoe cement
- Shut in back side while mixing and pumping shoe cement
- Displace shoe cement with latch-down dart
- Pump +/- 20 bbls of accelerated un-foamed cap cement down backside
- Pressure test casing
- Allow cement to cure 24 hours before resumption of drilling operations

8.4.2 INTERMEDIATE CASING CEMENTING PLAN

Well Conditions: The intermediate 13-⅜ inch casing will be set at 4500 ft with a bottom-hole static temperature (BHST) of 328 °F and an expected bottom-hole circulation temperature (BHCT) of +/- 200 °F. Lost circulation may be a minor risk during placement of the cement.

Circulation Method: The circulation method will be reverse with the use of a stab-in drill pipe. This will require the use of a stab-in float collar for the 13-⅜ inch casing that will be placed 1 joint above the bottom of the 4500 ft long casing string. Reverse circulation will allow for the staging of cement retarder as the slurry is pumped in the hole, with higher levels of retarder injected into the slurry that is placed near the bottom of the casing, and less or no retarder in the cement closer to the surface at lower well temperature. This will help minimize the set time for the cement. This method will also help minimize the amount of excess cement that will need to be mixed and pumped, which will reduce the cost of the job, and reduced waste cement disposal.

Cement Design: The density of the base cement slurry will be 15.4 lb/gal with 50% silica flour (fine crystalline silicon dioxide), 7.46 gal/sk mixing fluid, and 1.76 ft^3/sk. A retarder will be injected in stages as needed to keep the cement slurry liquid during placement. Foaming surfactants will be injected into the mixed based cement slurry to provide foam stability after placement while the cement sets. The base slurry will be foamed to a density of 12 lb/gal. Foam cement has been chosen because of its superior mechanical properties, which will help prevent brittle failure of the cement during cyclic loading due to pressure and temperature changes over the life of the well. The foam cement will also provide a lightweight cement to mitigate potential lost circulation. The foam cement strategy will help ensure that a full column of cement will be placed.

Job Procedure:

- Pump 100 bbls of water.
- Pump 50 bbls of chemical flush (foamed if significant lost circulation occurs during circulation).
- Pump 50 bbls of foamed water.
- Pump open-hole volume of cement plus 35% excess for wash-outs. Foam base slurry down to 12 lb/gal.
- Take returns and foamed fluid returns from the drill pipe to a holding tank after all drilling fluid has been circulated out of hole.
- Once foamed cement is seen at surface, indicating that the entire annulus has been filled with cement, turn off nitrogen and pump an un-foamed shoe and shoe track cement down the drill-pipe while holding the annulus closed. The shoe track will be 40 ft long and the shoe cement in the annulus will be 300 to 500 ft in length.
- Displace foam cement down the drill pipe with a latch down dart. The dart provides positive surface indication when cement is completely displaced down the drill pipe. The dart also provides

a means of preventing reverse flow of cement into the casing from the annulus after the job is completed. Land dart with 500 psi and then un-stab drill pipe and check that the flapper valve is holding.

- Pump (accelerated) base cement down the annulus to provide 100 ft cap cement.
- Pressure test casing.
- Allow cement to cure 24 hours before resumption of drilling operations.

8.4.3 DEEP LINER AND LONG STRING CEMENTING PLAN

Well Conditions: The deep 9-⅝ inch liner or long string will be set at 7500 ft with a BHST of 500°F and BHCT of +/-250°F. Lost circulation will be a minor risk during placement of the cement.

Circulation Method: If a liner is used, the circulation method will be conventional. An expandable liner hanger will be used to hold the cement in place and hold the liner in place after cementing. If a long string of casing is used, a reverse circulation cement job will be done. Reverse circulation will allow for the staging of cement retarder as the slurry is pumped in the hole, with higher levels of retarder injected into the slurry that is placed near the bottom of the casing, and less or no retarder in the cement closer to the surface at lower well temperature. This method will help minimize the set time for the cement. This method will also help minimize the amount of excess cement that will need to be mixed and pumped, which will reduce the cost of the job and need to dispose of waste cement.

Cement Design: The density of the base cement slurry will be 15.4 lb/gal with 50% silica flour (fine crystalline silicon dioxide), 7.46 gal/sack mixing fluid, and 1.76 ft^3/sk. A retarder will be injected in stages as needed to keep the cement slurry liquid during placement. Foaming surfactants will be injected into the mixed based cement slurry to provide foam stability after placement while the cement sets. The base slurry will be foamed to a density of 12 lb/gal. Foam cement has been chosen because of the superior mechanical properties which will help prevent brittle failure of the cement during cyclic loading due to pressure and temperature changes over the life of the well. The light-weight foam cement will minimize potential lost circulation. This strategy will help ensure that a full column of cement will be placed.

Job Procedure:

- Pump 100 bbls of water.
- Pump 50 bbls of chemical flush (foamed if significant lost circulation occurs during circulation).
- Pump 50 bbls of foamed water.
- Pump open-hole volume of cement plus 25% excess for wash-outs. Foam base slurry down to 12 lb/gal. Un-foamed tail cement slurry will be pumped at the end of the job to cover between 300 and 500 ft of annulus at the bottom of the 9-⅝ inch liner.
- Place diverter packer at surface between the drill pipe and the 13-⅜ inch last casing string to hold back pressure in case the foamed fluids return to surface during the job.
- Displace shoe cement down the dart that latches into the 9-⅝ inch top plug. Continue to displace the top plug until it lands on 9-⅝ inch casing shoe and apply an additional 500 psi.
- Set expandable liner hanger, un-set drill pipe from top of liner and circulate out any cement on top of the liner.
- Pull drill pipe out of the hole.
- Pressure test casing.
- Allow cement to cure 24 hours before resumption of drilling operations.

8.4.4 OPEN HOLE CEMENT PLUGS

8.4.4.1 LOST CIRCULATION PLUGS

In situations where extreme lost circulation is encountered and an open-hole cement plug is necessary the following guidelines should be followed:

- Use base cement slurry consisting of Class G cement with 35% silica flour. Additional material such as Perlite may be added to the blend to help solve lost circulation.
- Estimate or measure the temperature of the drilling fluid while circulating drilling fluid through drill pipe (Bottom Hole Circulation Temperature, BHCT)
- Test the cement slurry for thickening time at estimated BHCT. The cement slurry should have a minimum of 2 hours of thickening time.
- Calculate the hole volume and do not use more than 100% excess above bit size to account for wash-outs. Use a plug length of +/-200 ft of open hole.
- The drill pipe should be run in the hole, open-ended, with no check valves or other tools in the work string that would hinder pulling DP after the cement has been emplaced.
- After a balanced plug has been placed, the drill pipe should immediately be pulled out of the plug to 1.5 plug lengths above the estimated top of cement.

8.4.4.2 KICK-OFF PLUGS

In the event that an open-hole kick-off plug must be set to side-track around a fish, the following guidelines will apply:

- Use no more than 50% open-hole excess for volume calculations.
- Use densified, high strength cement slurry.
- Test cement at estimated BHCT. Use static temperature gradient, return fluid temperature while circulating at depth, and possibly temperature simulation to estimate BHCT.
- Design cement to have +/-3 hours of thickening time to allow for safe placement of the slurry.
- Use open-ended drill pipe with no check valves or other attachments that would impede pulling drill pipe out of the hole after cement plug placement.
- After placement of cement, pull completely out of cement plug and at least one plug length above estimated plug top before stopping to circulate hole.

8.5 LOGGING PLAN

Each new production well will be immediately logged after total depth is reached while the drilling rig is still onsite. To prepare the well for possible stimulation the hole will be circulated with viscous sweeps and drilling fluid after drilling operations have reached the target depth. The drill pipe will then be removed from the well, the bottom-hole assembly will be laid down, and the drill pipe will be run open-ended to the bottom of the well. The hole will be circulated with viscous sweeps, then fresh water to remove all solids from the hole in preparation for a possible stimulation. The hole will be circulated with fresh water for 12 hours to cool the well. The drill pipe will again be tripped out of the hole and the BHTV will be immediately run into the well. An attempt will be made to run the BHTV as deep as possible without exceeding the temperature capabilities of this logging tool.

Because of the relative importance of the data, the BHTV will be run first. The other logs will be run after the BHTV. The second logging suite includes an induction log to measure resistivity, a sonic log to measure interval transit time, lithodensity or spectral density logs to measure electron density, and natural gamma ray log to measure the presence of uranium, thorium and potassium in the rock formations. A static and

injecting PTS survey will also be performed along with a caliper survey. The static PTS survey will be run immediately following the open-hole logging run. A second static pressure-temperature survey will be conducted approximately three to seven days after the first, so that a comparison between the two surveys can be made and the well heat-up rate can be determined. Table 8-5 summarizes the available high temperature logging tools and their temperature limitations.

Table 8-5. High temperature tool options for open-hole logging and their temperature limitations.

High-Temperature Tool Options	Temperature Rating
Halliburton HEAT suite (GR, spectral density, full-wave sonic, induction, neutron density)	260°C (500°F)
Schlumberger Xtreme suite (GR, neutron density, full-wave sonic, induction,	260°C (500°F)
Baker Atlas Nautilus suite (GR, neutron density, full-wave sonic, induction, lithodensity)	260°C (500°F)
Tiger Energy Services Acoustic Formation Imaging Technology tool	300°C (572°F)
USGS ALT acoustic televiewer, non-commercial tool	268°C (514°F)
Tiger PTS data-relay tool	260°C (500°F)
Tiger PT memory tool	350°C (662°F)
Welaco PTS data-relay tool	260°C (500°F)
Pacific Process Systems PT memory tool	316°C (600°F)

8.6 RISK MITIGATION AND CONTINGENCIES

8.6.1 SAFETY

- General - Daily safety meetings will be held wherein pending operations are reviewed, safety hazards and incidents are discussed and the emergency plan and evacuation route are reviewed.
- Safety Training - Safety training will be required for all personnel who come to location during drilling operations. This will be monitored and overseen by drilling rig contractor personnel.
- PPE - All personnel on location curing drilling operations will be required to wear appropriate personal protection equipment (PPE) while working on site. This will include leather gloves, hard hat, safety glasses and steel-toed footwear, at a minimum.
- H_2S Monitoring - H_2S monitoring equipment and contractors certified in their proper use will be utilized on site during stimulation, drilling and flow test operations. During active rig operations, the drilling contractor will be responsible for H_2S monitoring. Windsocks are installed on location to aid in wind direction determination in case of an emergency.
- Driving – All personnel visiting or working at the site will be informed of the 25 mph speed limit on FS roads, lease roads and well pads. There are no speed limit signs posted so the rig operator will be required to inform all staff and contractors to observe these speed limits on all FS roads.
- Parking - All passenger vehicles will be required to park in designated parking areas. In addition, all passenger vehicles will be required to follow the first-out-forward rule. That is, all vehicles will be required to be parked in such a way that their first movement when leaving location will be forward. The drilling contractor or site supervisor will be responsible for monitoring and enforcing this rule.
- Personnel Access to Rig Site - Personnel on location will be required to first register when they arrive on location. They will also be required to sign out when leaving location. The drilling contractor will be required to monitor and enforce this policy.

8.6.2 DRILLING RISK MITIGATION

Drilling risks are outlined below, along with the plans and procedures that will be implemented to mitigate these risks.

8.6.2.1 LOST CIRCULATION

Lost circulation is a known risk for wells drilled at Newberry, especially in the top 1,000 ft of the well. To mitigate this risk the following steps will be taken.

- Conventional lost circulation materials in the drilling fluid will be used while drilling the top 1000 ft interval. If this does not stop major losses, the drilling fluid will be lightened by aeration. This should allow for drilling of this interval to the target depth.
- In cases of severe lost circulation, an open-hole cement plug will be set to seal off the zone. The optimal cement design is a slurry with low to moderate compressive strength to help minimize the chance of kicking off the plug and starting a new hole. To achieve this outcome, the density of the cement should be 13.0 lb/gal or less. Another more effective method would be to spot an open-hole foam cement plug. This strategy would lower the compressive strength of the resulting plug. It would also provide a means of lowering the cement density to as low as 9 lb/gal or less while still providing a competent cement to seal the lost circulation zone. Finally, the foam cement would expand into the lost circulation zone after placement to fill large voids.

This same general procedure will be used to address the problem of lost circulation while drilling the remainder of the well except in the open-hole interval, where the use of conventional lost circulation materials will be avoided. LCM will be avoided in order to minimize formation/fracture damage, which could ultimately impede flow into the wellbore during the long term circulation test.

8.6.2.2 STUCK PIPE

Getting the drill pipe stuck during drilling is a significant risk. To minimize the risk of stuck pipe, the hole must be kept clean of cuttings. This will be accomplished by pumping viscous sweeps periodically while drilling to help clean drill cuttings from the well. Also, minimizing lost circulation with aeration and/or lost circulation material will greatly reduce the possibility of getting stuck from cuttings falling out of the drilling fluid around the bit.

To aid in reducing the risk of stuck pipe extra mud pumps or high capacity pumps will be on location to aid in achieving increased pump rates to help reduce the risk of stuck pipe. In addition, air compressors will be on site to aid in lightening the drilling fluid as needed to both reduce the risk of stuck pipe and aid with potential lost circulation problems.

Another rule that must be followed during drilling operations to prevent cuttings from falling out around the drill bit is to never stop circulation while the bit is on the bottom of the hole.

Another operational practice to reduce the risk of getting the drill pipe stuck is to never by-pass the shale shakers in the mud pits when circulating the drilling fluid in the well. This practice is sometimes employed when circulation losses occur. The thinking is that the additional solids that remain in the drilling fluid will help seal off the lost circulation zones. The problem is that these same solids can fall out of the drilling fluid and stick the drill pipe and the drilling assembly. In addition, the solids can cause significant damage to the mud pumps at surface leading to equipment failure and rig down-time.

If the drill pipe does get stuck the following guidelines will be followed:

- Attempt to get loose
    - Jarring with pipe lubricant
    - Attempt to pump hole clean, using aeration and/or viscous sweeps as needed
- If cannot get loose
    - Do free point
    - Back off drill pipe

    - Drill over with wash pipe
- If the drill pipe is still stuck after a total of 3 days, a cement plug will be placed on top of the fish (follow best practices for plug cementing) and the drilling rig will either be skidded over and a new hole started (if total depth of the well is still shallow) or the well will be side-tracked.

8.6.2.3 LOSS OF DRILLING EQUIPMENT IN OPEN HOLE

The loss of expensive mud motors and drilling assemblies not only poses a significant cost risk to the operation but could also significantly delay the completion of the well. AltaRock will mitigate this risk by addressing the issue of stuck pipe as discussed above. We will also use mud coolers to minimize temperature at the bottom of the hole and thus minimize risk of exceeding temperature limits of mud motors and down-hole equipment. We will also monitor drilling fluid return temperatures and use temperature simulation software to estimate BHCT to ensure that existing temperature limitations of the equipment are not exceeded.

8.6.2.4 INCOMPLETE ANNULAR FILL

A major risk in drilling of geothermal well completion is having a cementing operation result in incomplete annular fill. Inadequate cement coverage can lead to casing collapse or other forms of casing damage if the casing is not supported over its entire length. To mitigate this risk a number of practices will be followed including:

- Use of lost circulation materials while drilling: If lost circulation can be reduced by treating the formations while drilling, it will reduce the risk of an incomplete annular fill.
- Use of light weight foam cement: A major cause of incomplete annular fill is loss circulation occurring during placement. This complication often results in incomplete annular fill. To reduce this risk, it is helpful to reduce the density of the cement system. Normal lightweight cements are limited to around 11 lb/gal and have very poor mechanical properties when set. Foam cement has improved mechanical properties (better than conventional normal weight cement) and can reduce the density of the cement during placement to as low as 9 lb/gal or less, while still providing an effective seal.
- Use of reverse circulation placement method: Another method of reducing the risk of loss circulation during cement placement is to pump in ‘reverse’, rather than conventionally (down the casing and up the annulus). This technique greatly reduces the pressure at the bottom of the hole during placement of the cement, thus minimizing the risk of lost circulation. A number of other associated advantages are achieved with this method as well, including reduction of the amount of excess waste cement that must be disposed of and shortening the waiting time for the cement to set.

8.6.2.5 DAMAGE TO STIMULATED FRACTURES

Another major risk while drilling is plugging or otherwise damaging permeability in the stimulated fractures due to the migration of drill cuttings and other drill solids into the stimulated fractures. To mitigate this risk the following procedures will be implemented:

- Underbalanced drilling: While drilling the open-hole section, an attempt will be made to drill underbalanced with respect to the pressure in the stimulated fractures. This method should prevent loss of drilling fluid and associated solids into the stimulated fractures. The pit levels will be monitored closely during this portion of the drilling operation for net fluid gain. It should not pose any significant drilling risk when this occurs, as the fluid is only hot water.

- Injection into NWG 55-29: Water will be injected into NWG 55-29 to maintain the pressure in the stimulated fractures. As the wellbore intersects the stimulated fractures a net flow of (hot) production fluid should occur into the wellbore preventing the infusion of drilling fluid, and associated solids, into the stimulated fractures.
- Non-damaging drilling fluid: The drilling fluid used while drilling the open-hole interval will contain a minimum of solids to reduce the risk of fracture damage. A minimum amount of bentonite clay will be used. High temperature polymers will be substituted as much as possible to add required viscosity to the drilling fluid. If lost circulation material is used, it will be a material like calcium carbonate, which can be readily removed with a mild acid or other treatment fluid. Other potential lost circulation materials could include proprietary diverter materials that can temporarily seal the fractures but will then degrade and dissolve over time in the presence of water and elevated temperature.
- Aeration: Aeration of the drilling fluid will also be used to reduce the density of the drilling fluid and aid in getting the well in an underbalanced pressure condition. Also, the aeration will aid in carrying drill solids and cuttings out of the well.
- Viscous Sweeps: Pump viscous sweeps (volume of highly viscous fluid) while drilling this hole section to help clean out excess drill solids and cuttings that may not be circulating out of the hole.

8.6.2.6 GENERAL OPERATIONS

All major operations that occur during the drilling operation will have written procedures. These procedures will be made available to both the operator and all vendors and personnel that will be involved in that given operation. In addition, safety meetings will be held prior to all major operations where the given procedure will be reviewed prior to the actual operation being performed.

8.6.2.7 WINTER DRILLING

Another major risk is the possibility of having to do a portion of the drilling during winter with freezing temperatures and deep snow. Drilling in severe winter conditions will not slow drilling if the following mitigation is applied:

- Retain drilling supervisor(s) with experience in winter operations
- Provide road clearing and transportation to the site from Highway 70
- Winterize drilling rig and associated equipment, including coverings for rig and floor
- Utilize boilers, fuel heaters and pipeline insulation to prevent fluids from freezing
- Supply heaters for mud tanks
- Add heaters to water meter cabinet and electric heat rap on all water lines

8.6.2.8 CORROSION OF PRODUCTION CASING

Another risk is the possibility of the produced geofluid causing corrosion of the production casing string. To address this risk the following steps will be taken:

- Sample and analyze produced fluids during flow testing to identify the corrosion potential.
- If the production fluid is determined to prevent a substantial corrosion risk, one or more of the following steps can be taken:
    - Apply appropriate chemical treatment, such as commonly used geothermal filming amines, to protect metallurgy from geofluid attack.
    - Change casing grade to increase corrosion resistance.

8.6.3 LOGGING CONTINGENCIES AND RISK MITIGATION

Concerns have been raised about the risks associated with open-hole logging and whether or not these risks outweigh the benefits of the data collection. Certain risk is inherent in all down-hole survey operations. Any time a tool is run in the open-hole, there is a risk that the tool will be lost or damaged. The logging risks associated with the Newberry demonstration site are outlined below:

1. Temperature – The wells will be exceptionally hot at depth, with temperatures exceeding 600°F at 10000 ft. The high temperature environment creates the greatest potential for internal tool damage. If the well has not been cooled by drilling operations, the open-hole 'triple combo' logging suite will not be utilized because these tools are rated to a maximum internal temperature of 500°F.
2. Thermal contraction – The pumping and circulation of cold water can cause volcanic formations to spall at the wellbore face and fall into the open-hole. During logging operations, the well remains static and begins to heat up, so spalling should not be a significant risk because the formation will be expanding and not contracting. The greatest potential for spalling occurs during circulation and injection.
3. Stuck tools from swelling clays – Swelling clays (e.g., illite, smectite) are only present in small quantities in this area, thus posing negligible risk.
4. Stuck tool due to well bore obstruction – Tools can become stuck if they hit a liner top or an unanticipated bottom or ledge at high speed. Written operating procedures will require that safe logging practices, including wireline speeds below 150 ft/min, are always followed. The wireline operators will be made aware of the wellbore configuration and will be required to slow down to 30 ft/min when approaching liner tops and any other known obstruction or constriction.

The logging companies have a vested interest in ensuring the safe operation of their tools, so many safety nets have been added to logging operations to decrease the likelihood of tool damage. The open-hole logging suites and BHTV tools will be run in conjunction with temperature and tension measuring devices. Temperature is monitored continuously to ensure that the maximum tool and wireline ratings are not exceeded. The temperature readings must be watched vigilantly to ensure that damage does not occur. Operating procedures will clearly communicate to the logging company that the limitations of the tool are not to be exceeded under any circumstances. In addition to temperature monitoring, the logging trucks also have built-in tension measurement. Halliburton and Schlumberger, for example, require a tension survey to be run in conjunction with their high-temperature tools, while other companies rely on weight indicators to determine if the wireline tension is increasing. Finally, weak points are intentionally built into all wireline assemblies in case a tool becomes stuck or is lost in the hole. In the case of a stuck tool, the line will break at the weak point where an engineered fishing neck is then exposed to aid in tool recovery.

Along with these built-in risk mitigation practices, relatively inexpensive tool insurance is available from each company. The details of each insurance plan differ and are summarized below. Each plan requires at least three attempts to recover the tool through competent fishing operations. Although down-hole wireline work is risky, it is a risk we must accept to collect the required data for a successful demonstration project.

Lost-in-hole charges in logging contracts are a standard everyday occurrence in the wireline business. Although we won't be able to completely mitigate the threat of damaging or losing a piece of equipment, the risk can be lessened by common sense logging practices, experienced logging personnel, built-in temperature and tension measurements and tool insurance.

Table 8-6. High temperature tools and insurance availability.

Company and Tool	Is Insurance Available	Cost of Insurance	Coverage	Lost-in-Hole Charges
Schlumberger Xtreme logs	Yes	$2,670 per tool (there are 5 tools)	Covers 50% of the tools' costs if lost in hole	$712,000 for five tools
Halliburton HEAT logs	Yes	$792 per tool (there are 5 tools)	Covers complete loss only, not repairs	Information requested
Tiger Energy AFIT tool	No	N/A	N/A	$460,000
Welaco PTS tool	Yes	$950 per well	Covers 50% of the tools' costs if lost in hole	$430,000 and additional costs for lost wireline
Tiger Energy PTS tool	No	N/A	N/A	Information requested, usually don't offer tool insurance
Pacific Process PTS tool	Yes	$500 per well	Covers 50% of the tools' costs if lost in hole	$200,000 and additional costs for lost wireline

8.7 SCHEDULE AND BUDGET

The production drilling schedule depends upon AltaRock finding a partner to share the drilling costs. As of January 2014, AltaRock is negotiating with potential partners. It is likely that the stimulation results, available in August 2014 will be needed in order to get a partner to commit. If that is the case, then the production drilling will not begin until spring of 2015 as soon as the snow melts.

Table 8-7. Schedule of upcoming drilling activities. Finer details of the schedule are left out because there will be activities that will be contingent upon the results of the restimulation effort.

Operation	Start Date	End Date
Drill Producer 55A-29	08/20/14	10/14/14
Re-mobilize rig	08/20/14	09/02/14
Purchase Casing / WH Valve / Run Conductor	08/20/14	08/22/14
Drill 55A-29	09/03/14	10/14/14
Stimulate 55A-29	10/15/14	01/08/15
Hookup DTS	01/09/15	01/15/15
Stimulate 3 weeks	01/16/15	02/13/15
Flow Back and Test Well	02/16/15	02/24/15

Table 8-8. Budget for the upcoming drilling effort at Newberry

Task Name	AltaRock Cost Share	DOE Cost Share	Project Total
Drill Production Well			
Project Meetings	$12,858	$1,250	$14,108
Integrate New Data and Design Production Well	$29,778	-	$29,778
Procure Casing	-	$1,624,748	$1,624,748
Procure High Pressure Wellhead	-	$139,650	$139,650
Prepare Well Site	$5,592	$63,195	$68,787
Mobilize/Demobilize Rig	$776,184	$2,500	$778,684
Drill Production Well	$3,467,012	$2,500,000	$5,839,347
Conduct Mini-Frac	$4,964	$232,600	$237,564
TOTAL	$4,296,388	$4,563,943	$8,732,666
Conduct Research Well Log Surveys			
Sonic-Gamma-Density	$1,861	$147,000	$148,861
Hot Hole FMS	$5,592	$65,000	$70,592
USGS Borehole Televiewer	$6,204	$51,300	$57,504
TOTAL	$13,657	$263,300	$276,957
Test Connectivity Between Injection and Production Well			
Project Meetings	$12,858	$24,912	$12,858
Maintain and Monitor MSA	$119,824	$23,400	$143,224
Rig Up Flow Test Equipment	$11,580	$21,675	$33,255
Pump Into Injection Well and Flow Production Well	$9,926	$209,000	$218,926
Monitor Injection and Production T, P, Q and H	$24,022	$76,000	$100,022
Sample and Analyze Production Well Weekly	$9,808	$5,194	$15,002
Inject Reservoir Tracer Compounds	$5,956	$20,000	$25,956
Conduct Injection PTS Wellbore Survey	$4,467	$20,000	$24,467
TOTAL	$198,441	$400,181	$573,710
Stimulate Production Well (contingent)			
Install DTS	$6,452	$27,250	$33,702
Stimulate Producer with Dual Stimulation Method	$24,319	$651,300	$675,619
Remove DTS	$1,588	-	$1,588
TOTAL	$32,359	$678,550	$710,909
Integrate Stimulation and Flow Test Data			
Update TOUGH-FLAC THM Model with Stress and Fracture Data	$3,309	$260,432	$263,741
Update TOUGHREACT Chemical Model	$14,891	$2,050	$16,941
Determine Equivalent Porous Matrix Using AltaStim	$4,757	-	$4,757
Evaluate Seismic and Hydraulic Monitoring Data	$34,898	$26,000	$60,898
Prepare Report: First Production Well Test Results	$20,717	$4,551	$25,268
TOTAL	$78,572	$293,033	$371,605
PROJECT TOTAL	**$4,619,417**	**$6,199,007**	**$10,665,847**

9 REFERENCES

AltaRock. 2011a. Phase I Report. Newberry EGS Demonstration, DOE Award: DE-EE0002777. Prepared by AltaRock Energy, Inc., August 26.

AltaRock. 2011b. Induced Seismicity Mitigation Plan. Newberry Enhanced Geothermal Systems Demonstration. Prepared by AltaRock Energy, Inc., August 3.

AltaRock. 2011c. Evaluation of Water Usage for the Newberry EGS Demonstration. Prepared by AltaRock Energy, Inc., February 9.

BLM. 2011. Environmental Assessment, Newberry Volcano Enhanced Geothermal System (EGS) Demonstration Project. United States Department of the Interior Bureau of Land Management (BLM). DOI-BLM-OR-P000-2011-0003-EA, DOE/EA-1897, December.

Baggeroer, A. B., Kuperman, W. A., and Mikhalevsky, P. N. 1993. An overview of matched field methods in ocean acoustics. IEEE Journal of Oceanic Engineering, 18, 401–424.

Bargar, K.E. and Keith, T.E.C. 1999. Hydrothermal Mineralogy of Core from Geothermal Drill Holes at Newberry Volcano, Oregon. USGS Professional Paper 1578, 92 p.

Bucker, H.P. 1976. Use of calculated sound fields and matched-field detection to locate sound sources in shallow water. Journal of the Acoustical Society of America, 59, 368-373.

Century West. 1982. La Pine aquifer management plan: Bend, Oregon. Prepared by Century West Engineering Corporation, 597p.

Charlaix, E., Guyon, E., Roux, S., 1987. Permeability of a random array of fractures of widely varying apertures. Transport in Porous Media, 2, 31–43.

Cladouhos, T., Petty, S., Callahan, O., Osborn, W., Hickman, S., and Davatzes, N. 2011a. The Role of Stress Modeling in Stimulation Planning at the Newberry Volcano EGS Demonstration Project, Proceedings, Thirty-Sixth Workshop on Geothermal Reservoir Engineering, Stanford University, Stanford, California, February 11-13.

Cladouhos, T., Clyne, Matthew, C., Maisie, N. Petty, S. Osborn, W. L., Nofziger, L. 2011b. Newberry Volcano EGS Demonstration Stimulation Modeling. Geothermal Resources Council Transactions, 35, 317-322.

Cladouhos, T., Petty, S., Nordin, Y., Moore, M., Grasso, K., Uddenberg, M., Swyer, M., Julian, B., Foulger, G. 2013. Microseismic Monitoring OF Newberry Volcano EGS Demonstration. Proceedings, Thirty-Seventh Workshop on Geothermal Reservoir Engineering Stanford University, Stanford, California, February 11-13.

Dames and Moore. 1994. Revised report Newberry geothermal project hydrology baseline study Newberry Volcano, Oregon Force Exploration Company. Prepared by Dames and Moore, May 4.

Davatzes N.C., Hickman S.H., Preliminary Analysis of Stress in the Newberry EGS Well NWG 55-29, GRC transactions, 35, 323-332, 2011.

Dorbath, L., Cuenot, N., Genter, A., Frogneux, M. 2009. Seismic response of the fractured and faulted granite of Soultz-sous-Forêts (France) to 5 km deep massive water injections. Geophysical Journal International, 177, 653-675.

Fetterman, J.A., 2011. Porosity Evolution in the Newberry Volcano Geothermal System, Oregon, USA: Feedback between deformation and alteration. Geothermal Resources Council Transactions, 35, 339-346.

Fetterman, J.A., Davatzes, N.C. 2011. Fracture Generated Porosity Evolution in the Newberry Volcano Geothermal System, OR: Feedback Between Deformation and Alteration, Geothermal Resources Council National Meeting.

Foulger Consulting. 2010. Newberry Calibration Shot Project. Internal Report to AltaRock Energy, Inc., 10/09/2010, 104 p.

Foulger, G.R., Julian, B.R. 2013a. Report To AltaRock Energy, Inc., Earthquake Seismicity Associated With the Newberry EGS Demonstration, Draft Report. 82p. Prepared March 18.

Foulger, G.R., Julian, B.R. 2013b. Seismological software for geothermal monitoring. Proceedings, Thirty-Eighth Workshop on Geothermal Reservoir Engineering, Stanford University, Stanford, California, February 11-13.

Gannett, M.W., Lite, K.E., Morgan, D.S., and Collins, C.A. 2001. Groundwater hydrology of the upper Deschutes Basin, Oregon. USGS Water-Resources Investigations Report 00–4162, 78 p.

Gueguen, Y., Dienes, J., 1989. Transport properties of rocks from statistics and percolation. Journal of Mathematical Geology 21, 1–13.

Häring, M.O., Schanz, U., Ladner, F., Dyer, B. 2008. Characterization of the Basel-1 enhanced geothermal system. Geothermics, 37, 469-495.

Harris, D.B., and Kvaerna, T. 2010. Superresolution with seismic arrays using empirical matched field processing. Geophysical Journal International, 182, 1455–1477.

Hudson, J.A., Pearce, R.G., Rogers, R.M. 1989. Source type plot for inversion of the moment tensor. Journal of Geophysical Research: Solid Earth, 94, 765–774.

James, R. 1970. Factors Controlling Borehole Performance. Geothermics-special issue, 2, 2, Pt. 2, 1502 pp.

Julian, B.R., Foulger, G.R. 1996. Earthquake mechanisms from linear-programming inversion of seismic-wave amplitude ratios. Bulletin of the Seismological Society of America, 86, 972-980.

Julian, B.R., Foulger, G.R. 2004. Microearthquake focal mechanisms – A tool for monitoring geothermal systems. Geothermal Research Council Bulletin, 33, 166-171.

Julian, B.R., Foulger, G.R., Monastero, F.C., Bjornstad, S. 2010. Imaging hydraulic fractures in a geothermal reservoir. Geophysical Research Letters, 37, L07305, 5p.

Julian, B.R., Miller, A.D., Foulger, G.R. 1997. Non-double-couple earthquakes at the Hengill-Grensdalur geothermal area, southeast Iceland, Geophysical Research Letters, 24, 743-746.

Julian, B.R., Miller, A.D., Foulger, G.R. 1997. Non-double-couple earthquakes at the Hengill-Grensdalur geothermal area, southeast Iceland. Geophysical Research Letters, 24, 743-746.

Julian, B.R., Miller, A.D., Foulger, G.R. 1998. Non-double-couple earthquakes 1. Theory. Reviews of Geophysics, 36, 525-549.

King, G. 1991. Technical Reconnaissance Report, Survey of Groundwater Resources, Upper Deschutes River Basin, Oregon, U.S. Bureau of Reclamation, In-house Report.

LBNL. 2013. Interactive Map of Earthquakes at the Newberry Caldera. Maintained by Lawrence Berkeley National Laboratory (LBNL), Earth Sciences Division. Available at: http://esd.lbl.gov/research/projects/induced_seismicity/egs/newberry.html.

Li, Y., Wang, J., Jung, W., Ghassemi, A. 2012. Mechanical Properties of Intact Rock and Fractures in Welded Tuff from Newberry Volcano. Proceedings, Thirty-Seventh Workshop on Geothermal Reservoir Engineering Stanford University, Stanford, California, January 30 - February 1.

Majer, E., Baria, R., Stark, M. 2008. Protocol for induced seismicity associated with enhanced geothermal systems. Report produced in Task D Annex I (9 April 2008), International Energy Agency-Geothermal Implementing Agreement (incorporating comments by: C. Bromley, W. Cumming, A. Jelacic and L. Rybach). Available at: http://www.iea-gia.org/publications.asp.

Majer, E.J., Robertson-Tait, N.A., Savy, J., Wong, I. 2011. Protocol for Addressing Induced Seismicity Associated with Enhanced Geothermal Systems (EGS). Available at: http://esd.lbl.gov/files/research/projects/induced_seismicity/egs/EGS-IS-Protocol-Final-Draft-20110531.pdf.

McGarr, A. 1976. Seismic Moments and Volume Changes. Journal of Geophysical Research, 81, 8, 1487–1494.

McGarr, A. 2014. Maximum Magnitude Earthquakes Induced by Fluid Injection. Journal of Geophysical Research: Solid Earth, 119.

Miller, A.D., Foulger, G.R., Julian, B.R. 1998. Non-double-couple Earthquakes 2. Observations. Reviews of Geophysics, 36, 551-568.

Morgan, D.S., Tanner, D.Q., Crumrine, M.D. 1997. Hydrologic, Water Quality, and Meteorological Data for Newberry Volcano and Vicinity, Deschutes County, Oregon, 1991-1995. USGS Open-File Report 97-4088, 72 p.

Osborn, W.L., Petty, S., Cladouhos, T.T., Iovenitti, J., Nofziger, L., Callahan, O., Perry, D.S., Stern P.L. (2011), Newberry Volcano EGS Demonstration, Phase I Results, GRC Transactions, 35, 499-505.

Parotidis, M., Shapiro, S.A., Rothert, E. 2004. Back Front of Seismicity Induced after Termination of Borehole Fluid Injection, Geophysical Research Letters, 31, L02612.

Petty, S., Nordin, Y., Glassley, W., Cladouhos, T., Swyer, M. 2013. Improving Geothermal Project Economics with Multi-Zone Stimulation: Results from the Newberry Volcano EGS Demonstration. Proceedings, Thirty-Eighth Workshop on Geothermal Reservoir Engineering, Stanford University, Stanford, California, February 11-13, 2013.

PNSN. 2013. Volcano Seismicity - Newberry. Pacific Northwest Seismic Network (PNSN). Available at: http://www.pnsn.org/volcanoes/newberry.

Rinaldi, A.P., J. Rutqvist, E.L. Sonnenthal, and T.T. Cladouhos, 2012. TOUGH-FLAC Coupled THM Modeling Of Proposed Stimulation at the Newberry Volcano EGS Demonstration. Proceedings, TOUGH Symposium 2012, Lawrence Berkeley National Laboratory, Berkeley, CA.

Roeloffs, E. 1996. Advances in Geophysics. Academic Press, San Diego, CA. v. 37 p. 168.

Sammel, E.A., and Craig, R.W., 1983, Hydrology of the Newberry Volcano Caldera, Oregon: U.S. Geological Survey Water Resources Investigations Report 83-4091.

Sammel, E.A., S.E. Ingebritsen, and R.H. Mariner (1988). The hydrothermal system at Newberry Volcano, Oregon, Journal of Geophysical Research, 93(B9), 10149-10162.

Shapiro, S., Krüger, O., Langenbruch, C., Dinske, C. 2010. Geometric Control of Earthquake Magnitudes by Fluid Injections in Rocks. Society of Exploration Geophysicists, Expanded Abstracts, 30, 1539-1543.

Sherrod, D.R., Taylor, E.M., Ferns, M.L., Scott, W.E., Conrey, R.M., and Smith, G.A. 2004. Geologic Map of the Bend 30 x 60-Minute Quadrangle, Central Oregon. USGS Geologic Investigations Series 1-2683.

Sonnenthal, E. L., Spycher, N., Callahan, O., Cladouhos, T., Petty, S., 2012. A thermal-hydrological-chemical model for the enhanced geothermal system demonstration project at Newberry Volcano, Oregon. Proceedings, Thirty-Seventh Workshop on geothermal reservoir engineering, Stanford University, Stanford, Ca, January 30 - February 1. SGP-TR-194.

URS, 2010. Evaluations of Induced Seismicity/Seismic Hazards and Risk for the Newberry Volcano EGS Demonstration. Prepared by URS Corporation, November 22.

Waldhauser, F. and W.L. Ellsworth, A double-difference earthquake location algorithm: Method and application to the northern Hayward fault, Bulletin of the Seismological Society of America, 90, 1353-1368, 2000.

Wang, J., Templeton, D., Harris, D., 2011. Mapping Diffuse Seismicity Using Empirical Matched Field Processing Techniques. Proceedings, Thirty-Sixth Workshop on Geothermal Reservoir Engineering, Stanford University, Stanford, California, January 31 - February 2.

Xu, T., Spycher, N., Sonnenthal, E. L., Zhang, G., Zheng, L., Pruess, K., 2011. TOUGHREACT Version 2.0: A simulator for subsurface reactive transport under non-isothermal multiphase flow conditions. Computers and Geosciences, 37, 763-774.

Wessel, P., and Smith, W. H. F., 1998. New, improved version of Generic Mapping Tools released, EOS Transactions American Geophysical Union, 79 (47), pp. 579.

Appendix A
Cultural Resources Report

Appendix B

Log of System Trips and Alarms Monitored and Performed by the Programmable Logic Control System

Appendix C
Stimulation Daily Field Progress Reports

Appendix D
Seismicity Reports

Appendix E
Groundwater Quality Analytical Results

Surface Water and Groundwater Quality Data, Newberry EGS Demonstration Project

			Field Parameters					Laboratory Analytical Results												
Monitoring Location	Sample Type	Date	Temp, (°C)	pH (SU)	Cond. (mS/m)	ORP (mV)	Turbidity (NTU)	Alkalinity, Total (mg/L CaCO3)	Alkalinity/HCO_3^- (mg/L $CaCO_3$)	Alkalinity/CO_3^{2-} (mg/L $CaCO_3$)	Alkalinity/OH^- (mg/L $CaCO_3$)	Aluminum (mg/L)	Ammonia (mg/L N)	Arsenic (mg/L)	Barium (mg/L)	Boron (mg/L)	Calcium (mg/L)	Cesium (mg/L)	Chloride (mg/L)	Chromium (mg/L)
PLHS	B	10/7/2011	49.9	6.09	0.99	81	–	540	540	<2	<2	<0.05	<0.1	0.015	0.28	0.76	48	0.004	7	<0.002
PLHS	B	7/26/2012	50.4	6.64-6.72	0.672-0.691	174	–	520	520	<2	<2	<0.05	<0.1	0.013	0.12	0.77	43	0.004	5	<0.002
PLHS	D	11/27/2012	46.8	6.33	0.917	145	0.08	660	660	<2	<2	<0.05	<0.1	0.014	0.24	0.9	56	0.004	7.5	<0.002
PLHS	P	1/6/2013	42.1	6.7	0.815	152	0.75	390	390	<2	<2	<0.05	<0.1	0.018	0.02	0.88	32	<0.002	3.8	<0.002
PLHS	P	2/9/2013	46.1	7.05	0.584	232	0.64	450	450	<2	<2	<0.05	<0.1	0.012	0.054	0.88	37	0.002	5.0	<0.002
PLHS	P	3/12/2013	39	6.35	0.764	176	0.08	550	550	<2	<2	<0.05	<0.1	0.022	0.011	0.72	50	0.004	7	<0.002
PLHS	P	4/10/2013	37.2	6.67	177	0.501	0.83	550	550	<2	<2	<0.05	<0.1	0.024	0.011	0.74	52	0.004	7.7	<0.002
PLHS	P	5/15/2013	39.8	6.53	174	0.793	-0.14	550	550	<2	<2	<0.05	<0.1	0.024	0.012	0.73	52	0.005	7.7	<0.002
PLHS	P	7/19/2013	52.4	6.2	–	–	0.07	580	580	<2	<2	<0.05	<0.1	0.011	0.2	0.76	50	0.004	6.8	<0.002
ELHS	B	10/6/2011	54.5	6.26	1.29	-37	28.1	740	740	<2	<2	<0.05	0.1	0.003	0.005	0.61	130	<0.002	4.5	<0.002
ELHS	B	7/26/2012	38.8	6.46	0.83	33	-	500	500	<2	<2	<0.05	0.2	<0.002	0.014	0.8	86	<0.002	1.7	<0.002
ELHS	D	11/29/2012	46.8	6.33	0.91	145	0.08	160	160	<2	<2	<0.05	<0.1	0.006	0.019	1	35	<0.002	1.4	<0.002
ELHS	P	1/6/2013	16	8.66	0.225	127	0.06	130	130	<2	<2	<0.05	<0.1	<0.002	0.019	0.98	29	<0.002	0.7	<0.002
ELHS	P	2/9/2013	28.4	6.58	0.684	134	0.1	510	510	<2	<2	<0.05	<0.1	<0.002	0.011	0.91	77	<0.002	3.8	<0.002
ELHS	P	3/12/2013	48.8	6.49	0.425	146	1.20	250	250	<2	<2	<0.05	0.2	<0.002	0.015	0.96	43	<0.002	2	<0.002
ELHS	P	4/10/2013	42	6.75	85	0.345	3.99	260	260	<2	<2	<0.05	<0.1	<0.002	0.013	0.95	46	<0.002	2.3	<0.002
ELHS	P	5/15/2013	22.9	6.77	132	0.289	0.47	150	150	<2	<2	<0.05	<0.1	<0.002	0.018	0.95	32	<0.002	0.8	<0.002
ELHS	P	7/19/2013	32.9	6.8	–	–	0.6	130	130	<2	<2	<0.05	<0.1	<0.002	0.017	1	30	<0.002	0.8	<0.002
PCG	B	7/26/2012	11.5	7.37	0.06	124	-	48	48	<2	<2	<0.05	<0.1	<0.002	0.003	<0.05	4.3	<0.002	1.7	<0.002
PCG	P	6/22/2013	9.7	7.98	108	0.48	0.12	44	44	<2	<2	<0.05	<0.1	<0.002	0.003	<0.05	4.4	<0.002	1.4	<0.002
PCG	P	7/23/2013	11.9	7.35	–	0.248	–	44	44	<2	<2	<0.05	<0.1	<0.002	<0.004	<0.05	4	<0.002	1.1	<0.002
VC	B	7/26/2012	7.9	6.43	0.051	142	err	44	44	<2	<2	<0.05	0.2	<0.002	0.005	<0.05	3.9	<0.002	1.4	<0.002
VC	P	6/22/2013	5.7	7.21	165	0.027	-0.12	41	41	<2	<2	<0.05	<0.1	0.002	0.004	<0.05	3.9	<0.002	1.2	<0.002
VC	P	7/23/2013	14.1	6.5	–	0.248	0.01	41	41	<2	<2	<0.05	<0.1	<0.002	<0.004	<0.05	4.2	<0.002	1	<0.002
NEWW	B	10/7/2011	8.6	7.27	0.064	124	0.55	50	50	<2	<2	<0.05	<0.1	<0.002	0.002	<0.05	5.5	<0.002	1.7	<0.002
NEWW	B	10/6/2011	9.1	7.38	0.093	120	Error	57	57	<2	<2	<0.05	<0.1	<0.002	0.002	<0.05	8.2	<0.002	2.4	<0.002
NEWW	B	7/26/2012	10.3	7.53	0.067	184	–	57	57	<2	<2	<0.05	<0.1	<0.002	0.004	<0.05	7.8	<0.002	2.3	<0.002
NEWW	P	1/18/2013	7.9	7.38	0.086	93	0.17	60	60	<2	<2	<0.05	<0.1	<0.002	0.003	<0.05	7.8	<0.002	2.3	<0.002
NEWW	P	2/28/2013	8.5	7.32	0.80	136	0.03	–	–	–	–	<0.05	–	<0.002	0.005	<0.05	7.9	<0.002	–	<0.002
NEWW	P	3/22/2013	8.7	7.20	0.077	137	-0.05	58	58	<2	<2	<0.05	<0.1	<0.002	0.004	<0.05	8	<0.002	2.4	<0.002
Pad 16 Water Well	B	8/16/2012	6	7.7	0.013	169	NA	42	42	<2	<2	<0.05	0.1	<0.002	0.002	<0.05	5	<0.002	0.7	<0.002
Pad 16 Water Well	D	11/26/2012	7.7	7.79	0.033	122	0.15	39	39	<2	<2	<0.05	<0.1	<0.004	<0.002	<0.05	5.1	<0.002	0.9	<0.002
Pad 16 Water Well	P	9/12/2013	6.88	8.2	-65	–	0.84	40	40	<2	<2	<0.05	<0.1	<0.002	0.003	<0.05	5.1	<0.001	0.8	<0.002
Pad 29 Water Well	P	8/10/2011	NA	NA	NA	NA	NA	240	240	<2	<2	<0.05	0.3	0.032	0.009	0.55	19	<0.002	4	<0.002
Pad 29 Water Well	B	8/12/2011	NA	NA	NA	NA	NA	240	240	<2	<2	<0.05	<0.1	0.032	0.007	0.57	19	<0.002	3.8	<0.002
Pad 29 Water Well	B	9/23/2011	NA	NA	NA	NA	NA	230	230	<2	<2	<0.05	<0.1	0.026	0.008	0.55	19	<0.002	3	<0.002
Pad 29 Water Well	D	10/18/2012	15.9	7.56	0.385	101	0.12	250	250	<2	<2	<0.05	0.1	0.033	0.008	0.59	19	<0.002	3.5	<0.002
Pad 29 Water Well	D	11/26/2012	16.7	7.69	0.368	170	0.02	250	250	<2	<2	<0.05	<0.1	0.034	0.007	0.58	20	<0.002	3.5	<0.002
Pad 29 Water Well	P	12/10/2012	14.5	7.54	0.345	71	0	250	250	<2	<2	<0.05	<0.1	0.033	0.008	0.56	19	<0.002	3.5	<0.002
Pad 29 Water Well	P	7/18/2013	16.7	7.15	–	0.305	0	250	250	<2	<2	<0.05	<0.1	0.028	0.007	0.57	19	<0.002	3.6	<0.002
Pad 29 Water Well	P	7/18/2013	16.3	7.23	–	0.333	0	250	250	<2	<2	<0.05	<0.1	0.028	0.01	0.56	19	<0.002	3.5	<0.002
Pad 29 Water Well	P	9/11/2013	7.25	24.3	-83	**	0.1	250	250	<2	<2	<0.05	0.1	0.029	0.007	0.57	19	<0.001	3.6	<0.002
NN-17	B	10/5/2012	13.1	6.92	0.53	NA	119	241	233	8	<2	<0.05	0.1	0.01	0.004	0.56	18	<0.002	3.1	<0.002
NN-17	D	10/18/2012	8.1	7.82	0.343	NA	17.2	240	240	<2	<2	<0.05	0.3	0.011	0.006	0.55	18	<0.002	3	<0.002
NN-17	P	1/7/2013	5.6	8.66	0.225	-75	4.57	240	240	<2	<2	<0.05	<0.1	0.011	0.006	0.55	16	<0.002	3.6	<0.002
NN-17	P	2/10/2013	6	8.26	0.145	-72	5.16	210	210	<2	<2	<0.05	<0.1	0.009	0.006	0.46	18	<0.002	2.8	<0.002
NN-17	P	3/14/2013	7.9	8.27	0.220	-61	4.65	210	210	<2	<2	<0.05	<0.1	0.009	0.009	0.42	18	<0.002	2.6	<0.002
NN-17	P	4/11/2013	4.6	8.2	129	0.214	0.83	242	233	9	<2	<0.05	0.2	0.013	0.006	0.56	18	<0.002	3.7	<0.002
NN-17	P	5/15/2013	8.6	7.78	-63	0.308	3.12	240	230	10	<2	<0.05	<0.1	0.014	0.005	0.55	18	<0.002	3.6	<0.002
NN-17	P	7/19/2013	9	7.3	–	–	3.26	250	250	<2	<2	<0.05	<0.1	0.014	0.005	0.56	18	<0.002	3.4	<0.002
NN-17	P	9/3/2013	7.74	9.9	-108	–	7.97	240	240	<2	<2	<0.05	<0.1	0.013	0.007	0.56	18	<0.002	3.4	<0.002
NN-18	B	10/9/2012	12.8	9.02	0.249	NA	16.8	171	80	91	<2	<0.05	<0.1	0.028	0.005	0.86	9.4	<0.002	6.5	<0.002
NN-18	D	10/18/2012	7.51	5.3	0.264	NA	2.86	190	190	<2	<2	<0.05	0.1	0.028	0.014	0.96	12	<0.002	6.6	<0.002
NN-18	P	1/7/2013	4.8	8.36	0.247	247	5.18	190	190	<2	<2	<0.05	<0.1	0.026	0.013	0.88	9.7	<0.002	6.3	<0.002
NN-18	P	2/10/2013	2.9	8.18	0.206	110	6.53	180	180	<2	<2	<0.05	<0.1	0.023	0.018	0.87	10	<0.002	6.3	<0.002
NN-18	P	3/14/2013	4.9	7.82	0.288	168	1.84	180	180	<2	<2	<0.05	<0.1	0.018	0.011	0.86	10	<0.002	6.3	<0.002
NN-18	P	4/11/2013	8	7.8	34	0.194	8.52	180	174	6	<2	<0.05	0.1	0.025	0.012	0.85	10	<0.002	6.1	<0.002
NN-18	P	5/17/2013	7.8	8.16	132	0.253	0.14	178	170	8	<2	<0.05	<0.1	0.025	0.012	0.82	9.6	<0.002	5.9	<0.002
NN-18	P	7/19/2013	14	7.93	–	–	–	180	180	<2	<2	<0.05	<0.1	0.026	0.012	0.85	9.7	<0.002	5.6	<0.002
NN-18	P	9/3/2013	7.69	13.9	-106	0.25	0.34	180	180	<2	<2	<0.05	<0.1	0.027	0.011	0.82	9.6	<0.002	5.7	<0.002

Surface Water and Groundwater Quality Data, Newberry EGS Demonstration Project (con't)

Monitoring Location	Sample Type	Date	Laboratory Analytical Results																
			F (mg/L)	Fe (mg/L)	Li (mg/L)	Mg (mg/L)	Mn (mg/L)	Hg (mg/L)	NO_3 (mg/L N)	P (mg/L)	K (mg/L)	Rb (mg/L)	SiO_2 (mg/L)	Na (mg/L)	Sr (mg/L)	SO_4 (mg/L)	TDS (mg/L)	δ^2H	$\delta^{18}O$
PLHS	B	10/7/2011	0.9	0.13	0.2	42	2.7	<0.0002	<0.5	0.2	13	0.032	160	110	0.2	3.5	720	-108.3	-14.44
PLHS	B	7/26/2012	0.6	<0.05	0.15	41	1.3	<0.0002	<0.5	0.14	11	0.032	150	96	0.18	3.2	630	-104.05	-13.75
PLHS(dup)	B	7/26/2012	–	–	–	–	–	–	–	–	–	–	–	–	–	–	–	-104.05	-13.78
PLHS	D	11/27/2012	0.9	<0.05	0.2	48	1.2	<0.0001	<0.5	0.13	16	0.04	220	140	0.2	3.5	820	–	–
PLHS	P	1/6/2013	0.8	<0.05	<0.1	41	0.031	<0.0001	1.3	0.04	6.6	0.016	58	58	0.11	4.9	380	–	–
PLHS	P	2/9/2013	0.8	<0.05	0.1	44	0.45	<0.0002	<0.5	0.06	8.8	0.022	100	78	0.15	3.4	500	–	–
PLHS	P	3/12/2013	0.8	<0.05	0.18	42	0.32	<0.0002	<0.5	0.18	13	0.039	180	110	0.15	12	690	–	–
PLHS	P	4/10/2013	0.9	<0.05	0.17	43	0.46	<0.0001	<0.5	0.17	13	0.038	170	110	0.2	12	690	-105.93	-14.19
PLHS	P	5/15/2013	0.9	<0.05	0.2	43	1	<0.0001	<0.5	0.18	13	0.04	170	110	0.21	12	710	-107.96	-14.35
PLHS	P	7/19/2013	0.5	<0.1	0.2	44	1.7	<0.0001	<0.5	0.12	14	0.034	210	120	0.2	3.4	740	-109.13	-14.41
ELHS	B	10/6/2011	0.5	0.15	<0.1	54	0.58	<0.0002	<0.5	0.15	13	0.012	180	90	0.36	<0.2	900	-113.6	-15.16
ELHS	B	7/26/2012	<0.1	0.56	<0.1	37	0.41	<0.0002	<0.5	0.12	9	0.015	110	63	0.27	26	590	-98.5	-12.4
ELHS(dup)	B	7/26/2012	–	–	–	–	–	–	–	–	–	–	–	–	–	–	–	-97.4	-12.2
ELHS	D	11/29/2012	0.2	0.17	<0.1	17	0.15	<0.0001	<0.5	0.08	4.8	0.013	37	32	0.11	54	270	–	–
ELHS	P	1/6/2013	0.2	0.06	<0.1	14	0.042	<0.0001	<0.5	0.03	4.2	0.011	19	27	0.12	61	230	–	–
ELHS	P	2/9/2013	0.3	<0.05	<0.1	39	0.45	<0.0002	<0.5	0.34	9.2	0.03	190	64	0.22	5.8	640	–	–
ELHS	P	3/12/2013	0.3	0.06	<0.1	21	0.23	<0.0002	<0.5	0.1	5.7	0.018	71	37	0.15	46	350	–	–
ELHS	P	4/10/2013	0.2	0.09	<0.1	22	0.33	<0.0001	<0.5	0.13	5.9	0.018	76	39	0.15	42	380	-92.5	-10.7
ELHS	P	5/15/2013	0.1	0.08	<0.1	14	0.098	<0.0001	<0.5	0.02	4.5	0.012	26	28	0.12	58	250	-82.9	-8.9
ELHS	P	7/19/2013	0.1	<0.1	<0.1	14	0.067	<0.0001	<0.5	<0.02	4.3	0.011	22	29	0.12	59	240	-79.87	-8.60
PCG	B	7/26/2012	0.2	<0.05	<0.1	3.5	<0.002	<0.0002	0.5	0.09	1.4	0.004	35	7.9	<0.05	1.5	70	-120.46	-16.2
PCG(dup)	B	7/26/2012	–	–	–	–	–	–	–	–	–	–	–	–	–	–	–	-120.22	-16.26
PCG	P	6/22/2013	0.1	<0.05	<0.1	3.7	0.003	<0.0001	<0.5	0.07	1.8	0.003	36	8.4	<0.05	0.6	76	-120.56	-16.14
PCG	P	7/23/2013	<0.1	<0.1	<0.1	3.4	<0.004	<0.0001	<0.5	0.07	1.5	0.003	37	7.8	<0.05	0.4	70	-120.09	-16.21
VC	B	7/26/2012	0.8	<0.05	<0.1	3	0.003	<0.0002	0.9	0.1	1.8	0.004	44	7.3	<0.05	0.4	76	-111.54	-15.4
VC(dup)	B	7/26/2012	–	–	–	–	–	–	–	–	–	–	–	–	–	–	–	-111.38	-15.37
VC	P	6/22/2013	0.7	0.07	<0.1	3.1	<0.002	<0.0001	<0.5	0.09	1.9	0.004	45	7.3	<0.05	0.4	86	-112.28	-15.3
VC	P	7/23/2013	0.6	<0.1	<0.1	3.1	<0.004	<0.0001	<0.5	0.08	1.9	0.004	47	7.1	<0.05	0.4	70	-112.16	-15.28
NEWW	B	10/7/2011	0.2	<0.05	<0.1	4.3	<0.002	<0.0002	<0.5	0.31	1.5	0.002	43	9.1	<0.05	0.5	92	-120.5	-16.14
NEWW	B	10/6/2011	0.2	0.1	<0.1	4.7	0.002	<0.0002	0.9	0.22	1.4	<0.002	42	10	<0.05	1.7	110	-119.8	-15.72
NEWW	B	7/26/2012	0.2	<0.05	<0.1	4.4	<0.002	<0.0002	1.9	0.18	1.4	<0.004	45	9.9	<0.05	2	100	-118.3	-15.8
NEWW	P	1/18/2013	0.2	<0.05	<0.1	4.5	0.002	<0.0002	1.3	0.17	1.4	<0.002	44	10	<0.05	1.5	96	–	–
NEWW	P	2/28/2013		<0.05	<0.1	4.6	0.002	<0.0002	–	–	1.4	<0.002	46	10	<0.05			–	–
NEWW	P	3/22/2013	0.1	<0.05	<0.1	4.5	0.002	<0.0002	1.1	0.18	1.4	<0.002	49	10	<0.05	1.5	100	-120.98	-15.68
Pad 16 Water Well	B	8/16/2012	0.2	0.08	<0.1	2.6	0.002	<0.0002	<0.5	0.12	1.1	0.003	41	6.8	<0.05	0.3	70	–	–
Pad 16 Water Well	D	11/26/2012	0.2	0.06	<0.1	2.5	0.002	<0.0001	<0.5	0.12	0.98	0.003	39	6.3	<0.05	0.3	76	–	–
Pad 16 Water Well	P	9/12/2013	0.2	<0.05	<0.1	2.6	0.003	<0.0001	<0.5	0.1	1.6	0.002	39	6.2	<0.05	0.3	74	-113.96	-15.58
Pad 29 Water Well	B	8/10/2011	0.8	0.1	<0.1	24	0.002	NA	0.29	0.15	4.7	0.014	59	44	0.08	2.5	280	–	–
Pad 29 Water Well	B	8/12/2011	0.8	0.07	<0.1	25	<0.002	NA	0.13	0.16	4.8	0.014	62	45	0.08	2.5	280	–	–
Pad 29 Water Well	B	9/23/2011	0.5	<0.1	<0.1	24	<0.002	NA	<0.5	0.2	5	0.012	60	42	0.08	2.5	270	–	–
Pad 29 Water Well	D	10/18/2012	0.7	<0.05	<0.1	25	0.003	<0.0002	<0.5	0.19	4.7	0.013	57	44	0.08	2.4	280	-110.8	-14.7
Pad 29 Water Well	D	11/26/2012	0.7	<0.05	<0.1	26	<0.002	<0.0001	<0.5	0.18	4.7	0.013	60	46	0.06	2.4	280	–	–
Pad 29 Water Well	P	12/10/2012	0.7	<0.05	<0.1	25	0.003	<0.0001	<0.5	0.18	4.7	0.012	55	46	0.05	2.5	280	-110.6	-14.72
Pad 29 Water Well	P	7/18/2013	0.5	<0.05	<0.1	25	<0.002	<0.0001	<0.5	0.15	5.2	0.012	58	44	0.08	2.5	280	–	–
Pad 29 Water Well(dup)	P	7/18/2013	0.6	<0.05	<0.1	25	<0.002	<0.0001	<0.5	0.15	5	0.012	58	43	0.07	2.6	280	–	–
Pad 29 Water Well	P	9/11/2013	0.6	<0.05	<0.1	25	<0.002	<0.0001	<0.5	0.2	5.1	0.012	60	44	0.08	2.5	280	-110.16	-14.71
NN-17	B	10/5/2012	0.7	<0.05	<0.1	24	0.092	<0.0002	<0.5	0.08	4.2	0.013	52	40	0.07	2.1	270	-111.4	-14.88
NN-17(dup)	B	10/5/2012	–	–	–	–	–	–	–	–	–	–	–	–	–	–	–	-112.3	-14.96
NN-17	D	10/18/2012	0.7	<0.05	<0.1	24	0.09	<0.0002	<0.5	0.09	4	0.013	51	39	0.07	1.9	260	-111.8	-14.77
NN-17(dup)	D	10/18/2012	–	–	–	–	–	–	–	–	–	–	–	–	–	–	–	-112.3	-14.96
NN-17	P	1/7/2013	0.8	0.27	<0.1	24	0.066	<0.0001	<0.5	0.1	4.2	0.014	55	40	0.07	1.9	240	–	–
NN-17	P	2/10/2013	0.6	0.13	<0.1	22	0.032	<0.0002	<0.5	0.12	3.6	0.009	50	34	0.08	2.1	230	–	–
NN-17	P	3/14/2013	0.6	0.13	<0.1	21	0.015	<0.0002	<0.5	0.14	3.4	0.009	50	31	0.06	2.2	230	–	–
NN-17	P	4/11/2013	0.7	0.08	<0.1	24	0.025	<0.0001	<0.5	0.1	4.5	0.014	53	41	0.07	1.8	260	-110.15	-14.87
NN-17	P	5/15/2013	0.7	0.16	<0.1	25	0.021	<0.0001	<0.5	0.1	4.4	0.014	54	42	0.12	1.8	270	-111.97	-14.99
NN-17	P	7/19/2013	0.6	0.2	<0.1	25	0.018	<0.0001	<0.5	0.09	4.4	0.014	55	41	0.1	1.9	270	-112.42	-14.92
NN-17	P	9/3/2013	0.6	0.24	<0.1	24	0.04	<0.0001	<0.5	0.1	4.7	0.013	55	41	0.1	1.8	260	-112.23	-15.08
NN-18	B	10/9/2012	0.4	0.09	<0.1	6.4	0.008	<0.0002	2.2	0.03	7.6	0.016	39	46	<0.05	13	190	-113.77	-15.13
NN-18(dup)	B	10/9/2012	–	–	–	–	–	–	–	–	–	–	–	–	–	–	–	-112.7	-15.13
NN-18	D	10/18/2012	0.5	<0.05	<0.1	14	0.015	<0.0002	<0.5	0.12	6.3	0.013	72	48	<0.05	4.9	240	-113.77	-15.14
NN-18	P	1/7/2013	0.5	<0.05	<0.1	13	0.012	<0.0001	<0.5	0.13	6.1	0.012	69	46	<0.05	4.7	230	–	–
NN-18	P	2/10/2013	0.5	0.26	<0.1	13	0.016	<0.0002	<0.5	0.12	6.1	0.013	67	47	<0.05	5	240	–	–
NN-18	P	3/14/2013	0.4	0.18	<0.1	13	0.009	<0.0002	<0.5	0.09	6.3	0.013	71	45	<0.05	4.7	240	–	–
NN-18	P	4/11/2013	0.4	0.2	<0.1	13	0.007	<0.0001	<0.5	0.1	6.3	0.012	68	46	<0.05	4.6	250	-113.47	-15.22
NN-18	P	5/17/2013	0.4	0.12	<0.1	13	0.006	<0.0001	<0.5	0.1	6.1	0.012	69	45	<0.05	4.4	250	-113.27	-15.25
NN-18	P	7/19/2013	0.3	0.2	<0.1	13	0.008	<0.0001	<0.5	0.1	6.3	0.012	70	46	<0.05	4.6	240	-111.32	-15.19
NN-18	P	9/3/2013	0.4	0.11	<0.1	13	0.004	<0.0001	<0.5	0.1	6.1	0.011	68	45	<0.05	4.6	250	-111.39	-15.16

B- background
D-during stimulation
P-post stimulation
(dup) – duplicate analysis
ELHS – East Lake Hot Springs
NEWW – Newberry Estates water well
PLHS – Paulina Lake Hot Springs
Cond. – Conductivity
TA – Total Alkalinity
Temp. – temperature
< – constituent was not detected above the laboratory reporting limit
"– " – data not collected

Appendix F
LLNL MFP Seismicity Report

Lawrence Livermore National Laboratory

Phase 2.1 Report

Newberry Volcano EGS Demonstration

Unclassified

October 18, 2013

LLNL-TR-635591-DRAFT

Lawrence Livermore National Laboratory is operated by Lawrence Livermore National Security, LLC, for the U.S. Department of Energy, National Nuclear Security Administration under Contract DE-AC52-07NA27344.

Disclaimer

Table of Contents

1 Seismic Data

1.1 SEISMIC STATION INSTRUMENTS

The Phase 2 Newberry Microseismic Network consists of 8 2-Hz 3-component Oyo Geospace HS-1 borehole geophones, 7 2-Hz 3-component Oyo Geospace HS-1 surface geophones, and 7 1-Hz 3-component Geotech GS-13 buried surface seismometers (Table 1). The NN stations are borehole stations. The NM and NB stations are surface stations. The Geospace HS-1 geophones were operated with the shunt open. The Geotech SMART-24R dataloggers with ADC Board version 06 were configured to 40 Vpp bipolar differential input range when paired with the GS-13 sensors, and configured to 5 Vpp bipolar differential when paired with the HS-1 sensors.

Station	Sensor	Recorder	Group
NM03, NM06, NN07, NM08, NN09, NN17, NN18, NN19, NN21, NM22, NN24, NN32, NM40 NM41, NM42	Geospace HS-1	Geotech SMART-24R	A
NB01, NB04, NB08, NB13, NB18, NB19	Geotech GS-13	Geotech SMART-24R	B
NB17	Geotech GS-13	Guralp CMG-DM24-S3	C

Table 1. Seismic instrumentation deployed at the Newberry site.

1.2 DATA PROCESSING

1.2.1.1 Converting to a Common Format

The raw data was converted to a common SAC format. Data from Groups A, B, and C were originally in suds, cd1.1, and gcf format, respectively.

1.2.1.2 Convert Raw Seismic Data to Physical Units

The raw seismograms output by the seismic recording systems are not proportional to physical units. To measure and model features in the seismograms, the effects caused by the recording systems themselves need to be quantitatively taken into account and the raw data converted into physically

meaningful units. See Appendix A for our specific procedure to convert the raw data in counts into physical units.

2 Identification of More Microearthquakes Using Empirical MFP

2.1 MFP EARTHQUAKE DETECTION

Our MFP technique differs from the established earthquake detection techniques and is an adaptation of a signal processing technique originally developed to locate continuous underwater acoustic sources [Bucker 1976; Baggeroer *et al*. 1993]. We calculate the wavefield structure across an array by estimating the structure directly from field calibration data, i.e., previously observed seismic events. Then we steer the array explicitly in the frequency domain using the complex phase and amplitude factors obtained from the field data (Harris and Kvaerna, 2010). We refer to this strategy as empirical MFP, in which the master templates created from the seismograms of previously detected micro-earthquakes contain contributions from direct and scattered seismic energy.

Empirical MFP largely eliminates the sensitivity of (correlation) matching operations to source time history variations by processing the observed data stream in a large number of narrow frequency bands. This makes MFP sensitive to the spatial structure of the signal at the observing aperture (controlled by mechanism and propagation), but not the temporal structure (controlled, in part, by source time history). In this way MFP can identify previously undiscovered events even if they bear little resemblance to the master event in the time domain.

2.2 ORIGINAL EARTHQUAKE CATALOG

We use the Foulger Consulting earthquake catalog as the original earthquake catalog. Between October 2012 and December 2012, the Foulger Consulting catalog identified and located 207 microearthquakes (Figures 1 and 2). Although the stimulation started on October 16, 2012, the first catalog event occurred on October 29, 2012. No microseismic events were identified in September 2012.

2.3 CREATION OF MASTER MATCHING TEMPLATES

Master templates are created from master events. They are used to identify new events in the seismic datastream. The master events are selected based on two criteria. First, calibration events cannot be superimposed on other events on the seismic record. Second, waveforms of master events must also have high signal-to-noise ratios (SNR), especially in the lower frequency ranges, on at least four three-component seismic stations. No other selection criteria based on magnitude, mechanism or location is taken into consideration. Using these criteria, we investigated all catalog events occurring between October 2012 and December 2012. We identify 75 events out of the original 207 catalog events that could be employed as master events (Figure 3).

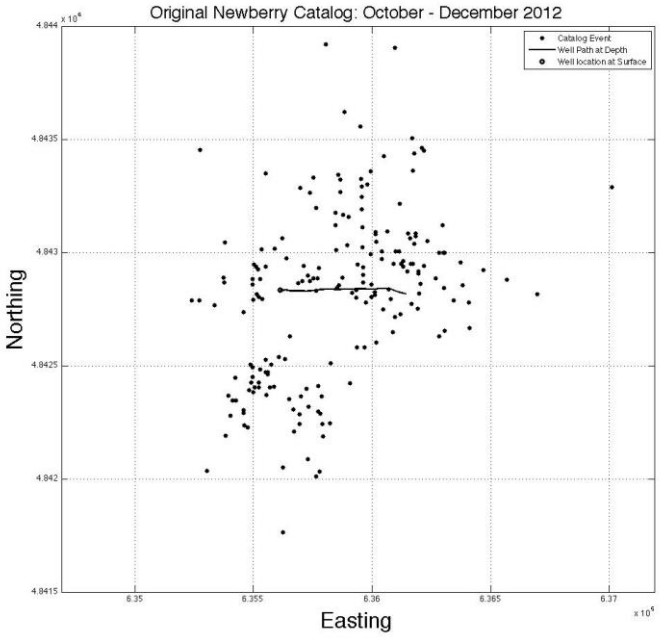

Figure 1. Map view of original catalog events between October 2012 and December 2012 plotted as black dots.

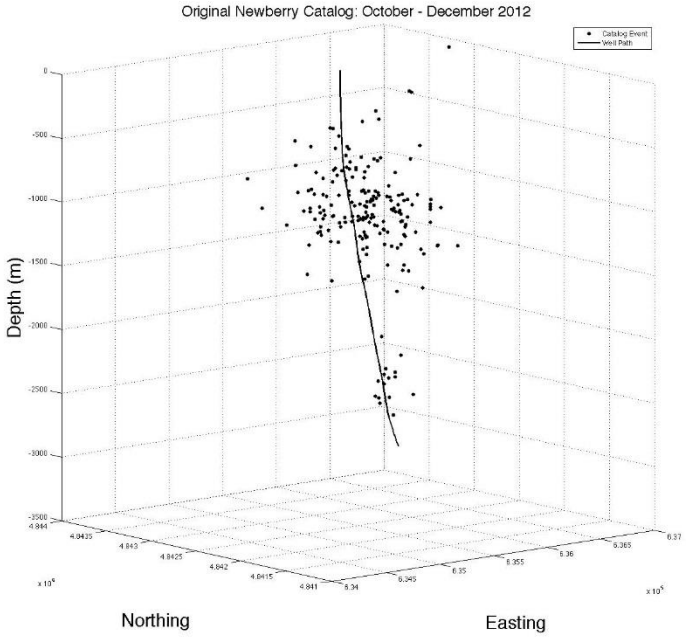

Figure 2. Depth view of original catalog events between October 2012 and December 2012 plotted as black dots.

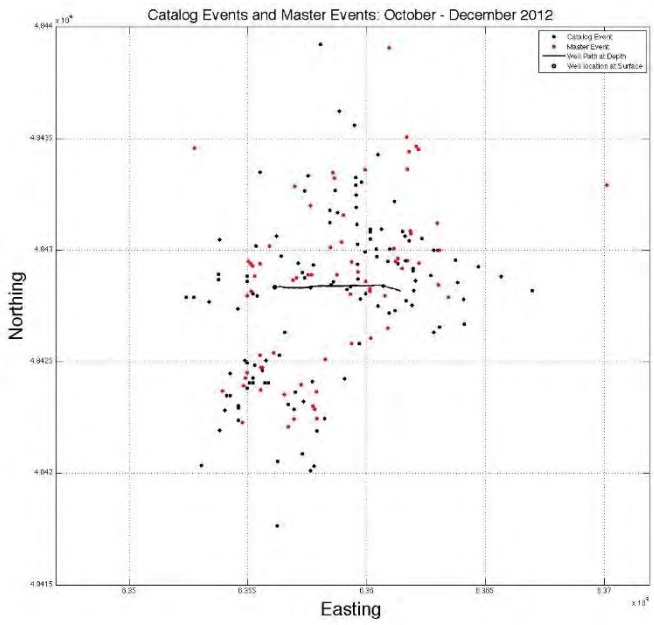

Figure 3. Map view of original catalog events that could be used as master events in red, and original catalog events that could not be used as master events in black.

2.4 APPLICATION OF MFP METHODOLOGY TO THE CONTINUOUS SEISMIC DATA

The empirical MFP code compared master templates to the continuous seismic data using a 21-sec sliding window that stepped forward at 1-second intervals. Comparisons between master events and new data were performed in the 6 – 12 Hz frequency band for continuous data between September 2012 and December 2012.

The original Foulger Consulting catalog reported 207 events. The MFP earthquake detection code was able to identify 240 additional events (Figures 4 and 5). Of the 75 master events used in the MFP, 65 identified at least one new event while 10 master events did not identify any new events.

An example of a newly detected event is shown in Figure 6. Notice how different noise sources obscure the signal in the time domain, but that the event can be identified more clearly in the frequency domain.

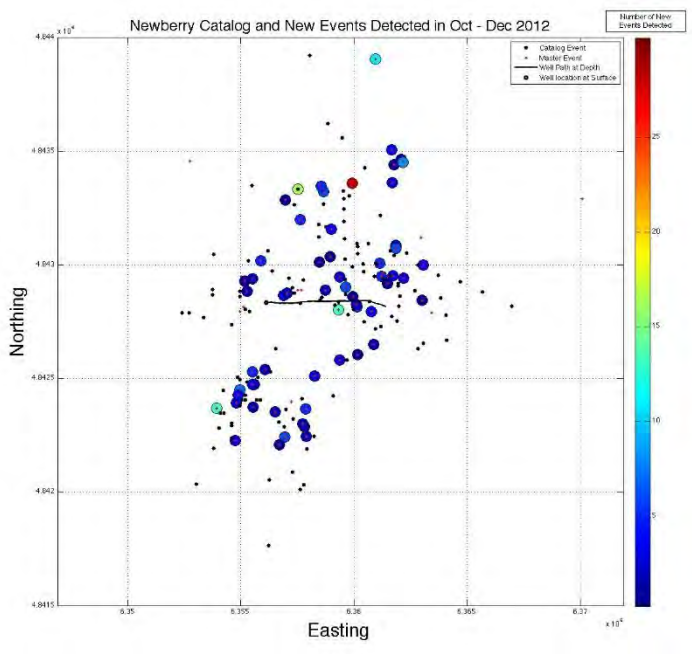

Figure 4. Plot in map view showing the location of the newly detected events as circles. The circles are color coded to indicate the number of new events the master events detected. Catalog events that were designated as a master event are plotted as red dots. Catalog events that were not used as master events are plotted as black dots.

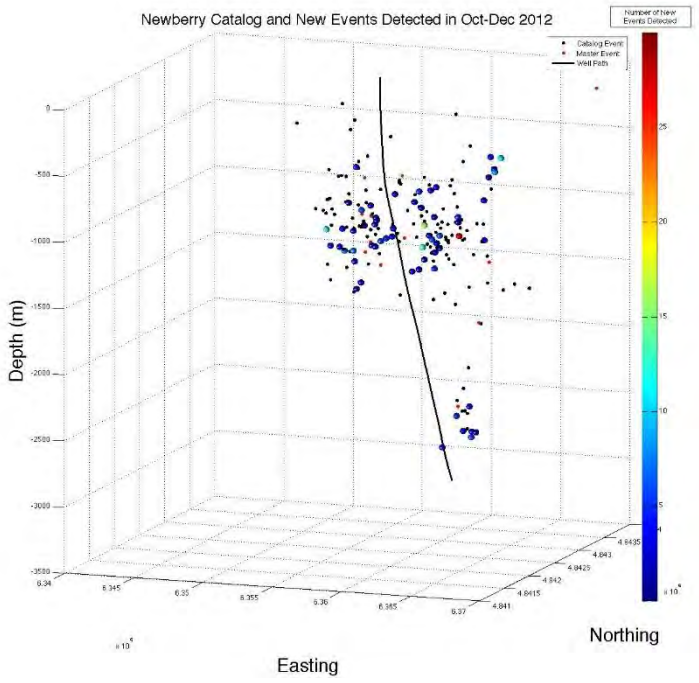

Figure 5. Plot in depth view showing newly detected events as spheres. The circles are color coded to indicate the number of new events the master events detected. Catalog events that were

designated as a master event are plotted as red dots. Catalog events that were not used as master events are plotted as black dots.

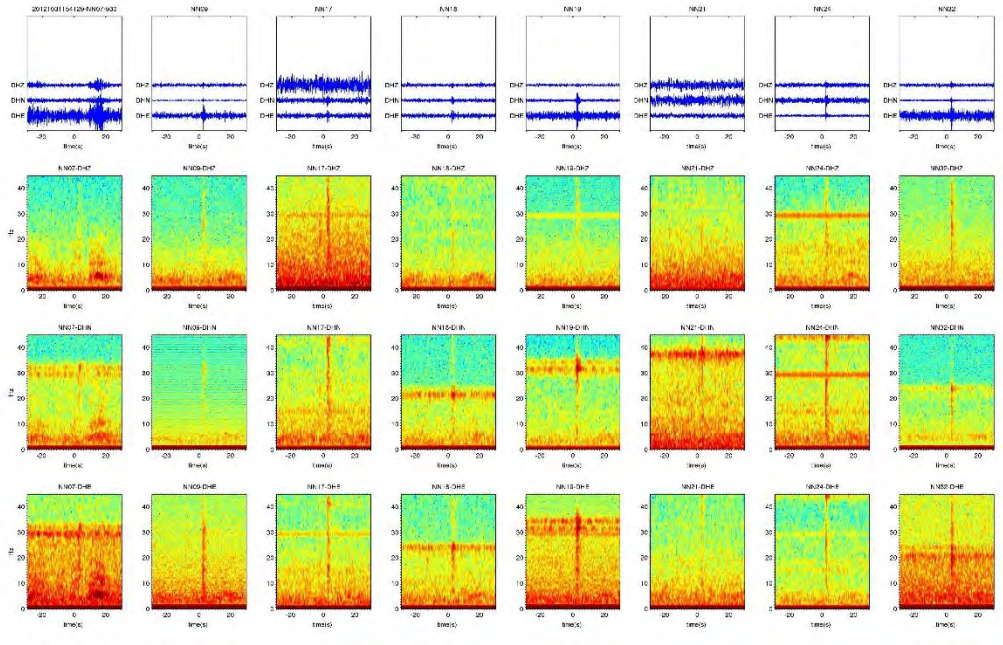

Figure 6. Example of a newly detected event not in the original catalog. Each column contains plots for one station. The first row shows the event in the time domain. The second, third and fourth rows show spectrograms of the vertical and horizontal components between 0 – 45 Hz.

Only one additional event was identified that occurred pre-stimulation. This event occurred on October 1, 2012 and was located in the shallow seismic zone (Figure 7). Additionally, one other event was detected post-stimulation, but pre-catalog. This second event occurred on October 20, 2012 and was also located in the shallow seismic zone (Figure 7). No other pre-catalog Newberry EGS events were detected between September 1, 2012 and October 28, 2012.

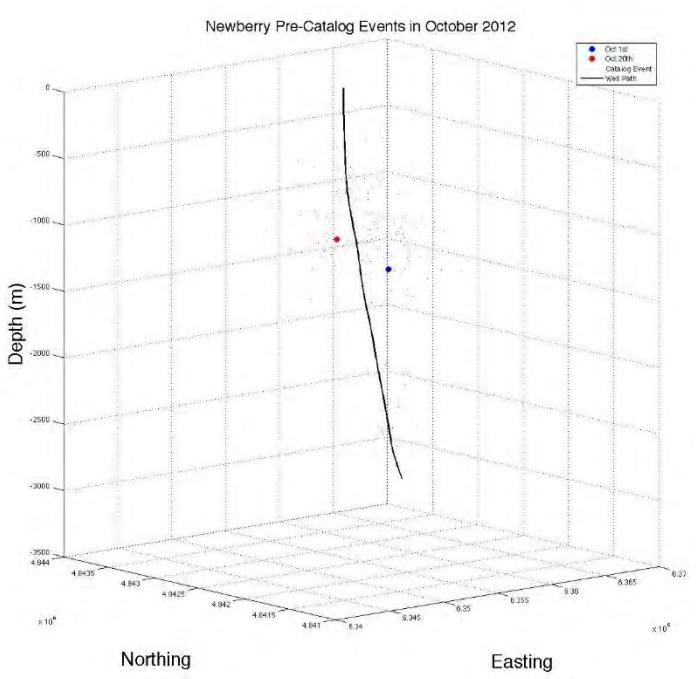

Figure 6. Plot in depth view showing the location of the October 1 pre-stimulation event in blue and the October 20 pre-catalog event in red.

2.5 POSSIBLE SEISMICALLY DELINEATED PLANES

Using the hypoDD relocated Foulger Consulting catalog, possible planar features in the subsurface can be delineated using a combined catalog of the original and newly detected events. We show an example of one in Figure 7. For all other analyses in this report, the original Foulger Consulting catalog was used since not all events from the original catalog are included in the relocated catalog.

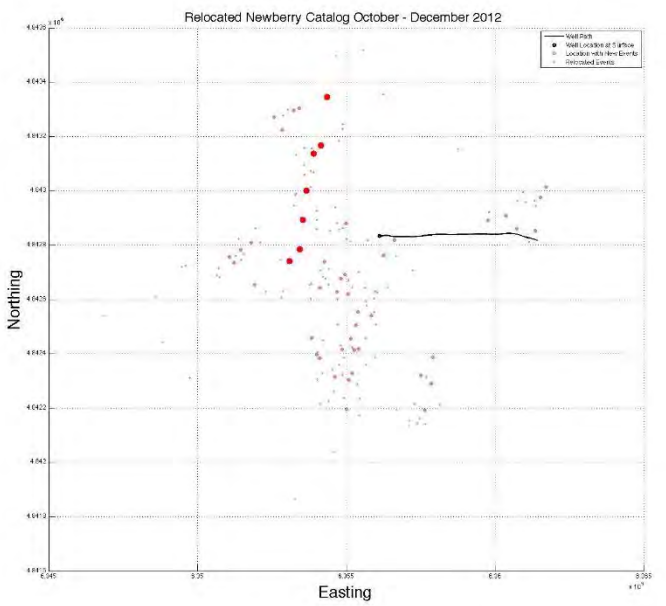

Figure 7. Plot in map view showing one fracture illuminated by the newly detected events. Newly detected events are in general much smaller than other events in the original catalog. This lineation would then indicate a small fracture that is "crackling".

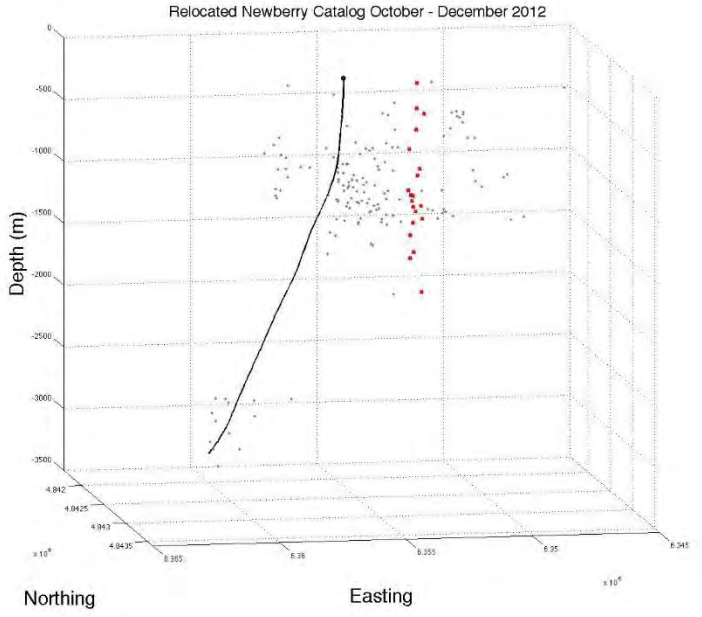

Figure 8. Plot in depth parallel view (12°) showing the fracture with both nearby original seismicity and newly detected events as red circles.

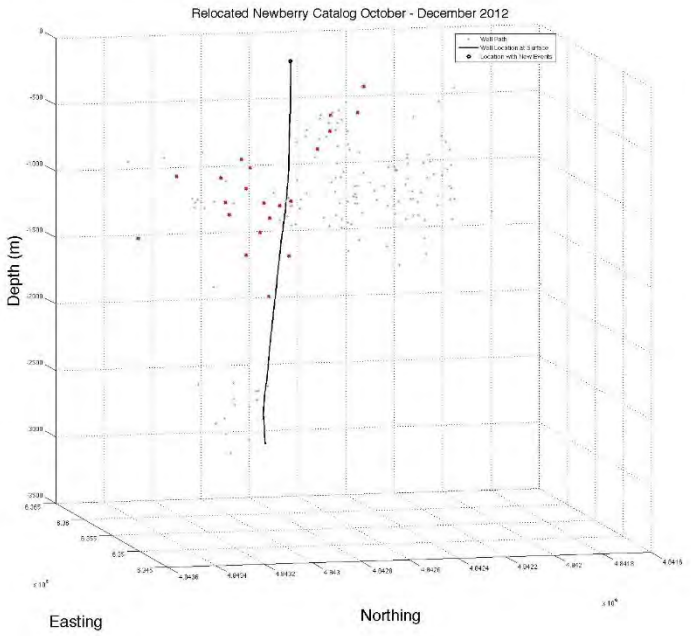

Figure 9. Plot in depth perpendicular view (102°) showing the fracture with both nearby original seismicity and newly detected events as red circles.

3 Comparison Between Seismicity and Injection Data

3.1 DAILY RATES

We plot the number of seismic events per day compared to the daily flow rate (Figure 8). There is a general relationship between the amount of fluids injected and the number of seismic events per day, however the seismicity is sometimes delayed. This is different from the behavior observed at The Geysers EGS experiment.

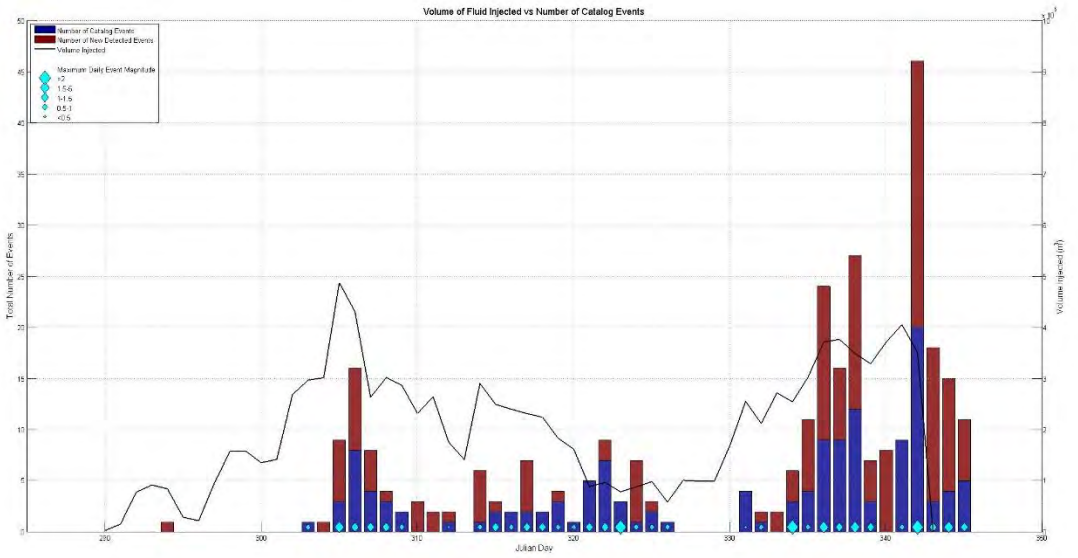

Figure 8. Comparison of the daily number of seismic events with the daily injected volume. The number of original catalog events are plotted as blue bars, the number of newly detected events are plotted as red bars. The horizontal axis is number of days since October 1, 2012. The daily injected volume is plotted as the black line. The maximum magnitude of events in a particular day is plotted as blue.

4 Creation of 3D Velocity Model

Ambient noise correlation (ANC) is a technique in which the data recorded at one seismometer are correlated with the data recorded at another to obtain an estimate of the Green's function (GF) between the two. The cross correlation of ambient noise between a pair of stations results in a waveform that is identical to the seismogram that would result if an impulsive source located at one of the stations was recorded at the other. Because of this, the techniques developed for earthquake seismology can be applied to the correlations themselves.

Using ANC, we created a 3D model of the Newberry site down to a depth of 5km. We collected continuous data for the month of October 2012, for the 22 stations in the Newberry network, together with 12 additional stations from the nearby CC, UO and UW networks. The data were instrument corrected, whitened and converted to single bit traces before cross correlation according to the methodology laid out in Benson (2007).

There are 231 unique paths connecting the 22 stations of the Newberry network. The additional networks extended that to 402 unique paths crossing beneath the Newberry site. Because we are particularly

interested in the very shallow seismic structure, we need high quality correlation waveforms at frequencies from 0.5-15 Hz. These particular data are very good and the GFs emerged quickly.

We treated each GF as a seismic record and inverted for the best fitting 1D model along each path. The objective function was to maximize the fit between the GF and synthetic seismograms, including the scattering energy in the coda. Short paths and high frequencies are most sensitive to the shallowest structures. Deeper structures are resolved for longer paths. We inverted simultaneously for Vp, and Vs and Qs, although Qs is poorly resolved. We broke the data into 3 groups. GFs for paths shorter than 5 km were filtered between 0.6 to 15 Hz and focused on matching details to 1 km. For paths between 5 - 10 km we filtered GFs between 0.5-8 Hz and data for the longest paths were filtered between 0.1 - 2 Hz. These longest paths, typically including at least one station outside the Newberry network, extended our depth coverage below 5km.

The individual 1D models were merged into a tomogram of the region using singular value decomposition. Two slices through the final 3D model are presented in Figure 9. Note how the seismicity generally follows the rapid change in velocity gradient between the highs and lows. This remarkable feature can be seen in most of the 2D slices throughout the model.

To test the accuracy of the model, we calculated synthetic seismograms for local earthquakes through both the original 1D and 3D models using the reflectivity method and the LLNL SW4 code, respectively. We compare the synthetics to a M1.85 earthquake that occurred on December 1, 2012. For clarity, we plot a representative set of data and synthetic waveform envelopes calculated through the 1D model (Figure 10). Notice how the 1D synthetics are only able to capture one or two peaks of the actual wavetrain. Waveform envelopes of the data and synthetics calculated through the 3D model are compared in Figure 11. The 3D synthetics are able to accurately capture the complexity of the surface waves, such as those observed at the NB19 surface station. Discrepancies in the phase and amplitude between the data and 3D synthetics can be due to lack of resolution of the current parameters, such as problems with the estimated Q value, or indicate a need for a longer time span of data. Refinements to the model based on comparisons such as these are expected to improve the overall robustness of the 3D velocity model.

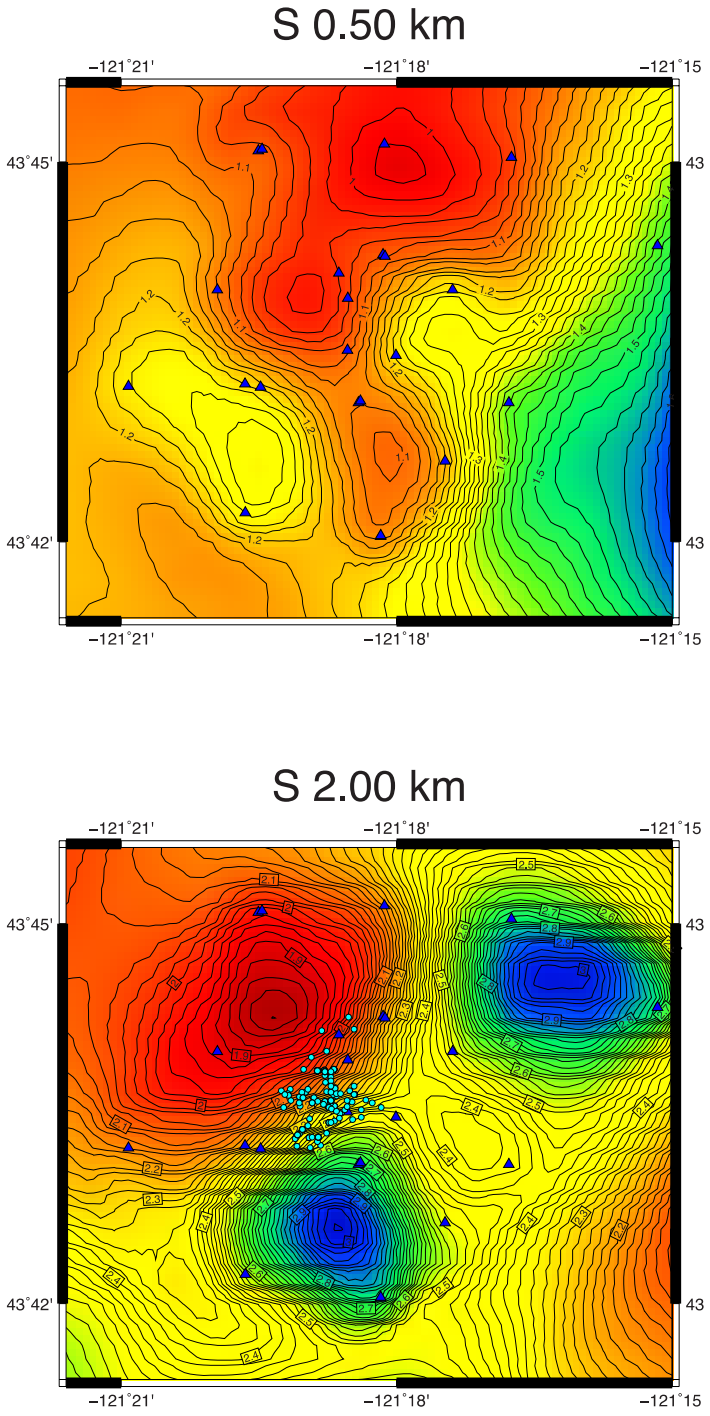

Figure 9. Slices through the shear velocity model at 0.5 and 2.0 km depth, including the independently located seismicity (cyan circles). Continuous data from Newberry network stations (blue triangles) and nearby seismic networks (off map) were used to constrain the velocity structure beneath the site down to 5 km.

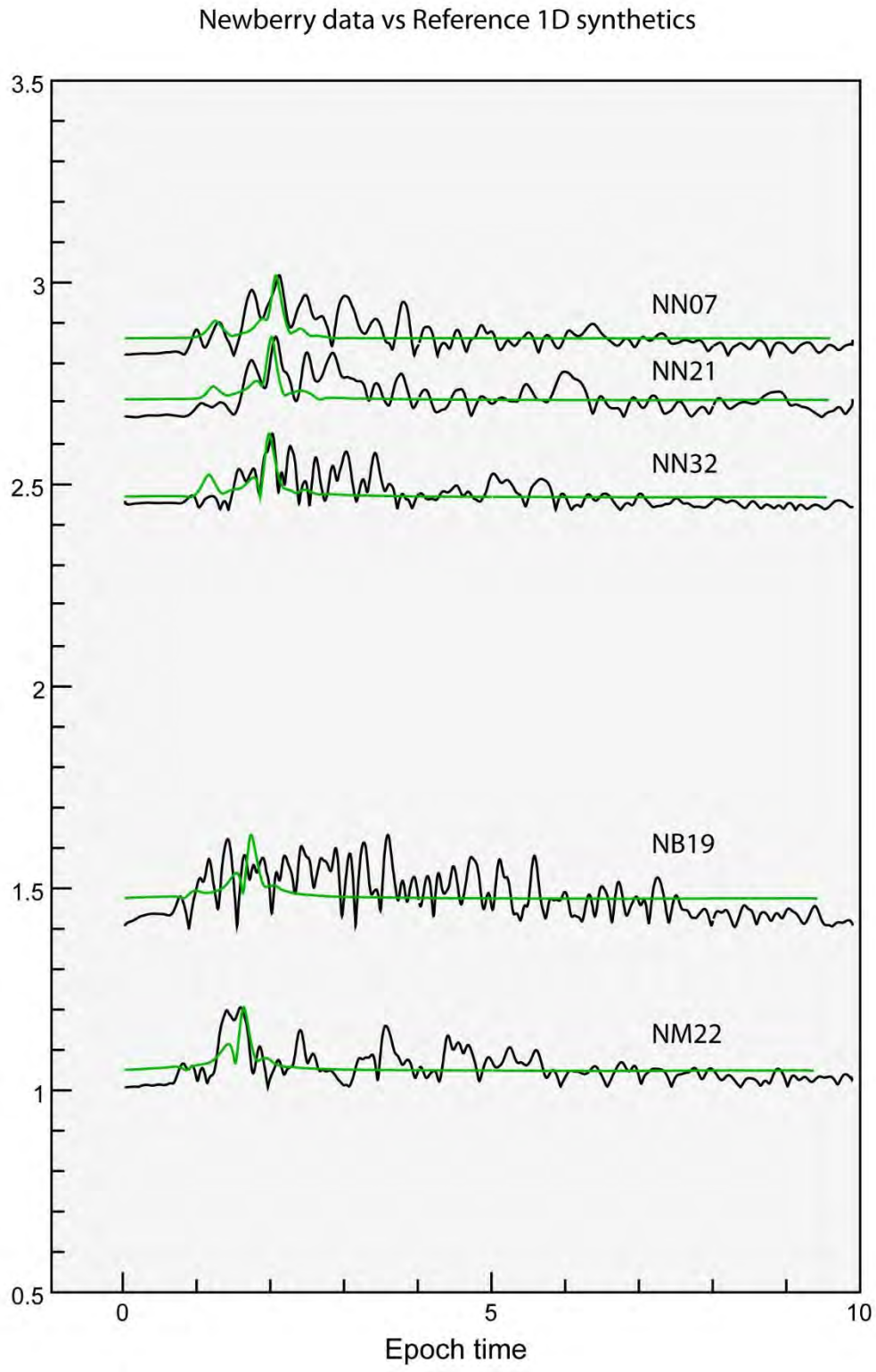

Figure 10. Envelopes of data for the 12/01/2012 event, recorded by the Newberry seismic network (black) compared to the synthetics calculated through reference 1D model (green).

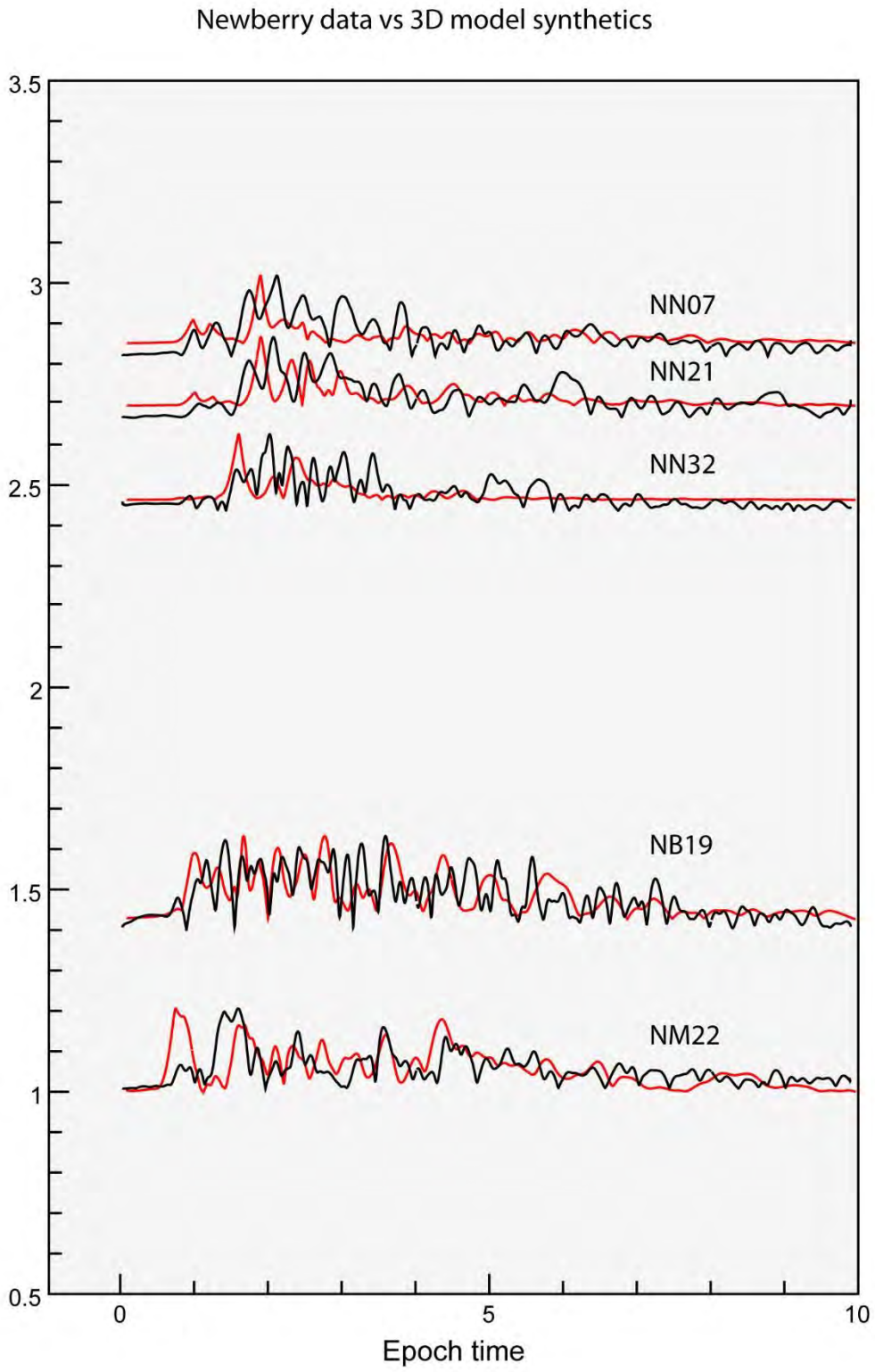

Figure 11. Envelopes of data for the 12/01/2012 event (black) and synthetics (red) calculated through the 3D model. Notice the improvement in fit to the data compared to the 1D model, especially when modeling the surface waves at NB19.

5 Preliminary Conclusions and Future Work

Using the empirical MFP method, we were able to identify 240 additional events occurring between September 2012 and December 2012 at the Newberry EGS site. There were 207 events in the original catalog during this same time period.

These new events were identified using 75 events from the original earthquake catalog as master events in the empirical MFP earthquake detection methodology. We apply the empirical MFP technique to continuous data from 8 borehole sensors from the time period between September 2012 and December 2012. The new events were primarily located in the shallow seismic swarm.

Combining the original and newly detected event catalog, possible seismic planes in the subsurface become illuminated. One such plane is shown in this DRAFT report. Comparisons between the number of daily seismic events and the daily injected volume show a similar trend, but not a strong one-to-one relationship.

Future work will include an extension in time of the above MFP earthquake detection method to identify more microearthquakes post-December 2012. The last observed event in the original catalog occurred in late February. We will determine how long the “crackling” will continue after the last known event occurs and which seismic lineations are the most active.

We will run a standard earthquake detection routine to verify the suitability of the AltaRock automatic STA/LTA parameters. All seismic studies that AltaRock initiated were based on the original automatically triggered catalog. Verifying the routine will be relatively straight-forward and provide evidence that no larger-events were originally missed.

We are currently applying the ambient noise correlation technique to the surface and subsurface seismic data to obtain an improved 3D velocity model of the subsurface. We will use this improved model to relocate the larger of the newly detected MFP events using an advanced earthquake location technique. The proposed technique can determine the Bayesian errors in the locations. A previous study showed that new events in a traditional geothermal field were within the error bars of their master events. We aim to prove that the same is true in an EGS as well.

Additionally, we will use the improved 3D model to apply the model-based MFP technique to the Newberry site to determine if any small events occurred in the aseismic zone between the deep and shallow seismically active areas. The ability of the model-based method to produce robust results will depend on the resolution of the 3D velocity model.

6 References

Benson, G.D., M.H. Ritzwoller, M.P. Barmin, A.L. Levshin, F. Lin, M.P. Moschetti, N.M. Shapiro, and Y. Yang (2007). Processing seismic ambient noise data to obtain reliable broad-band surface wave dispersion measurements, Geophys. J. Int 169, 1239-1260

Eaton, J.P. (1975). Harmonic Magnification of the Complete Telemetered Seismic System, from Seismometer to Film Viewer Screen, U.S. Geol. Surv. Open-FileReport 75-99, 40 pages.

Healy, J.H. and M.E. O-Neill (1977). Calibration of Seismographic Systems: USGS Stations in the Central California Network, U.S. Geol. Surv. Open-File Report 77-736, 176 pages.

Scherbaum, F. (2001). Of Poles and Zeros: Fundamentals of Digital Seismology, Dordrecht: Kluwer Academic Publishers.

Appendix A

Conversion of Seismic Data From Raw Counts to Physical Units

Determine Form of Transfer Function

To account for the distortion that seismic recording systems necessarily introduce into the ground motion signals they are measuring, the Laplace transform is applied to the equation of motion for the seismometer. In general, the Laplace transform converts a function from the time-domain to the frequency-domain, where the equations become functions of the complex angular frequency, *s*. Conceptually, we see that the Laplace transform of the output recorded signal, Y(s), is equal to the Laplace transform of the input true ground signal, X(s), multiplied by the Laplace transform of the transfer function, T(s):

$$Y(s) = T(s)X(s)$$

This transfer function can be specified using a variety of different parameters. Here we describe the transfer function using the poles and zeros of the transfer function together with a gain factor. Assuming that the seismic sensor can be represented using a simple mass, spring, and dashpot system, the velocity transfer function for the velocity sensors in this study can be written in the form

$$T_{vel-rad}(s) = \frac{Y(s)}{X(s)} = -c_{vel}\frac{-s^2}{s^2 + 2\beta\omega_0 s + \omega_0^2}$$

where $T_{vel-rad}(s)$ is the velocity transfer function in units of radians, c_{vel} is the frequency independent scale factor for the velocity form in units of V/m/s, β is the sensor total damping constant in percent of critical, and ω_0 is the natural frequency of the seismometer in radians (Scherbaum, 2011). The frequency independent gain factor is sometimes also referred to as the scale factor and has units of the sensor output signal units divided by input signal units (e.g., V/m/s for a velocity sensor). The frequency dependent portion is dimensionless.

ω_0, in radians, can be calculated using the natural frequency of the sensor, f_0, in Hz using the simple relationship

$$\omega_0 = 2\pi f_0$$

The sensor toal damping constant, β, in units of percent of critical, is defined as

$$\beta = \beta_o + \beta_c$$

where β_o is the open circuit damping due to the mechanical properties of the sensor (usually provided on the sensor specification sheet) and β_c is the current damping due to the electrical properties of the sensor and datalogger. The current damping can be determined using

$$\beta_c = \frac{G_0^2}{2\omega_0 m R_t}$$

where G_0^2 is the instrinsic sensitivity of the velocity sensor in V/m/s (usually provided on the sensor specification sheet sheet), m is the mass of the sensor in kg (usually provided on the sensor specification sheet), and R_t is the total resistance of the entire system in ohms. The total resistance can be determined using

$$R_t = R_c + R_{load}$$

where R_c is the feedback coil resistance in ohms (usually provided on the sensor specification sheet), and R_{load} is the parallel sum of all the parallel resistors in the system (e.g., a shunt resistor, a preamplifier or resistor, and/or a datalogger, Z_{amp}). In this study there were no series resistors installed in the seismic system, so we will ignore any possible contribution from series resistors in this formulation.

We installed a parallel external damping resistor, R_s, between the GS-13 seismic sensors and the digitizers to attenuate the signal. The appropriate value of the resistor was determined by

$$R_{s-theoretical} = \frac{CDR}{0.7} - R_c$$

where *CDR* is the instrument critical damping resistance in ohms at 1.0 Hz (provided on the sensor specification sheet), R_c is the main coil resistance in ohms (provided on the sensor specification sheet), and 0.7 indicates our choice of relative damping value. The actual resistors, R_s, were fabricated in the laboratory for each station with values as close as possible to $R_{s-theoretical}$.

In general, R_{load} can be determined for an arbitrary number of parallel resistors using the relationship

$$\frac{1}{R_{load}} = \sum_{x=1}^{n} \frac{1}{R_x}$$

In the special case where there may be only two resistors (e.g., a damping resistor and a datalogger), the following much simpler formula to find the resistance value is often used

$$R_{load} = \frac{R_s \cdot Z_{amp}}{R_s + Z_{amp}}$$

In the special case where there may be only one resistor (e.g., only a datalogger), R_{load} simplifies to

$$R_{load} = Z_{amp}$$

For passive electrodynamic sensors, the input impedance of the datalogger should be at least 2 orders of magnitude larger than the total resistance of the disconnected sensor. If this is true, then the datalogger will not significantly influence the sensor electronics or change the damping and sensor poles (IRISa, 2013). This is not an issue for active sensors since the input impedance of the recording device does not influence the sensor's characteristics (Asch, 2009).

Determine Poles and Zeros of Transfer Function

The poles of the transfer function are determined from the roots of the *T(s)* denominator. The zeros of the transfer function are the zeros in the T(s) numerator. In this case, we can see that for the velocity transfer function $T_{vel-rad}(s)$ there are two zeros at zero and for the displacement function $T_{disp-rad}(s)$ there are three zeros at zero.

For the underdamped case ($\beta < 1$), the poles for both velocity and displacement become

$$p_{1,2} = -\beta\omega_0 \pm i\omega_0\sqrt{1-\beta^2}$$

where ω_0 is again the undamped seismometer eigenfrequency in radians and β the total sensor damping constant (Scherbaum, 2001).

Determine the Pole-Zero Constant

The pole-zero constants can be determined using

$$CONSTANT_{vel-rad} = A0_{vel-rad} * G_s * G_d$$

where $A0_{vel-rad}$ is the velocity normalization factors. The sensor gain, G_s, describes the effective sensitivity of the sensor. The digitizer gain, G_d, describes the sensitivity of the digitizer, in units of counts/V.

To determine the *A0* constant, we must define the relationship between the output (counts) of the seismic recording system and the input (ground motion). To do so we evaluate the complex angular frequency of the transfer functions on the imaginary axis such that

$$s = i\omega$$

to determine the velocity frequency response function

$$T_{vel-rad}(i\omega) = C_{vel-rad}F_{vel-rad}(i\omega) = C_{vel-rad}\frac{(i\omega)^2}{(i\omega)^2 + 2\beta\omega_0(i\omega) + (\omega_0)^2}$$

The normalization factors are calculated such that the modulus of the frequency-dependent $F(i\omega)$ term, in the frequency response function, multiplied by the *A0* factor is unity at the calibration frequency ω_c, or

$$A0_{vel-rad} = \frac{1}{|F_{vel-rad}(i\omega_c)|}$$

The calibration frequency, ω_c, should be within the passband of the instrument. The units of ω_c are in radians.

To determine G_s, the effect of additional resistors and the datalogger on the seismometer's generator constant, G_0, is taken into account such that

$$G_s = \frac{G_0 R_{load}}{R_t}$$

(Eaton, 1975; Healy and O'Neil, 1977).

The digitizer gain, G_d, can be determined by taking the inverse of the digitizer's bit weight, *BW,* which is in units of V/counts (sometimes provided on the digitizer calibration sheets or log files). The BW is essentially equivalent to the digitizer's least significant bit (LSB). The LSB is defined as the voltage per count.

If a gain is set on the digitizer, the effective LSB can be calculated using

$$LSB_{eff} = \frac{LSB}{GAIN}$$

Conversion Between Hz and Radian

Often sensor data sheets will have calibrated pole-zero and A0 information for each individual sensor on the sensor specification sheet. If the values are given in Hz, the values can be converted to radians using

$$Pole_{rad} = Pole_{Hz} \cdot (2\pi)$$
$$Zero_{rad} = Zero_{Hz} \cdot (2\pi)$$

$$A0_{rad} = A0_{Hz} * (2\pi)^{np-nz}$$

where np is the number of poles and nz is the number of zeros.

Seismic System Parameters

Parameter	Value
f_0	2.0 Hz
G_{0-avg}	78.74 V/m/s
m	0.023 kg
β_{0-avg}	0.61
R_{c-avg}	3800 Ω
R_s	0 Ω
$Z_{amp-HS1-S24}$	250,000 Ω
GAIN	8

Table 1. HS-1-LT geophone sensor specifications. Average values are listed by the subscript avg. These average values are input into the actual calculations since sensor specification sheets were not available for these instruments. f_0 = natural frequency of the sensor, G_0 = intrinsic sensitivity of the sensor (often also called the main coil generator constant), m = internal mass, β_0 = open circuit damping, R_c = main coil resistance, R_s = external damping resistor, $Z_{amp-HS1-S24}$ = SMART-24 datalogger input resistance, and *GAIN* = digitizer gain.

Parameter	Value
f_0	1.0 Hz
G_{0-avg}	2300 V/m/s
m	5 kg
β_{0-avg}	0.01
R_{c-avg}	9200 Ω
R_{s-avg}	111K Ω
$Z_{amp-GS13-S24}$	2M Ω
$Z_{amp-DM24}$	1M Ω
GAIN	1

Table 2. Sensor and digitizer specifications for sites with GS-13 sensors. Average values are indicated by the subscript *avg*, and are listed for informational purposes only. The true values from the sensor specification sheets are input into the actual calculations. f_0 = natural frequency of the sensor, G_0 = intrinsic sensitivity of the sensor (often also called the main coil generator constant), m = internal mass, β_0 = open circuit damping, R_c = main coil resistance, R_s = external damping resistor, $Z_{amp-GS13-S24}$ = SMART-24 datalogger input resistance, $Z_{amp-DM24}$ = DM24-S3 datalogger input resistance, and *GAIN* = digitizer gain.

Appendix B

List of Master Events

Date (UTC)	Time (UTC)	Latitude	Longitude	Depth AMSL (km)	Magnitude (Mw)
2012/10/31	02:13:05.23	43.7271	121.3093	0.88	0.81
2012/10/31	03:58:01.23	43.7261	121.3077	0.86	0.60
2012/10/31	17:31:25.33	43.7283	121.3091	0.91	1.51
2012/11/01	06:46:36.25	43.7271	121.3099	0.77	0.71
2012/11/01	13:38:26.95	43.7266	121.3130	-0.33	0.75
2012/11/01	20:48:36.26	43.7282	121.3091	0.95	1.25
2012/11/02	08:51:15.90	43.7256	121.3072	0.02	1.23
2012/11/02	12:19:11.30	43.7294	121.3143	-0.85	1.02
2012/11/04	01:57:21.95	43.7266	121.3143	-0.56	0.72
2012/11/04	19:03:09.89	43.7308	121.3114	-0.50	0.76
2012/11/09	10:30:33.30	43.7222	121.3180	-0.57	0.83
2012/11/10	18:25:56.04	43.7276	121.3100	-0.72	1.21
2012/11/11	04:13:18.52	43.7271	121.3122	-0.92	0.87
2012/11/11	04:17:36.46	43.7286	121.3077	-0.37	0.70
2012/11/13	16:50:34.91	43.7232	121.3137	-0.71	1.16
2012/11/14	04:27:55.59	43.7258	121.3123	-0.52	0.76
2012/11/14	07:37:01.95	43.7308	121.3092	-0.78	0.65
2012/11/17	00:18:25.37	43.7259	121.3113	-0.36	0.63
2012/11/17	07:04:55.84	43.7219	121.3142	-0.46	1.36
2012/11/18	13:45:40.33	43.8058	121.3110	2.02	2.05
2012/11/18	17:49:06.97	43.8081	121.3118	2.13	1.88
2012/11/21	05:56:42.95	43.7208	121.3154	-0.89	0.88
2012/11/27	11:35:06.79	43.7318	121.3203	-0.87	0.76
2012/11/29	09:31:09.96	43.7300	121.2988	-1.70	1.07
2012/11/29	20:29:23.62	43.7208	121.3142	-0.79	1.34
2012/11/29	20:31:23.47	43.7271	121.3175	-0.70	2.04

2012/12/01	00:42:50.09	43.7290	121.3126	-0.90	0.85
2012/12/01	21:20:48.34	43.7266	121.3145	-1.03	0.81
2012/12/01	21:56:55.84	43.7260	121.3175	-0.45	1.16
2012/12/01	22:40:19.55	43.7272	121.3176	-0.50	1.45
2012/12/01	22:45:22.12	43.7271	121.3170	-0.67	1.85
2012/12/01	23:23:46.23	43.7258	121.3177	-0.74	0.85
2012/12/02	00:07:44.00	43.7277	121.3133	-0.77	0.93
2012/12/02	01:58:48.03	43.7272	121.3098	0.70	0.71
2012/12/02	04:24:39.86	43.7270	121.3087	0.69	0.78
2012/12/02	14:04:22.41	43.7222	121.3150	-0.81	0.91
2012/12/02	22:37:35.00	43.7270	121.3174	-0.48	1.33
2012/12/02	23:01:44.79	43.7207	121.3181	-0.61	1.17
2012/12/03	03:53:51.03	43.7212	121.3143	-0.83	1.06
2012/12/03	04:19:00.29	43.7264	121.3153	-0.57	0.95
2012/12/03	08:17:57.40	43.7279	121.3127	-0.56	1.52
2012/12/03	11:48:36.38	43.7266	121.3173	-0.79	0.62
2012/12/03	13:50:52.10	43.7229	121.3170	-0.45	0.77
2012/12/03	21:15:49.33	43.7265	121.3151	-0.89	0.74
2012/12/05	09:23:40.64	43.7263	121.3115	-0.74	1.35
2012/12/05	11:19:29.40	43.7268	121.3096	-0.70	1.08
2012/12/05	11:44:02.80	43.7275	121.3076	-0.56	0.58
2012/12/05	16:02:12.01	43.7257	121.3105	0.98	1.06
2012/12/05	19:06:34.46	43.7238	121.3123	-0.38	1.60
2012/12/07	01:28:51.28	43.7321	121.3092	-1.08	0.57
2012/12/07	04:22:57.30	43.7317	121.3087	-1.00	0.54
2012/12/07	09:34:38.47	43.7220	121.3171	-0.91	0.95
2012/12/07	16:25:15.69	43.7229	121.3171	-0.53	2.39
2012/12/07	16:41:58.16	43.7234	121.3171	-1.15	1.82
2012/12/07	18:12:06.15	43.7225	121.3179	-0.70	0.89
2012/12/07	18:15:09.54	43.7229	121.3171	-0.63	1.64
2012/12/08	03:40:51.72	43.7240	121.3113	-0.47	1.21
2012/12/08	03:41:53.78	43.7244	121.3104	-0.59	1.04

2012/12/08	23:46:57.83	43.7260	121.3113	-0.48	0.42
2012/12/09	08:07:06.37	43.7267	121.3119	-0.56	0.45
2012/12/09	13:42:39.74	43.7306	121.3144	-0.57	1.50
2012/12/09	16:15:18.45	43.7219	121.3142	-0.64	1.36
2012/12/09	22:19:38.60	43.7218	121.3159	-0.32	1.07
2012/12/10	11:14:37.37	43.7213	121.3144	-0.61	1.07
2012/12/11	02:57:04.58	43.7302	121.3151	-0.75	1.17
2012/12/11	07:09:13.66	43.7366	121.2365	2.09	1.14
2012/12/12	05:08:56.09	43.7220	121.3191	-0.70	0.87
2012/12/12	06:45:15.75	43.7205	121.3157	-0.30	1.05
2012/12/12	21:53:56.46	43.7315	121.3091	-0.94	1.25
2012/12/19	14:41:51.66	43.7305	121.3130	-0.50	2.34
2012/12/19	14:50:23.56	43.7307	121.3131	-0.40	2.01
2012/12/20	09:27:39.55	43.7278	121.3165	-0.52	2.07
2012/12/20	14:03:32.83	43.7316	121.3086	-0.98	1.57
2012/12/21	00:06:06.27	43.7357	121.3100	-0.99	1.44
2012/12/24	00:33:57.57	43.7235	121.3164	-0.71	1.71

Appendix C

Catalog of New Events with Preliminary Locations

Date (UTC)	Time (UTC)	Latitude	Longitude	Depth AMSL (km)	Magnitude	
10/01/12	09:27.9	43.7316	-121.3086	0.79	0.83	Md
10/20/12	33:22.4	43.7306	-121.3144	1.20	0.02	Md
10/29/12	02:21.2	43.7283	-121.3095	2.66	0.83	Mw
10/30/12	17:53.5	43.7271	-121.3093	2.65	0.53	Md
10/31/12	53:25.2	43.7357	-121.3100	0.78	0.29	Md
10/31/12	49:31.6	43.7257	-121.3105	2.75	0.23	Md
10/31/12	41:29.4	43.7282	-121.3091	2.72	0.29	Md
10/31/12	06:37.3	43.7261	-121.3077	2.63	0.33	Md
10/31/12	08:58.4	43.7282	-121.3091	2.72	0.45	Md
10/31/12	27:29.3	43.7266	-121.3130	1.44	0.33	Md
10/31/12	13:05.2	43.7271	-121.3093	2.65	0.81	Mw
10/31/12	58:01.2	43.7261	-121.3077	2.63	0.6	Mw
10/31/12	31:25.3	43.7283	-121.3091	2.68	1.51	Mw
11/01/12	57:38.4	43.7282	-121.3091	2.72	0.39	Md
11/01/12	06:37.5	43.7271	-121.3093	2.65	0.34	Md
11/01/12	31:49.6	43.7271	-121.3099	2.54	0.43	Md
11/01/12	13:14.4	43.7306	-121.3144	1.20	0.45	Md
11/01/12	31:16.4	43.7308	-121.3114	1.27	0.66	Md
11/01/12	46:36.2	43.7271	-121.3099	2.54	0.71	Mw
11/01/12	06:59.1	43.7270	-121.3119	1.67	0.46	Mw
11/01/12	07:08.6	43.7287	-121.3133	1.05	0.79	Mw
11/01/12	07:20.0	43.7286	-121.3119	1.12	0.43	Mw
11/01/12	07:35.5	43.7305	-121.3119	1.26	0.65	Mw
11/01/12	38:26.9	43.7266	-121.3130	1.44	0.75	Mw

11/01/12	48:36.3	43.7282	-121.3091	2.72	1.25	Mw
11/01/12	54:20.2	43.7291	-121.3129	1.43	0.65	Mw
11/02/12	12:26.1	43.7290	-121.3126	0.87	0.53	Md
11/02/12	26:38.4	43.7306	-121.3144	1.20	0.17	Md
11/02/12	46:22.5	43.7302	-121.3151	1.02	0.29	Md
11/02/12	51:15.9	43.7256	-121.3072	1.79	1.23	Mw
11/02/12	22:03.8	43.7359	-121.3136	1.27	1.26	Mw
11/02/12	37:38.2	43.7300	-121.3130	1.35	0.81	Mw
11/02/12	19:11.3	43.7294	-121.3143	0.92	1.02	Mw
11/03/12	37:24.4	43.7306	-121.3144	1.20	0.23	Md
11/03/12	34:14.9	43.7283	-121.3112	1.25	0.6	Mw
11/03/12	44:31.7	43.7265	-121.3147	0.13	0.68	Mw
11/03/12	44:37.4	43.7261	-121.3144	0.79	1.03	Mw
11/04/12	57:22.0	43.7266	-121.3143	1.21	0.72	Mw
11/04/12	03:09.9	43.7308	-121.3114	1.27	0.76	Mw
11/05/12	59:46.7	43.7267	-121.3119	1.21	0.47	Md
11/05/12	59:57.7	43.7267	-121.3119	1.21	0.17	Md
11/05/12	00:20.7	43.7267	-121.3119	1.21	0.46	Md
11/06/12	34:22.4	43.7317	-121.3087	0.77	0.47	Md
11/07/12	52:29.1	43.7267	-121.3090	1.19	0.34	Mw
11/09/12	36:19.8	43.7271	-121.3122	0.85	0.1	Md
11/09/12	35:17.5	43.7259	-121.3113	1.41	0.38	Md
11/09/12	30:33.3	43.7222	-121.3180	1.20	0.83	Mw
11/10/12	25:56.0	43.7276	-121.3100	1.05	1.21	Mw
11/10/12	39:09.9	43.7280	-121.3085	1.10	0.52	Mw
11/11/12	13:18.5	43.7271	-121.3122	0.85	0.87	Mw
11/11/12	17:36.5	43.7286	-121.3077	1.40	0.7	Mw
11/12/12	46:38.5	43.7275	-121.3076	1.21	0.24	Md
11/12/12	25:32.4	43.7260	-121.3113	1.29	0.57	Md
11/12/12	59:46.4	43.7232	-121.3137	1.06	0.48	Md

11/12/12	41:23.7	43.7267	-121.3119	1.21	0.52	Md
11/12/12	02:14.4	43.7165	-121.3164	1.60	0.42	Mw
11/12/12	02:17.3	43.7208	-121.3138	1.20	1.15	Mw
11/13/12	09:05.5	43.7258	-121.3123	1.25	0.35	Md
11/13/12	50:34.9	43.7232	-121.3137	1.06	1.16	Mw
11/13/12	16:31.2	43.7275	-121.3077	1.09	0.63	Mw
11/14/12	27:55.6	43.7258	-121.3123	1.25	0.76	Mw
11/14/12	37:01.9	43.7308	-121.3092	0.99	0.65	Mw
11/14/12	44:53.5	43.7255	-121.3094	1.36	0.39	Mw
11/15/12	27:36.6	43.7263	-121.3115	1.03	0.24	Md
11/15/12	23:27.5	43.7314	-121.3107	0.60	0.7	Mw
11/16/12	26:17.6	43.7230	-121.3174	0.33	1.07	Mw
11/16/12	26:26.6	43.7223	-121.3167	0.24	0.89	Mw
11/16/12	25:50.7	43.7262	-121.3133	1.09	0.84	Mw
11/16/12	26:10.6	43.7263	-121.3132	0.87	0.72	Mw
11/16/12	26:25.8	43.7255	-121.3064	1.28	0.52	Mw
11/17/12	13:52.9	43.7268	-121.3096	1.07	0.3	Md
11/17/12	48:34.5	43.7275	-121.3076	1.21	0.19	Md
11/17/12	18:25.4	43.7259	-121.3113	1.41	0.63	Mw
11/17/12	18:47.2	43.7261	-121.3123	0.73	0.32	Mw
11/17/12	40:49.8	43.7262	-121.3067	0.92	0.47	Mw
11/17/12	40:51.3	43.7264	-121.3044	1.50	0.68	Mw
11/17/12	04:55.8	43.7219	-121.3142	1.31	1.36	Mw
11/17/12	46:15.1	43.7256	-121.3118	1.20	0.48	Mw
11/17/12	46:18.1	43.7250	-121.3103	1.22	1.26	Mw
11/18/12	04:26.4	43.7253	-121.3109	1.12	0.71	Mw
11/18/12	45:40.3	43.8058	-121.3110	3.79	2.05	Mw
11/18/12	49:07.0	43.8081	-121.3118	3.90	1.88	Mw
11/19/12	08:00.5	43.7258	-121.3123	1.25	0.16	Md
11/19/12	10:22.5	43.7258	-121.3123	1.25	0.58	Md

11/19/12	13:29.5	43.7258	-121.3123	1.25	0.26	Md
11/19/12	17:03.4	43.7260	-121.3113	1.29	0.54	Md
11/19/12	12:02.5	43.7251	-121.3100	1.57	0.73	Mw
11/20/12	41:24.5	43.7258	-121.3123	1.25	0.3	Md
11/20/12	09:33.5	43.7229	-121.3171	1.24	0.41	Md
11/20/12	39:06.9	43.7265	-121.3081	1.30	0.85	Mw
11/20/12	12:39.9	43.7284	-121.3112	1.39	0.45	Mw
11/21/12	56:42.9	43.7208	-121.3154	0.88	0.88	Mw
11/26/12	05:59.5	43.7267	-121.3148	0.78	0.14	Mw
11/26/12	06:02.6	43.7270	-121.3142	1.01	0.39	Mw
11/26/12	43:02.1	43.7280	-121.3112	1.35	0.42	Mw
11/26/12	43:13.9	43.7271	-121.3103	0.76	0.31	Mw
11/27/12	35:06.8	43.7318	-121.3203	0.90	0.76	Mw
11/28/12	54:47.7	43.7219	-121.3142	1.13	0.42	Md
11/29/12	39:06.1	43.7270	-121.3087	2.46	0.46	Md
11/29/12	31:10.0	43.7300	-121.2988	0.07	1.07	Mw
11/29/12	29:23.6	43.7208	-121.3142	0.98	1.34	Mw
11/29/12	31:23.5	43.7271	-121.3175	1.07	2.04	Mw
11/30/12	43:47.6	43.7271	-121.3099	2.54	0.43	Md
11/30/12	55:55.5	43.7272	-121.3176	1.27	0.43	Md
11/30/12	18:38.8	43.7266	-121.3145	0.74	0.1	Md
11/30/12	48:52.6	43.7308	-121.3092	0.99	0.11	Md
11/30/12	38:37.3	43.7303	-121.3116	0.94	0.5	Mw
11/30/12	08:56.8	43.7259	-121.3174	0.85	0.59	Mw
11/30/12	26:51.3	43.7295	-121.3099	1.62	0.52	Mw
11/30/12	07:14.9	43.7266	-121.3177	0.96	0.86	Mw
12/01/12	41:34.1	43.7270	-121.3087	2.46	0.21	Md
12/01/12	18:59.9	43.7271	-121.3170	1.10	0.54	Md
12/01/12	25:38.5	43.7258	-121.3123	1.25	0.22	Md
12/01/12	39:36.4	43.7282	-121.3091	2.72	0.26	Md

12/01/12	39:50.5	43.7271	-121.3093	2.65	0.55	Md
12/01/12	03:17.5	43.7258	-121.3123	1.25	0.31	Md
12/01/12	19:58.5	43.7258	-121.3123	1.25	0.11	Md
12/01/12	26:15.7	43.7267	-121.3119	1.21	0.33	Md
12/01/12	28:29.7	43.7267	-121.3119	1.21	0.6	Md
12/01/12	33:04.4	43.7308	-121.3114	1.27	0.21	Md
12/01/12	18:12.8	43.7279	-121.3092	2.19	0.53	Mw
12/01/12	42:50.1	43.7290	-121.3126	0.87	0.85	Mw
12/01/12	20:25.3	43.7276	-121.3102	1.09	0.59	Mw
12/01/12	18:04.9	43.7292	-121.3133	0.86	0.52	Mw
12/01/12	20:48.3	43.7266	-121.3145	0.74	0.81	Mw
12/01/12	56:55.8	43.7260	-121.3175	1.32	1.16	Mw
12/01/12	40:19.6	43.7272	-121.3176	1.27	1.45	Mw
12/01/12	45:22.1	43.7271	-121.3170	1.10	1.85	Mw
12/01/12	23:46.2	43.7258	-121.3177	1.03	0.85	Mw
12/02/12	09:33.1	43.7290	-121.3126	0.87	0.66	Md
12/02/12	33:59.5	43.7258	-121.3123	1.25	0.7	Md
12/02/12	07:44.0	43.7277	-121.3133	1.00	0.93	Mw
12/02/12	58:48.0	43.7272	-121.3098	2.47	0.71	Mw
12/02/12	18:01.6	43.7264	-121.3119	1.26	0.43	Mw
12/02/12	24:39.9	43.7270	-121.3087	2.46	0.78	Mw
12/02/12	04:22.4	43.7222	-121.3150	0.96	0.91	Mw
12/02/12	04:25.9	43.7258	-121.3028	1.51	0.57	Mw
12/02/12	33:35.9	43.7259	-121.3090	1.09	0.72	Mw
12/02/12	37:35.0	43.7270	-121.3174	1.29	1.33	Mw
12/02/12	01:44.8	43.7207	-121.3181	1.16	1.17	Mw
12/03/12	04:44.6	43.7257	-121.3105	2.75	0.34	Md
12/03/12	13:42.4	43.7282	-121.3091	2.72	0.21	Md
12/03/12	14:51.4	43.7283	-121.3091	2.68	0.44	Md
12/03/12	53:51.0	43.7212	-121.3143	0.94	1.06	Mw

12/03/12	19:00.3	43.7264	-121.3153	1.20	0.95	Mw
12/03/12	17:57.4	43.7279	-121.3127	1.21	1.52	Mw
12/03/12	28:13.0	43.7224	-121.3127	1.54	0.53	Mw
12/03/12	52:24.1	43.7215	-121.3149	1.04	0.59	Mw
12/03/12	48:36.4	43.7266	-121.3173	0.98	0.62	Mw
12/03/12	50:52.1	43.7229	-121.3170	1.32	0.77	Mw
12/03/12	59:58.9	43.7281	-121.3094	2.54	0.83	Mw
12/03/12	52:18.7	43.7223	-121.3144	0.75	0.69	Mw
12/03/12	10:22.2	43.7268	-121.3090	2.49	0.74	Mw
12/03/12	15:49.3	43.7265	-121.3151	0.88	0.74	Mw
12/03/12	55:11.8	43.7212	-121.3154	0.97	0.67	Mw
12/04/12	05:48.8	43.7222	-121.3180	1.20	0.22	Md
12/04/12	26:38.3	43.7357	-121.3100	0.78	0.21	Md
12/04/12	50:46.1	43.7271	-121.3150	1.25	1.24	Mw
12/04/12	37:12.2	43.7234	-121.3161	1.12	1.04	Mw
12/04/12	30:47.7	43.7228	-121.3170	1.07	0.66	Mw
12/05/12	18:18.5	43.7275	-121.3076	1.21	0.72	Md
12/05/12	11:13.1	43.7231	-121.3178	1.07	1.17	Mw
12/05/12	23:40.6	43.7263	-121.3115	1.03	1.35	Mw
12/05/12	18:37.1	43.7268	-121.3056	1.56	0.92	Mw
12/05/12	19:29.4	43.7268	-121.3096	1.07	1.08	Mw
12/05/12	43:21.1	43.7276	-121.3109	1.11	1.01	Mw
12/05/12	44:02.8	43.7275	-121.3076	1.21	0.58	Mw
12/05/12	02:12.0	43.7257	-121.3105	2.75	1.06	Mw
12/05/12	06:34.5	43.7238	-121.3123	1.39	1.6	Mw
12/05/12	02:02.7	43.7227	-121.3187	0.97	1.05	Mw
12/06/12	44:50.8	43.7548	-121.2115	7.88	1.75	Mw
12/06/12	26:42.8	43.7271	-121.3094	2.50	0.55	Mw
12/06/12	39:52.4	43.7270	-121.3098	2.42	0.41	Mw
12/06/12	27:30.1	43.7281	-121.3191	0.74	0.59	Mw

12/06/12	18:46.9	43.7258	-121.3115	1.29	0.65	Mw
12/06/12	20:46.9	43.7261	-121.3106	0.96	0.7	Mw
12/06/12	23:45.2	43.7260	-121.3125	1.02	0.49	Mw
12/06/12	55:33.4	43.7274	-121.3159	0.47	0.69	Mw
12/06/12	27:23.3	43.7238	-121.3119	1.13	0.5	Mw
12/07/12	48:37.6	43.7257	-121.3105	2.75	0.45	Md
12/07/12	14:06.5	43.7321	-121.3092	0.69	0.73	Md
12/07/12	28:17.2	43.7234	-121.3171	0.62	0.62	Md
12/07/12	27:09.7	43.7229	-121.3171	1.14	0.26	Md
12/07/12	29:27.7	43.7218	-121.3159	1.45	0.76	Md
12/07/12	49:28.5	43.7271	-121.3093	2.65	0.51	Md
12/07/12	11:39.4	43.7260	-121.3113	1.29	0.86	Md
12/07/12	11:56.4	43.7306	-121.3144	1.20	0.61	Md
12/07/12	30:50.1	43.7276	-121.3100	1.05	0.76	Md
12/07/12	55:02.3	43.7208	-121.3154	0.88	0.79	Md
12/07/12	28:51.3	43.7321	-121.3092	0.69	0.57	Mw
12/07/12	22:57.3	43.7317	-121.3087	0.77	0.54	Mw
12/07/12	19:41.0	43.7293	-121.3119	1.25	0.33	Mw
12/07/12	20:05.6	43.7284	-121.3106	1.73	0.46	Mw
12/07/12	34:38.5	43.7220	-121.3171	0.86	0.95	Mw
12/07/12	25:12.5	43.7227	-121.3178	0.92	1.15	Mw
12/07/12	25:15.7	43.7229	-121.3171	1.24	2.39	Mw
12/07/12	26:32.6	43.7223	-121.3175	0.86	0.61	Mw
12/07/12	41:58.2	43.7234	-121.3171	0.62	1.82	Mw
12/07/12	08:46.9	43.7263	-121.3089	2.31	0.66	Mw
12/07/12	20:25.4	43.7232	-121.3168	0.90	0.57	Mw
12/07/12	21:37.6	43.7258	-121.3209	1.04	0.71	Mw
12/07/12	56:49.4	43.7213	-121.3183	1.02	0.74	Mw
12/07/12	12:06.2	43.7225	-121.3179	1.07	0.89	Mw
12/07/12	12:46.2	43.7223	-121.3177	1.22	0.72	Mw

12/07/12	15:09.5	43.7229	-121.3171	1.14	1.64	Mw
12/07/12	15:39.9	43.7225	-121.3175	1.36	0.73	Mw
12/07/12	17:14.2	43.7223	-121.3169	0.98	0.56	Mw
12/07/12	07:03.2	43.7271	-121.3068	0.81	0.45	Mw
12/07/12	55:26.3	43.7278	-121.3119	1.12	0.71	Mw
12/08/12	46:31.4	43.7306	-121.3144	1.20	0.18	Md
12/08/12	20:42.2	43.7234	-121.3171	0.62	0.9	Md
12/08/12	58:33.9	43.7222	-121.3180	1.20	0.6	Md
12/08/12	34:47.8	43.7238	-121.3123	1.39	0.91	Md
12/08/12	42:29.8	43.7238	-121.3123	1.39	0.54	Md
12/08/12	28:53.8	43.7238	-121.3123	1.39	0.79	Md
12/08/12	06:28.7	43.7219	-121.3142	1.13	0.64	Md
12/08/12	16:10.7	43.7267	-121.3119	1.21	0.84	Md
12/08/12	07:42.4	43.7308	-121.3114	1.27	0.2	Md
12/08/12	20:36.7	43.7267	-121.3119	1.21	0.89	Md
12/08/12	30:51.4	43.7308	-121.3114	1.27	0.43	Md
12/08/12	00:07.6	43.7307	-121.3131	1.37	0.59	Md
12/08/12	40:51.7	43.7240	-121.3113	1.30	1.21	Mw
12/08/12	41:53.8	43.7244	-121.3104	1.18	1.04	Mw
12/08/12	46:57.8	43.7260	-121.3113	1.29	0.42	Mw
12/09/12	38:54.4	43.7306	-121.3144	1.20	0.76	Md
12/09/12	43:04.4	43.7308	-121.3114	1.27	0.07	Md
12/09/12	57:30.4	43.7306	-121.3144	1.20	0.64	Md
12/09/12	37:15.7	43.7229	-121.3171	1.14	0.61	Md
12/09/12	25:00.5	43.7229	-121.3171	1.24	0.39	Md
12/09/12	29:15.2	43.7234	-121.3171	0.62	0.76	Md
12/09/12	34:54.4	43.7306	-121.3144	1.20	0.56	Md
12/09/12	07:06.4	43.7267	-121.3119	1.21	0.45	Mw
12/09/12	42:39.7	43.7306	-121.3144	1.20	1.5	Mw
12/09/12	15:18.5	43.7219	-121.3142	1.13	1.36	Mw

12/09/12	19:38.6	43.7218	-121.3159	1.45	1.07	Mw
12/10/12	09:45.7	43.7219	-121.3142	1.13	0.71	Md
12/10/12	08:00.5	43.7243	-121.3158	1.14	0.43	Mw
12/10/12	14:37.4	43.7213	-121.3144	1.16	1.07	Mw
12/10/12	57:46.4	43.7326	-121.3119	0.75	0.32	Mw
12/10/12	10:10.9	43.7189	-121.3144	0.94	0.49	Mw
12/10/12	44:16.3	43.7204	-121.3193	0.88	1.42	Mw
12/11/12	28:45.5	43.7220	-121.3191	1.07	0.44	Md
12/11/12	57:04.6	43.7302	-121.3151	1.02	1.17	Mw
12/11/12	09:13.7	43.7366	-121.2365	3.86	1.14	Mw
12/11/12	24:04.7	43.7253	-121.3091	0.22	0.36	Mw
12/11/12	04:20.5	43.7187	-121.3146	0.95	0.53	Mw
12/11/12	05:57.4	43.7194	-121.3150	0.48	0.65	Mw
12/12/12	08:56.1	43.7220	-121.3191	1.07	0.87	Mw
12/12/12	45:15.7	43.7205	-121.3157	1.47	1.05	Mw
12/12/12	53:56.5	43.7315	-121.3091	0.83	1.25	Mw
12/13/12	38:26.4	43.7306	-121.3144	1.20	0.6	Md
12/13/12	51:19.0	43.7214	-121.3157	1.02	0.41	Mw
12/14/12	04:43.8	43.7218	-121.3187	0.83	0.67	Mw
12/14/12	55:56.9	43.7218	-121.3189	0.84	0.63	Mw
12/14/12	02:01.2	43.7256	-121.3197	0.75	0.49	Mw
12/15/12	43:59.4	43.7308	-121.3114	1.27	0.21	Md
12/15/12	24:31.2	43.7357	-121.3100	0.78	0.4	Md
12/15/12	00:53.8	43.7264	-121.3153	1.20	0.86	Md
12/15/12	59:02.5	43.7278	-121.3165	1.25	0.21	Md
12/16/12	18:00.5	43.7220	-121.3191	1.07	0.3	Md
12/16/12	19:00.5	43.7220	-121.3191	1.07	0.21	Md
12/17/12	41:34.5	43.7229	-121.3171	1.24	0.1	Md
12/17/12	41:35.3	43.7208	-121.3154	0.88	0.18	Md
12/17/12	27:39.5	43.7220	-121.3191	1.07	0.5	Md

12/17/12	28:22.5	43.7220	-121.3191	1.07	0.72	Md
12/17/12	41:25.4	43.7306	-121.3144	1.20	0.6	Md
12/17/12	55:32.8	43.7264	-121.3153	1.20	0.95	Md
12/17/12	56:50.4	43.7317	-121.3087	0.77	0.65	Md
12/18/12	53:07.4	43.7308	-121.3114	1.27	0.14	Md
12/18/12	46:56.1	43.7229	-121.3170	1.32	0.32	Md
12/18/12	18:26.4	43.7306	-121.3144	1.20	0.39	Md
12/18/12	58:14.4	43.7306	-121.3144	1.20	0.28	Md
12/18/12	58:38.4	43.7306	-121.3144	1.20	0.79	Md
12/18/12	39:50.4	43.7306	-121.3144	1.20	0.63	Md
12/18/12	52:00.5	43.7321	-121.3092	0.69	0.28	Md
12/18/12	00:08.6	43.7307	-121.3131	1.37	1.26	Md
12/18/12	18:26.5	43.7305	-121.3130	1.27	0.59	Md
12/19/12	29:46.2	43.7357	-121.3100	0.78	0.26	Md
12/19/12	32:25.5	43.7305	-121.3130	1.27	0.18	Md
12/19/12	35:38.4	43.7306	-121.3144	1.20	0.15	Md
12/19/12	54:01.5	43.7220	-121.3191	1.07	0.22	Md
12/19/12	44:51.5	43.7305	-121.3130	1.27	-0.19	Md
12/19/12	59:47.6	43.7307	-121.3131	1.37	0.14	Md
12/19/12	01:15.2	43.7357	-121.3100	0.78	0.78	Md
12/19/12	20:53.5	43.7305	-121.3130	1.27	0.8	Md
12/19/12	49:55.5	43.7305	-121.3130	1.27	0.37	Md
12/19/12	32:00.4	43.7308	-121.3114	1.27	0.26	Md
12/19/12	58:00.2	43.7357	-121.3100	0.78	0.16	Md
12/19/12	29:06.6	43.7307	-121.3131	1.37	0.25	Md
12/19/12	41:51.7	43.7305	-121.3130	1.27	2.34	Mw
12/19/12	50:23.6	43.7307	-121.3131	1.37	2.01	Mw
12/20/12	27:16.9	43.7316	-121.3086	0.79	0.46	Md
12/20/12	31:31.9	43.7316	-121.3086	0.79	0.21	Md
12/20/12	52:31.9	43.7316	-121.3086	0.79	0.13	Md

12/20/12	25:52.4	43.7306	-121.3144	1.20	0.24	Md
12/20/12	51:50.5	43.7220	-121.3191	1.07	0.21	Md
12/20/12	27:39.6	43.7278	-121.3165	1.25	2.07	Mw
12/20/12	03:32.8	43.7316	-121.3086	0.79	1.57	Mw
12/21/12	06:43.4	43.7308	-121.3114	1.27	0.32	Md
12/21/12	09:18.2	43.7357	-121.3100	0.78	0.72	Md
12/21/12	06:06.3	43.7357	-121.3100	0.78	1.44	Mw
12/21/12	19:18.8	43.7212	-121.3190	0.91	2.32	Mw
12/21/12	20:52.2	43.7214	-121.3183	0.90	1.29	Mw
12/21/12	20:52.2	43.7208	-121.3183	0.59	1.41	Mw
12/21/12	20:42.7	43.7273	-121.3109	1.22	1.49	Mw
12/22/12	10:29.9	43.7306	-121.3144	1.17	1.66	Mw
12/22/12	40:36.5	43.7191	-121.3163	-0.05	1.15	Mw
12/22/12	03:13.9	43.7219	-121.3153	1.31	1.76	Mw
12/22/12	55:29.2	43.7302	-121.3119	0.88	1.1	Mw
12/22/12	44:54.9	43.7232	-121.3179	0.69	1.07	Mw
12/22/12	52:24.5	43.7221	-121.3178	0.66	1.91	Mw
12/22/12	06:10.9	43.7258	-121.3205	1.54	1.54	Mw
12/22/12	07:24.3	43.7264	-121.3177	1.12	1.43	Mw
12/24/12	33:57.6	43.7235	-121.3164	1.06	1.71	Mw
12/24/12	47:49.5	43.7298	-121.3119	1.30	1.46	Mw
12/25/12	59:07.9	43.7278	-121.3172	1.18	1.81	Mw
12/26/12	04:24.6	43.7332	-121.3127	1.11	0.83	Mw
12/26/12	39:21.0	43.7282	-121.3161	1.15	1.33	Mw
12/26/12	02:23.4	43.7258	-121.3172	0.59	0.93	Mw
12/26/12	09:37.6	43.7770	-121.3241	1.76	1.34	Mw
12/27/12	19:45.5	43.7278	-121.3165	1.25	0.6	Md
12/27/12	32:08.6	43.7996	-121.2756	2.08	1.67	Mw
12/27/12	33:51.0	43.7971	-121.2733	1.89	1.49	Mw
12/27/12	23:43.1	43.8057	-121.2927	3.66	1.73	Mw

12/27/12	29:00.8	43.7960	-121.2886	4.45	1.47	Mw
12/27/12	53:37.0	43.7665	-121.1870	9.60	1.5	Mw
12/27/12	37:55.4	43.7308	-121.3169	1.28	1.89	Mw
12/27/12	44:09.9	43.8101	-121.2828	2.41	2.62	Mw
12/27/12	44:41.2	43.7913	-121.2787	3.80	1.26	Mw
12/27/12	49:51.2	43.7253	-121.3182	1.61	0.87	Mw
12/27/12	07:45.5	43.7275	-121.3115	1.14	0.81	Mw
12/27/12	32:22.8	43.7190	-121.3203	0.21	1.09	Mw
12/28/12	02:02.9	43.7316	-121.3086	0.79	0.24	Md
12/28/12	44:35.0	43.7971	-121.2769	3.84	1.26	Mw
12/28/12	19:43.1	43.7245	-121.3064	1.15	0.91	Mw
12/28/12	08:09.0	43.7300	-121.3146	1.05	1.2	Mw
12/28/12	01:42.8	43.7242	-121.3080	1.14	1.76	Mw
12/28/12	04:27.4	43.7244	-121.3077	1.07	1.24	Mw
12/29/12	25:27.2	43.7225	-121.3179	1.07	0.25	Md
12/29/12	40:16.7	43.7219	-121.3142	1.13	0.11	Md
12/29/12	45:26.7	43.7275	-121.3079	1.84	0.67	Mw
12/30/12	43:08.5	43.7220	-121.3191	1.07	0.25	Md
12/30/12	44:36.5	43.7220	-121.3191	1.07	0.13	Md
12/30/12	52:34.7	43.7203	-121.3142	0.89	0.81	Mw
12/31/12	24:24.5	43.7267	-121.3192	1.34	1.64	Mw
12/31/12	56:04.8	43.7265	-121.3192	0.90	1.41	Mw

Appendix G
Foulger Consulting Micro-seismicity Report

Appendix H
Directional Survey

Appendix I
Work Over Plan for Well NWG55-29

Appendix J
Proposed 2014 Amendments to Induced Seismicity Mitigation Plan